UNIVERSITÀ DEGLI STUDI
DI MODENA E REGGIO EMILIA

DOCTORAL RESEARCH IN
INDUSTRIAL INNOVATION ENGINEERING

PhD cycle **XXXIV**

Competition Sector: **09/B1**
Scientific Disciplinary Sector: **ING-IND/16**

Numerical and Experimental Optimization on the Extrusion Process of Light Alloys

Candidate: **Riccardo Pelaccia**

Supervisor (Tutor): **Prof. Barbara Reggiani**

Director/Coordinator of the PhD course: **Prof. Franco Zambonelli**

Academic Year 2020/2021

Abstract (Italian):

L'estrusione a caldo di leghe leggere è un processo di formatura dove, imponendo grandi deformazioni ed elevate velocità di deformazione, è possibile ottenere profili a sezione costante di alta complessità, come profili multi-cavità e/o con spessori variabili. Negli ultimi anni, la richiesta di requisiti sempre più stringenti in termini di resistenza, qualità e precisione, combinata all'aumento della concorrenza di mercato, ha reso necessario un attento controllo e ottimizzazione del processo già in fase di progettazione per produrre componenti privi di difetti, per massimizzare la produttività e ridurre gli scarti di materiale.

In questo scenario, l'obiettivo della presente tesi di dottorato è il monitoraggio e l'ottimizzazione del processo di estrusione sia in termini di identificazione e controllo dei parametri più significativi, sia in termini di progettazione degli utensili e analisi dei difetti. In particolare, il lavoro si è focalizzato sullo studio del processo di estrusione con matrice raffreddata ad azoto liquido per evitare difetti nel profilo e per migliorare la vita utile degli utensili e sull'analisi e la previsione dei difetti di charge welds e billet skin.

Con riferimento alla prima tematica, anche se l'utilizzo dell'azoto nell'estrusione è una pratica industriale consolidata, lo stato dell'arte è carente di un approccio sistematico per la progettazione e l'ottimizzazione dei canali di raffreddamento. Infatti, i canali sono solitamente realizzati sulla base dell'esperienza del progettista, rendendo difficile la gestione e il controllo delle numerose variabili in gioco relative, per esempio, alla geometria e alla posizione del canale, alle proprietà del refrigerante e ai parametri di processo. In questo contesto, l'uso di modelli numerici avanzati può supportare l'implementazione di una metodologia sistematica per garantire un design efficiente in termini di raffreddamento già durante la fase di progettazione della matrice.

In termini di scarto di materiale, i difetti di charge welds e billet skin riducono di molto le proprietà meccaniche ed estetiche del profilo per la presenza di zone di transizione con diversa microstruttura, alterazioni chimiche e presenza di contaminanti (ossidi, lubrificanti...). Pertanto, per la minimizzazione degli scarti risulta necessario uno studio approfondito dei difetti per poterne prevedere la comparsa e l'evoluzione durante il processo.

Durante il progetto sono state eseguite diverse campagne sperimentali per monitorare sia l'evoluzione del campo termico durante il processo di estrusione con raffreddamento ad azoto sia per valutare l'influenza dei parametri di processo sull'evoluzione dei difetti. Inoltre, gran parte del lavoro è stato dedicato all'implementazione e alla validazione di modelli numerici da utilizzare come supporto mirato all'ottimizzazione di processo.

Tra i risultati più significativi, il modello numerico per il raffreddamento ha evidenziato che modellando l'azoto come fluido monofase (liquido o gassoso), si ottengono buoni risultati macroscopici sull'evoluzione del campo termico, ma i limiti riscontrati hanno spinto verso un modello più complesso per tenere conto del cambiamento di fase. Il confronto numerico-sperimentale ha mostrato errori medi inferiori all'8% sia con raffreddamento sia senza.

Anche in termini di estensione ed insorgenza dei difetti di charge welds e billet skin sono stati ottenuti buoni risultati numerici, soprattutto se paragonati con le attuali formulazioni teoriche ed empiriche presenti in letteratura (errori superiori al 50%).

I risultati ottenuti suggeriscono l'affidabilità degli strumenti di simulazione sviluppati e la loro facile integrabilità industriale come supporto sia per l'ottimizzazione di processo che per la progettazione degli stampi.

Abstract (English):

The hot extrusion of light alloys is a forming process widely used to manufacture constant cross-section profiles of any complexity, as multi-hollow and variable thicknesses profiles, by imposing high deformations rates. In the last years, requirements for high strength, quality and precision continuously increased, together with a steep increasing of the market competition, thus making mandatory an accurate setting and optimization of the extrusion process at the design stage to produce defect-free profiles, to maximize the production rates and to reduce the material scraps.

In this scenario, aim of the present PhD thesis was a comprehensive monitoring and optimization of the extrusion process in terms of key-parameters identification and control, tooling design and defects assessment. More specifically, work has been focused on the investigation of the process performed with a die cooled with liquid nitrogen to avoid thermal defects in the profile and to improve the tooling set life, and on the analysis and prediction of charge welds and skin defects to reduce the material scrap.

Concerning the first topic, even if the use of nitrogen in extrusion is an industrial consolidated technology, a systematic approach for the design, optimization and testing of the cooling channel is still missing in literature. Cooling channels are usually manufactured according to the designer's experience, thus making extremely challenging the managing of the many variables involved, such as those of the channel geometry and position, of the coolant properties and of the cooling parameters. However, the use of advanced numerical tools can support the implementation of an efficient approach for the selection of an optimal cooling solution at the process-die design stage.

In terms of material scrap, charge welds (front-end) and billet skin (back-end) are both defects that drastically reduce the mechanical and the esthetical properties of the final profile due to the presence of transition zones with different microstructure, altered chemical composition and contaminants (oxides, lubricants...). Then, an in-depth knowledge and an accurate predictability of these defects evolution represent a mandatory requirement for the scrap minimization.

During the PhD period, different experimental campaigns have been performed to monitor the thermal field during the extrusion process with a nitrogen cooled die as well as to assess the influence of process parameters on the charge-skin defects evolution. In addition, an extensive numerical work has been accomplished by implementing and validating predictive models to be used as key support tools for process optimization.

As main outcomes of the work, the proposed numerical model for nitrogen cooling showed that a discrete modelling approach (gaseous or liquid-only cooling), even if providing useful indications on the average thermal distribution, show some limitations thus pushing toward a more sophisticated mixed model to account the nitrogen phase-change. The experimental-numerical comparison showed a good matching of the results in terms of temperature prediction with average errors below 8% both in uncooled and in nitrogen cooled conditions.

A good numerical prediction was found also in terms of charge welds and billet skin evolution in the investigated profiles. Numerical results evidenced a good predictability in terms of defects extend and onset, especially if data are compared with the theoretical formulas reported in literature that showed errors greater than 50% with respect to experimental data.

The achieved results suggest the reliability of the developed and tested simulation tools and their easy integrability in a flexible procedure to be used for process and die-design optimization.

Table of Contents

1 Introduction

The hot extrusion process of light alloys is a forming process widely used to obtain components with constant cross-section of almost any complexity by imposing high deformation rates [1-2]. Notably, a pre-heated cylindrical billet is inserted within the container, and it is forced to flow within the shaped die by means of the ram of the hydraulic press (Fig. 1). The billet-material flow fills the die openings, passing through intermediate pre-form, in order to obtain at the exit of the die the final profile shape. The good deformability of the light alloys at high temperatures (range of 450-570 °C for aluminum alloys) allows to easily achieve profiles of high geometric complexity (Fig.2) such as multi-hollow profiles, thin gauges, profiles with sophisticated appendixes and wings etc. without giving up to high production rates [1-2]. In addition, the capability of remarkably varying geometrical design, the high strength-to-density ratio and the almost unmatched corrosion resistance have raised the use of aluminum extrudates at the forefront in many fields, such as furniture design, automotive, aeronautics, railway transportation and construction, among the many [3].

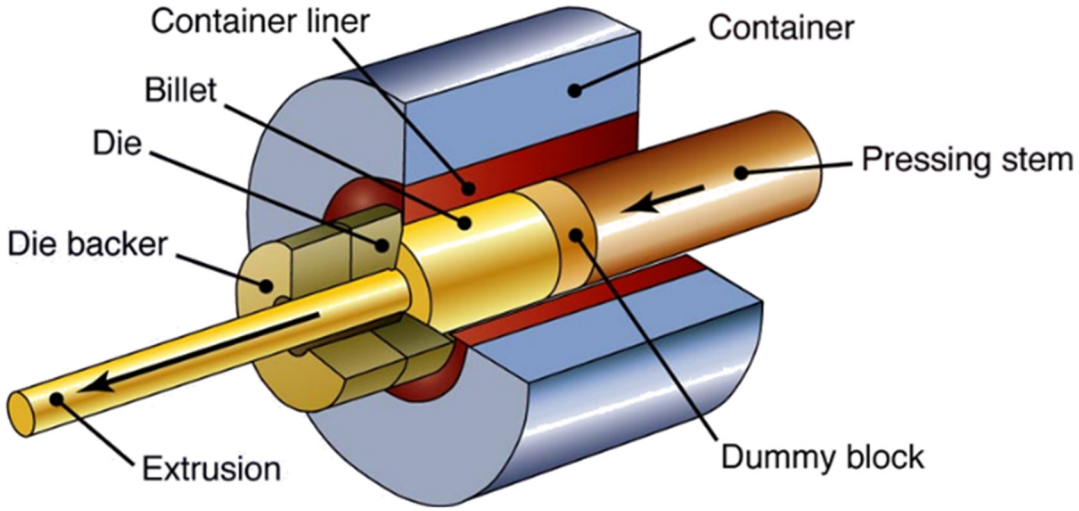

Fig. 1 The hot extrusion process

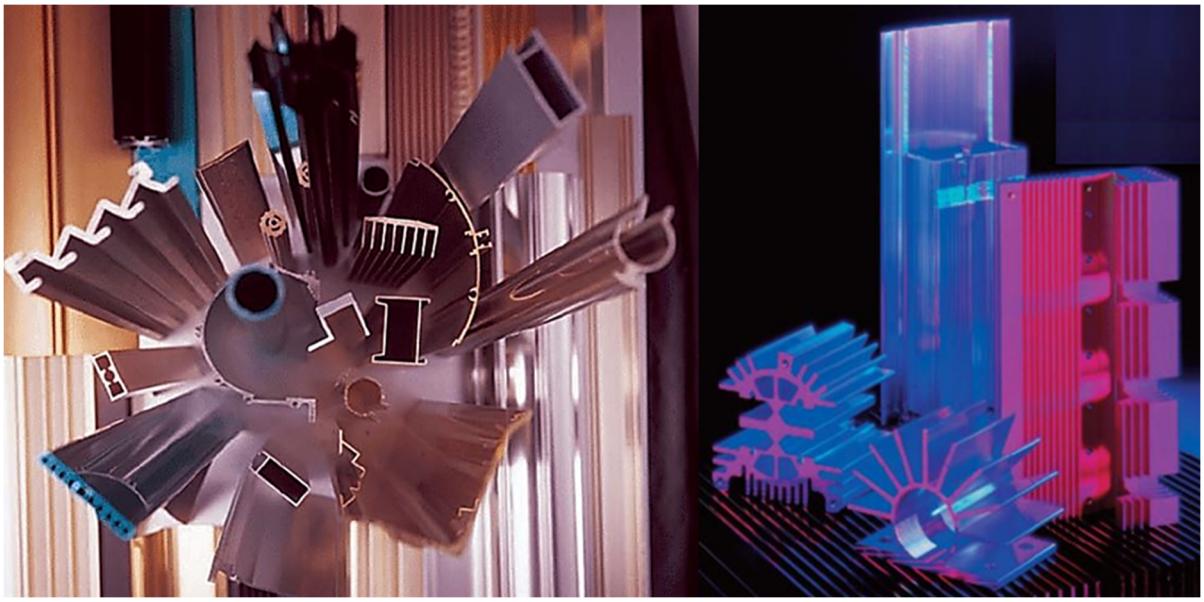

Fig. 2 Examples of profiles achievable with the hot extrusion process [3]

In the industrial context, the high required quality standards at reduced costs, combined with the increased market competition, makes it necessary an accurate setting and optimization of the extrusion process to produce defect-free profiles, to maximize the process productivity as well as to reduce the material scrap [4-5]. In this framework, the motivation of the research lies in a comprehensive monitoring of the extrusion process in terms of process parameters control, tooling design and defects assessment. The combination of the experimental and numerical analysis is a mandatory activity for the understanding of the process and for the implementation of valid Finite Element (FE) predictive models to be used as support tool for process optimization, also with the further aim to limit the time with respect to expensive and cost consuming experimental campaigns. Therefore, the main objective of this PhD project is identified in the development of numerical models to be used for the optimization of the extrusion process in the main aspects of industrial interest. The defects in the extrusion process may be of a different nature: burns and cracks due to the excessive profile temperature, geometrical problem resulting from an excessive deformation of the die, the decay of the mechanical properties of same portions of the profile for the occurrence of impurities (charge weld, billet skin), esthetic defects due to not correct process design and so on. In this scenario, this work is projected towards two aspects of large industrial interest: the use of liquid nitrogen cooling within the die to reduce the defects induced by high temperature as well as to increase the tool life and the production rate; the control and the minimization of industrial unavoidable scraps, since they are characteristic of the process, such as the charge welds and the billet skin contamination.

About the first topic, companies and researchers are focused on the control and the reduction of the critical process temperatures in order to avoid defects in the profile and to improve the tool lifetime. In addition, their great efforts in the use of nitrogen cooling are conveyed to the productivity gain, especially for complex profiles, where the high temperatures, generated to overcome friction and to plastically deform the material, strongly depend on the extrusion speed. The use of the liquid nitrogen is a well-known technology in the industrial framework, however, a systematic methodology for the design of the cooling channel has not been proposed yet. Cooling channels are manufactured according to the designer's experience, without a robust criterion to obtain the optimal design that depends on many variables, such as the channel geometry and position, coolant properties and cooling parameters. Thereby, the use of numerical tools as the Finite Element Method (FEM) could be extremely useful for the analysis and selection of an optimal cooling solution in relation to the process parameters and the geometrical features of the profile.

About scrap reduction, the research activity is focused on the experimental analysis and the numerical prediction of the charge welds and billet skin in industrial profiles, both representing important material scraps due to the lower mechanical properties of the profile portion contaminated by these defects. Indeed, the charge welds and the billet skin contaminations drastically reduce the mechanical properties of the final profile, due to the presence of transition zones with different microstructure, altered chemical composition and contamination derived by previous processes. The current industrial practice, based on experiences and simplified theoretical approaches, underestimates or overestimates very frequently the scrap material, thus selling a low-quality products in the first case and discarding grade material in the second case. Again, the understanding and the numerical prediction of these defects could be a valid aid for the optimization of the process in term of scrap minimization.

The study of the properties, peculiarity and of the technological limits of the extrusion process is a mandatory preliminary activity for the subsequent research works. Particularly, it is required to study the thermodynamics and the tribology specific of the extrusion process in order to gain a thorough knowledge of the process itself and to extrapolate the main parameters to be monitored. In addition,

the analysis of aluminum alloy in terms of mechanical and physical properties allows figuring out better the flow material behavior under different process parameters. Simultaneously, it requires an in-depth know-how of the numerical tools nowadays available to simulate the process, meaning a deep knowledge of the finite element method theory, of the ways to process the CAD geometries within the simulation codes, of the optimal meshing of the components and of the optimal settings of the input parameters. Furthermore, the extrusion process with nitrogen cooling requires the study of the fluid-dynamics theory and of the behavior of pressurized fluids within a channel with the aim to quantify the influence of parameters such as the channel design and the fluid properties on the cooling performances. Concerning the experimental identification and the analysis of the internal defects in the profile, such as the charge welds and the billet skin, it also requires a specific knowledge for the sample preparation in terms of metallographic and metallurgical issues.

Therefore, in the second chapter it will be presented a brief but detailed overview of the fundamentals of the hot extrusion process of aluminum alloys with the aim to acquire the necessary know-how for the identification of the key-parameters for the process control, tooling design and defects assessment. In the third chapter, the state of art on thermal process control and charge –skin prediction was deeply presented and discussed in order to frame the main issues and challenges that will be addressed within this PhD thesis. Afterwards, the preliminary setting and the performing of three experimental campaigns will be addressed within the chapter 4, collecting and analyzing interesting data in terms of thermal field and cooling efficiency during the extrusion process with nitrogen cooling of real industrial profiles. With the same aim, the chapter 6 will report two experimental analyses for the evaluation of the scrap length in terms of charge welds and billet skin, showing the careful, but very time-consuming, metallographic analysis for the defects detection. The acquired data in terms of extrusion load, temperature monitoring and control as well as in terms of defects onset and evolution will be used for the implementation and validation of comprehensive numerical models of the extrusion process. Notably, the modelling concept, the numerical settings and assumptions as well as the experimental-numerical comparison of the results will be addressed within the chapters 5 and 7, respectively for the nitrogen cooling and for the defect prediction. The simulation performances, the advantages and the limits of the proposed models will be deeply assessed and discussed.

2 Principles of Hot Extrusion Process

2.1 *The Hot Extrusion Process*

The hot extrusion is a forming process where a pre-heated cylindrical billet is inserted within the container and it is forced to flow by compression through the die opening of a smaller cross-sectional area than that of the original billet [1-2]. The billet diameter is slight lower than the container one to allow the billet insertion; thereby, the compression firstly causes only the billet upsetting until its diameter does not match that of the container. Then the compression forces lead to high deformation within the billet and the material starts to fill the die openings generating the desired shaped profile at the die exit. Fig. 3 shows a 2D schematization of a direct extrusion process where the main components are indicates: the ram of the press that compresses the billet into the die-container walls, the container that acts as the housing of the billet and the die that gives the final shape at the profile. The billet is not completely extruded, but a billet rest is discarded to avoid the profile contamination with lubricant, inclusions, undesired oxides etc. (see section 2.5).

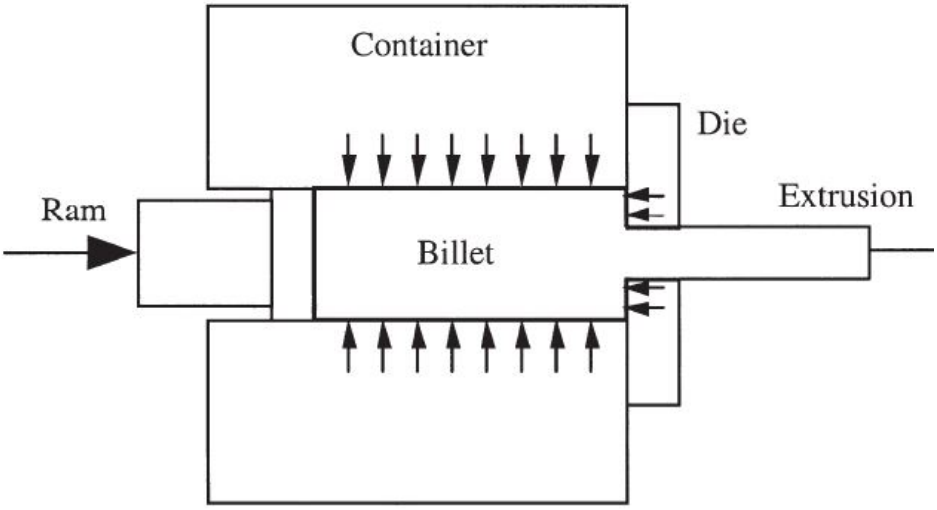

Fig. 3 Schematization of the Direct Extrusion Process [1]

Schematization of Fig.3 well describes an example of a direct extrusion process, where the material flow direction coincides with that of the ram, resulting in friction forces that act at the billet/container /die interfaces [1-2]. Instead, in an indirect process, the extrusion direction is opposed to the ram motion (Fig.4), resulting in no friction at the billet/container interface and in a twofold increasing in billet weight and extrusion speed along with a 30-45% decrease in extrusion force [1-2,6]. However, the main drawback of the indirect process lies in the maximum achievable profile dimensions and shape complexity since the die has to flow into the container and to act as ram, thus bounding the indirect extrusion to simple profiles (solid and hollow), but at high production rates [7-8].

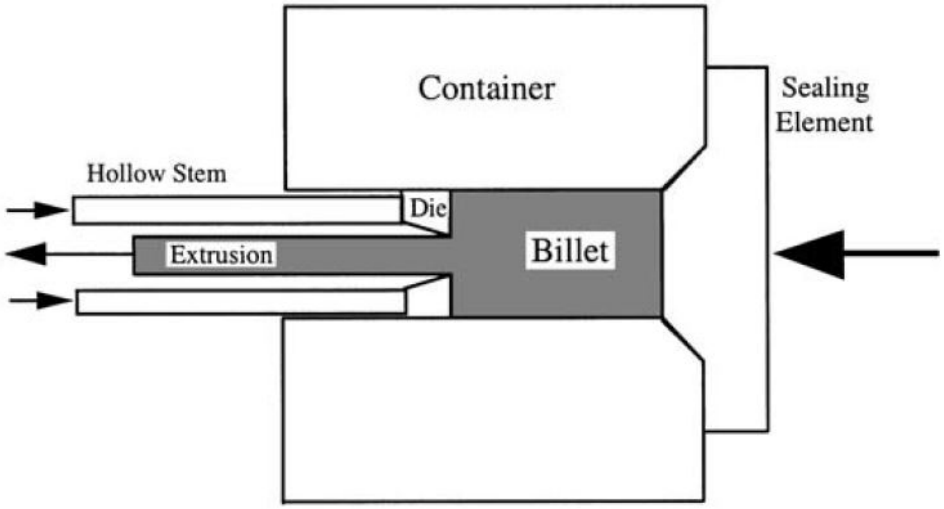

Fig. 4 Schematization of the Indirect Extrusion Process [1]

During the hot extrusion the material flow is subjected to high deformations at high strain rate and temperature [1-2,9]. A deep assessment of the deformation mechanics involved in the process is mandatory to highlight the key-parameters that must be investigated and monitored as well as to generate reliable numerical models. This assessment can be structured in the following main steps:

- Friction model and material flow
- Thermodynamics of the hot extrusion process
- Extrusion load - process parameters correlations
- Intrinsic defects of the process (charge welds and billet skin)

- Die design

The aforementioned aspects will be discussed with the aim to acquire the necessary know-how for the numerical models implementation and validation of the hot direct extrusion process of light alloys (Al and Mg), aim of the present PhD thesis.

2.2 Friction model and material flow

Friction forces depend on the process configuration, such as direct or indirect, and occur at the billet-tools interfaces (ram–billet back-end; billet-container walls; billet-die walls) (Figs. 3,4) [1,6,9]. The well-known Coulomb friction model [10] considers the surfaces in contact only at random asperity peaks, resulting not suitable for the extrusion process where the contact of the surfaces is deeper and the involved pressures are very high (Fig.5a). A valid alternative is offered by the Siebel, or shear, friction model for which the friction force F_f is assumed to be proportional to real contact area [11,12]:

$$F_f = m\tau_f A_r \tag{1}$$

with m the friction factor, τ_f the material shear strength and A_r the real contact area. According to the Von Mises yield criteria [13-14], the shear stress τ_f to overcome (Fig.5) is equal to $\sigma/\sqrt{3}$, where σ being the material flow stress.

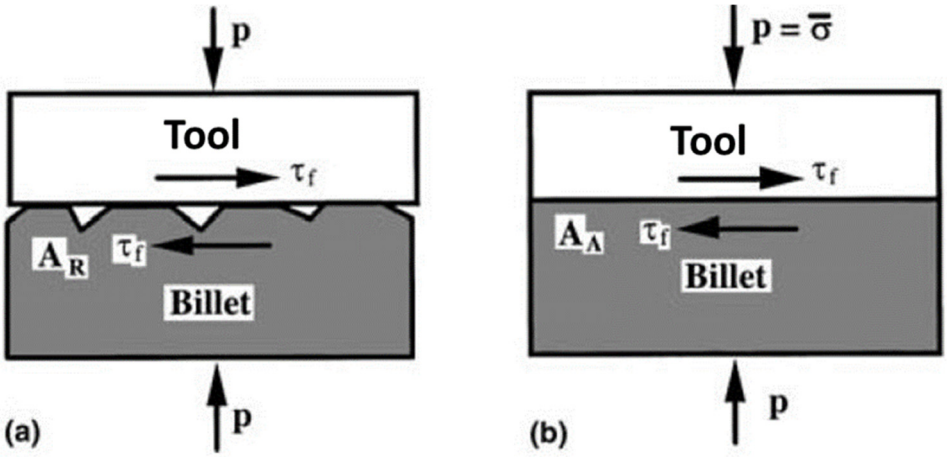

Fig. 5 Friction Condition in the Extrusion Process: a) Sliding friction condition, b) Sticking friction condition [1]

The friction forces must be analyzed for each billet/tool interface because they influenced the extrusion load necessary to perform the process and, more importantly, they affect the material flow within the die and everything else that depends on it (die filling, profile quality, defect evolution etc.). Starting from the container walls, during the direct extrusion process, the contact area gradually increases after the billet upsetting, rapidly reaching the total apparent contact area A_a. Therefore, in the billet-container interface a sticking friction condition rapidly occurs. Friction factor is equal to 1 in unlubricated state, representing the common condition on the container walls in order to avoid profile contamination (see section 2.5). At the ram-billet interface, the sticking condition is reached for high pressures applied on the billet under deformation. The friction factor is in the range of 0.8-1 depending on the use of lubricant to avoid the ram-billet adhesion. Indeed, in this case the contamination with the lubricant generally remains within the billet rest (see section 2.5). On the die walls high pressures promote the formation of an adhesion layer, also developed due to the strong adhesion of materials such as aluminum with the tool steel with which the dies are constructed [15]. Therefore, the sticking friction condition is predominant within the die. Different considerations must

be integrated about the bearings (or forming) zones, where the profile obtains the final shape (Fig.6). The bearings surfaces are usually treated (such as nitriding or thin hard coatings) to increase the surface hardness and the wear resistance [15-16] with the aim to preserve the profile tolerances and consequently to improve the die life. The presence of the surface treatment reduces the aluminum adhesion on the bearings surfaces, resulting in a sliding friction condition modelled by a friction factor m significantly lower than 1. Thereby, some studies concern the evaluation and the modelling of the friction conditions on the bearings surfaces [9,17]. Similar considerations can be done for the indirect extrusion but recalling the absence of billet-container relative motion that leads to lower flow resistance and load. Table 1 summarizes what discussed in terms of friction factor and friction conditions.

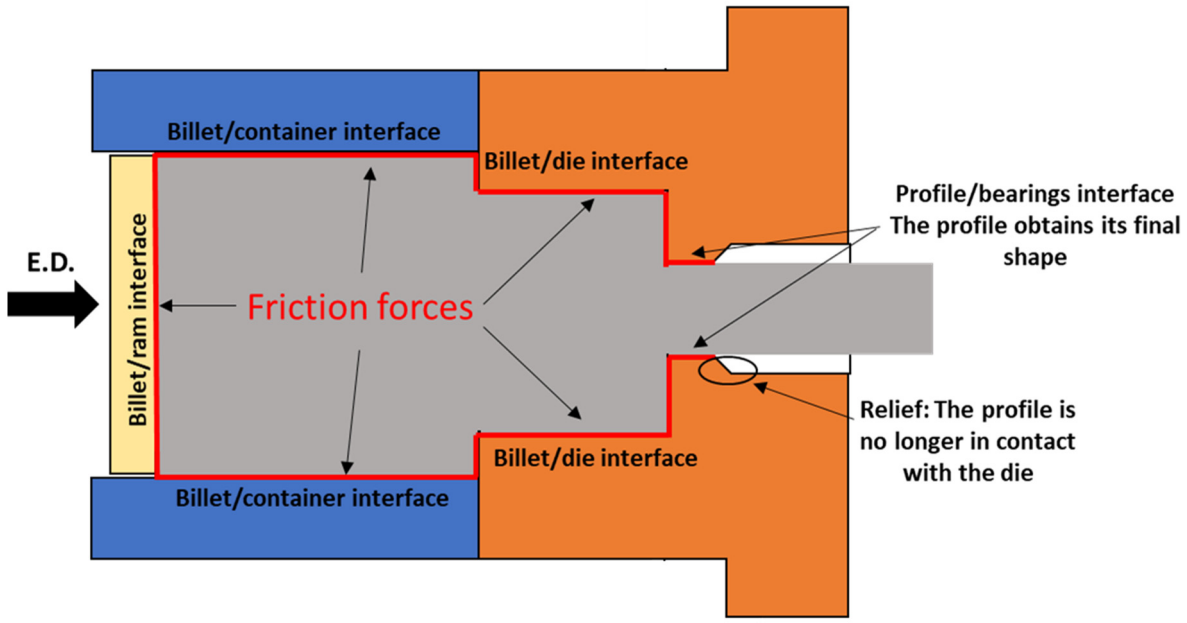

Fig. 6 Friction forces on the aluminum-tools interfaces

Table 1 Friction conditions and the corresponding friction factors at the billet-tools interfaces

Billet-Tool interface	Friction Condition	Friction Factor
Billet-Ram	Sticking	0.8-1
Billet-Container	Sticking (Direct Extrusion)	1
Billet-Die	Sticking	1
Aluminium-Bearings	Sliding	0.3-0.8

As previously mentioned, the friction forces at the billet-tools interfaces impact on the material flow inside the die leading to a slower flow of the peripheral part of the billet than that of the center, phenomena that causes severe shear deformation. The force required to push the billet into the container surface exceeds the shear strength of the billet material, and consequently deformation proceeds by shear in the bulk of the billet. Fig. 7 shows an example of material flow in both the indirect and direct extrusion. Flow pattern A is typical of indirect extrusion with the presence of friction at the die-billet but not at the container-billet interface. Instead, flow pattern B occurs when friction acts in both container and die interfaces (direct process). In both cases, material at the center

of the billet flows faster than that at the periphery. In the corner of the leading end of the billet, a separate zone is formed between the die face and the container wall, known as a dead-metal zone. The material near the surface undergoes shear deformation compared with the pure deformation at the center, and it flows diagonally into the die opening to form the outer shell of the profile. It is worth nothing that an extended dead-metal zone is formed during the direct process, also showing a more shear deformation compared with that in flow pattern A. Friction between the dead-metal zone and the flowing material is no more than the shear stress of the material, then the friction stress is also given by Eq. 1 with friction factor equal to 1.

Visio-plastic analyses can be usually performed in aluminum extrusion in order to measure the friction effect at the billet-container interface (Fig. 8) [18-19]. A first approach consists in splitting the billet into two parts, then imprinting a grid on one part and finally recomposing the original billet with a thin layer of a release agent in the middle. The two slices are then extruded together. A second way is to drill equally spaced holes in the billet, then to fill them with rods of a different alloy having a similar flow stress but a dissimilar color. Another method consists in the analysis of the billet rest microstructure visible after chemical etching.

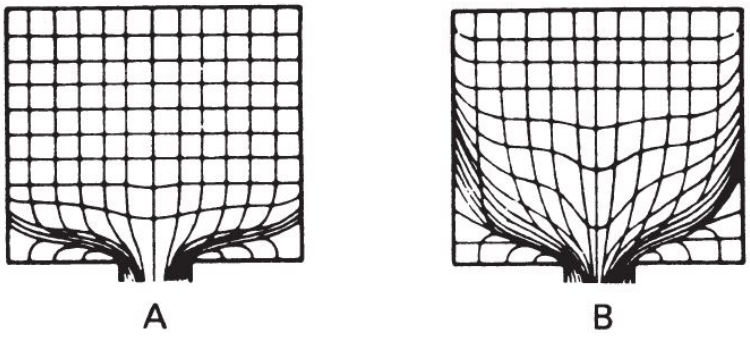

Fig. 7 Schematization of possible flows pattern during the extrusion process: A) Indirect Process, B) Direct Process [1]

Fig. 8 presents some example of flow patterns during the direct extrusion got with different visio-plastic approaches. In all examples, the fast material flow at the center of the billet as well as the dead-metal zones are clearly visible. In addition, Fig. 8c shows a "ram effect" on the material flow: the starting point of some rods moved radially from the surface to the inside of the billet since during each stroke the ram rasps material from the surface pushing it inside where higher speeds are present. The way of material flowing affects many aspects of the process in terms of extrusion load, heat generation as well as of profile quality and properties, thus motivating the several papers presented in literature on the experimental-numerical visio-plastic analyses of aluminum extrusion [18-20].

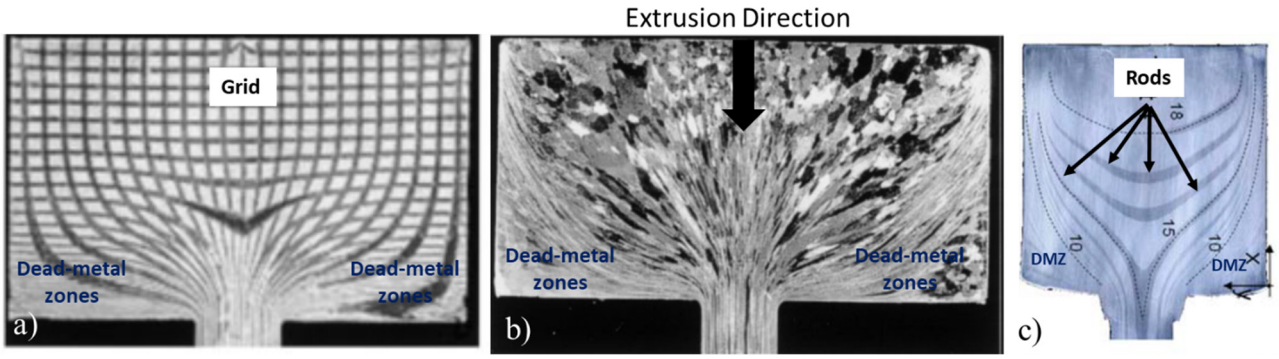

Fig. 8 Experimental analysis of the material flow in the container: a) Flow pattern evaluated with a grid [18], b) Micrographic analysis of the billet rest [18], c) Flow pattern evaluated with rods inserted within the billet [19]

2.3 Thermodynamics of the hot extrusion process

Temperature control during aluminum extrusion is a mandatory activity in order to produce defect-free profiles and to optimize process productivity [1-2,9,12,21]. Therefore, temperature is one of the most important parameters in extrusion: the flow stress is reduced if temperature is increased and, consequently, the material forming comes easier; however, the maximum extrusion speed is constrained since localized high temperatures can lead to incipient melting of the specific alloy [1-2,9]. In terms of generated thermal field, the extrusion process can be schematized as shown in Fig. 9.

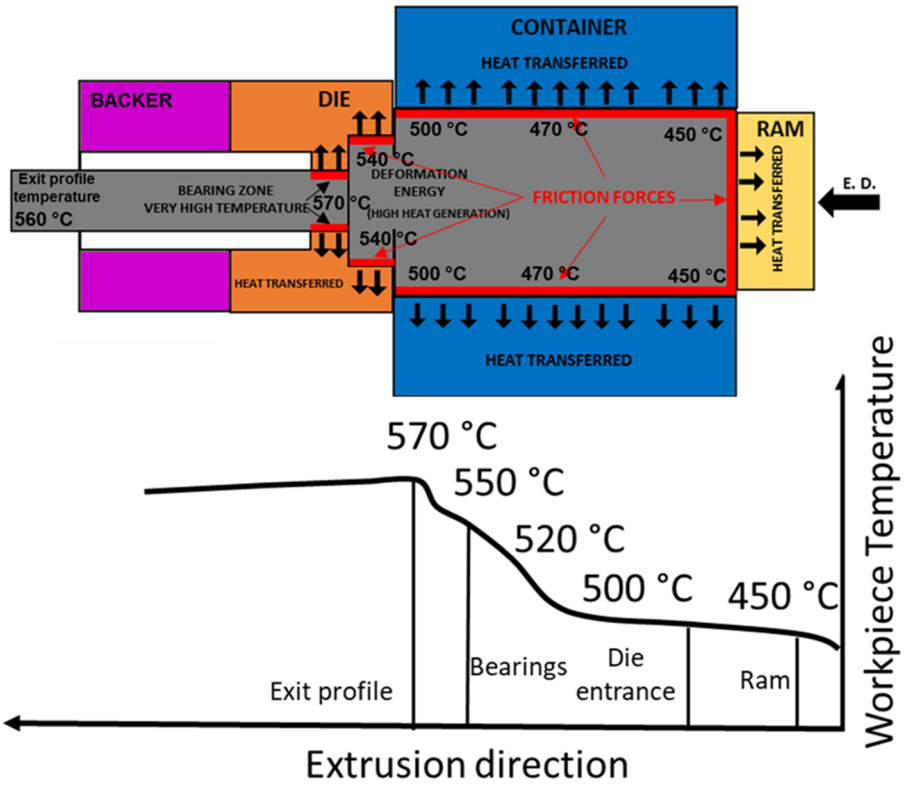

Fig. 9 Schematic of hot-extrusion process in terms of heat transfer and temperature history

The preheated billet (450°C-480°C) is slightly cooled by the contact with the ram (300°C-400°C) and the container (400°C-450°C), but the friction energy generated at the billet-tool interfaces and the high deformation energy used to form the final profile are largely converted into heat (80-90%). Therefore, the exit profile temperature can reach values of about 550°C-580°C for aluminum alloys. The billet preheating is necessary to guarantee the billet deformation and the right die filling during the process. The extrusion die is preheated at high temperature (450°C-500°C) to avoid in-service breakdowns and it is warmed during the process by the forming material. In summary, the main contributions to the resulting thermal field are:

- The heat generated for plastic deformation
- The heat generated for friction at the aluminium-tools interfaces
- The heat generated from the intermetallic friction at dead metal zones
- The heat exchanged for convection by billet with air during the billet transferring from the pre-heating oven to the container
- The heat exchanged for conduction by billet with the container walls before the process starting

- The heat exchanged for conduction by billet with the whole tooling set during process
- The heat exchanged for convection by the profile with the air at the die exit

During the process, the profile exit temperature cannot exceed a critical threshold (related to the specific alloy) in order to avoid surface defects, such as burns, cracks and hot tearing (Fig. 10 [22-25]), as well as to limit the decrease of the die life and wear strength for the creep-thermal fatigue detrimental interaction [26].

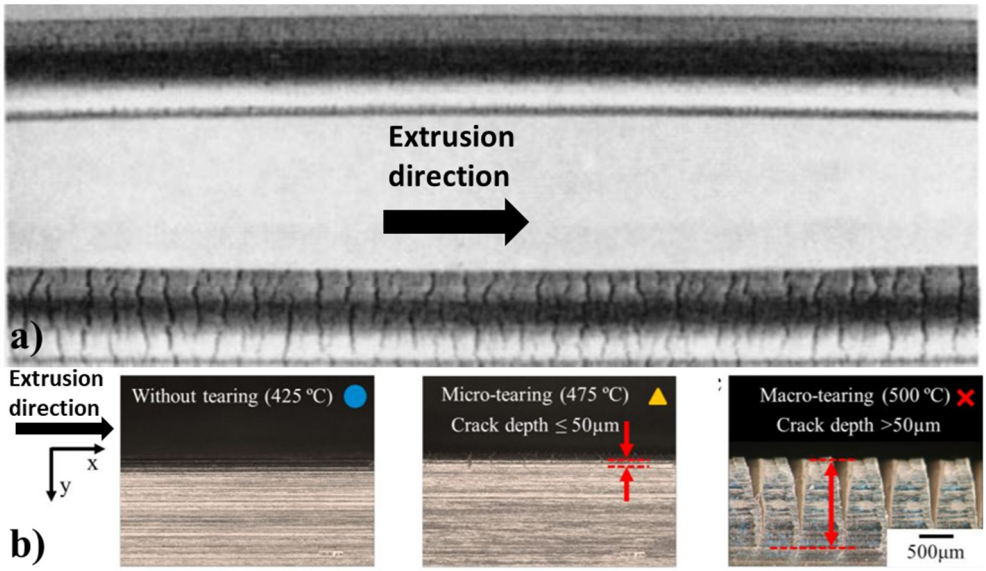

Fig. 10 Examples of hot cracks and tearing in the extrusion process: a) Picture from literature [22] about AA2014 aluminum alloy, b) Picture from literature [23] about AA7075 aluminum alloy

The temperature distribution in the billet and in the profile during the extrusion depends on several factors, such as billet material properties, friction conditions at the material-tools interfaces, die design parameters as well as process parameters (ram speed, extrusion ratio, outside perimeter of the profile etc.). Some of these effects are summarized as follows [1,9]:

- *Materials properties*: The mechanical properties of the billet material considerably affect the magnitude of the heat generated due to deformation and boundary friction. In terms of deformation, the dissipated heat strongly depends on the flow stress of the material at a given temperature, strain rate, and strain. In terms of friction, the temperature increase is proportional to the friction shear stress. In addition, the thermal properties of both the billet material and the tool ones (thermal conductivity, heat transfer coefficients etc.) influence the temperature increase as well as the heat transfer.
- *Friction*: As previously mentioned, the heat generation heavily depends on the friction factor at the billet-container interface, as well as at material-die one. Higher friction factors and higher friction shear stresses cause an increase in temperatures, assuming other variables as constant. Additionally, temperature increases also occur due to higher friction shear stress at the dead metal zone interface.
- *Ram speed*: The temperatures developed in extrusion increase with increasing ram speed. Indeed, the strain rate is directly proportional to the ram speed, and the magnitude of the generated heat is proportional to the strain rate. In addition, the lower the ram speed, the more time available for the generated heat to flow towards the tools since the heat conduction is also more pronounced with aluminium because of its high conductivity.

- *Extrusion ratio*: The extrusion ratio is defined as the ratio between the billet area after the upsetting and the cross-section area of the final profile. In the case of larger extrusion ratios, the exit temperature becomes higher due to severe plastic deformation at higher strain.
- *Outside profile perimeter*: The exit temperature developed in extrusion increases with increasing outside perimeter of the die openings. This increase occurs because the die bearing frictional area increases with the increase of outside perimeter for the same bearing length.

At this point, it comes clear that an in-depth assessment of the generated thermal field is mandatory for the process optimization. In chapter 3, the thermodynamics of the extrusion process will be resumed and deeply discussed in terms of research activities reported in literature and in terms of die cooling with liquid nitrogen as an advanced solution to control the thermal field of the die and of the profile as well as to increase the production rate.

2.4 Extrusion load- process parameters correlations

The load required during the process shall not exceed the press capacity, making it mandatory the knowledge of the main affecting variables such as the material flow stress, as mainly, the pre-heating billet temperature, the extrusion ratio, the friction condition at the material-tool interfaces and the ram speed. The evolution of the extrusion load during both the direct and the indirect process is shown in Fig. 11. After the billet upsetting, the extrusion load rapidly increases due to the friction forces and the die filling, thus reaching the peak when the material starts to exit from the bearings zones. After the peak, the load gradually decreases due to a temperature rise (leading to a lower flow stress) and to a frictional area reduction within the container as the billet length decreases with the ram stroke. The sharp rise at the end of the ram stroke depends on the billet rest length because it contains impurities, and the flow would start to be radial making it difficult to extrude (see section 2.5).

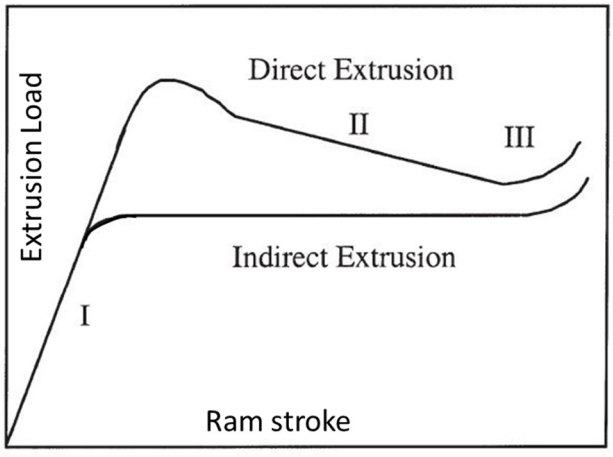

Fig. 11 Evolution of the extrusion load during the ram stroke

In detail, the main variables affecting the extrusion force are [1-2,9]:

- Extrusion ratio
- Working temperature
- Extrusion Speed
- Flow stress

Extrusion Ratio: The extrusion ratio (ER) of a multi-hole die is defined by:

$$ER = \frac{A_C}{n * A_e} \quad (2)$$

where n is the number of symmetrical holes, A_C is the area of container, and A_E is the area of extrusion. The extrusion ratio is a clear indication of the amount of mechanical working that will occur to achieve the final profile shape. Indeed, the effective strain is a function of the extrusion ratio, thereby, the extrusion load required to deform the material depends on it. The decrease of the extrusion ratio causes a decrease of the extrusion load because the amount of plastic strain and deformation work will be less. When the extrusion ratio is high, the extrusion pressure required to push the metal through the die will be higher due to a higher amount of plastic strain. The extrusion ratio in the industry practice is in the range of 10-35 and 10-100 for hard and soft alloys, respectively. However, these ranges should not be considered absolute because the actual shape of the extrusion affects the results. It is worth noting that aluminum profiles extruded with a low extrusion ratio present a micro-structure similar to that of as-cast aluminum (coarse grain and low mechanical properties); thereby, it is not recommended to extrude shapes with very low extrusion ratio in order to obtain the desired mechanical properties.

Extrusion Temperature: Extrusion is carried out at elevated temperatures for metals and alloys that do not have sufficient plasticity range at room temperature and to reduce the forces required for extrusion. As mentioned in the previous section, the flow stress, and consequently the extrusion load, decreases with a temperature rise, keeping in mind the constraints already discussed in terms of surface defect at elevated temperature. From a thermal point of view, the load changes during the extrusion have been deeply investigated by analyzing the relations with the billet temperature, the heat transfer from the billet to the container and the heat developed by deformation and friction [27-31].

Extrusion Speed: Increasing the ram speed produces an increase in the extrusion load. Indeed, the strain rate is directly proportional to the ram speed, while the magnitude of the generated heat is proportional to the strain rate. Even if the temperature developed in extrusion increases with increasing ram speed (lower stress), the effect of the strain-rate is predominant in terms of load increase.

Material Flow Stress: A true stress-strain curve gives the stress required to any given strain. The flow stress of the material is influenced by the following factors:

- Chemical composition and the metallurgical structure of the material
- Temperature of deformation, the strain ε and the strain-rate $\dot{\varepsilon}$

The definition of the stress-strain curve is mandatory for the numerical analysis, because as previously discussed, the flow stress influences the extrusion load, the friction condition, the thermal field and more generally it affects how the material fills the die openings and the quality of the final profile. Therefore, the flow stress must be described in an analytical form to be implemented within the numerical model. The flow stress depends on the temperature, the strain and the strain-rate, thereby, in its most general form it can be written as:

$$\sigma = f(\varepsilon, \dot{\varepsilon}, T) \quad (3)$$

The experimental analysis of the flow stress during the extrusion process is not possible because at every point there are different conditions in terms of temperature, strain and strain rate, usually also affected by variable friction condition. Thereby, over the years, different experimental material characterizations have been proposed to evaluate the flow stress under different condition of

temperature, strain and strain-rate, trying to replicate conditions similar to the process ones. The methods most commonly used for obtaining the flow stress are the tensile, uniform compression and torsion tests [32]. Tensile test is the most popular and used when small strains are required (usually limited to 0,3-0,5); indeed, the limit of the test is the occurrence of necking that constraints the maximum range of achievable strain before fracture [33-34]. The compression test requires optimal lubrication of the specimen faces thus generating relevant complexity with hot testing; moreover, severe barreling of the specimen usually occurs at strain around the unity thus superiorly limiting again the strain field [35-37]. In this context, torsion test appears the most suitable method to characterize alloys for hot extrusion because the strain is superiorly limited only by the specimen brake that usually occur at strain higher than 5 thus matching with bulk processes requirements like extrusion where the strain field can reach locally values up to 10 [32, 38-42].

Starting from the experimental data, different flow-stress models can be selected. In the context of the hot extrusion process, two models are widely used: the hyperbolic sine law proposed by Zener and by Sellars and Tegart [43], and the equation proposed by Hensel-Spittel [38, 44]. The former can be expressed as follow:

$$\bar{\sigma}\,(T,\dot{\varepsilon}) = \frac{1}{\alpha} sinh^{-1}[\frac{1}{A}\dot{\varepsilon}\exp\left(\frac{Q}{RT}\right)]^{\frac{1}{n}} = \frac{1}{\alpha} sinh^{-1}[(\frac{Z}{A})]^{\frac{1}{n}} \tag{4}$$

where σ is the flow stress, $\dot{\varepsilon}$ is the strain rate, Q is the activation energy, R is the gas constant, T is the temperature, n, A and α are material constants, while Z is defined as the Zener-Hollomon parameter. Eq. 4 is generally used to relate peak or steady state stress with temperature and strain rate, but the strain dependence is neglected unless supposing that A, α, n, and Q are strain-dependent parameters, as suggested by some authors [45-52]. Polynomial equations are therefore almost invariably used to quantify the dependence of these parameters on strain well describing the hot workability of steels [45-46], Al [47-50], and Mg alloys [51-52]. The major problem in these analyses is that extrapolation above the maximum experimental strain can lead to negative values of the flow stress [42]. However, in its original form, it is widely used in forming process as the extrusion where the strain rates are very high and to neglect the strain dependence of the stress can be sometimes acceptable. Indeed, as it will be clear in the next chapters, using an Eulerian numerical approach, the Zener-Hollomon flow stress allows avoiding the integration of the strain rate to obtain the strain for the evaluation of the material flow behaviour, thus reducing the computational time. Instead, the Hensel-Spittel flow stress takes into account the stress dependence on strain, strain rate and the temperature:

$$\bar{\sigma} = A \cdot e^{m_1 T} \cdot \bar{\varepsilon}^{-m_2} \cdot \dot{\bar{\varepsilon}}^{-m_3} \cdot e^{\frac{m_4}{\bar{\varepsilon}}} \cdot (1+\bar{\varepsilon})^{m_5 T} \cdot e^{m_7 \bar{\varepsilon}} \cdot \dot{\bar{\varepsilon}}^{m_8 T} \cdot T^{m_9} \tag{5}$$

where σ is the flow stress, A, m1, m2, m3, m4, m5, m7, m8 and m9 are material constants, ε is the strain, $\dot{\varepsilon}$ is the strain rate, T is the temperature. Starting from the experimental data, parameters of the HS equation can be estimated by a multi-linear regression procedure [53]. The behavior of the metal flow is predicted more accurately due to the strain dependence modelling, being more suitable for numerical analyses of die filling and of defects prediction like charge welds and billet skin contamination. Within the implemented numerical models that will be presented in this PhD thesis both flow stress models are used in accordance with the needs.

2.5 Intrinsic defects of the process: Charge welds and the Billet skin contamination

Charge Welds: Charge welds or transverse welds are intrinsic defects of the process generated since multiple billets are consecutively extruded. Indeed, at the end of the ram stroke, even if the billet rest

is removed, the die remains completely filled by the material (Fig. 12). When the new billet is loaded into the press and the subsequent extrusion starts, the new material and the old one interacts with each other, thus creating a transition zone of a certain length in extrusion direction where the profile presents a mixture of new and old billet material. This transition zone is defined as charge welds extent. As it is visible in Figs. 12c, d, the charge welds extend along the profile to a variable length depending on die design and processing parameters [54-55]. The new billet material present in the transition zone is usually contaminated by oxides, dust, or by lubricant collected during the loading into the press [56]. Therefore, the profile length contaminated by the charge welds must be discarded due to its lower mechanical properties if compared with the rest of the profile length. The contaminated material is discarded starting from the stopmark, an evident mark generated on the profile in contact with the bearings zones during the billet change. Indeed, during this dwell time the material within the die cools down and sticks to the bearing zones, then, when the extrusion process starts again the material pulls away from the bearings generating the stopmark. Fig. 12 shows the movement of the stopmark along the extrusion direction during the charge welds evolution. As convention, the scrap length for the charge welds is evaluated as a positive distance from the stopmark because the defect is extruded after the stopmark in the extrusion direction.

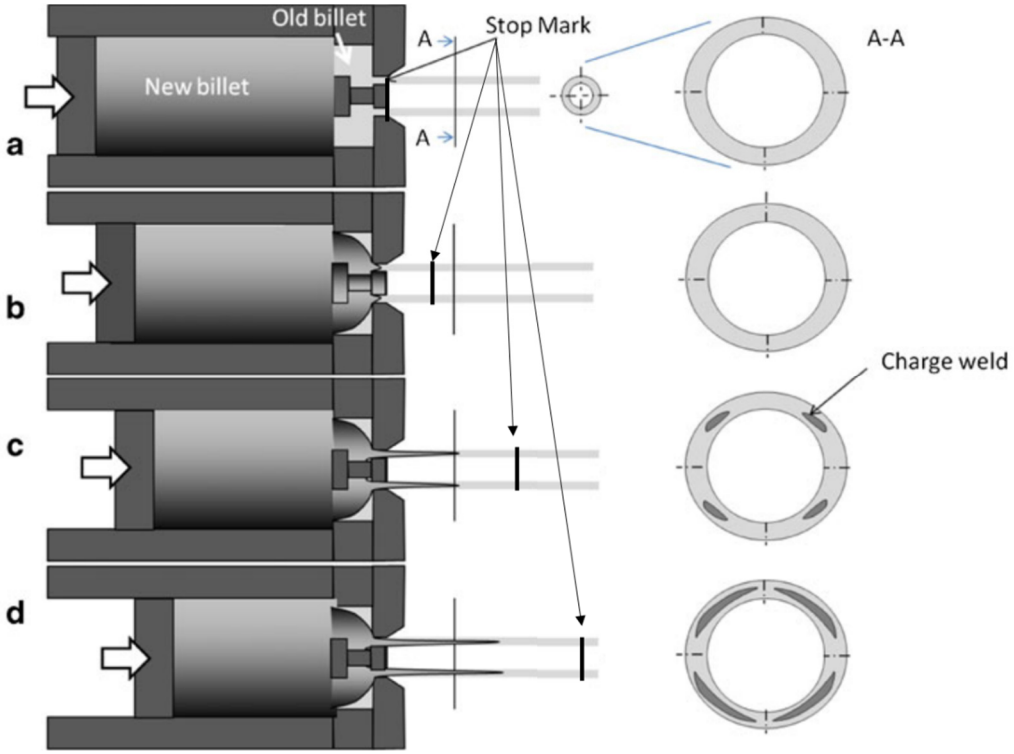

Fig. 12 Charge Welds evolution during billet-on-billet extrusion

The experimental evaluation of the charge welds extent consists in cutting the profile into several samples of defined length, polishing and chemical etching the cross section of the samples with the aim to reveal the charge welds defect and to evaluate the percentage of the old-material replacement with the new one. The industrial practice considers the extinction of the charge welds defect when the 95% of the cross-section area of the profile is replaced by the new billet material (Fig. 13). However, the experimental analysis of the charge welds extent is a very time and cost consuming activity and it is not possible to make for each profile within a framework of industrial production. Currently, the determination of the zone to be discarded in industrial everyday practice for weld contamination is still performed by intuition, analogy with similar profile shapes, and experience (see section 3.2).

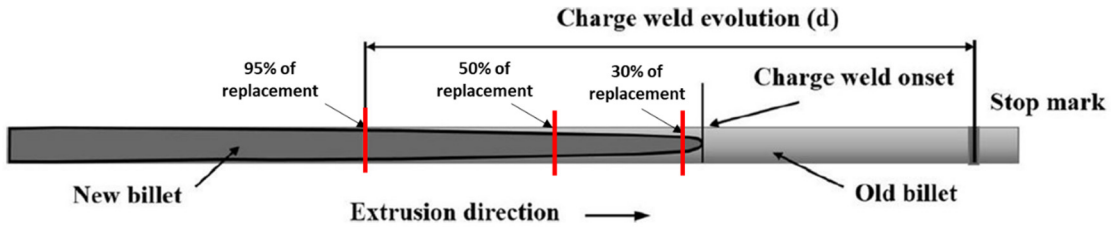

Fig. 13 Extrusion length with a transition zone

Billet Skin Contamination: As previously discussed (section 2.2), the friction at the billet-container interfaces produces an imbalanced material flow with the formation of dead metal zones and complex material flow inside the die. In relation to the high friction factor with the container, during the ram stroke. the billet skin does not flow towards the die, but it is accumulated in the proximity of the ram (Fig. 14). At the end of the process, if the billet rest length is enough (Fig. 14 a), the skin does not flow inside the die and the contamination is entirely discarded with the billet rest. Instead, if the billet rest length is inadequate, the billet skin can flow inside the die and eventually also into the profile (Fig.14 b).

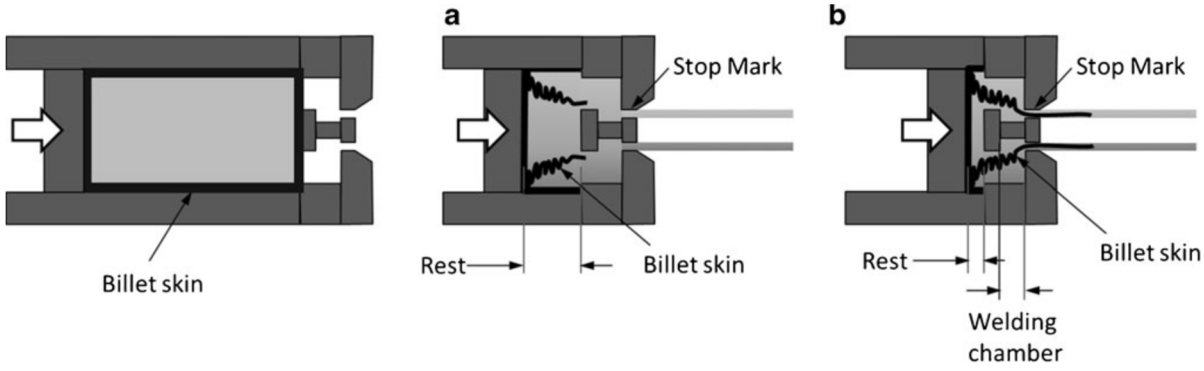

Fig. 14 Billet skin contamination in the direct extrusion process

The skin of the billet is usually marked by a different chemical composition or microstructure than the inner material [57]. This difference can be either the result of an altered chemical composition (i.e. depended on the cooling from casting) or of a contamination such as oxides, dust and oil accumulated during the preparation of the billet (billet transport, pre-heating in the oven, loading in the press etc.). Therefore, also in this case, the profile length contaminated by the billet skin must be discarded for its lower mechanical properties. Analysing the Fig. 14, it is worth noting that the skin contamination can be found before the stopmark if it enters within the profile before the end of the ram stroke. Thereby, the scrap length for the skin contamination is evaluated as negative distance from the stopmark. The skin present after the stopmark usually interacts and mixes with the charge welds defect and it is discarded within the scrap length designed for the charge welds. The same consideration discussed for the charge welds apply for the experimental evaluation of the skin contamination within the profile. According to industry practice, standard billet rest for direct extrusion is kept to 10 to 15% of the billet length [1-2].

At this point it is clear the need to evaluate the appropriate billet rest and scrap length to minimize the discarded material since the industrial practice usually overestimates or underestimates the defect extent within the profile. The implementation of reliable numerical model can offer the possibility to minimize the material discarded but also to support the optimization of the die design with the aim to reduce the defect extent during the process.

2.6 Die design

There are three basic types of extrusion dies [2-3, 58]: solid dies, semi-hollow dies, and hollow dies, which produce solid profiles, semi-hollow profiles, and hollow profiles respectively. Extrusion dies are essentially thick, circular steel disks containing one or more orifices of the desired profile. They are generally manufactured in H-13 tool steel and heat-treated to obtain the desired condition of high mechanical resistances at high temperature to withstand to the extrusion pressure, and good wear resistance to ensure a long die life in relation to the productivity. Taking as an example a direct extrusion process, the extrusion die will be placed in the extrusion press along with several supporting tools, also made from hardened tool steel. These tools are generally known as backers, bolsters and sub-bolsters (Fig.15) and they provide support for the die during the extrusion process, thus contributing to load resistances and to the improvement of tolerance controls and extrusion speeds [2-3, 58].

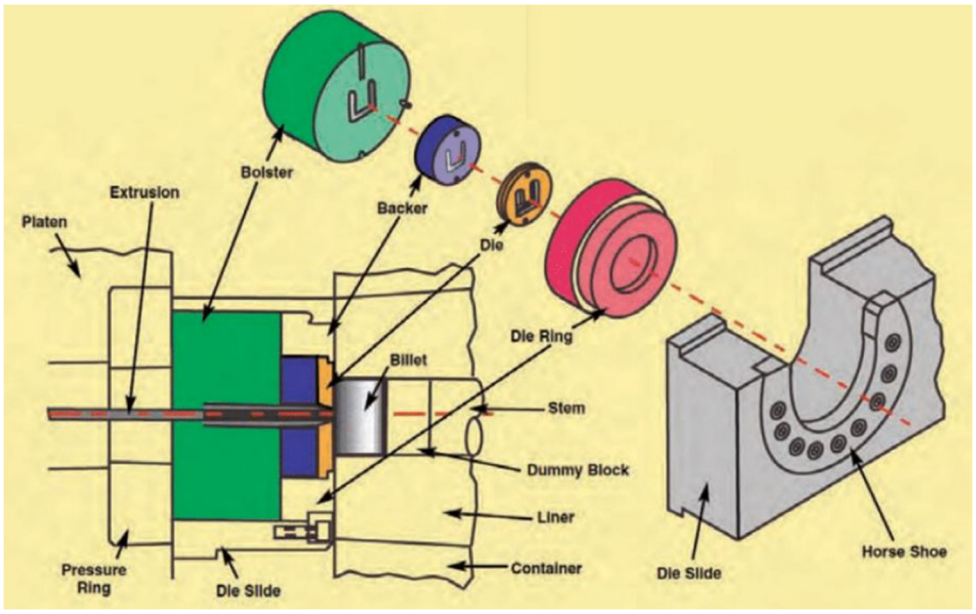

Fig. 15 Tooling set of the direct extrusion process [3]

Solid dies: Solid dies are used to produce profiles that do not contain any voids. Various styles of solid dies are used, depending on the equipment and manufacturing philosophy of the extruder in relation to the shape complexity of the profile [58]. The simplest solid die is the flat-face die that has a totally flat face with openings that exactly match the shape of the extrusion. The material from the aluminum billet goes directly through these openings. Instead, the pocket die has a cavity built into the front of the final die opening that is slightly larger than the width of the profile. This cavity helps the control of the metal flow, thus improving the welding of subsequent billets during the continuous extrusion. A feeder die (or weld plate) has a separate feeder plate that gets pinned or bolted onto the front of the final die. Like the pocket die, it allows for continuous extrusion. The feeder can help the control contour or the spread of the aluminum to different areas of the die. Another advantage of a feeder die is that it prevents direct contact between the billet and the face of the die during billet deformation. Fig. 16 shows an example of both flat-face die and a pocket die used to realize U-shaped profiles. Instead, Fig.17 presents an example of complex feeder die to realize a heat sink. In this case, the feeder allows a strict control of the material flow to satisfy high requirements in terms of geometrical tolerances.

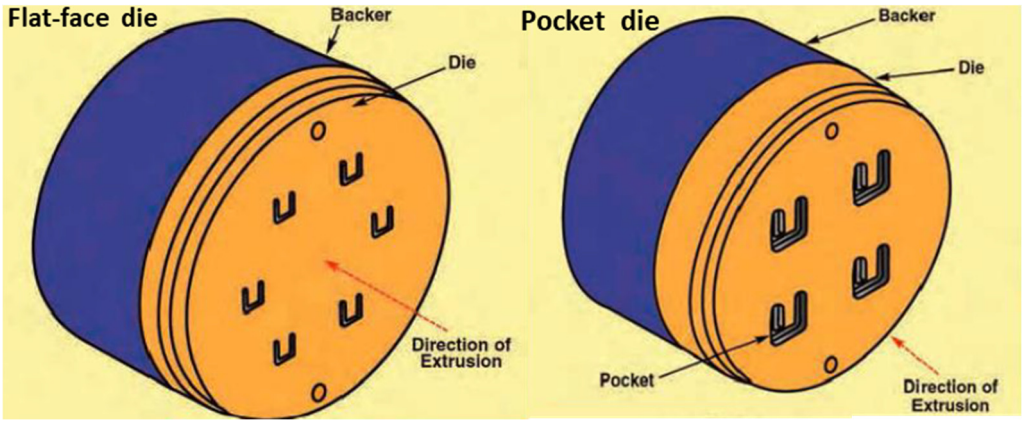

Fig. 16 Types of solid dies: Flat-face die on the left, Pocket die on the right [3]

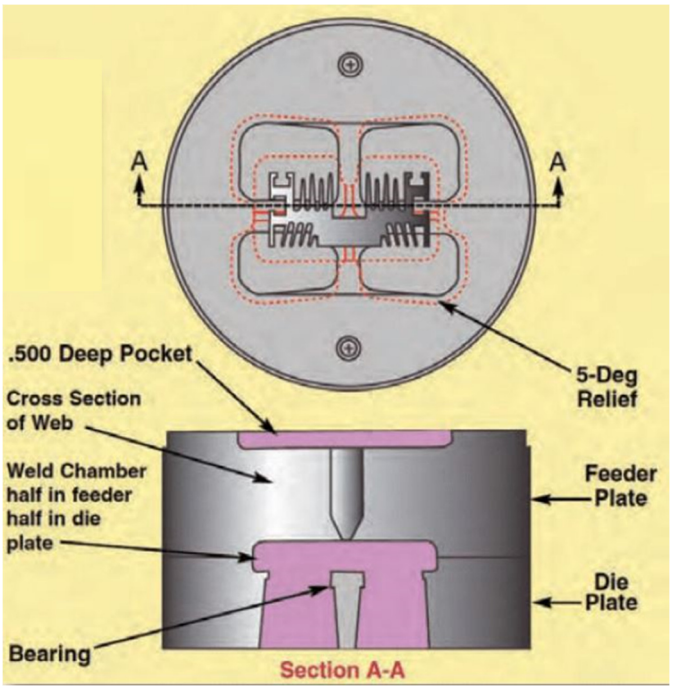

Fig. 17 Example of feeder die [3]

Hollow and Semi-Hollow dies: Hollow dies produce profiles with one or more voids. Examples of hollow profiles are simple tubes or profiles with many detailed openings (Fig. 2). The most common type of hollow die is the porthole die, which consists of a mandrel and cap section (Fig. 18). The mandrel, also known as the core, generates the internal features of the profile. The mandrel has two or more ports; where the material flow separates into each port and rejoins in the weld chamber prior to enter to the bearings zones. The ports are separated by webs, also known as legs, which support the core or mandrel section. The cap (or die), which creates the external features of the profile, is assembled with the mandrel. The backer, when used, provides critical tool support and is in direct contact with the exit side of the cap. Also for hollow dies, the shape complexity of the openings allows controlling the material flow in the mandrel and in the cap according to the quality standards required for the extrudate. Similar to a hollow shape, a semi-hollow profile has a void or voids, but they are partially enclosed, however, a solid shape also may partially enclose a void, and the distinction may not be obvious. The semi-hollow classification derives from a comparison between the area of the partially enclosed void and the mathematical square of the size of the gap (called tongue ratio). Depending on the tongue ratio semi-hollow dies can be constructed as flat, recessed pocket, weld-plate, or porthole design, with a prevalence of the latter.

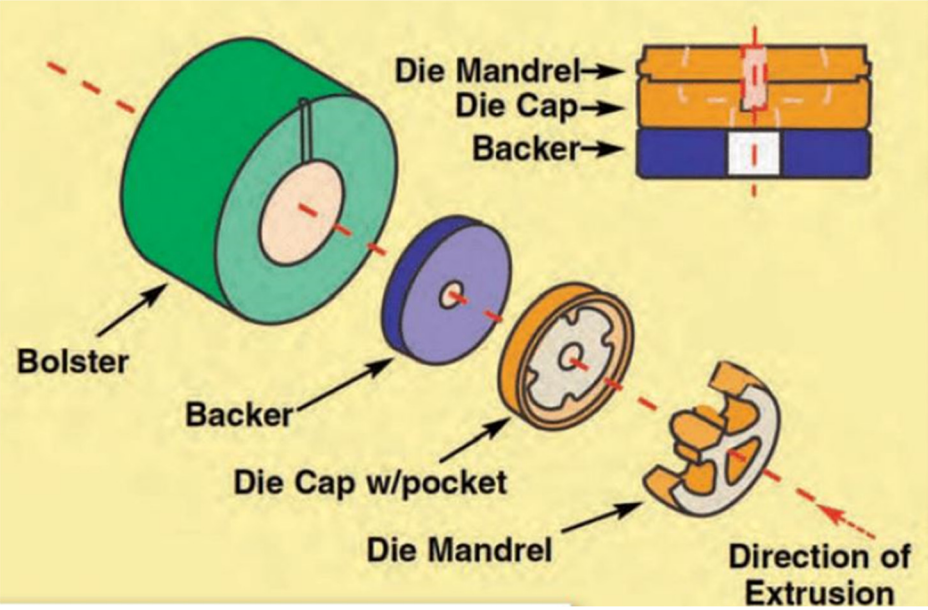

Fig. 18 Schematization of tooling set for hollow profile ("Pancake" hollow die) [3]

Overall, failure to utilize custom tooling when appropriate could result in excessive die deflection, breakage, and/or an inability to meet tight dimensional tolerances. Notably, if well designed, the life cycle of an extrusion die is generally determined by the wear of the bearing. As previously discussed, the bearings zones are the surfaces of the extruding aperture where the profile obtains its final shape. The bearings, therefore, are the primary determinant of control and finish of the profile. Any deterioration of the bearings (considering the surface finish required) will lead to premature failure of the die. One of the most applied methods to extent the bearings life and consequently the die life is nitriding [15]. Nitriding is heat-treat process that makes the bearing surfaces extremely hard, thus increasing their wear resistance. If monitored properly, this process can be repeated several times before a new die needs to be made.

3 State-of-the-art on thermal process control and charge –skin prediction

The brief overview reported in the previously chapter about the fundamentals of the hot extrusion process evidences the large role of the temperature field in terms of material flow, loads and profile quality. In addition, it was noticed how the charge welds and the billet skin contamination result intrinsic defect of the process, since their formation are the consequence of the nature of the process. However, the experimental assessment of these defect is quite hard and very expensive, making their numerical evaluation of strong interest. Therefore, in the chapter 3, the state of art of the hot extrusion process will be presented, focused on the temperature control and monitoring and on the experimental-numerical assessment of the defects evolution.

3.1 Liquid nitrogen cooling

As reported in a number of works [9,12, 59-60], during extrusion the profile exit temperature increases as a result of the great amount of both friction energy at the billet/tool interface and billet deformation energy converted into heat. In addition to that, if the ram speed or the extrusion ratio increase, the temperature rises even further, potentially leading to detrimental surface defects as well as to the reduction of the die life [24-26, 61]. With the aim of achieving maximum production rates without giving up the profile quality, optimal working conditions have to be identified in narrow

processing windows [2, 9, 62]. In the recent years, many extrusion companies focused their attention on the process thermal field evolution by installing on their presses pyrometers for the contactless monitoring of the billet and of the profile temperatures along the whole production chain. By analyzing the data acquired through pyrometers, many companies realized that many defects are related to excessively high exit temperature thus limiting the production rates. In this context, many research activities are focused on the numerical investigation and prediction of the thermal field during the extrusion process leading to an evolution over the years of the numerical tools and methodologies to gain sufficient accurate solving capabilities [63-66]. In 2010, L. Donati et al. [64] compared six different FEM codes for the extrusion process of two overlapped AA6082 U-shape profiles: one with fully supported opening, the other with partially supported opening. The experimental-numerical comparison showed a good codes prediction in terms of thermal field and extrusion load. From 2011 to 2012, N. Biba et al. [65-66] tested the potentiality of the software Qform-Extrusion taking into account the influence of the die deformation on the material flow through the die. The comparison with different experimental case studies showed that the die deformation causes the alteration of the bearing area and the friction condition, thus influencing the profile temperature and the material flow.

A possible strategy to limit the exit profile temperature consists of reducing the billet preheating temperature; however, this could have a negative impact on plastic formability and die life by implying higher press loads and mechanical stresses [60]. Another option consists of using a billet-temperature tapered along its axis and an air-cooled container as a first method to obtain the so-called isothermal extrusion [1-2, 67-68]. The billet with a tapered thermal field holds a lower temperature at the contact with the ram and a higher temperature at the entrance of the die (Fig. 19). In this way, the billet material increases its temperature due to the friction and the deformation energy within the container and, only at the entrance of the die, it reaches the temperature to promote the proper die filling. The air-cooled container can support the control of the billet thermal field during the ram stroke. The aim of the isothermal extrusion is the selection and the control of the proper exit profile temperature that shall be constant throughout the production process [67-69]. For example, Farjad Bastani et alii [69] analyzed the isothermal extrusion process of aluminum by the use of the 3D FE software Altair HyperXtrude and the 2D finite element software ALMA2π. They provided the best combination of process parameters and the so called “Isothermal maps” for each phase of the press cycle. As an alternative, or complementary to the first approach, isothermal extrusion can be operated by adjusting ram speed on a retroactive temperature feedback from the profile at the exit [67-69]. Specifically, the speed of the ram is increased or decreased as a function of the temperature monitored by the pyrometer on the profile. However, even if the isothermal extrusion can provide a valid solution to avoid surface defects, the need for increasing production rate can be hardly met by an approach practically based on speed reduction.

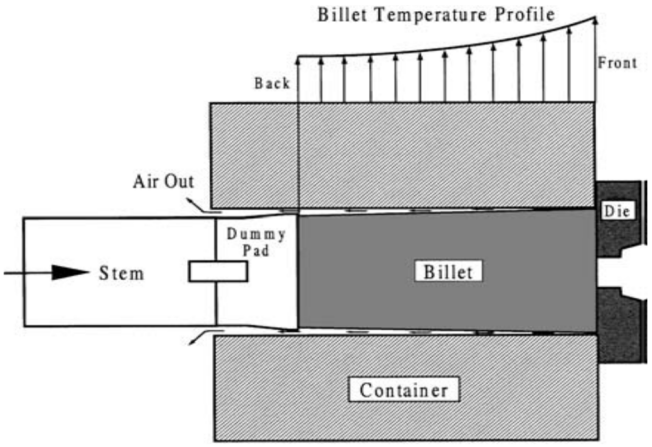

Fig. 19 An example of tapered billet thermal field [1]

So, the cooling of the profile nearby the bearing zones – where the profile reaches its final shape and where the higher temperature values and gradients occur – has become mandatory in achieving performance targets, which promoted extensive research on this subject, especially in the last decade [70-71]. The main advantages of dissipating the excessive heat generated in the die are related to the possibility of increasing the production rates and the improvement of the surface quality with a minimal increase of the extrusion force by shifting the thermal conduction path from the forming zone to the cooling source.

Recently, in industry, the use of nitrogen cooling has become a widely adopted solution to address most of the aforementioned issues: the cooling channels are typically manufactured in the tooling set near the exit of the profile, in order to perform heat removal only at the locations where it is required. Previously, gaseous nitrogen was employed as the coolant for the tooling set, but liquid nitrogen has then replaced it, owing to its higher cooling capacity [72-73]. Fig. 20 shows an example of industrial setting of the extrusion process with nitrogen cooling. The industrial practice provides the manufacture of the cooling channel in the backer, a tool that is not in involved in the aluminum deformation, but it is positioned in contact with the exit die surface to withstand to high-pressure loads imposed by the aluminum under deformation (see section 2.6). Notably, the temperature drop is localized only nearby the exit profile, not involving the whole billet in deformation even where it is not necessary or backfired (for example at the entrance of the die). The cooling channel surrounds the exit of the profile, while transferring holes are made in the die to connect the path of the nitrogen with the exit of the profile from the bearing zones. The liquid nitrogen subtracts heat in the tooling set and indirectly in the profile surface, then, at the exit of the cooling path, the hot nitrogen in a gaseous form surrounds the exit profile, thus limiting the profile oxidation. The temperatures in the die and in the profile should not reduce excessively to avoid the die damaging for excessive thermal gradient as well as to guarantee the exit of the profile.

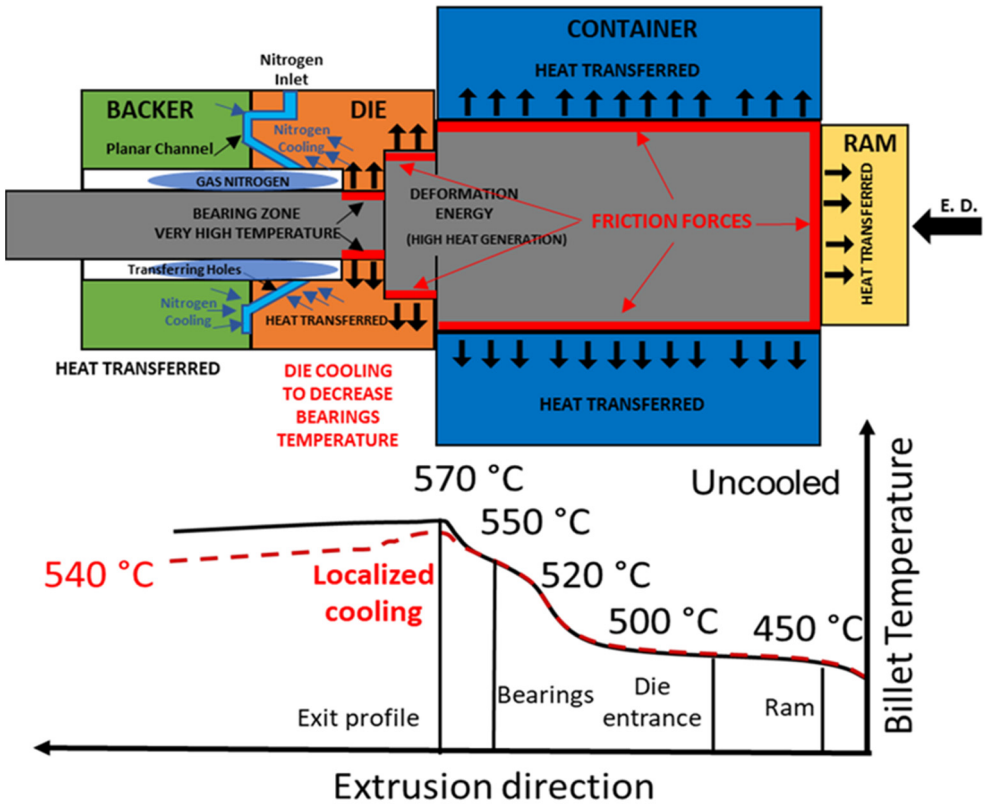

Fig. 20 Schematic of hot-extrusion process with nitrogen cooling and temperature history

In this context, the available literature includes some studies that focus on the cooling potential of liquid-nitrogen systems. These works show that it is possible to obtain a remarkably higher heat removal in a wide range of extrusion applications with respect to water or air cooling [72-76], doubling in some cases the extrusion speed. For instance, Stratton [73] proposed an overview of selected industrial techniques based on nitrogen cooling of the extrusion process, providing evidence of the specific benefits from using liquid nitrogen to cool the die. In this context, several papers on gas and liquid nitrogen applications aimed at increase dies performances were presented at the International Aluminium Extrusion Technology (ET) seminars [74-76]. In a different study, Donati et alii [77] analyzed the effect of liquid nitrogen in the extrusion of hollow profiles, recording a maximum temperature decrease of 80 °C in the bearing zones. In dedicated studies, Hölker et al. [78], Hölker and Erman Tekkaya [79] and Reggiani and Todaro [80] assessed and evaluated the possibility to increase the cooling efficiency by manufacturing a conformal channel around the bearing zones to better conveying the cooling in the hottest regions by additive SLM (Selective Laser Melting) technology.

All the above mentioned works mainly focus on design and manufacturing of cooling channels, whereas not so many studies are available in literature with regard to the physics involved in nitrogen cooling of extruded parts and the development of models capable of predicting its performance. Despite the increased industrial use of liquid nitrogen cooling in the aluminum extrusion context, a comprehensive methodological investigation of its effect on the thermal process efficiency is still limited. Cooling channels are usually manufactured according to the designer's experience, thus making extremely challenging the managing of the many variables involved, such as those of the channel geometry and position, of the coolant properties and of the cooling parameters.

The FE modeling of cooling channels has been reported in literature but mainly for plastic injection molding and die casting applications [81-82]. In addition, a consistent part of the published work used

water as cooling media flowing in the channels or made use of simplified convective coefficients applied to the channels' walls.

In order to fill the outlined literature gap, aim of the present PhD project is to model, for the first time, a hot extrusion process accounting for liquid nitrogen cooling. The numerical modelling has been performed by means of FE analyses that were validated against industrial experimental data. The global aim of the work is to offer to the industrial scenery a more faithful model of the extrusion cooled with liquid nitrogen in order to better finalize the process optimization.

3.2 Experimental-Numerical assessment of the charge welds and billet skin evolution

As discussed in section 2.5, the charge welds and the billet skin contamination strongly reduce the mechanical properties of the extrudate so that they must be discarded. Many experimental works have been done to investigate charge welds evolution and metal flow in complex dies, focused on the influence of the charge welds on the quality and strength of the produced profiles. For instance, Loukus et al. [83] studied an A-pillar made of AA6082-T4 alloy contaminated by charge welds by means of tensile testing and microstructural analyses: tensile specimens were prepared with the weld located at 0°, 45°, and 90° to the tensile axis. Comparison of failure strains and fracture modes revealed that weld regions are less ductile than the no-weld regions. Zhu and Young [84] investigated the effects of charge welds on the strength of 6063-T5 and 6061-T6 heat-treated aluminum alloy columns with respect to the section slenderness on simple square and round profiles. The longitudinal tensile tests shown that the transverse welds reduce the 0.2% proof stress of aluminum alloy for up to 68%. Bingöl and Keskin [85] discussed the effect of billet temperature and ram speed on the structure morphology of the charge welds, while Zhang et al. [56] reported oxide distribution and microstructure analyses in the charge welding zones obtained by SEM and optical microscopy for a single cross section of the profile. Concerning skin contamination, the defect evolution has been investigated mainly by experiments [57, 86-88]. For instance, Kim et alii [57] examined the effects of some direct extrusion parameters (friction condition, temperature, ram stroke) on the flow behavior of the billet skin layer in a porthole die for direct extrusion. It was found that the flow of the surface layer could be divided into an inward flow along the back face of the billet and a forward flow along the boundary of the dead zone. The container friction strongly influences the balance between the two flows, while the extrusion temperature had little influence on the flow pattern. Jowett et alii [87] verified that the quantity of metal containing skin contamination was about the 14 % for the majority of the analyzed profiles. In addition, skin defect tends to flow earlier at the top of the billet due to uneven upset. This means that multi-holes dies could show more advanced flow of cored material in the upper holes.

Nevertheless, since the experimental assessment of the scrap length is a time and cost consuming activity, the determination of the zone to be discarded in industrial everyday practice for weld contamination is still performed by intuition, analogy with similar profile shapes, and experience. For example, as guideline in function of the extrusion ratio ER, 1000 mm for ER<30, 2000 mm for 30<ER<40, and 3000 mm for ER>40 is scrapped.

In this scenario, some simplified theoretical formulations have been proposed to evaluate the scrap extent estimation [87-88]. About the charge welds extent, the first formulation proposed by Saha [88] can be expressed as follow:

$$d = \frac{V_1 + V_2}{A_e * n} \tag{6}$$

where the charge weld extent (d) has been related to the volume of material present in the die ports V_1, to the volume of material present in the welding chambers V_2, to the exit profile section area A_e and to the number of the profile openings in the die n. Main limit of such equation is the hypothesis of a constant material flow in all die ports and chambers, while it is commonly known that friction deeply affect material flow thus generating both fast and dead metal zones. Thereby, the second formulation [87] involves a corrective factor of 1.5 to modify the first one and to better match the experimental evidence. To the best author's knowledge, only one empirical formula has been reported in literature by Jowett et al. [87] for skin contamination length prediction:

$$s = \frac{(0.14*V_b - 0.75*(V_1+V_2) - V_{rest})}{A_e*n} \quad (7)$$

where V_b and V_{rest} are the billet and the billet rest volume respectively, and the other terms follow the definitions used in Eq. 6.

These theoretical formulations can offer a fast estimation of the scrap extent, but the comparison with a lot of experimental data highlighted their limits. Therefore, the implementation of numerical models to predict the extrusion defects by means of FE codes has become a mandatory activity in order to control and minimize the extent of the profile to be discarded at the design stage of the process. In terms of charge welds, it is reported in literature that the way of interaction and replacement of the old-new billet is primarily influenced and driven by the die geometry [89–92]. Other process parameters such as profile alloy, billet pre-heating temperature, extrusion speed, and friction level have been reported to be negligible factors in the definition of the charge weld onset and extension [92–96]. Reggiani et alii [97] showed the potentiality of the ALE numerical codes in terms of charge welds prediction reporting the experimental-numerical comparison for four industrial profiles. In terms of skin prediction, some works were proposed but concerning 2D simulations of simplified case studies [98-100]. Instead, Lou et alii [101] tried to compare the outputs of numerical simulations with experimental data on an extruded profile with a complex geometry, however, the comparison was made on the billet discard and not on the evolution within the profile.

In this context, this PhD projects will be focused on the testing and validation of reliable numerical models for the prediction of the defect onset and evolution. Although the several studies reported in literature about the defects prediction, further investigations are still needed in order to validate the accuracy of FEM codes against industrial profiles of variable geometries, material properties and process parameters, especially regarding to the skin contamination. In addition, the experimental campaigns, that will be deeply discussed in the chapter 6, will evidence the great limits of the industrial practice and the theoretical approaches compared to the numerical capabilities.

4 Experimental assessment of the hot extrusion process using liquid nitrogen cooled die

In this chapter, three different experimental campaigns will be analyzed: the Benchmark 2011 case study taken from the literature [77], the Multi-Die case study and the Profilati case study. The first one is assumed as reference to know how to set an experimental campaign for the monitoring of the thermal gradient during the hot extrusion process among an industrial production line. The temperature history of the process was acquired by several thermocouples inserted on the tooling-set and the process was carried out to evaluate the nitrogen cooling efficiency at different percentage of nitrogen flow rate. The Multi-Die case study was the first experimental campaign carried out during this PhD project at a laboratory press, where it was analyzed the potentiality of conformal cooling channel manufactured by means of an additive technology. Then, a comprehensive experimental

campaign for both the temperature monitoring of the process and for the assessment of the extrusion defects was carried out with the Profilati case study, analyzing a complex industrial hollow profile. The collected data and the experimental evidence will be deeply discussed, then, the results in terms of temperatures and extrusion loads will be used as comparison for the validation of the implemented FE models (see, chapter 5).

4.1 Benchmark 2011 case study [77]

4.1.1 Experimental Setting

In these sections they will be deeply analyzed the methods for temperatures and loads monitoring and the obtained results at different cooling conditions taken from the Benchmark 2011 case study [77]. In Fig. 21 the industrial hollow profile selected for the experimental campaign is shown. The tooling set was composed by three components: the mandrel, the die and the backer (Fig. 22). In the mandrel, the aluminum flow was divided by five portholes, then, it rejoined in the welding chamber, where the aluminum was constrained to flow in the cavity between the mandrel and the die (Fig. 24), thus obtaining the final hollow profile in the bearing zones.

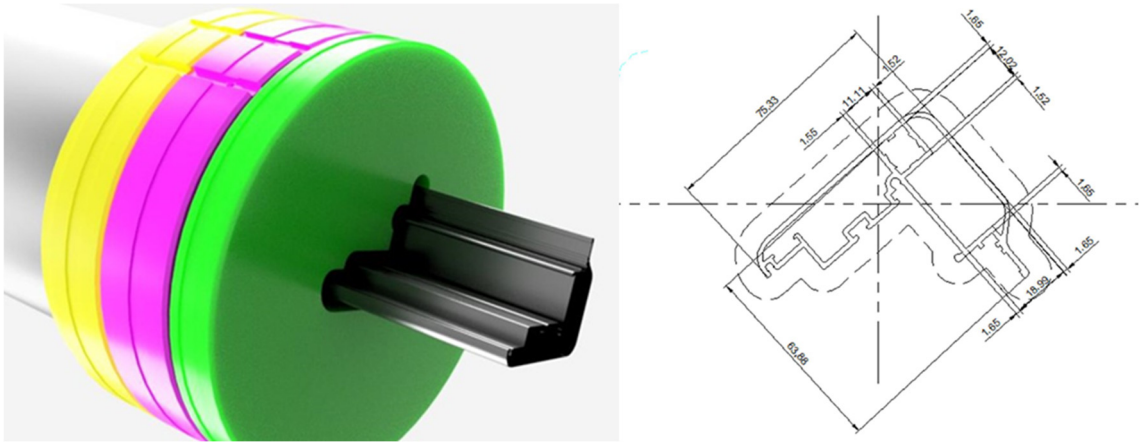

Fig. 21 The industrial hollow profile selected for the experimental campaign

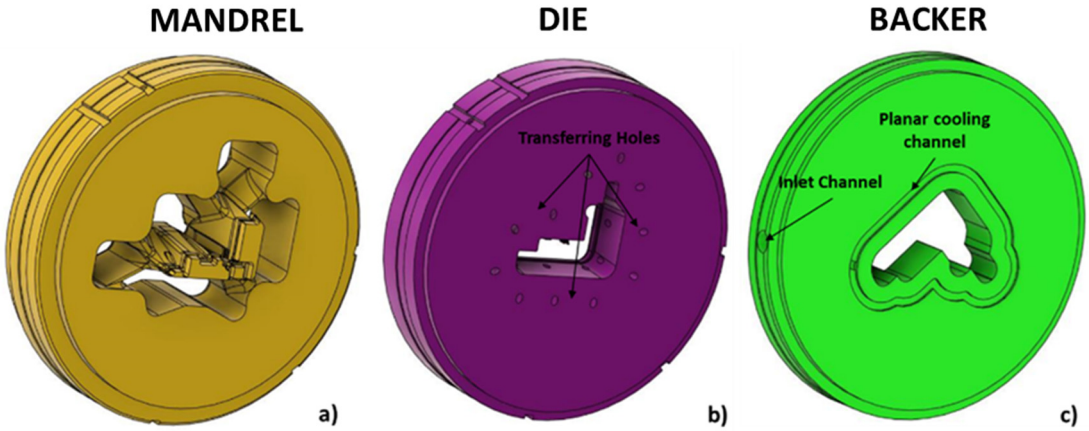

Fig. 22 The Tooling Set: a) The Mandrel; b) The Die; c) The Backer

In the backer surface in contact with the die (at 37 mm far from the bearing zones), a planar cooling channel was realized with a rectangular cross section (6mm x2.1mm, width per depth), as shown in the Figs. 22c and 24. Eleven transferring holes were manufactured in the die (circular section of 5

mm diameter) to invest the exit profile with a gas nitrogen atmosphere in order to reduce the profile oxidation.

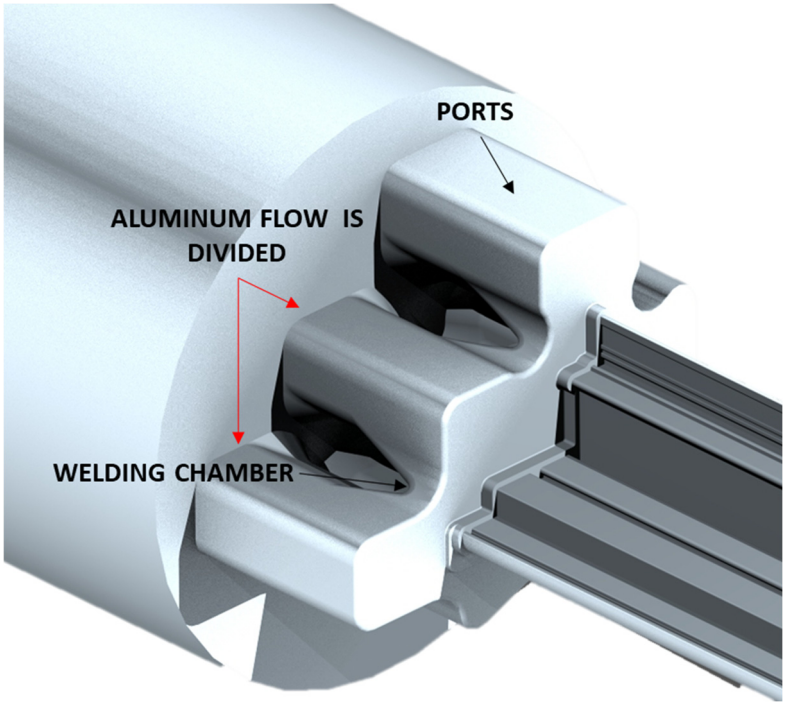

Fig. 23 Material Flow within the portholes die

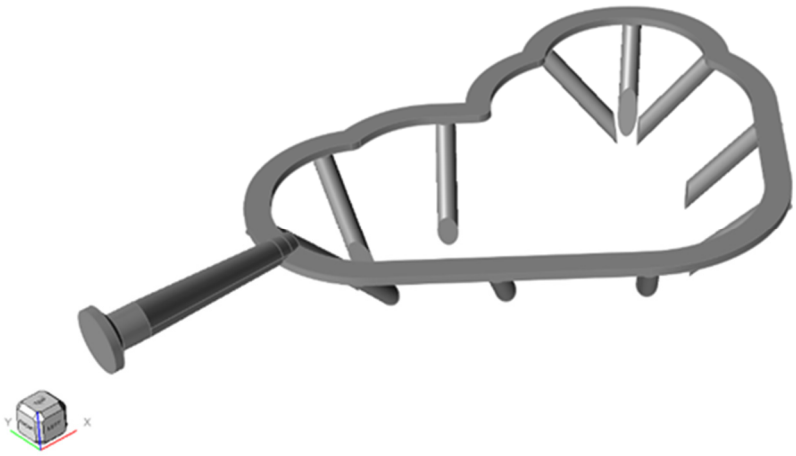

Fig. 24 Computer Aided Design (CAD) drawing of the cooling channel.

The thermal field in the tooling set was monitored by means of five thermocouples K-type (Fig. 25): three in the die (T1, T3 and T5) are positioned at about 15 mm far from the bearing zones to monitor the temperature where the highest heat generation is obtained; two in the mandrel (T2 and T4) nearby the welding chamber where high deformations occur. The exit profile temperature was recorded by a pyrometer positioned at 1625 mm far from the backer face.

Ten cylindrical billets in AA6060 (diameter of 205 mm and length of 790 mm) were extruded with the extrusion speed of 2.71 mm/s in different condition of nitrogen flow rate. A conical taper heating of 499-445°C (front-back) was applied in the billet along its axis. A temperature of 427°C and 413°C was set for container and ram respectively, while a die pre-heating of 490°C was selected.

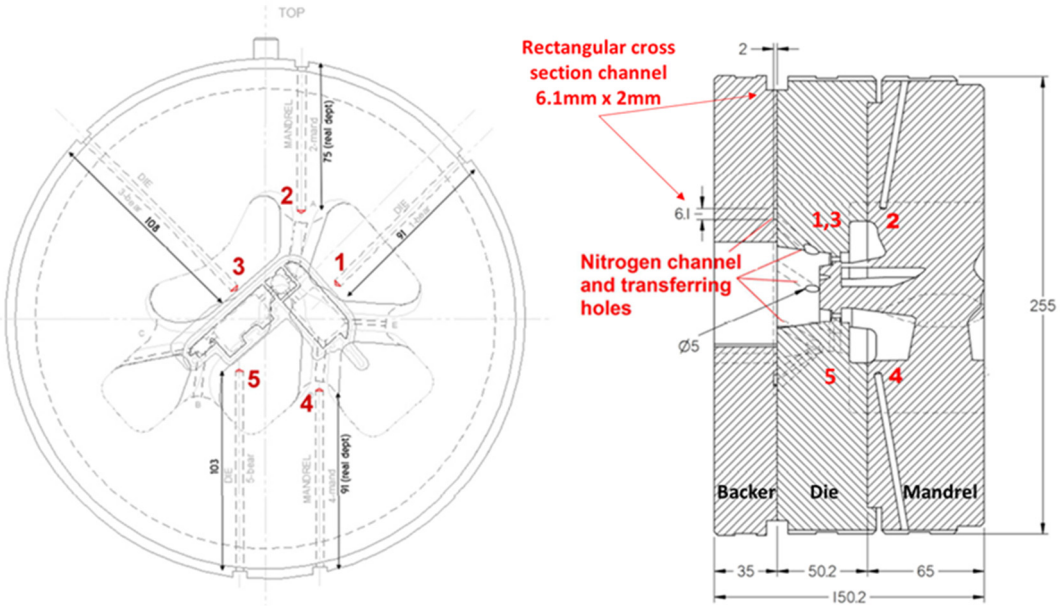

Fig. 25 Thermocouples location.

4.1.2 Experimental Results

The Fig. 26 shows the thermal history of the extrusion process acquired by the thermocouples and the pyrometer. During the initial 500 seconds the thermocouples were connected to the system and the tooling set positioned into the press. The process setting was indicated with a negative time in order to position the beginning of the first extrusion to zero time. The first billet was extruded at reduced ram speed to engage the profile into the puller and to homogenize the thermal field in the tooling set. It is clear in the figure the stop for connecting the puller at about 80s, resulting in temperatures decrease both in the die and in the profile caused by the heat transfer with the press and the air.

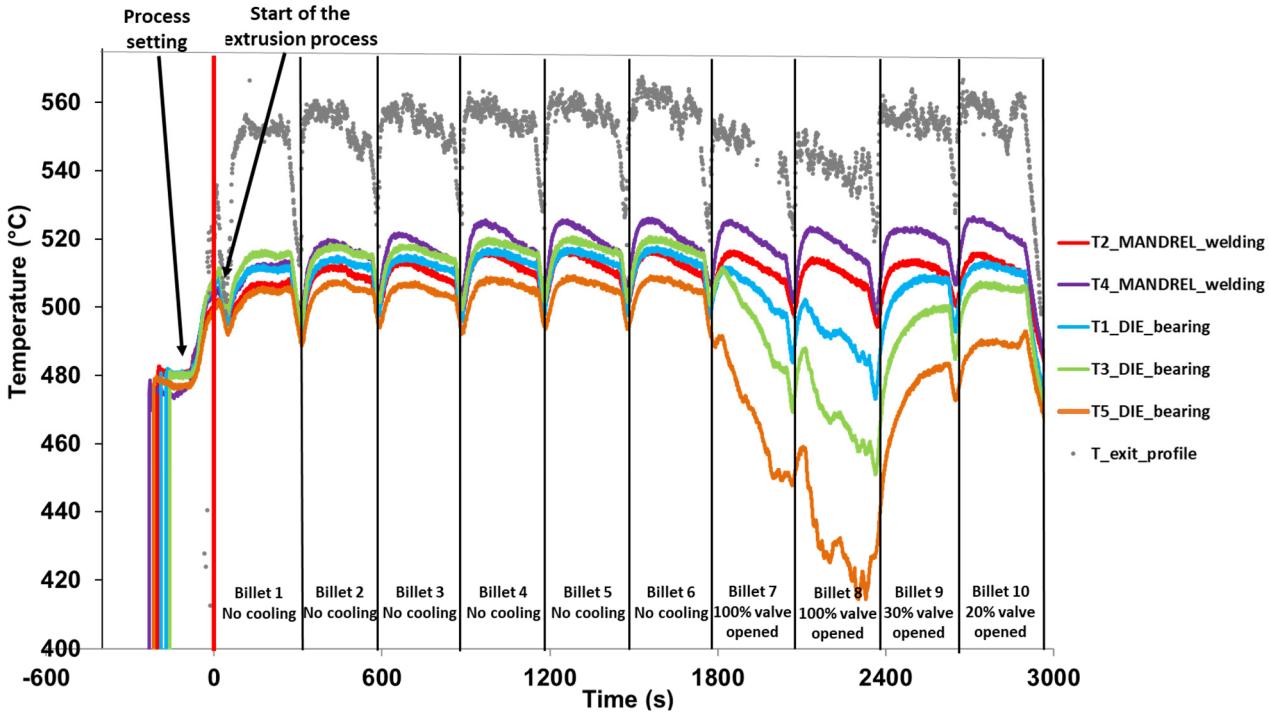

Fig. 26 Temperature history of the data registered by the thermocouples and the pyrometer during the experimental trials [77]

The subsequent five billets were extruded at the selected ram speed of 2.71 mm/s and without nitrogen cooling to reach the steady state uncooled condition as a point of comparison to evaluate the cooling efficiency. Indeed, from billet 1 to 4 a constant increase of the temperatures was registered both for the die (510 to 515°C for T1) and for the profile (550 to 560°C), while from billet 4 the process can be considered stationary. During each ram stroke, profile temperature initially increased then decreased at the end of the stroke as well as in the tooling set, where the temperatures rose to a peak during the extrusion then dropped down during the billet change for the heat exchange with the air and the colder material of the press.

From billet 4 the process can be considered stationary, and it is possible to notice that the maximum temperature, as expected, was in the profile with values higher of 40°C respect to the die temperatures. Indeed, analyzing the extrusion of billet 6, an exit profile temperature of 560 °C was obtained. In the die, the thermocouples T1 and T3 recorded a maximum temperature of 520 °C, while T5 registered a value of 510 °C. In the mandrel, temperatures of 510 °C and 525 °C was found for T2 and T4 respectively, confirming the great heat generation occurred in the welding chamber due to the material under deformation.

Before extruding billet 7, the liquid nitrogen valve was completely opened and a marked reduction of die temperature was immediately visible. The channel design promoted the cooling in the bottom part of the die, obtaining the most drop of temperature in T5 (from 510°C to 450 °C), significant cooling in T3 (from 510 °C to 475 °C) and less effective in T1 (from 510 °C to 490 °C). The drop of temperatures in the mandrel was negligible, as expected, due to the great distance of the cooling channel from the welding chamber.

Billet 8 was extruded with the same condition of trial 7 and, despite of a slight initial rise of temperatures at the beginning of the stroke, temperatures dropped down to 430°, 460° and 480°C in T5, T3 and T1 respectively. As consequence of die temperature decreasing, also profile temperature decreased, recording a maximum drop of 20°C during the trial 8 (from 560°C to 540°C). The localized cooling in the die did not involve a significantly increase of the extrusion load obtaining a value of 19.9 MN against the maximum of 19.1 MN registered without cooling.

In the ninth extrusion, temperatures immediately rose again to higher values due to the decrease of nitrogen flow rate till 30%, obtaining in thermocouple T5 a temperature of 480°C against the 430°C reached with the maximum flow rate. Similarly, the exit profile temperature increased of about 10°C. In the last extrusion, a thermal condition comparable to the uncooled one was obtained using the 20% of nitrogen flow rate.

In this experimental campaign, the liquid nitrogen cooling showed its potentiality in terms of heat removal rate with only a slightly increase of extrusion load. Moreover, the obtained results evidenced the limit of the channel design in terms of cooling balance, recording a great gradient of temperature around the bearings zones that can reduce the die life as well as lead to profile distortion for inhomogeneous cooling. Indeed, the three thermocouples in the die recorded a great difference in terms of drop of temperatures, although they recorded about the same temperature without the cooling. The use of FEM for the design of the cooling channel could provide a support to obtain the best cooling solution during the design phase, thus saving time and costs for inefficient solutions.

4.2 Conformal Cooling Channel: Multi-die case study

4.2.1 Multi-die conceptualization and manufacturing

As evidenced in the chapter 3, one limitation of the current industrial practice could be that cooling channels are manufactured only by means of convectional machining techniques thus deeply constrain the cooling channels design. Moreover, channels are usually obtained by milling the backer (also named third plate), thus limiting the cooling efficiency on the bearings where the highest temperatures are reached. In this contest, the additive manufacturing (AM) technologies provide the opportunity of realizing conformal channels inside the die with a greater design freedom, following the shape of the bearings and of the die [78,102-104]. Dies can be separated in two parts in order to encompass the high manufacturing costs of additive manufacturing: a small insert made by AM, where bearings and the cooling channel are realized; a housing die made by conventional technologies which contains the insert and the adduction channel for the liquid nitrogen. In this way, the manufacturing cost of the die can be deeply reduced and, once the die has worn out, only the insert will need to be replaced, thus avoiding the re-manufacturing of the whole extrusion die.

In the project, a round bar of 10 mm in diameter was extruded. The die was split into two H13 steel parts (Fig.27): an external steel housing (75 mm in outer diameter and 76.5 mm in axial length), designed and manufactured by the die maker Almax Mori Srl (TN) Italy, and the insert in additive manufacturing (25 mm of diameter and 20 mm of axial length) produced at University of Bologna. The feeding chamber (30 mm in diameter and 20 mm in axial length) connected the material flow to the bearings zones of the insert with a constant length of 5 mm.

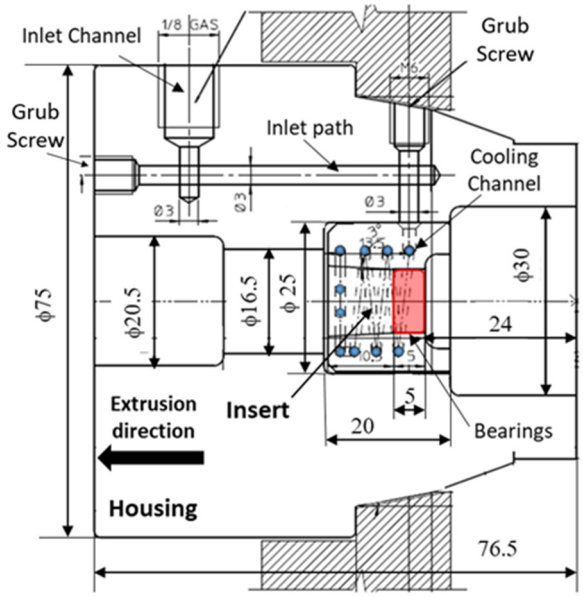

Fig. 27 Die concept design

It was selected a helicoidally cooling channel that surrounded the bearings zones in the extrusion direction with the aim to obtain a targeted and homogeneous cooling. Moreover, the geometrical parameters of the helicoid had to be chosen ensuring the insert functionality, the printing feasibility as well as the cooling efficiency [105]. As example (Fig. 28), small helix diameter and pitch imply a low distance between the channel and the bearings achieving a higher cooling effect. However, the mechanical resistance of the insert must be ensured not only during the printing process, but also during the hot extrusion. In a similar way, a big channel diameter reduces the pressure drop and promotes the liquid nitrogen flow at the expense of the resistance of the insert. At the end of the

helicoid, a toroidal channel with radial exit holes was picked to invest the exit profile with gaseous nitrogen.

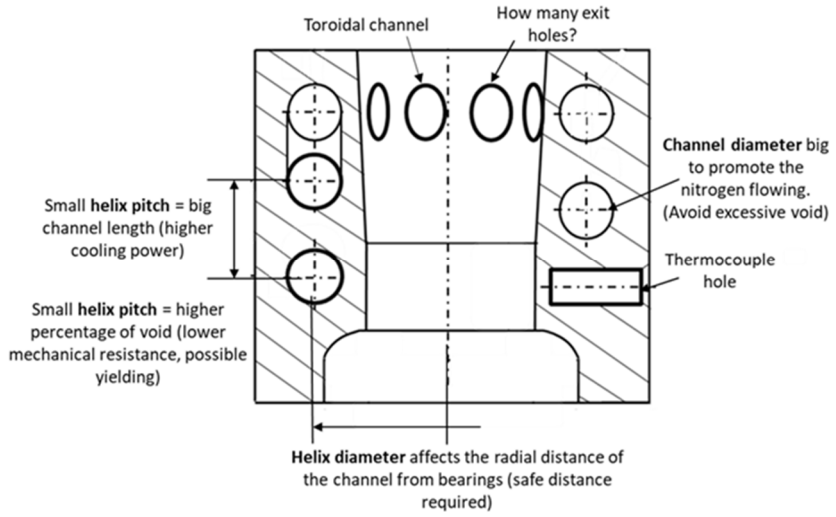

Fig. 28 Cooling Channel Concept Design

Figs. 29 a, b show the final insert design used in the experimental trials with 3 mm of channel diameter, 16 mm of helix diameter, 5 mm of helix pitch and 8 exit radial holes. In addition, one thermocouple hole was planned to monitor the temperature nearby the bearings during the tests.

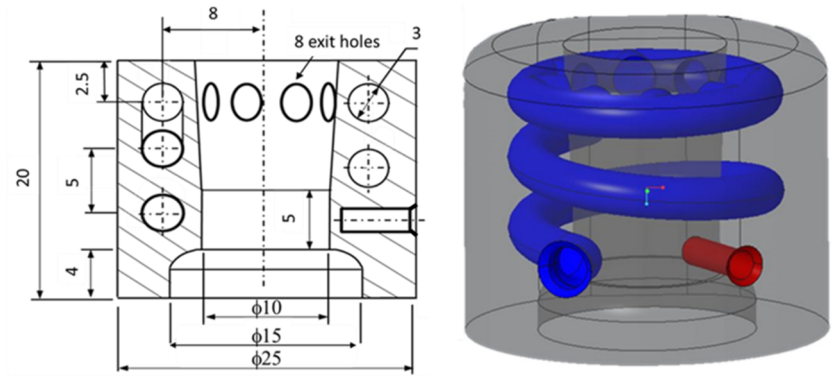

a) b)

Fig. 29 Final insert design: a) section view, b) 3D CAD model

The insert was printed with the Selective Laser Melting (SLM) technology on a SISMA Industries MYSINT 100 RM machine located at University of Bologna laboratories. The selection of the proper printing parameters allowed the achievement of a dense structure also with the H13 tool steel [80,102, 106-107], the most used for the manufacturing of the extrusion dies. The density of the final components (Figs. 30 a, b) was higher than 98% and the printed material evidenced an ultimate tensile strength of the tested specimens of 1600 ± 50MPa. The quality of the inserts was proved by x-ray and microscope analyses as shown in Figs. 30 c, d: x-ray evidenced the absence of detectable cracks within the insert and microstructural analyses confirmed a low amount of porosity as well as the presence of a typical structure of mid-carbon tempered steels.

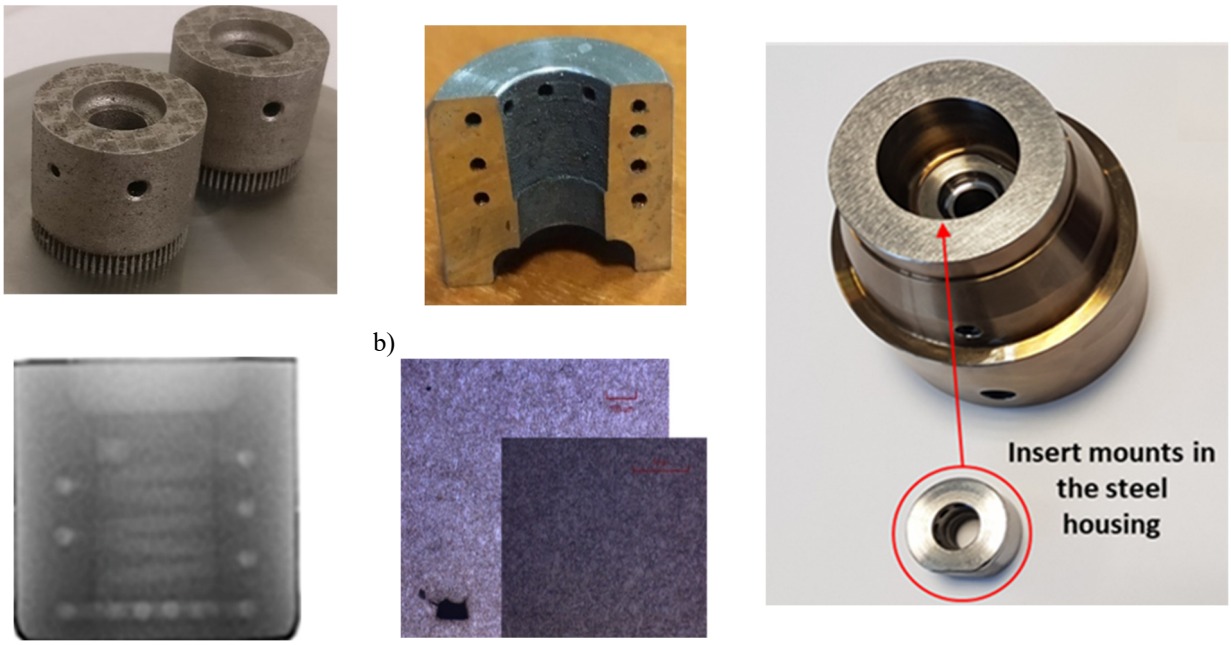

Fig. 30 Printed inserts: a) Inserts on the platform after powder removal; b) visual inspection of the channel section; c) X-rays analysis; d) Microscope analysis; e) Die set before insert assembling

The bearings and the outer insert surfaces were machined with the Electrical Discharge Machining (EDM) process. Actually, the roughness left by the SLM process (Ra= 7 μm) in the bearings zones was not adequate to achieve a good quality of the extrudate surface. Moreover, the outer surface of the insert required strict tolerances for the shrink-fit in the housing (fig. 30e). Finally, the heat treatment was performed to get the required hardness for the extrusion process (45 HRC). In detail, for H13 tool steel it consisted in an austenitization at 1020 °C, gas quenching using forced pressure nitrogen and two tempering (at 550°C and 585 °C, respectively).

4.2.2 The Experimental Trials

Experimental trials were performed on a reduced scale industrial press (2.5MN) at the Alubin plant, Haifa, Israel. The press was equipped with an acquisition system able to record over time the main cylinder oil pressure, the billet stroke, the ram speed and the die temperature through a K-type thermocouple. The experimental setting consisted in the extrusion of several billets made by AA6063 aluminum alloy and ZM21 magnesium alloy, with the purpose of testing the insert functionality as well as the cooling efficiency. Billet length and diameter were 100 mm and 45mm, respectively for both alloys. The liquid nitrogen was stored at about 5 bars in a tank of 230 liters and supplied by a 4m-length pipe. The potentiality of the conformal cooling channel was evaluated by using the 100% of nitrogen flow rate at different extrusion speeds. In Tab.2 are reported the process parameters for the extrusion of both alloys. The preheating temperatures of billet and die as well as the container one were chosen based on the experiences of the extruder (partner of the project) and on the data founded in literature about the selected materials to be extruded [39, 44,108]. The data acquired during the process were the thermocouple temperature of the insert and the extrusion load. The data of the profile temperature recorded by a pyrometer were not reliable, due to the not negligible profile fluctuations and sunlight reflections.

Table 2 Process parameters for the experimental tests

Process Parameters	AA6063	ZM21
Billet Length	100 mm	100 mm

Billet Diameter	45 mm	45 mm
Container Diameter	50 mm	50 mm
Billet Stroke	90 mm	90 mm
Preheated Billet Temperature	450 °C	300 °C
Container Temperature	376 °C	376 °C
Preheated Die Temperature	450 °C	300 °C
Ram speed	2/4.2/6.5 mm/s	4 mm/s
Extrusion Ratio	25	25

- *Testing of AA6063 billets*

Twenty-four billets were extruded: from billet 1 to billet 7 the extrusion process was performed without cooling; from billet 8 to billet 24 the valve of nitrogen was fully opened 100%. In terms of extrusion speed, the first third billets were extruded at low speeds (2 mm/s) with the aim to homogenize the temperatures in the tooling set. From billet 4 to billet 21 the extrusion speed was fixed at 4.2 mm/s, while billets 22 to 24 were processed at 50% higher ram speed (6.5mm/s). In Fig. 31, the monitored parameters history is reported with the thermocouple temperature in red line and the extrusion load in green line.

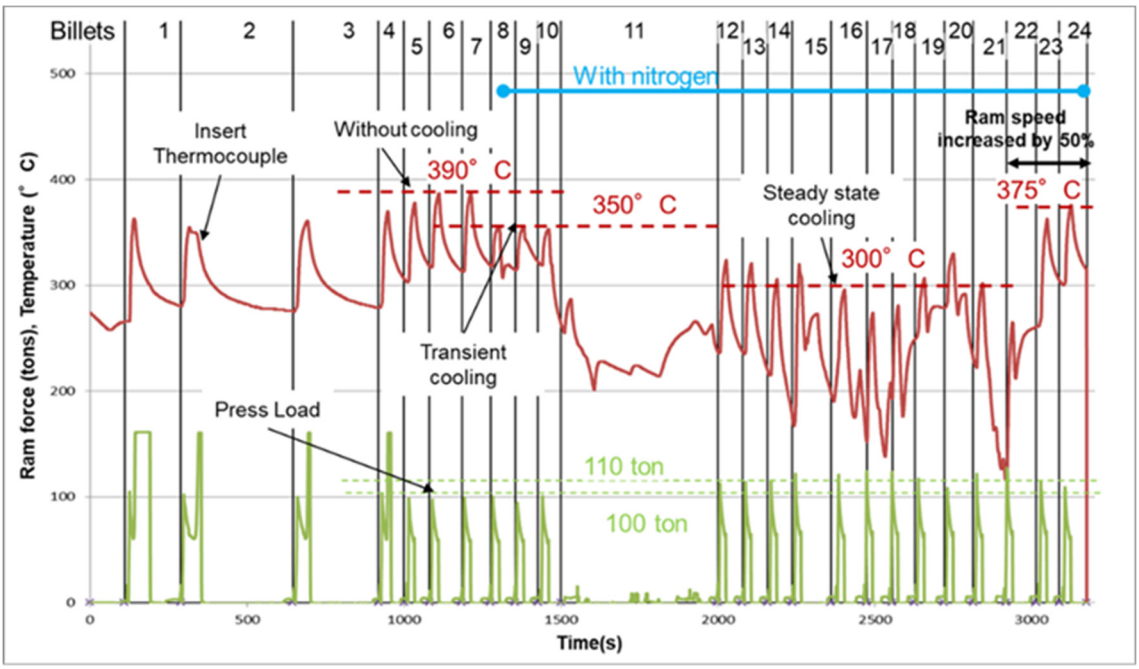

Fig. 31 Temperature history of the data registered by the thermocouples during the experimental trials (AA6063)

During the uncooled process, the sixth and seventh extrusion reached a stationary process condition, showing a maximum thermocouple temperature of 390 °C and a value of 100 tons in terms of extrusion load. At the beginning of the cooled process (billets 8-10), the decrease of temperature was immediately evident and in the order of 40 °C, due to the reduced dimensions of the press and the tooling set compared with the standard industrial scale. However, the presence of high percentage of gaseous nitrogen within the channel was supposed and confirmed during this transitory phase by the lack of ice in the external surface of the connecting pipes. During the eleventh extrusion the dummy

block was changed following the suggestions of the extruder, because a large amount of aluminum from the previous billets was stuck to the dummy block wall with the risk of having some issues with the subsequent extrusions. The long stop of the test to change the dummy block of the ram resulted in a generally cooling of the tooling set. Therefore, starting from billet 12, the pipe rapidly started to be covered by ice, the liquid nitrogen reached the die inlet, and the die temperature showed an average drop of 90°C. In order to limit the decrease in die temperature, from billet 12 the nitrogen valve was manually closed during all billet changes. The manually handling of the nitrogen valve caused the lack of the noticeable stationarity during the cooled process, but an average thermocouple temperature of 300 °C and a minimum of 280 °C were registered respectively. Indeed, in relation to the reduced press scale, the die temperature oscillations are quite big (90-150°C) if compared to the ones achievable in conventional scale processes. The effect was also visible in the uncooled condition where a temperature drop of around 90°C was recorded during the billet exchange. In order to control the extent of the temperature oscillation, in industrial practice nitrogen valve is usually software controlled (opening, closing and level opening 0-100%) thus avoiding the extreme decrement recorded during the extrusion of billets 17 and 21. The potentiality of nitrogen cooling was widely proved when the extrusion speed was increased (billets 22 to 24), obtaining a die temperature 15°C lower than the uncooled one at lower ram speed. In terms of extrusion load, the localized cooling around the bearings did not cause a significant increase of the value, obtaining a maximum of 110 tons against the 100 tons of the uncooled condition. The most important result in terms of functionality was that the insert did not reveal traces of damage or wear at the end of the extrusions.

- *Testing of ZM21 billets*

During the preliminary test, the exit holes of the cooling channel were obstructed by magnesium deposition, as shown in Fig. 32a. The problem was probably related to the small exit angle at the end of the bearings (3°), thus triggering the pick-up defect. It was attempted to open again the channels by grinding, ball blasting and compressed air, but without success. For this reason, an alternative non-conformal cooling channel was used during the test (Fig. 32b) with the aim ensure a cooling effect. In terms of billet pre-heat, the preliminary test suggested to reduce the value at 300°C (table 2) respect the 450°C used for aluminum alloy, thus avoiding surface defects for excessive exit profile temperature. During the experimental campaign (Fig.33), 18 billets were extruded at constant ram speed of 4 mm/s, thus generating a profile exit speed of 6 m/min: the first three extrusions were performed without cooling to homogenize the tooling set temperature; from billet 4 to 10 the nitrogen valve was fully opened; from billet 11 to 18 the nitrogen valve was closed again.

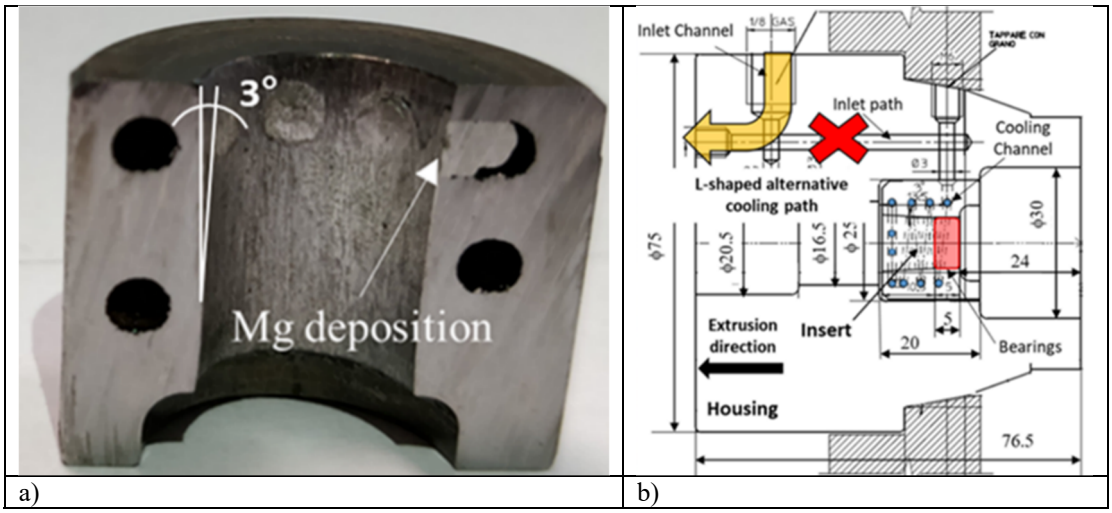

a) b)

Fig. 32 a) Pick-up defect during magnesium test, b) alternative cooling path (in yellow)

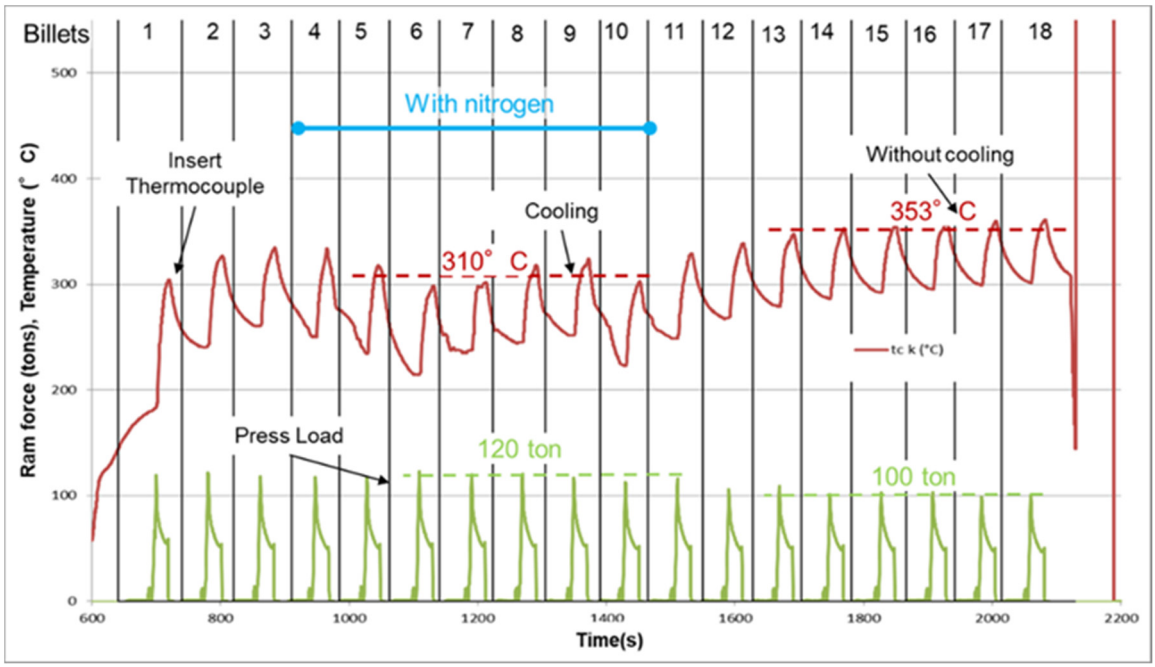

Fig. 33 Temperature history of the data registered by the thermocouples during the experimental trials (ZM21)

The nitrogen flow rate was reduced to 50% during the billet-change, but not removed because the non-conformal solution led to a decrease of the die temperature not as efficient as in the aluminum test. However, a temperature drop of about 40 °C (from 353 °C to 310 °C) registered during the test can be considered a quite good result. In terms of extrusion load, an increase of 20% with respect to the uncooled process was found (from 100 tons to 120 tons), because the rheological behavior of the magnesium alloy is more affected by the temperature if compared to the aluminum alloy [39, 108].

As positive remarks, the insert resisted also to the second cycle of experimental tests without any evident failure. In addition, a good profile quality was achieved both with and without nitrogen (Fig. 34), thus representing an important outcome also considering that the thermal field and the production rate were in the range of the industrial standards for ZM21 alloy [109].

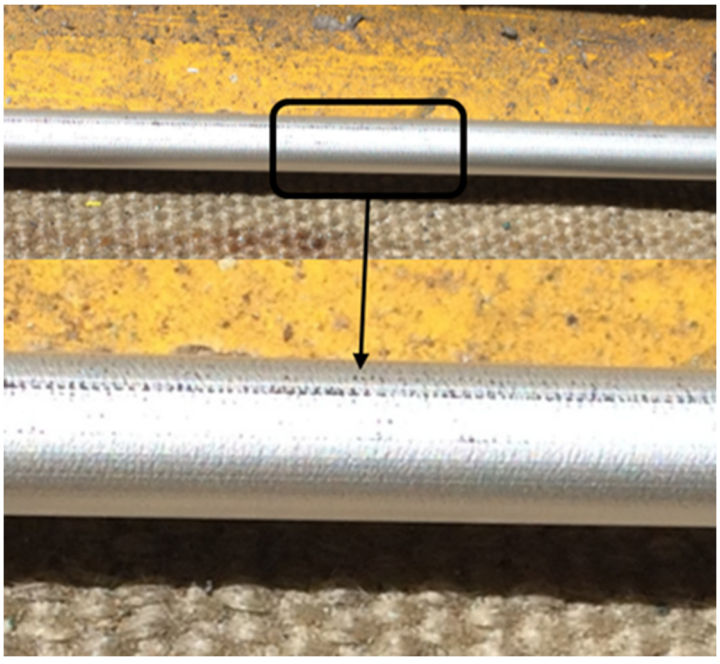

Fig. 34 Visual inspection of ZM21 exit profile surface

4.3 Profilati case study

4.3.1 Die design and liquid nitrogen cooling system

The industrial hollow profile depicted in Fig. 35 was selected for the experimental tests. Three tools composed the porthole die (Fig. 36): the mandrel with two portholes, an external diameter of 385 mm and axial length of 112 mm; the die and the backer with the same external diameter and axial length of 72 mm and 23 mm respectively. The cooling channel was realized in the backer surface in contact with the die, thus, positioned at 33 mm far from the bearings zones. As showed in Fig 36c and 37b, the channel had a not-constant rectangular section along the cooling path (depth per width 3x5mm and 4x6mm), while sixteen transferring holes (depth per with 2x5 mm) surrounded the outgoing profile.

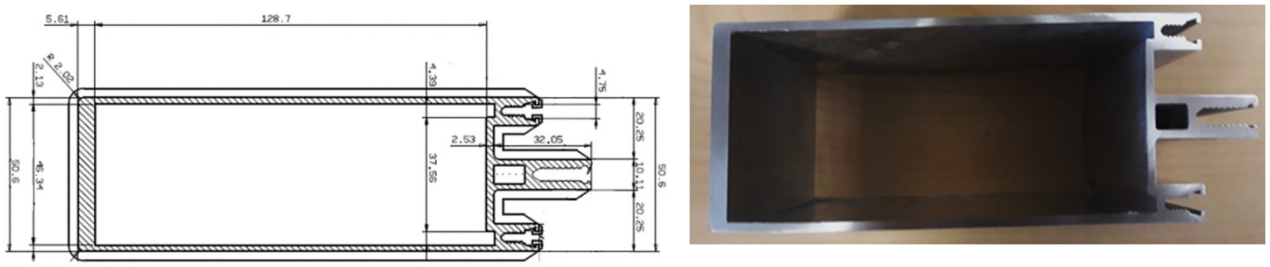

a) b)

Fig. 35 The hollow profile selected for the experimental tests: a) Profile drawing, b) Profile sample

a) b) c)

Fig. 36 Porthole die: a) The mandrel; b) The die; c) The backer with the cooling channel

The inlet channel was positioned in the die and connected to the planar path of the backer through the L-shaped circular channel with a diameter of 8 mm (Fig. 37a). The liquid nitrogen was stored in a large tank outside the industrial plant (pressure of 7 bars), and a pipeline 100 m long with a diameter of 15 mm connected the tank with the porthole die (Fig. 38). The inlet nitrogen pressure at the die was about 4.5 bar (at least as the regulating valve is fully open) and in such operating condition the boiling point is about -180 °C [110]. The inlet nitrogen temperature was governed by the sub-cooler positioned upstream of the die, where the liquid nitrogen under pressure was cooled by means of tapped nitrogen brought to ambient pressure and consequently with lower boiling point (-196 °C at 1.01325 bar). Therefore, the liquid nitrogen entered within the channel with temperature equal or higher than -196 °C and very close to the boiling point at its operating pressure. The maximum flow rate declared for this nitrogen plant was 80 Kg/h when the valve was fully opened.

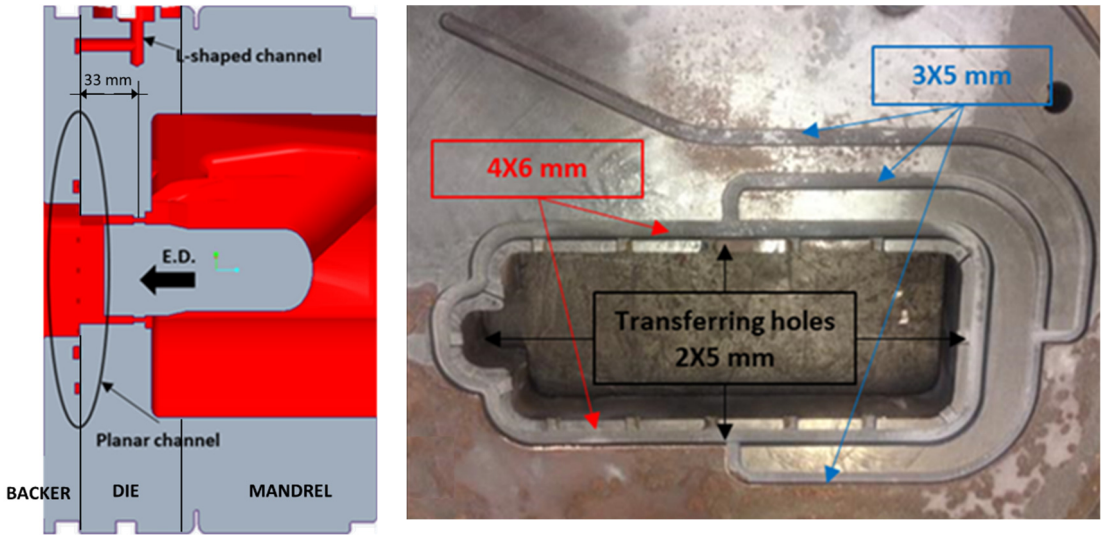

a) b)

Fig. 37 The cooling channel design: a) The L-shaped inlet channel; b) The rectangular section design of the planar channel

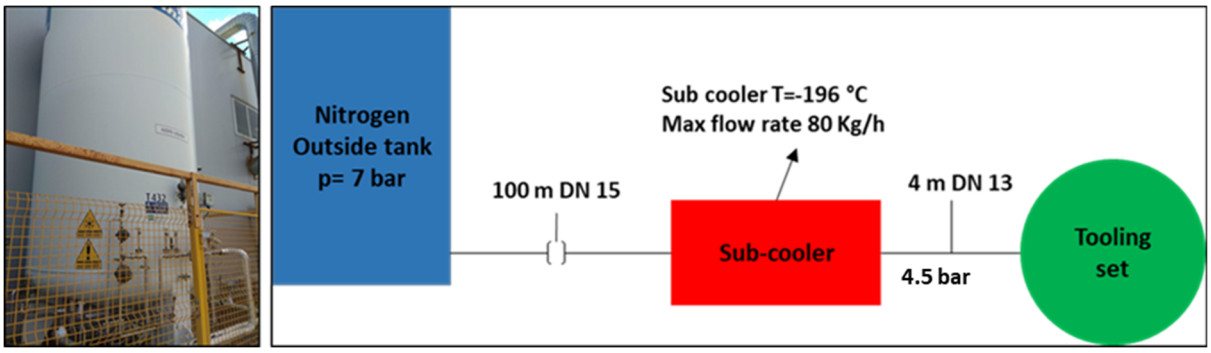

Fig. 38 The scheme of the nitrogen plant

Eleven K-types thermocouples were positioned in the tooling set to monitor the thermal state evolution during the extrusion process: six were located in the backer to follow the cooling channel path (P1 to P6 in Fig. 39b); five were placed in the die (M3 to M7 in Fig. 39a) to record the temperature around the bearing zones. During the installation of the thermocouples, the depth of the holes in the tooling set was verified and the quotes acquired and saved.

In the die and the backer, an external rectangular-shaped groove was made to allow the thermocouples passage avoiding their breakage during the assembly in the ring (Fig. 40). Moreover, soft alloy pins were used for clamping the thermocouples further avoiding their movement from the seat. The thermocouple temperatures were recorded by means of Agilent acquisition system connected to a laptop, while the exit profile temperature was monitored with the Williamson contactless pyrometer connected with the control system of the press.

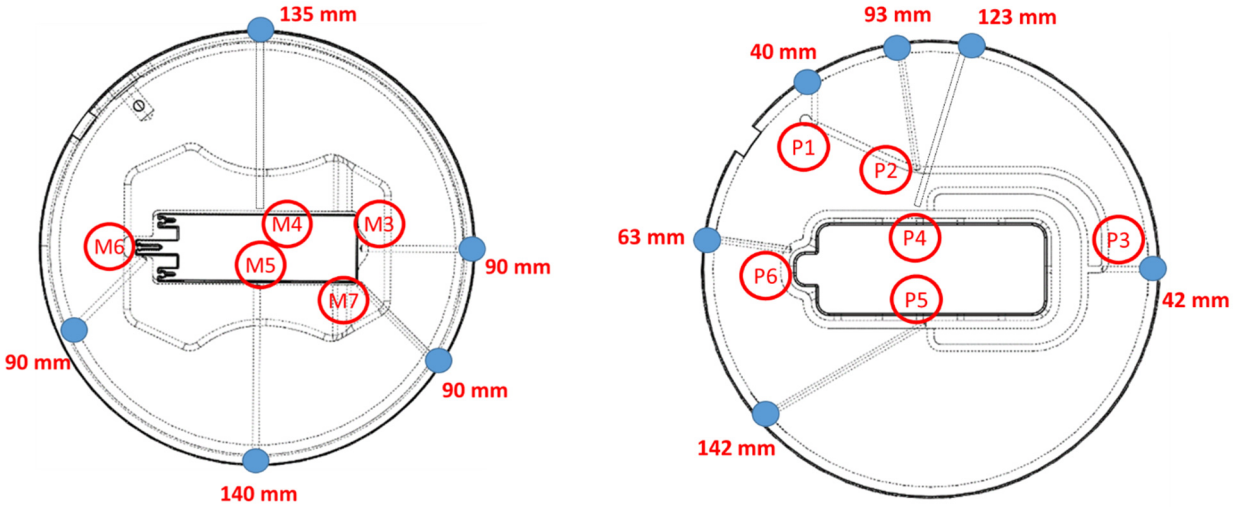

a) b)

Fig. 39 Positions of the thermocouples: a) Die, b) Backer; numbers report the acquired depths of the thermocouple holes.

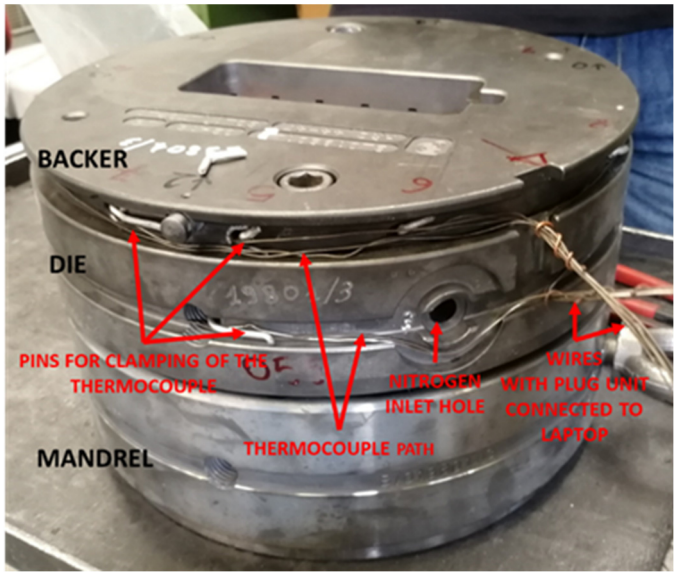

Fig. 40 The installation of the thermocouples in the die and backer

4.3.2 Experimental campaign

The experimental campaign consisted in the extrusion of seventeen AA6060 billets in different conditions of extrusion speed and nitrogen flow rate. The length and the diameter of the billets were 950 mm and 203 mm, respectively. A conical taper heating from 480°C to 440°C (front-back) was applied in the billet along its axis; the pre-heating die temperature was set to 520 °C and the container temperature to 400 °C.

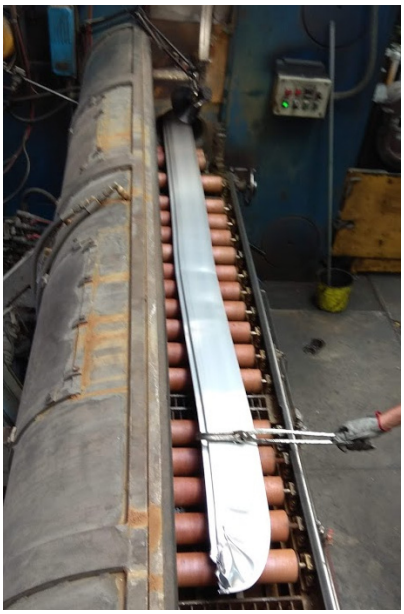

Fig. 41 The extrusion of the first billet

Fig. 42 reports the whole extrusion process in terms of temperature monitoring, showing in black line the exit profile temperature, on the top the temperatures in the die, on the bottom the temperatures in the backer.

The connection of the thermocouple to the acquisition system was performed at around 250s, after the transfer of the die assembly from pre-heating oven to the press. During this setup time, the thermocouples placed in the backer (P1-P6) already registered lower values than thermocouples placed in the mandrel (M3-M6) as consequence of the greater heat exchange of the backer with the air and the die holder in the press. The thermocouple M7 got broken during die loading and it did not acquire valid data.

The first extrusion started at around 400s (Fig.41): temperatures in the die immediately increased due to the hot aluminum flowing in the mandrel and in the die, while the temperatures in the backer strongly decreased because the extrusion load promoted the contact between the backer and the colder press and consequently caused a higher heat-exchange. Extrusion of billet 1 lasted up to 600s due to the selected low ram speed (4 mm/s) and the stop for puller clamping of the profile.

During the long dwell time for the first billet change (600 to 900s), the die cooled down, consequently heating up the backer. From 900s, three billets were extruded at the extrusion speed of 8 mm/s without any cooling to obtain, with billet 4, the steady-state condition for the uncooled process. In this process condition, the backer showed a thermal field very stable with small gradient during the billet change, because the cooling during the dwell time was balanced by the heat exchange with the hot die. Therefore, the cooling down in the die was higher during the billet change, with a drop recorded by the thermocouple of about 30°C.

By analyzing the thermal history of fourth extrusion (steady-state condition of the uncooled process), it was found an exit profile temperature of 556 °C, slightly lower than the peak temperature reached in the bearing zones. Indeed, thermocouple M3, closer to the short side of the profile without wings (Fig.39b), recorded the highest value in the bearings zones of 565 °C. Moreover, M6 and M5, positioned respectively near the wings and at the center of lower side, acquired a temperature only 5°C lower than M3. The lowest temperature in the bearing zones was recorded by M4 (525 °C), located symmetrically with respect to M5. In the backer, the lower temperature was registered in P1 (300 °C), located nearby the entrance of the cooling channel. Thermocouples P3, P4, P5 and P6 were

positioned as the corresponding thermocouples of the die, recording temperatures of 313 °C, 355 °C, 360 °C and 345 °C, respectively. The thermocouple P2, located immediately following P1 along the channel, provided a value of 311 °C.

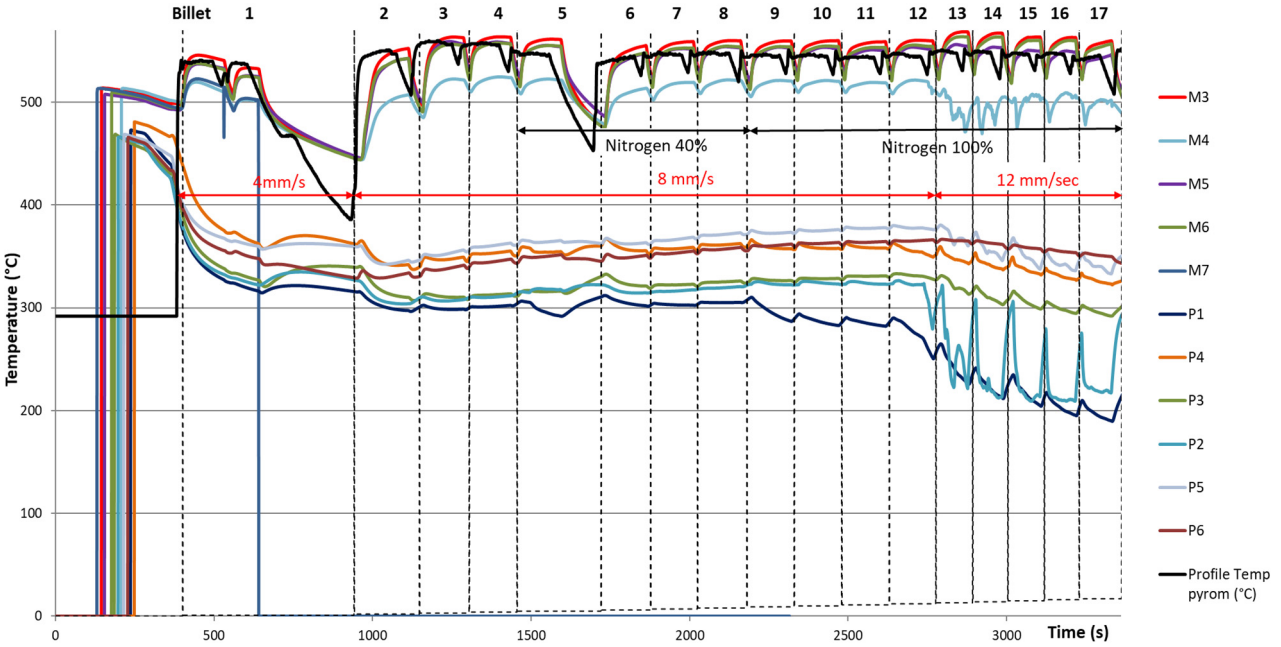

Fig. 42 Temperature history of the extrusion process: Thermocouples temperature and the exit profile temperature

From the fifth to the eighth extrusion, the ram speed remained constant, but the nitrogen valve was opened at 40%. Billet 8 was considered the steady-state condition for an extrusion speed of 8 mm/s and liquid nitrogen flow rate of 40%. In order to understand the behavior of the nitrogen in the channel, it is possible to simplify the scheme as a tube with a pressure at the inlet, distributed pressure losses along the tube and outlet at atmosphere pressure (1 bar). If nitrogen enters as liquid and then changes its state in gaseous, an increase of volume of 177 times occurs thus preventing nitrogen flow. The selected channel design did not promote the liquid nitrogen flow using the 40% of nitrogen flow rate, thus causing the formation of a large amount of nitrogen gas within the channel. This was also experimentally confirmed by the absence of ice in the external surface of the nitrogen connecting pipe as well as by the lack of temperature variation in the tooling set. Otherwise, sensors in P2-P6 even showed a slight increase, as one can expected by a 'warm' gas nitrogen flow in the channel.

From billet 9 to billet 12, the valve of the nitrogen was opened to 100%, keeping the extrusion speed at 8 mm/s. The connecting pipe started to be partially covered by ice, as confirmed by thermocouple P1 that, as first, recorded a temperature of 250 °C against 300 °C of the uncooled condition. The effect of liquid nitrogen cooling reached P2 during billet 12 and finally reached P3 only during the extrusion of billet 13. The acquired data suggested a very slow replacement of gaseous nitrogen by liquid nitrogen within the channel and the coexistence of gaseous and liquid nitrogen phases in the channel. In these conditions, the heat subtracted in the die resulted negligible. In addition, it is worth noting that during the extrusion of billet 12 a steady state condition in terms of thermal field was not still reached. However, only for further comparison with the numerical results discussed later (see section 5.5), billet 12 was considered like the steady-state condition for the extrusion speed of 8 mm/s and the 100% of nitrogen flow rate.

During the extrusion of billet 13, and subsequent billets, the extrusion speed was increased at 12 mm/s and the nitrogen valve was kept at maximum opening. The increase of the extrusion speed leads to an increase of heat generation and consequently to a general increase in temperatures (see section

2.3). However, in the backer, the mixture of gaseous and liquid nitrogen began to show a visible cooling effect also in P4-P6 despite the greater generation of heat related to extrusion speed increase. Therefore, at this point the transitory phase of the cooling consisted in a continuous partially replacing of the large amount of gas nitrogen present along the channel with the liquid nitrogen pumped from the external pipeline, thus leading to a more effective cooling. Moreover, at the beginning of the last extrusion, the connecting pipe was completely iced and the thermocouples P1 and P2 registered the highest drop of temperature with 196 °C and 219 °C against 300 °C and 311 °C of the uncooled condition, respectively. In the die, the cooling began to be now visible and small effective, reaching a maximum drop of 23°C in M4 (from 525°C to 502°C), followed by M5 with 13°C (from 560° to 547°C). In addition, the pyrometer recorded a decrease of around 10°C in the exit profile temperature (from 555°C to 545°C). As positive remark in terms of cooling efficiency, it has to be reminded that the final temperature decrease was obtained at 50% higher ram speed that, on the contrary, promotes a generally temperature rise.

In terms of extrusion loads, a peak of 23.3 MN (billet 4) was acquired in uncooled condition while 24 MN was recorded during the cooled one (billet 12). During the extrusion of the last five billets, the combination of increased ram speed and of the low cooling effect caused a moderate raise of the extrusion load (below 10 %), with a maximum registered value of 25.5 MN in billet 17.

A good design of the cooling channel should lead to a condition with uniform temperatures all around the bearings as well as to a short transient from gas to liquid, however, the experimental trials highlighted the limits of the proposed cooling system that was not as effective as expected. As previously explained, the cooling was negligible with the 40% of nitrogen flow rate, and it began quite effective, where necessary in the die, only after nine extrusions with the nitrogen valve fully opened. Moreover, the acquired data suggested that during the extrusion of the last billet a mixture of gas and liquid nitrogen was still flowing into the cooling channel, thus indicating that the steady-state cooled condition was not still reached. In addition, the long transitory was also favored by automatically closing of the nitrogen valve during the billet change, that it was usually used to avoid an excessive die cooling, but that in this situation was self-defeating.

Also in terms of balanced cooling, the limits were evident: temperatures in the die were not uniform around the profile, with differences from M3 to M4 up to 44°C in the cooled condition (billet 12) and up to 58 °C at higher extrusion speed (billet 17), against the 35°C of the uncooled one (billet 4). Differences became more relevant in the backer: a maximum delta of 154°C was found from P1 to P5 (billet 17) compared to 60°C of the uncooled condition (billet 4).

In conclusion, the experimental campaign clearly showed again the necessity of developing a reliable channel design criteria or numerical tools in order to gain optimal cooling conditions. Indeed, the tested design seemed initially a good solution to the press technicians, but it actually turned out to be very ineffective.

5 Numerical assessment of the hot extrusion process with nitrogen cooling

The following chapter is focused on the numerical modelling of the extrusion process with nitrogen cooling. The 3D model of the extrusion process is integrated with the 1D model of the cooling channel. It is worth noting that the fluid-dynamics equations are solved over the coordinate identified by the unit tangent vector to the channel axis, following the complex 3D path of the channel within the tooling set. A 1D approach is preferred to three-dimensional approaches to avoid excessive computational complexity without limiting the reliability of the numerical results. The full

comprehensive numerical model of the extrusion process is implemented in the COMSOL Multiphysics software that allows coupled analysis of thermal, structural and fluid dynamics problems [111]. The three case studies previously discussed will be modelled with the aim to test the accuracy of the proposed model as well as to show its potentiality and limit. Even if the first proposed model does not consider the nitrogen phase change within the channel, it offers good results in terms of temperature prediction at low computational time.

The potentiality of the model predictability will be confirmed for all case studies, thus evidencing how the numerical approach can be useful to support the die design in terms of performances optimization, where the based-experience approaches show their greatest limits. Moreover, the next proposed step will be the integration of the FE model within an optimization platform with the aim to test a large number of designs in automatic way. This approach will be tested with the Benchmark 2011 case study that evidenced an unbalanced cooling around the bearings. Then, a new 1D numerical model will be proposed based on the homogenous fluid approach with the aim to consider the gas formation within the cooling channel. The model will be tested with the Profilati case study, for which the single-phase model shows its greatest shortcomings.

5.1 1D Numerical Model of nitrogen cooling

A one-dimensional (1D) approach is used to model the nitrogen flow within the cooling channels, thus resolving momentum-conservation and continuity equations over the coordinate identified by the unit tangent vector to the channel axis. In this first model, the phase change is not considered, then, it is possible to simulate steady state conditions with 100% of liquid or gas nitrogen within the channel. However, helpful evaluations can be obtained also for transitory conditions (liquid-gas mixture) that are located between the two extreme condition (fully liquid or gaseous).

Notably, the following assumptions are applied in the proposed model [111-112]:

- The phase change is not considered
- The equations are valid for incompressible or weakly compressible gas/fluid
- The velocity profile is fully developed with an entire pipe section.
- The curvature of the pipe segment gives rise to insignificant pressure loss in comparison with wall friction.
- Shocks are neglected
- All velocity components normal to the pipe axis is assumed to be 0

The proposed model allows defining and varying the channel cross-section geometry within the pipe segments (e.g., shape, dimensions) to calculate some involved variables (e.g., Reynolds number, pressure drop). To this end, the mean hydraulic diameter $d_h = 4A/P$ can be generally used, where A is cross-sectional area and P is the wetted perimeter. Continuity and momentum conservation are expressed by the following equations, respectively:

$$\frac{\partial A_c \rho}{\partial t} + \nabla \cdot (A_c \rho u) = 0, \tag{8}$$

$$\rho \frac{\partial \boldsymbol{u}}{\partial t} \cdot \bar{\boldsymbol{t}} + \rho u \nabla \cdot (u) = -\nabla p \cdot \bar{\boldsymbol{t}} - \frac{1}{2} f_D \frac{\rho}{d_h} u|u| + \boldsymbol{F} \cdot \bar{\boldsymbol{t}}, \tag{9}$$

where ρ is the density of the fluid, c refers to the channel section, t is time, $\boldsymbol{u}$ is the cross-section averaged velocity of the fluid, with u being its component along the coordinate tangential to the

channel axis, $\bar{\boldsymbol{t}}$ is the unit tangent vector, p is the fluid pressure, f_D is the Darcy friction factor and $\boldsymbol{F}$ is gravity expressed as a force per unit volume. Friction losses due to viscous shear stresses are embodied by the second term on the right-hand side of Eq. (9).

Quantifying the friction factor is performed through the well-established Churchill correlation [112-113], which is largely implemented in pipe-flow simulations to the purpose, since it applies to laminar and turbulent flow, as well as the transition region. Its formulation is presented in the following relationship:

$$f_D = 8 \cdot \left\{ \left[\left(\frac{8}{Re} \right)^{12} (\theta_1 + \theta_2)^{-1.5} \right]^{\frac{1}{12}} \right\}, \tag{10}$$

where the Reynolds number is expressed as $Re = \rho u d_h / \mu$, μ is dynamic viscosity, θ_1 and θ_2 are empirical parameters that depend on Re and relative roughness ε / d_h, with ε being absolute surface roughness, through the following expressions:

$$\theta_1 = \left\{ -2.457 \cdot ln \left[\left(\frac{7}{Re} \right)^{0.9} + 0.27 \frac{\varepsilon}{d_h} \right] \right\}^{16}, \tag{11}$$

$$\theta_2 = \left(\frac{37530}{Re} \right)^{16}. \tag{12}$$

Pressure drops due to lumped energy losses can be also added in the nodes of the channel under the generic relationship $\Delta p = \frac{1}{2} K_f \rho u^2$, where K_f is the loss coefficient pertaining to the specific change in the flow geometry that generates additional resistance (e.g., bends, T and Y junctions, contractions, expansions). Examples of available standard loss coefficients, K_f, for Newtonian fluid [111-112] are shown in the table 3. Obviously, it is also possible to add user-defined coefficients or to select directly an imposed Δp.

Table 3 Loss Coefficients for additional flow resistances

Feature	Description	Loss Coefficient K
Bends	90° standard elbow	0.9
Bends	45° standard elbow	0.5
Valves	Globe, fully open	10
Valves	Angle, fully open	4.4
Valves	Gate, fully open	0.2
Valves	Ball, fully open	4.5
Valves	Butterfly, fully open	0.6
Valves	Swing check, fully open	2.5
T-junction	T-junction split/merger	0.1 side/ 2.1 main

In terms of heat exchange, the conservation of energy is also included within the model to predict temperature distribution in the channel as well as the thermal interaction between nitrogen and die; its formulation was expressed as:

$$\rho A_c c_p \frac{\partial T}{\partial t} + \rho A_c c_p u \cdot \nabla T = \nabla \cdot A_c k \nabla T + f_D \frac{\rho A_c}{2 d_h} u^3 + Q_{wall}, \quad (13)$$

where c_p is specific heat capacity at constant pressure (c for incompressible matter as liquid), T is nitrogen temperature, k is nitrogen thermal conductivity and Q_{wall} is a source term that accounts for the heat exchanged by nitrogen with the surrounding die. It is also worth noting that the second term on the right-hand side of Eq. (13) embodies the heat dissipated by friction within the fluid. Notably, Q_{wall} is calculated through the following equation:

$$Q_{wall} = hP(T_{die} - T), \quad (14)$$

where h is convective heat transfer coefficient and *die* refers to each node of the die around the channel. Therefore, temperature at those locations is calculated by continuity equation for heat flux even within the die:

$$\rho_{die} c_{die} \frac{\partial T_{die}}{\partial t} = \nabla \cdot k \nabla T_{die} - Q_{wall} \quad (15)$$

The convective heat transfer coefficient depends on thermophysical properties of the involved fluid and on the flow type; it is expressed by Nusselt number $Nu = h \cdot d_h / k$ in non-dimensional form. Nusselt number was evaluated employing correlations typical of forced convection in pipe flow; notably, Eqns. (16) and (17) express the selected formulations for laminar and turbulent flow [113], respectively:

$$Nu = 3.66 \quad (16)$$

$$Nu = \frac{(f_D/8)(Re-1000)\cdot Pr}{1+12.7\sqrt{f_D/8}\cdot(Pr^{2/3}-1)}, \quad (17)$$

where Pr is Prandtl number $\left(\frac{\nu}{\alpha} = \frac{\mu \cdot c_p}{k}\right)$ and n is dynamic viscosity (μ/ρ) and a is thermal diffusivity. So, convective coefficient is not considered *a priori* constant along the channel, but it is function of the thermo-fluid-dynamics phenomena involved within the cooling path. Liquid or vapor/gas physical properties (density, viscosity…) are then implemented in the calculations by merely resorting to datasheets available for nitrogen [110,114].

5.2 3D Numerical Model of the Hot Extrusion Process integrated with 1D Model of Cooling Channel

The full comprehensive numerical model of the extrusion process is implemented on Comsol Multiphysics software that allows coupled analysis of thermal, structural and fluid dynamics problems. The extrusion process is modelled with pure Eulerian approach, requiring the geometry of the material flow in already deformed condition (Fig. 43). Overall, the tooling set (mandrel, die, backer…) are combined into one solid tool to avoid the contact analysis, while the ram and the container, indispensable only for a Lagrangian approach, are replaced by proper thermal and frictional boundary conditions. In table 4 are collected all parameters and boundary conditions necessary to prepare a steady state 3D simulation of the extrusion process integrated with the 1D model of the cooling channel. The specific values for each case study will be reported in their respective sections.

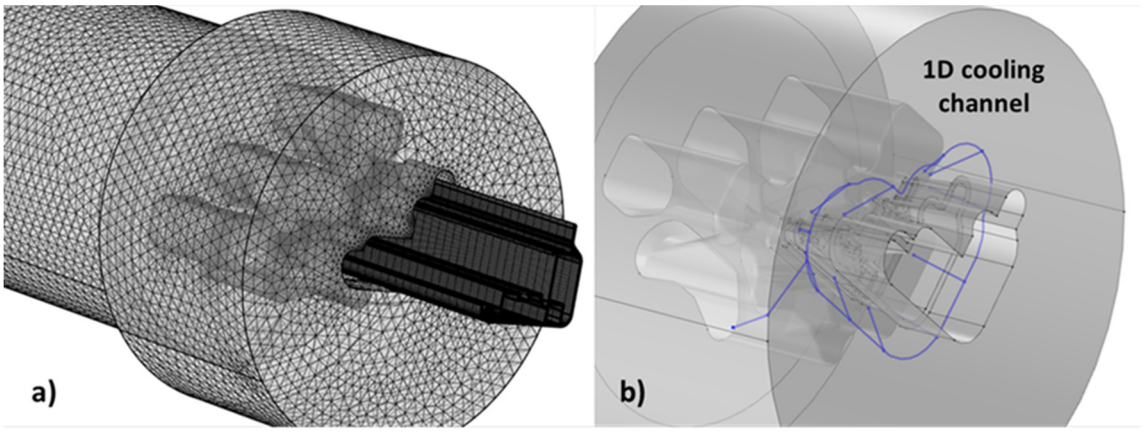

Fig. 43 Example of FE model from Benchmark 2011 case study: a) The billet and the tooling set; b) The 1D cooling channel integrated in the tooling set

Table 4 Process Parameters and boundary conditions set in the numerical models

Process Parameters	**Value**
Billet Temperature	Depends on the case study
Die Temperature	Depends on the case study
Container Temperature	Depends on the case study
Ram Temperature	Depends on the case study
Ram Speed	Depends on the case study
Ram, Container/billet interface	No slip condition + Heat exchange by convection
Die/billet interface	No slip condition + Heat exchange by conduction
Bearings/billet interface	Slip condition + Heat exchange by conduction
Inlet Nitrogen Pressure or Inlet nitrogen flow rate	Depends on the case study
Inlet Nitrogen Temperature	-196 [°C]
Nitrogen Density (Liquid/Gas) (-196 °C, room pressure)	806.59/4.56 [kg/m^3]

Dynamic Viscosity (Liquid/Gas) (-196 °C, room pressure)	1.6137E-4/5.4273E-6 [Pa*s]
Nitrogen heat capacity at constant pressure Cp (Liquid/Gas) (-196 °C, room pressure)	2.041/1.123 [J/g*K]
Nitrogen thermal conductivity k (Liquid/Gas) (-196 °C, room pressure)	0.1465/0.00700 [W/m*K]
Surface roughness of the channel (ε)	Commercial steel (0.046 mm)

The aluminium flow is modelled as non-Newtonian fluid with the dynamic viscosity being a function of temperature and strain rate. In the extrusion process, accurate numerical results have been achieved using the Perzyna's model of viscoplasticity [115], where the dynamic viscosity is computed as the ratio of the effective deviatoric flow stress to the effective strain rate, while the flow stress is calculated with the Sellars-Tegart inverse sine hyperbolic model (see section 2.4) [43]:

$$\eta(T,\dot{\varepsilon}) = \frac{\sigma(T,\dot{\varepsilon})}{3\dot{\varepsilon}} \tag{18}$$

$$\bar{\sigma}\,(T,\dot{\varepsilon}) = \frac{1}{\alpha} sinh^{-1}\left[\frac{1}{A}\dot{\varepsilon}\exp\left(\frac{Q}{RT}\right)\right]^{\frac{1}{n}} = \frac{1}{\alpha} sinh^{-1}\left[\left(\frac{Z}{A}\right)\right]^{\frac{1}{n}} \tag{19}$$

where η is the dynamic viscosity, σ the flow stress, $\dot{\varepsilon}$ the strain rate, Q the activation energy, R the gas constant, T the temperature, n, A and α are material constants, while Z is defined as the Zener-Hollomon parameter.

About the wall conditions, a sticking condition is imposed at the billet/container, billet/die and billet/ram interfaces, then, a slip condition depended on the aluminium viscosity is selected in the bearings zones and at the exit of the die. A heat transfer coefficient of 11,000W/m^2°K is set between aluminium and the tool system not modelled (container and ram), while 3,000W/m^2°K is chosen in tool-to-tool contacts with the container and the tool-housing in the press, thus simulating where necessary an equivalent heat exchange by convection. For heat exchange with air, the heat transfer is set equal to 50 W/m2°K with an air temperature of 50°C. Instead, the heat transfer is calculated resolving the contact analysis in the interfaces between the material flow and the modelled tools.

About the nitrogen cooling an inlet temperature of -196 °C is imposed as suggested by nitrogen plant supplier; in addition, the inlet pressure or the nitrogen flow rate must be imposed as boundary condition. The physical properties of the nitrogen (density, viscosity…) are imposed constant for both liquid and gaseous state, choosing the boiling point at room pressure (-196 °C). The small differences in the application range (1/5 bars; -196/-170°C) do not justify the use of properties depended by temperature and pressure. However, a different approach will be used when the phase change shall be taken into account, because it is already clear in table 4 the great differences in terms of properties between liquid and gas nitrogen.

As discussed in the following sections, steady-state simulations will be performed comparing the numerical results with the experimental ones at the middle of each billet extrusion in terms of temperature and extrusion load. The initial die filling and the end of the extrusion process (in

proximity of the billet rest) cannot be easily assessed with a pure Eulerian approach; however, this is not a limit for the aim of the model to capture the macroscopic effects of the nitrogen cooling as well as to evaluate rapidly the efficiency of the selected cooling channel design.

5.3 Benchmark 2011 Case Study: Experimental-Numerical comparison

The numerical model described in the section 5.1 was firstly tested with the Benchmark 2011 case study taken from the literature [77]. The process parameters, the boundary condition and the flow stress parameters discussed from a general point of view in the section 5.2 are reported in tables 5 and 6 for this specific case study. Recalling the experimental campaign, ten AA6060 billets were extruded in different cooling conditions (Fig. 44). Therefore, for the validation of the numerical model, three different steady-state extrusion conditions were tested: the uncooled condition (6th billet), the cooled condition with the 100% of nitrogen flow rate (8th billet) and the cooled condition with the nitrogen valve opened at 20% (last billet).

Table 5 Process Parameters and boundary conditions set for Benchmark 2011 case study

Process Parameters	**Value**
Billet Temperature	460 °C
Die Temperature	500 °C
Container Temperature	427 °C
Ram Temperature	413 °C
Ram Speed	2.71 mm/s
Ram, Container/billet interface	No slip condition + Heat exchange by convection
Die/billet interface	No slip condition + Heat exchange by conduction
Bearings/billet interface	Slip condition + Heat exchange by conduction
Inlet Nitrogen Pressure or Inlet nitrogen flow rate	2 bar (100%) 1.1 bar (20%)
Inlet Nitrogen Temperature	-196 [°C]
Nitrogen Density Liquid (-196 °C, room pressure)	806.59 [kg/m^3]
Dynamic Viscosity Liquid (-196 °C, room pressure)	1.6137E-4 [Pa*s]
Nitrogen heat capacity at constant pressure Cp	2.041 [J/g*K]

Liquid (-196 °C, room pressure)	
Nitrogen thermal conductivity k Liquid (-196 °C, room pressure)	0.1465 [W/m*K]
Surface roughness of the channel (ε)	0.046 mm

Table 6 Flow stress parameters of Zener-Hollomon model for AA6060 [116]

Flow stress parameters	AA6060
Q parameter of Zener-Hollomon model	161 [KJ/mol]
A parameter of Zener-Hollomon model	7.6301*1010 [1/s]
n parameter of Zener-Hollomon model	4.67
a parameter of Zener-Hollomon model	0.035 [1/MPa]

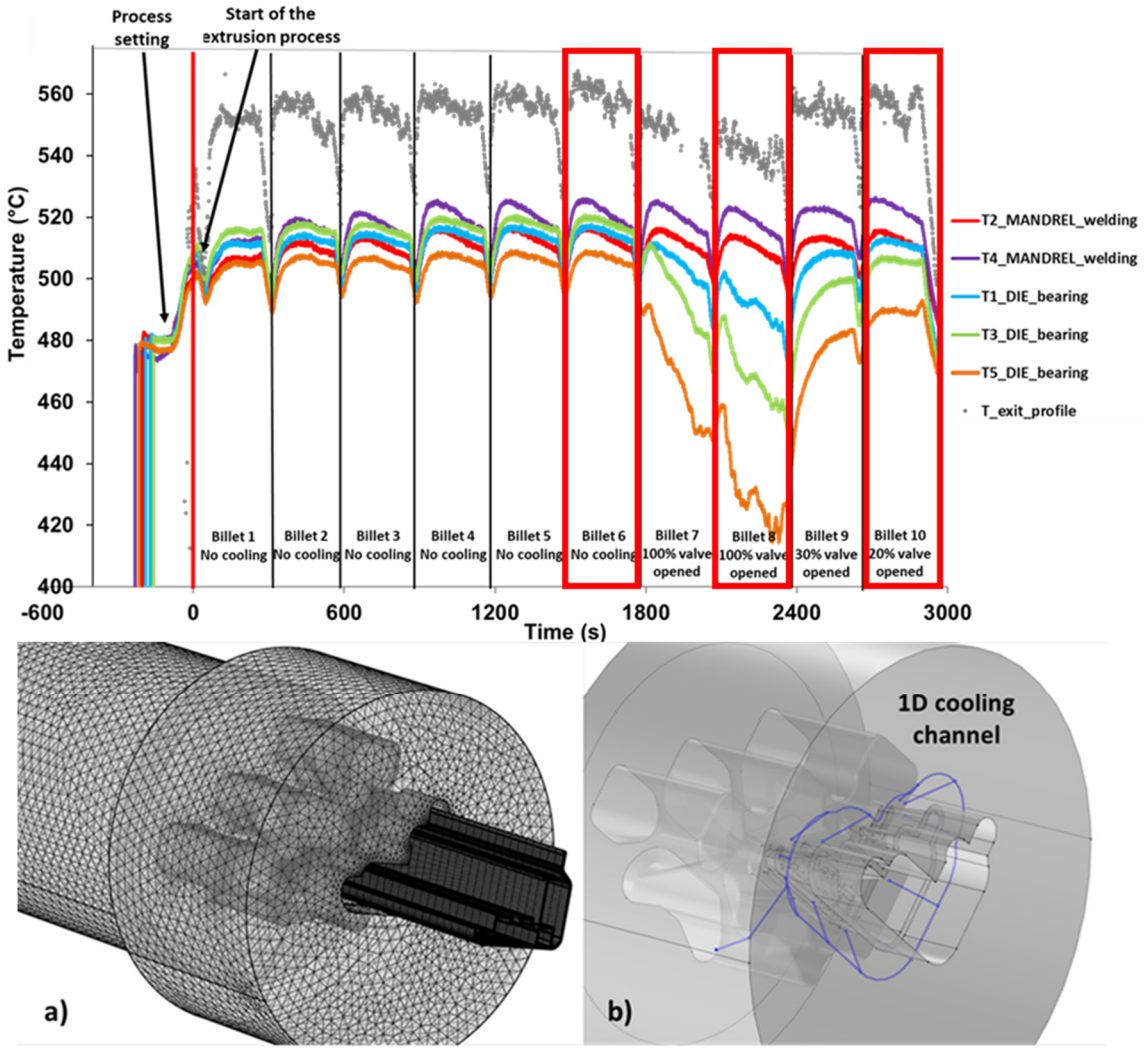

Fig. 44 Selection of the extrusion conditions for the Experimental-Numerical comparison

The die mesh consisted of 712068 tetrahedral mesh with 10 mm of maximum element size and 1 mm of minimum element size. The cooling channel was meshed with 380 edge elements to obtain an average size of 2 mm and a minimum size of 0.5 mm. The aluminium domain consisting of 800595 elements was divided into two parts: the exit profile meshed with a structured hexahedral mesh, the billet and the material under deformation meshed with tetrahedral elements.

Figs. 44, 45 and 46 show the thermal map in the mandrel and in the die where the thermocouples were positioned, comparing the uncooled and the cooled conditions respectively. In the mandrel, a general underestimation of the temperatures was found in the uncooled process (Fig. 45a) even if with very low percentage errors (maximum of -2.8% in T4). The nitrogen cooling did not affect substantially the thermal map of the mandrel confirming the experimental evidence (Fig. 45b). In this case, the numerical-experimental errors in terms of thermocouples' temperature were below 4%.

The efficiency of the cooling was clearly visible in the die when the nitrogen valve was fully opened (Fig. 46), evidencing the strong differences between the uncooled and cooled conditions. Notably, in Fig. 46b, not only it is immediately noticeable the great heat removal registered in the die, but also the unbalanced cooling around the profile as found during the experimental campaign. Slight overestimations of the die temperatures (T1, T3 and T5) were observed without cooling; however even in this case, a peak error of 2.5% was found in T5. Using the 100% of nitrogen flow rate, the peak experimental-numerical discrepancy was registered for thermocouple T1, with a value of 3.9%. Even if the contribution of the gas nitrogen cooling that surrounded the exit profile was not simulated, the difference in the exit profile temperature was low (1.9%), confirming probably its small cooling effect.

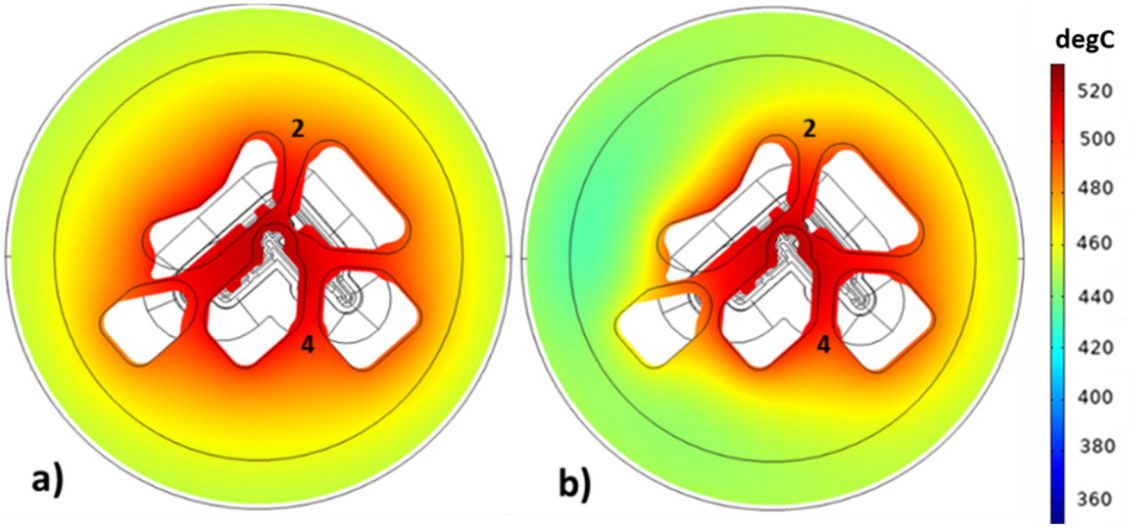

Fig. 45 Thermal field in the thermocouple plane of the mandrel: a) Uncooled b) Cooled process (100%)

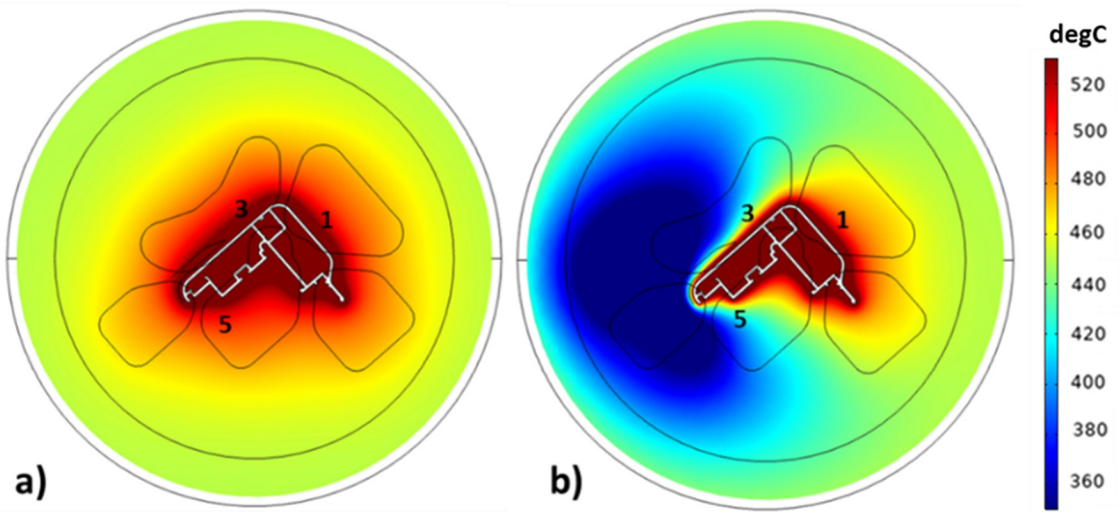

Fig. 46 Thermal field in the thermocouple plane of the die: a) Uncooled b) Cooled process (100%)

In Fig. 47 the numerical results with the 20% of nitrogen flow rate revealed an ineffective cooling as emerged by the experimental campaign. In addition, the numerical-experimental comparison in terms of temperature in the thermocouples and profile showed a maximum peak error of -3.3% in T2. In terms of extrusion load, the underestimation of 6.5% founded in the cooled condition (100%) is considerably acceptable. Concluding, the achieved results (tables 7 and 8) confirmed the goodness of the numerical prediction under different extrusion conditions. Therefore, the numerical analysis confirmed, as previously mentioned, the experimental evidence: the low cooling of the mandrel, the unbalanced cooling in the die, the ineffective cooling with the 20% of valve opening as well as the small increase of the extrusion load with the nitrogen cooling.

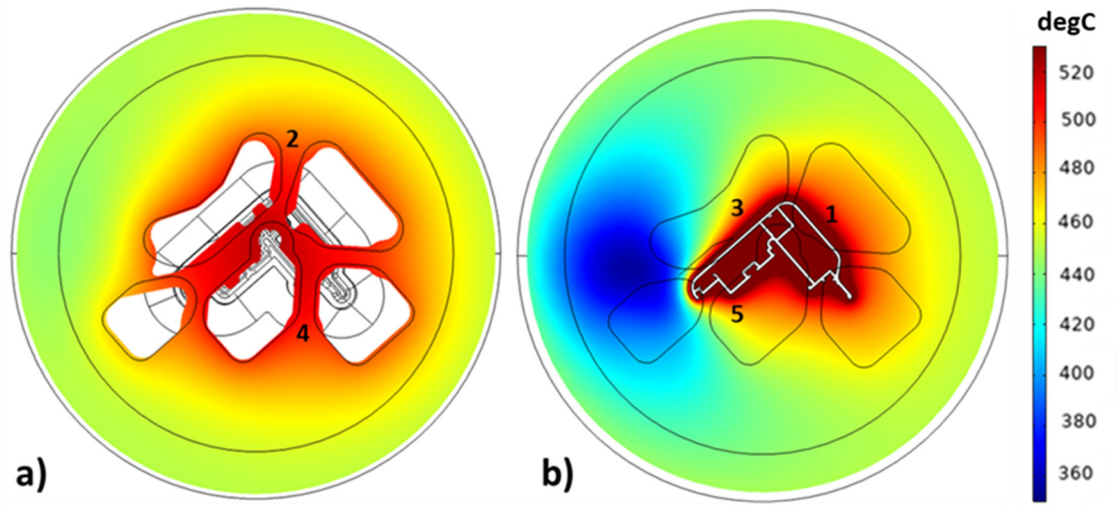

Fig. 47 Thermal field in the thermocouple plane of the die: a) Uncooled b) Cooled process (20%)

Table 7 Experimental-Numerical comparisons (Billet 6 – NO cooling, Billet 8 - YES cooling)

	Thermocouples Temperature [°C]					**Profile Exit T [°C]**	**Load [MN]**	**Cooling 100% valve opening**
	T1	**T2**	**T3**	**T4**	**T5**			
Exp.	518	517	520	525	510	560	19.1	NO
Num.	530	505	530	510	523	563	18	NO

Err%	2.3	-2.3	1.9	-2.8	2.5	-0.7	-5.8	
Exp.	490	508	460	523	430	540	19.9	YES
Num.	509	500	450	505	430	550	18.6	YES
Err%	3.9	-1.6	-2.2	-3.5	0	1.9	-6.5	

Table 8 Experimental-Numerical comparisons (Billet 10, 20% valve opening)

	Thermocouples Temperature [°C]					**Profile Exit T [°C]**	**Load [MN]**
	T1	**T2**	**T3**	**T4**	**T5**		
Exp.	510	517	508	525	490	560	19.1
Num.	520	500	510	510	495	558	18.2
Err%	2.0	-3.3	0.4	-2.9	1.0	-0.4	-4.7

5.4 Multi-die case study: Experimental-Numerical Comparison

The second validation of the 3D numerical model of the extrusion process integrated with the 1D model of the cooling channel was performed with the Multi-Die case study. For the first time, the gas nitrogen numerical model was also evaluated to compare the numerical results with the experimental ones during the transitory phase of the cooling. Indeed, recalling the experimental campaign with AA6063 billets (Fig. 48), when the nitrogen valve was fully opened (billet 8) a transitory cooling phase of about three extrusions was registered, probably related to the formation of a large amount of gas nitrogen within the channel. In addition, other three conditions were simulated for the aluminum alloy: the uncooled condition (billet 7), the steady-state cooling condition (billet 17), and the cooling condition at higher extrusion speed (billet 24). About ZM21 magnesium alloy, two conditions were tested (Fig. 49): cooled condition with L-shaped cooling path (billet 10, see section 4.2.2**)** and the uncooled one (billet 17). For the nitrogen cooling, an inlet pressure of 4 bar was set in the cooling channel, assuming a pressure drop of about 1 bar in the first pipeline. An inlet nitrogen temperature of -196 °C was set, considering negligible the drop from the tank to the cooling channel in the steady-state condition. Steady-state simulations were carried out in order to evaluate the thermal fields in the regime conditions. Notably, tables 9 and 10 report the process parameters, the boundary conditions, and the flow stress parameters for both alloys.

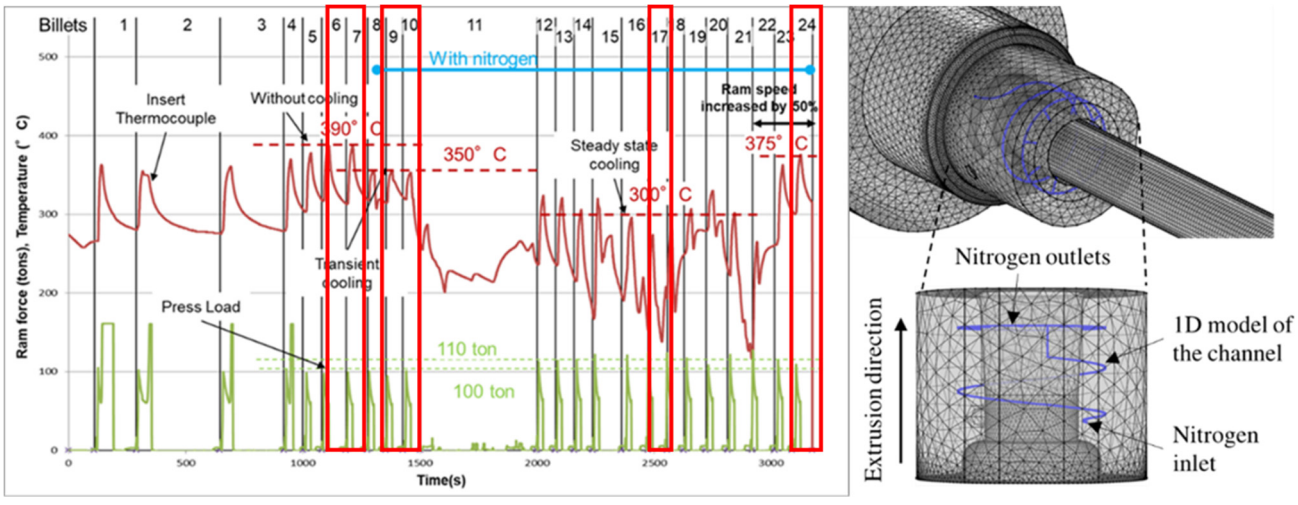

Fig. 48 Selection of the extrusion conditions for the Experimental-Numerical comparison (AA6063)

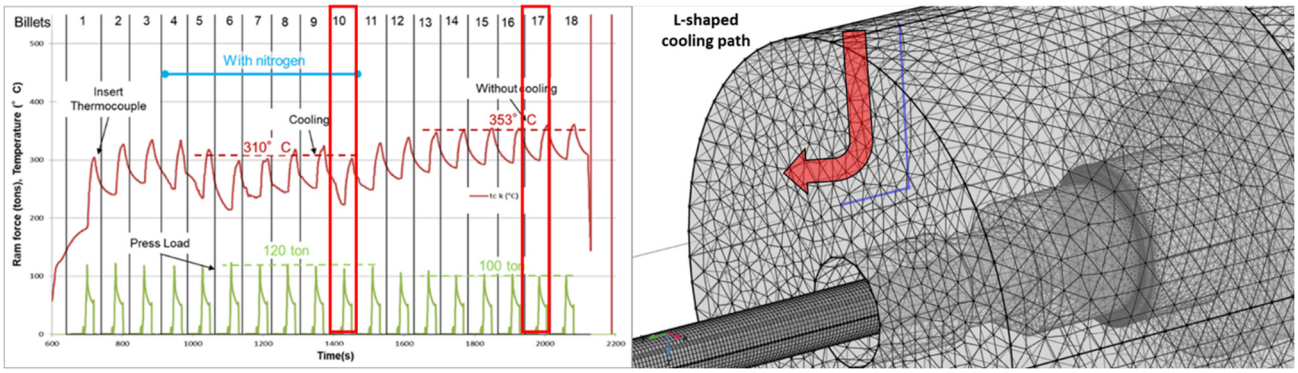

Fig. 49 Selection of the extrusion conditions for the Experimental-Numerical comparison (ZM21)

Table 9 Process Parameters and boundary conditions set for Multi-Die case study

Process Parameters	**Value (AA6063)**	**Value (ZM21)**
Billet Temperature	450 °C	300 °C
Die Temperature	450 °C	300 °C
Container Temperature	376 °C	376 °C
Ram Temperature	430 °C	280 °C
Ram Speed	4.2/6.5 mm/s	4 mm/s
Ram, Container/billet interface	No slip condition + Heat exchange by convection	No slip condition + Heat exchange by convection
Die/billet interface	No slip condition + Heat exchange by conduction	No slip condition + Heat exchange by conduction
Bearings/billet interface	Slip condition + Heat exchange by conduction	Slip condition + Heat exchange by conduction
Inlet Nitrogen Pressure or Inlet nitrogen flow rate	4 bar (100%)	4 bar (100%)
Inlet Nitrogen Temperature	-196 [°C]	-196 [°C]
Nitrogen Density (Liquid/Gas) (-196 °C, room pressure)	806.59/4.56 [kg/m^3]	806.59 [kg/m^3]
Dynamic Viscosity (Liquid/Gas) (-196 °C, room pressure)	1.6137E-4/5.4273E-6 [Pa*s]	1.6137E-4 [Pa*s]
Nitrogen heat capacity at constant pressure Cp (Liquid/Gas) (-196 °C, room pressure)	2.041/1.123 [J/g*K]	2.041 [J/g*K]

Nitrogen thermal conductivity k (Liquid/Gas) (-196 °C, room pressure)	0.1465/0.00700 [W/m*K]	0.1465 [W/m*K]
Surface roughness of the channel (ε)	0.046 mm	0.046 mm

Table 10 Flow stress parameters of Zener-Hollomon model for AA6063 [44] and ZM21 [39]

Flow stress parameters	**AA6060**	**ZM21**
Q parameter of Zener-Hollomon model	203.399 [KJ/mol]	141.441 [KJ/mol]
A parameter of Zener-Hollomon model	$6.063*10^{12}$ [1/s]	$1.35*10^{12}$ [1/s]
n parameter of Zener-Hollomon model	5.108	3.6
α parameter of Zener-Hollomon model	0.0456 [1/MPa]	0.0238 [1/MPa]

The die mesh consisted of 442107 tetrahedral mesh with 5 mm of maximum element size and 0.5 mm of minimum element size. The cooling channel was meshed with 593 edge elements to obtain an average size of 0.5 mm. The aluminum domain consisting of 218695 elements was divided into two parts: the exit profile meshed with a structured hexahedral mesh, the billet and the material under deformation meshed with tetrahedral elements. About the L-shaped cooling channel for magnesium alloy 200 edge elements were used with average size of 0.5 mm. Overall, it may be noted a smaller average size of the mesh compared to the Benchmark 2011 case study, since the dimension of the channel and the tooling set were reduced compared to the industrial standard, thus obtaining fewer elements despite the use of finer mesh.

5.4.1 Aluminum Alloy (AA6063)

Fig. 50 shows the axial section of the three simulated conditions: uncooled, stationary cooling, cooling with higher extrusion speed, respectively. The 17th extrusion was chosen for the comparison with the liquid nitrogen cooling model, because it registered the lowest thermocouple temperature, probably related to the highest percentage of liquid phase in the channel. The colder blue regions around the bearings in Figs. 50b, c highlighted the relevant thermal effect of the conformal cooling in the insert. The impact on the profile was also significant with a decrease of 30 °C in the exit temperature (from 405°C to 370°C). In the condition at higher ram speed, a profile exit temperature comparable to the uncooled condition at lower ram speed was obtained, showing the potential to increase the production rates with nitrogen cooling.

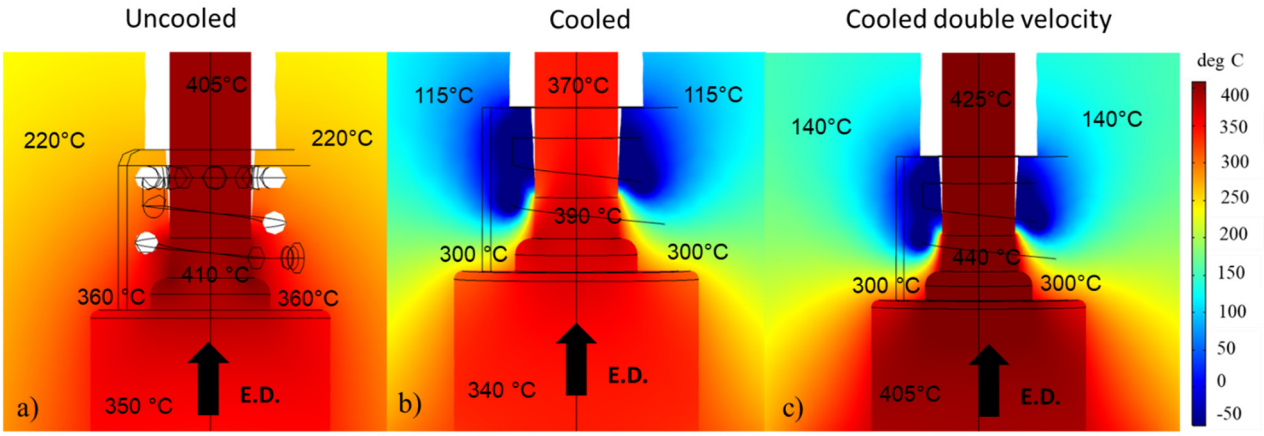

Fig. 50 Thermal field of the simulated extrusion processes (AA6063): a) uncooled condition (billet 7); b) stationary cooled condition (billet 17); c) cooled condition at higher extrusion speed (billet 24)

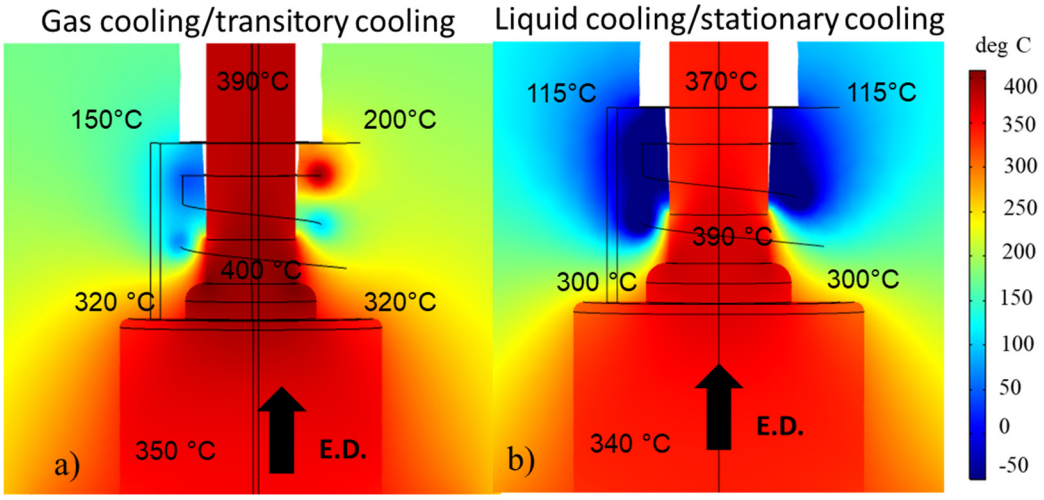

Fig. 51 Comparison between the transitory cooling with gas nitrogen model (billet 10) and the stationary cooling with liquid nitrogen model (billet 17)

Fig. 51 highlights the differences between the transitory (billet 10) and the stationary (billet 17) cooling. It is immediately clear the lower cooling effect of the gas nitrogen that, in this case, well represented the transitory cooling phase found during the experimental campaign. However, since the phase change was not considered, the accurate assessment of the cooling evolution (i.e. liquid/gas mixture within the channel) was limited to the evaluation of two extreme conditions (only gas or only liquid) even if with very low computational time.

Tables 11 summarizes the comparisons between numerical and experimental results in terms of insert temperature and extrusion load. The accuracy of the numerical model was confirmed by the reduced discrepancies with maximum percentage errors of -6.3 % and 14.0% in terms of temperature (billet 24) and extrusion load (billet 10), respectively. About the extrusion load the error was considerable acceptable, because of this entity it cannot affect the selection of the extrusion press (always enough oversized), and in addition, it did not significantly impact in terms of thermal field prediction.

Table 11 Experimental-Numerical comparison for AA6063

Extrusion Process Condition	Temperature (°C)	Load (MN)
Experimental no cooling	387	0.98
Numerical no cooling	392	1.09

% Err (Billet 7)	1.3 %	11 %
Experimental cooling	275	1.21
Numerical cooling	285	1.19
% Err (Billet 17)	3.6 %	-1.7 %
Experimental cooling with higher extrusion speed	375	1.08
Numerical cooling with higher extrusion speed	353	1.02
% Err (Billet 24)	-6.3 %	-5.6 %
Experimental transitory cooling	353	0.99
Numerical transitory cooling	342	1.13
% Err (Billet 10)	-3%	14%

5.4.2 Magnesium Alloy (ZM21)

For the magnesium alloy, the extrusion of 10th billet was used as benchmark for the simulation with nitrogen cooling, while the 18th billet for the uncooled one. Fig. 52 shows the results of the simulation performed by considering the alternative non-conformal channel used during the experimental trials. The cooling effect was lower than the one achieved in the conformal solution of aluminum test, but it was not negligible. Indeed, in the bearings, as well as in the exit profile, a decrease of temperature of 20 °C with respect to the uncooled condition was detected.

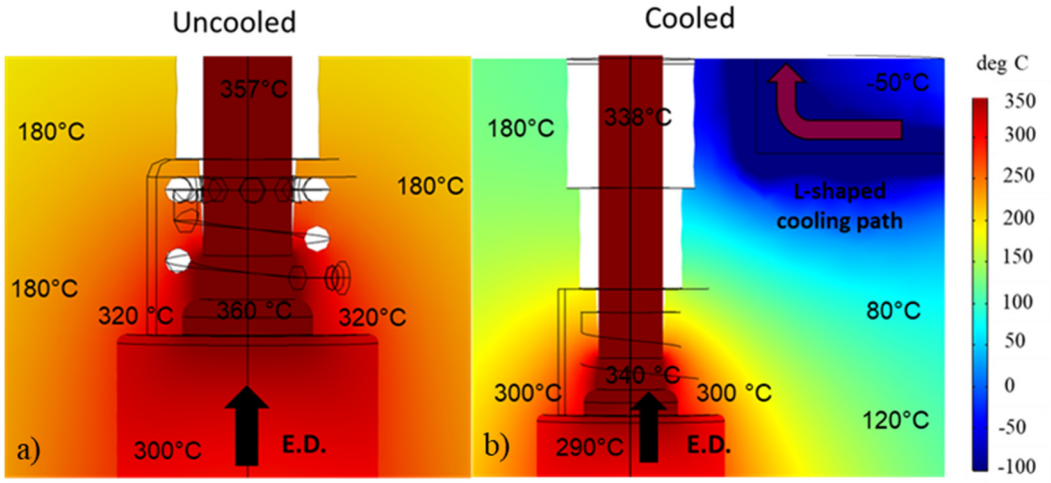

Fig. 52 Thermal field of the simulated extrusion processes (ZM21): a) uncooled condition; b) cooled condition

A peak error of 7.5% detected in terms of temperature prediction as well as the underestimation of 4.5% found in terms of extrusion load (billet 10), confirmed again the accuracy of the numerical model (table 12).

Table 12 Experimental-Numerical comparison for ZM21

Extrusion Process Condition	Temperature (°C)	Load (MN)
Experimental no cooling	361	0.99
Numerical no cooling	347	1.03
% Err (billet 18)	-3.9 %	4 %
Experimental cooling	308	1.11
Numerical cooling	331	1.06
% Err (billet 10)	7.5 %	-4.5 %

5.5 Profilati Case Study: Experimental-Numerical Comparison

For Profilati case study transient simulations were implemented for the first time, testing both the gas and liquid nitrogen models with the aim to capture the evolution of the thermal field during the whole extrusion campaign. Actually, Eulerian approach considers the billet as a continuous fluid that flows within the container and the die; thus, during the transient simulation, the model simulated the extrusion of a single virtual billet for the whole simulation time. For this reason, the numerical results showed an initial peak of temperatures generated by the billet in deformation then, after the transitory, the temperatures reached a steady-state condition. On the contrary, the experimental results showed a peak of temperatures and a cooling down during each billet change.

After the transitory analysis, three steady state conditions were evaluated (Fig. 53): without any cooling for comparison with the 4th billet, using the gaseous nitrogen model for the comparison with the 12th billet (connecting pipe partially covered by ice), then using the liquid nitrogen model only as comparison with the 17th billet (highest cooling obtained experimentally). Even if the phase change was not considered as declared in the previous sections, in this case it will be shown how the analysis of the nitrogen thermal map could give significant qualitative information about the gas nitrogen formation along the cooling path. For the billet and the material inside the die a tetrahedral mesh with 1200053 elements (maximum size of 5 mm) were used (Fig. 53). For the die a tetrahedral mesh with 953700 tetrahedral elements (maximum size of 10 mm) were used. In the bearings and the profile, a mesh with 202000 hexahedral elements were chosen obtaining a minimum of 3 elements within the profile thickness in order to guarantee a correct calculation of temperature and velocity field. The process parameters and the boundary conditions were set to replicate the experimental setting and they are reported in Table 13. Specifically, the uncooled simulation used, as initial values, the initial conditions of billet 1, while the cooled simulations both started from the steady-state condition obtained in the uncooled simulation (billet 4). In the backer surfaces in contact with press, a heat flux with a constant temperature of 280 °C was imposed, experimentally suggested by the temperature of 300 °C registered by P1 in the steady-state uncooled condition. In both simulations with nitrogen cooling, the same pressure gradient was imposed between the inlet and the outlets of the channels and equal to the amount needed to get 80 Kg/h of liquid nitrogen flow rate, value suggested by the nitrogen plant supplier. In Table 14 are reported the flow stress parameters of Zener-Hollomon model for AA6060, the same used in the Benchmark 2011 case study.

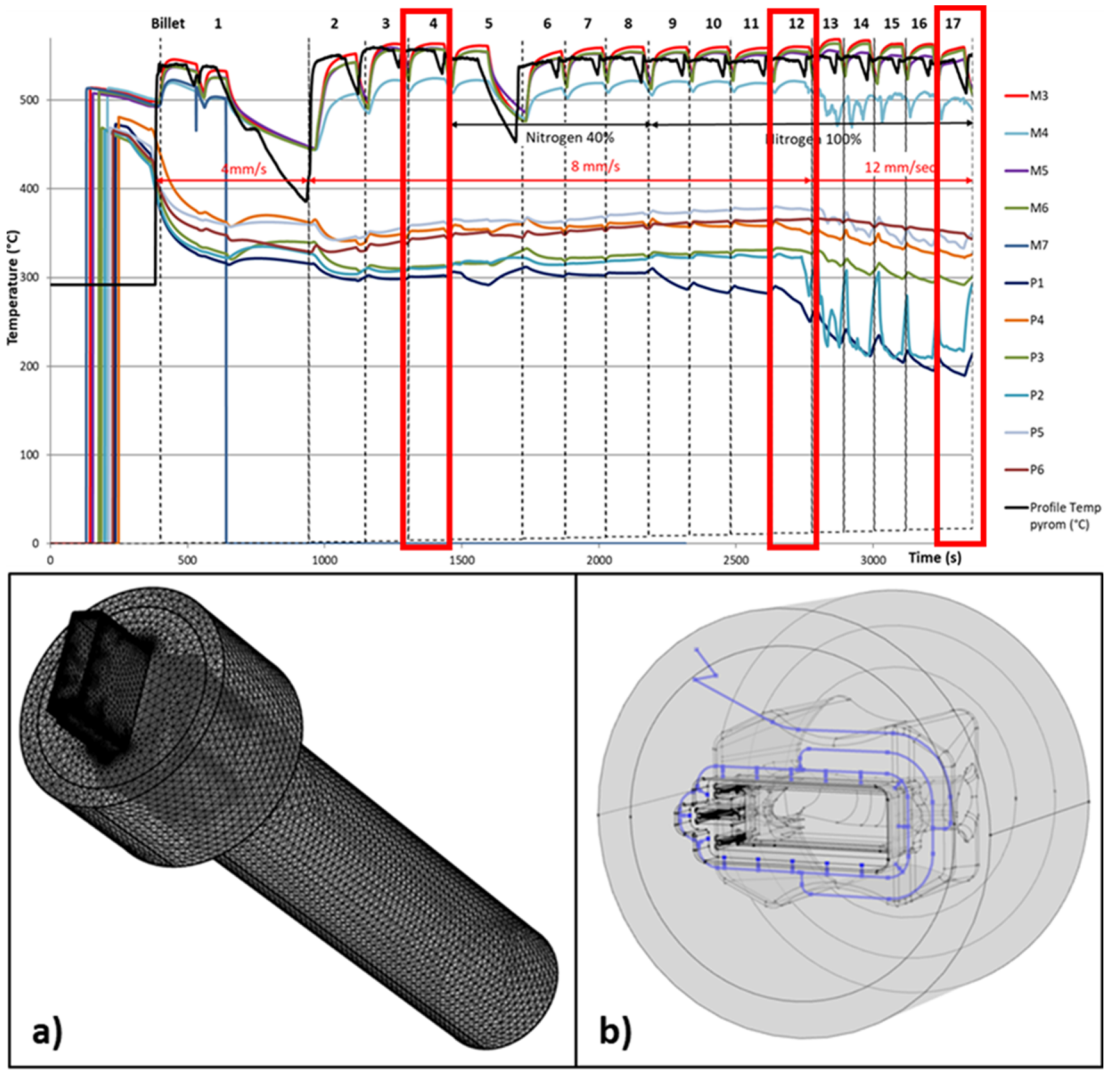

Fig. 53 Selection of the extrusion conditions for the Experimental-Numerical comparison

Table 13 Process parameters, boundary conditions and nitrogen properties for Profilati case study

Process Parameters	Uncooled Process	Gas nitrogen cooling	Liquid nitrogen cooling
Billet Temperature	480 °C	480°C	480 °C
Die Temperature	510 °C	Initial value steady state uncooled simulation (End of Billet 4)	Initial value steady state uncooled simulation (End of Billet 4)
Container Temperature	430 °C	430°C	430°C
Ram Temperature	440 °C	440°C	440°C
Temperature of backer surfaces in contact with press	280 °C	280 °C	280 °C
Ram Speed	8 mm/s	8 mm/s	12 mm/s

Ram, Container/billet interface	No slip condition + Heat exchange by convection	No slip condition + Heat exchange by convection	No slip condition + Heat exchange by convection
Die/billet interface	No slip condition + Heat exchange by conduction	No slip condition + Heat exchange by conduction	No slip condition + Heat exchange by conduction
Bearings/billet interface	Slip condition + Heat exchange by conduction	Slip condition + Heat exchange by conduction	Slip condition + Heat exchange by conduction
Inlet Nitrogen Flow Rate	-	6.04 Kg/h	80 Kg/h
Inlet Nitrogen Temperature	-	-196°C	-196°C
Nitrogen Density (-196 °C, room pressure)	-	4.56 kg/m^3	806.59kg/m^3
Dynamic Viscosity (-196 °C, room pressure)	-	1.6137E-4 [Pa*s]	5.4273E-6 [Pa*s]
Nitrogen heat capacity at constant pressure Cp (Liquid/Gas) (-196 °C, room pressure)	-	1.123 J/g*K	2.041 J/g*K
Nitrogen thermal conductivity k (Liquid/Gas) (-196 °C, room pressure)	-	0.00700 W/m*K	0.14605 W/m*K
Surface roughness of the channel (ε)	-	0.046 mm	0.046 mm

Table 14 Flow stress parameters of Zener-Hollomon model for AA 6060 [116]

Flow stress parameters	**AA6060**
Q parameter of Zener-Hollomon model	161 KJ/mol
A parameter of Zener-Hollomon model	7.6301*10^{10} 1/s
n parameter of Zener-Hollomon model	4.67
a parameter of Zener-Hollomon model	0.035 1/MPa

Figs. 54 and 55 show the computed thermal map of the die and the backer in the thermocouple mid-plane for the three different cooling conditions. In the simulation without cooling, the thermal map presented a range of temperatures around 560 °C nearby the bearing zones, and it was immediately clear that the simulation with gas nitrogen cooling did not impact significantly to the die thermal map (Fig. 54b). Using the liquid nitrogen cooling, a noticeable drop of temperatures towards the external surface of the die was obtained, however, the small cooling effect around the bearings confirmed the experimental evidence. Notably, the small temperature drop was clear and visible around M4, M5 and M7, while a minor effect nearby M3 and M6 was observed.

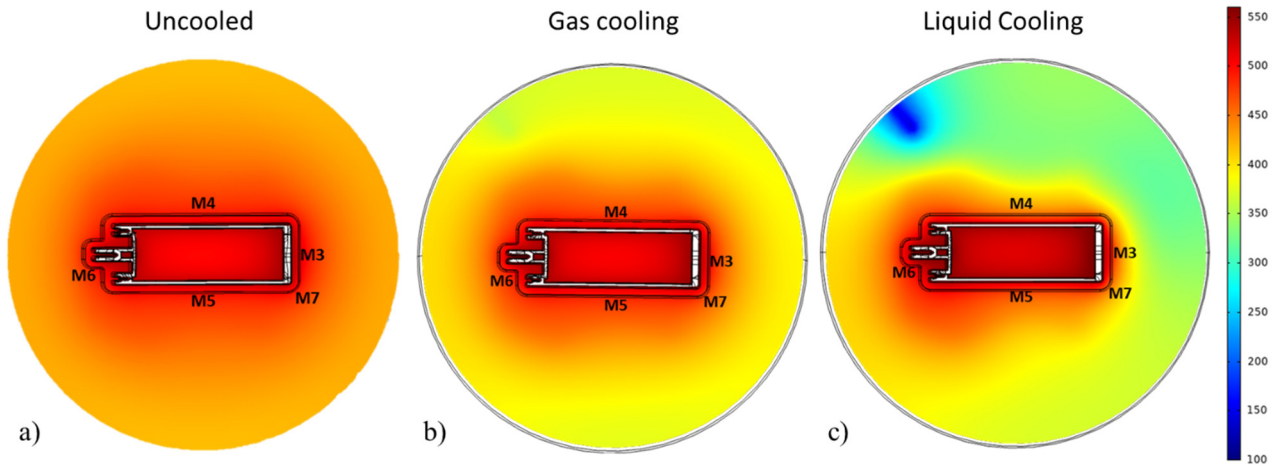

Fig. 54 Thermal map of the die in steady state condition: a) uncooled, b) gas cooled process, c) liquid cooled process

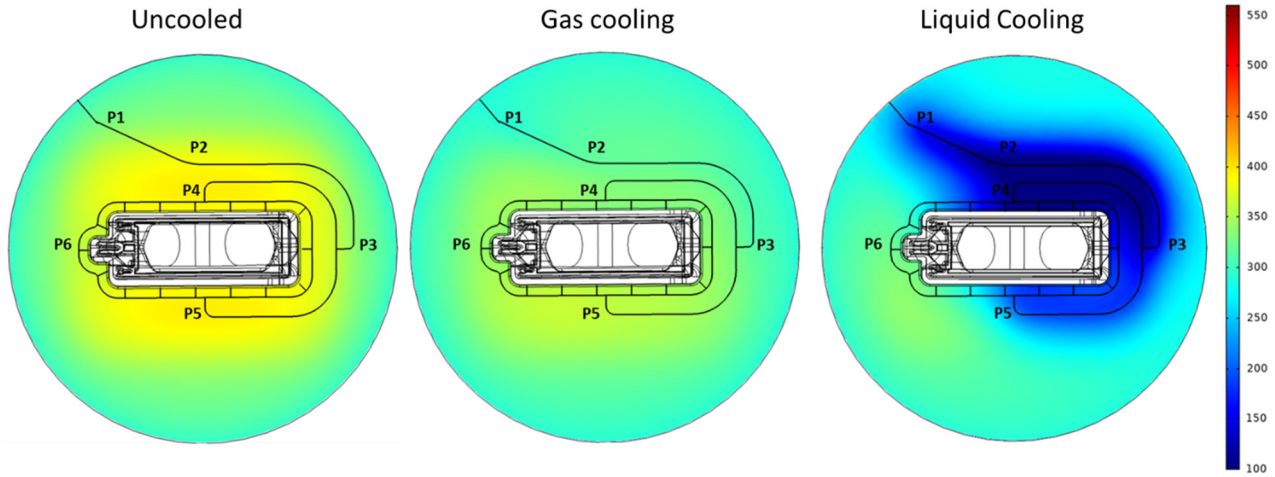

Fig. 55 Thermal map of the backer in steady state condition: a) uncooled, b) gas cooled process, c) liquid cooled process

In the backer, the thermal map of the gas cooled condition showed a small cooling effect, obtaining the maximum drop of temperatures of about 20 °C in the region around P1. The liquid nitrogen underlined a greater cooling effect, made clear by the deep blue region across the channel. However, the cooling turned out to be less effective around P5 and negligible nearby P6, thus clearly pointing out the limits of the channel design.

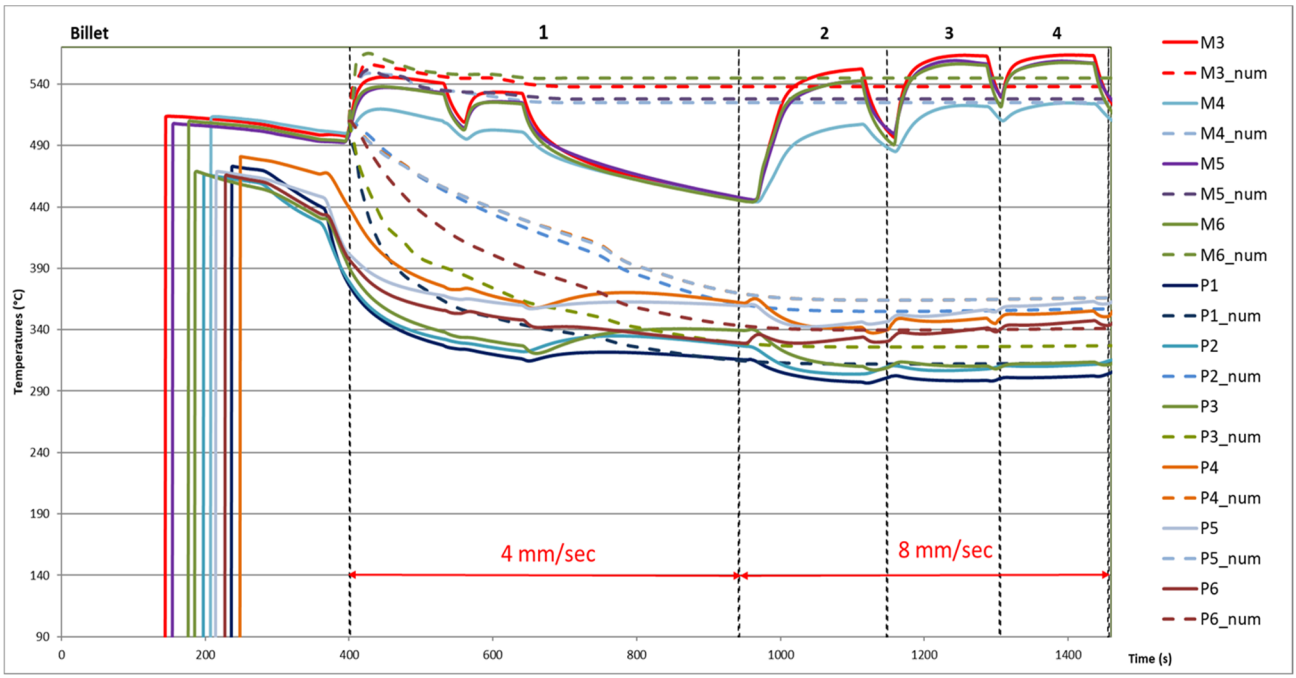

Fig. 56 Temperature history of the extrusion process: Experimental-numerical comparison without cooling

In Fig. 56, the experimental data of all the thermocouples were overlapped to the values computed by the transient uncooled simulation (from billets 1 to 4). As previously discussed, the Eulerian approach considers the billet as a continuous fluid that flows within the container and the die; for this reason, numerical results in the die (M3-M6) showed an initial peak of temperatures generated by the billet in deformation then, after the transitory, the temperatures reached a steady-state condition for the whole process, unlike the experimental data that showed a peak of temperatures and a cooling down during each billet change. Similar considerations can be drawn for backer locations (P1-P6) unless the initial thermal increase not detected in both experimental and numerical data. The reached numerical steady-state condition evidenced a cooling down after the initial peak of temperature, related to the simulated billet cooling in the container. Indeed, the boundary condition in the billet replicated a convective heat transfer with the container at constant temperature (430 °C). This condition cooled excessively the "long virtual billet" during the transient analysis, while the preheated temperature of each new real billet was higher (480 °C). However, the maximum underestimation of 32 °C registered in M5 (528 °C against 560°C) did not affect the reliability of the predicted results in terms of die thermal field. In the backer, the experimental-numerical comparison at the end of the transitory showed a good matching with small overestimation except for P2 (357 °C num. against 311 °C exp.). Moreover, the boundary conditions set to replicate the heat exchange with the air and the "cold" part with the press well captured the transitory phase experimentally observed in the backer during the first extrusion (Fig. 56). Tabs. 15 and 16 summarized the experimental-numerical comparisons for the steady-state uncooled condition. The accuracy of the numerical predictions was assessed by the errors always below the 6% in all thermocouples except for P2 (14.8%). In terms of extrusion load, a peak of 20.5 MN was predicted against 23.3 MN experimentally acquired, with an error of the 12%.

Table 15 Comparison between the experimental acquired temperatures in the backer and the predicted numerical results (Billet 4)

Billet 4	**Thermocouples Temperature [°C]**	**Cooling**

	P1	P2	P3	P4	P5	P6	
Experimental	300	311	313	355	360	345	**NO**
Numerical	313	357	327	366	366	341	**NO**
Err%	+4.3%	+14.8%	+4.5%	+3.1%	+1.7%	-1.2%	

Table 16 Comparison between the experimental acquired temperatures in the die and the predicted numerical results (Billet 4)

Billet 4	**Thermocouples Temperature [°C]**					**Profile Exit T [°C]**	**Cooling**
	M3	**M4**	**M5**	**M6**	**M7**		
Experimental	565	525	560	560		556	**NO**
Numerical	538	525	528	545	525	549	**NO**
Err%	-4,8%	0%	-5,7%	-1,3%		-1,3%	

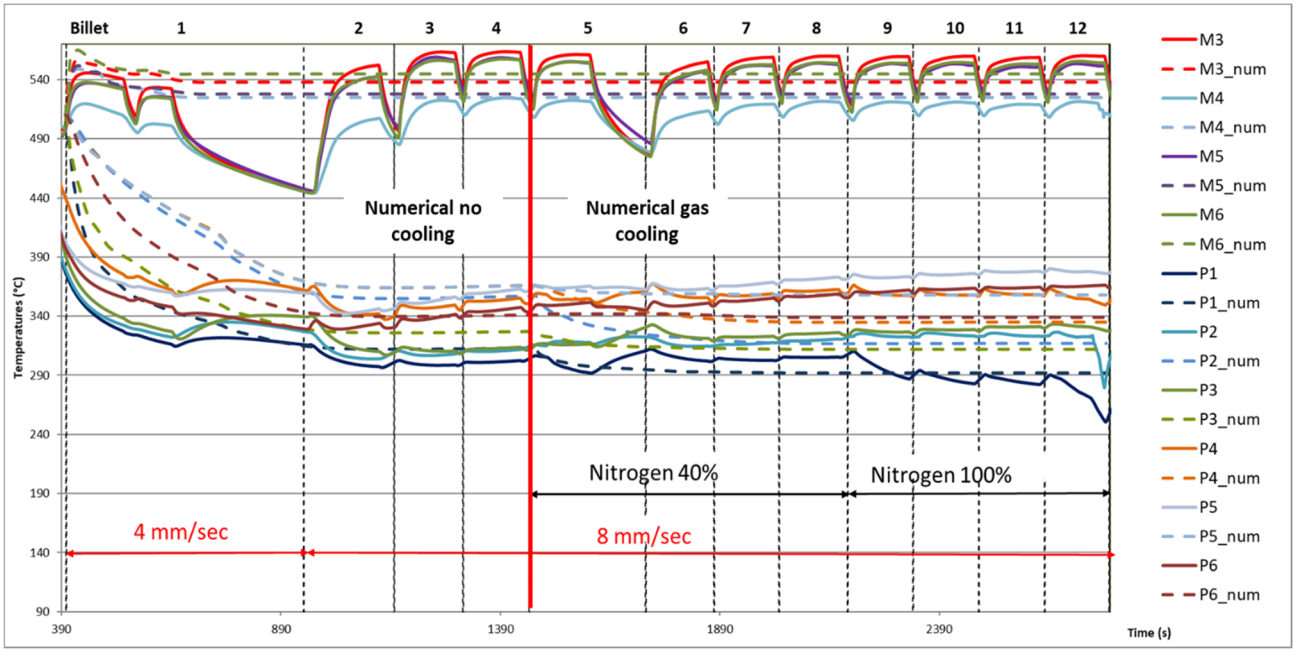

Fig. 57 Temperature history of the extrusion process: Experimental-numerical comparison in the gaseous cooled condition

The simulation of gaseous nitrogen cooling was compared to the experimental results, starting from the 5th billet up to the 12th (Fig. 57). The numerical computation started from the steady-state uncooled thermal condition (end of billet 4) using gaseous model, 100% valve opening and 8 mm/s of ram speed. Indeed, regardless of nitrogen flow rate (40% or 100%) the connecting pipe started to be covered by ice only from billet 12 while, during the previous extrusions, only gas nitrogen was flowing within the channel.

In the die, the numerical outcomes matched the experimental cooling inefficiency, further underlining the minor cooling effectiveness of gas nitrogen. In the backer, during the extrusion of billets 5 to 11,

a fine accuracy of the numerical model was found for locations P1 to P3 whilst for locations P4 to P6 the simulation provided a slight underestimation of the temperatures. However, at the end of the 12th extrusion the liquid nitrogen started experimentally flowing in P1, thus affecting also P2. The remaining locations were affected by the effect of gaseous-liquid mixture with a drop of temperatures higher respect the previous extrusions. Therefore, a better matching was achieved in locations P2 to P4 if data at the end of the billet 12 were analysed, obtaining consequently a numerical overestimation of the experimental temperature in P1. Tables 17 and 18 reports the comparison of simulated and experimental temperatures at the middle of billet 12 with errors always below the 8%. In terms of extrusion load, a simulated peak value of 21 MN was obtained against 24MN experimentally acquired (error of 12.5%).

Table 17 Comparison between the experimental acquired temperatures in the backer and the predicted numerical results (Billet 12)

Billet 12	**Thermocouples Temperature [°C]**						**Cooling**
	P1	**P2**	**P3**	**P4**	**P5**	**P6**	
Experimental	272	325	329	351	360	347	**Gaseous**
Numerical	292	317	312	335	358	339	**Gaseous**
%Err	+7.4%	-2.5%	-5.2%	-4,6%	-0.6%	-2.3%	

Table 18 Comparison between the experimental acquired temperatures in the backer and the predicted numerical results (Billet 12)

Billet 12	**Thermocouples Temperature [°C]**					**Profile Exit T [°C]**	**Cooling**
	M3	**M4**	**M5**	**M6**	**M7**		
Experimental	560	516	552	554		545	**Gaseous**
Numerical	538	525	528	545	525	548	**Gaseous**
%Err	-3.9%	+1.7%	-4.3%	-1.6%		+0.6%	

The simulation data of the liquid cooled condition (100% valve opening and an extrusion ram speed of 12 mm/s) were overlapped with the experimental data for billets 13 to 17 (Fig.58). In the die, the increase of ram speed caused an initial raise of temperature in all thermocouples, as visible during the processing of billet 13. Liquid nitrogen cooling generated a decrease of temperatures in M4 and M5, while a negligible cooling was detected in the other thermocouples, in good agreement with the experimental results. In the backer, the numerical cooling was more effective than in the experimental trials, with a good temperature matching only for P1 due to the presence of liquid-gas mixture nitrogen within the whole channel (from P2 to P5). Finally, a good correlation was also found for P6 with a negligible temperature decrease both in the numerical and the experimental results.

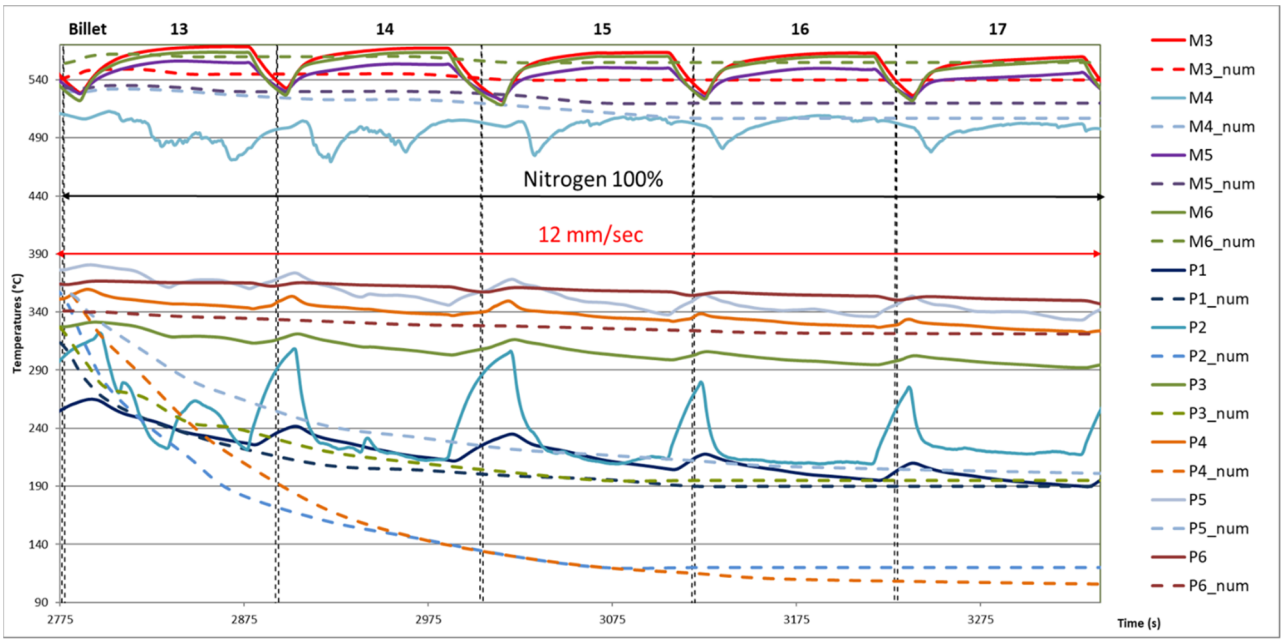

Fig. 58 Temperature history of the extrusion process: Experimental-numerical comparison in the liquid cooled condition

Tables 19 and 20 summarize in detail data for billet 17. In the backer, a peak error of -67.8% was found in P4 temperature prediction, but in P1 and in P6 the error was of 3.1% and 8.3%, respectively. In the die, errors were always below 5%. In terms of extrusion load, both in the numerical prediction and in the experimental results, the increase of loads remained under 10% (numerically, from 20.5 MN of billet 4 to 22 MN of billet 17, experimentally from 23.3 MN to 25.5 MN).

Table 19 Comparison between the experimental acquired temperatures in the backer and the predicted numerical results (Billet 17)

Billet 17	**Thermocouples Temperature [°C]**						**Cooling**
	P1	**P2**	**P3**	**P4**	**P5**	**P6**	
Experimental	196	219	296	326	340	350	**Liquid**
Numerical	190	120	195	105	200	321	**Liquid**
%Err	-3.1%	-45.2%	-34.1%	-67.8%	-41.2%	-8,3%	

Table 20 Comparison between the experimental acquired temperatures in the die and the predicted numerical results (Billet 17)

Billet 17	**Thermocouples Temperature [°C]**					**Profile Exit T [°C]**	**Cooling**
	M3	**M4**	**M5**	**M6**	**M7**		
Experimental	560	502	547	557		541	**Liquid**
Numerical	540	507	520	555	490	555	**Liquid**

%Err	-3.6%	+1.0%	-4.9%	-0.4%	+2.6%

Finally, even if the numerical model of nitrogen cooling did not consider the phase change, the analysis of the nitrogen temperature within the channel could provide information about nitrogen phase. With the assumption that all pressure drops in the channel are negligible, the range of pressure within the channel is about 3-4 bars and, in this condition, the boiling temperature of nitrogen is about -186 °C (Fig. 58) [18]. The information obtained by the liquid nitrogen thermal map (Figs. 59a, b) of billet 12 confirmed the presence of a big amount of gas along the channel. As can be deduced from the Fig. 60a, the temperature was higher than the boiling temperature along the channel, with values of -50 °C nearby P4 and P5 and of about 10 °C nearby P6. Figure 60b shows in red all the points of the cooling path with temperatures higher than the boiling point at 3 bars of pressure. Only nearby the inlet channel, the obtained temperatures suggested the presence of liquid nitrogen as also experimentally evidenced.

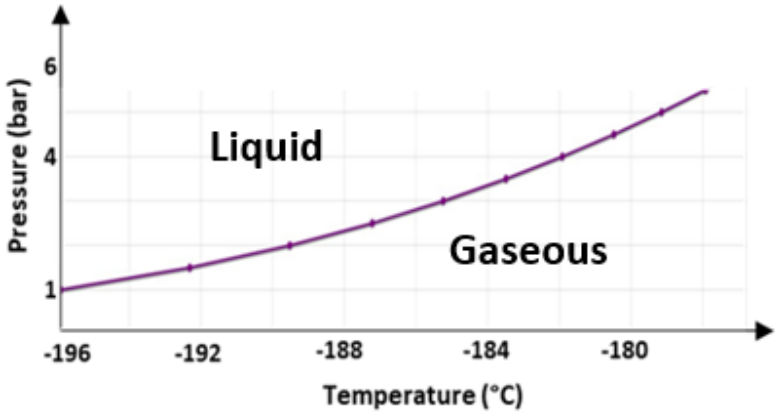

Fig. 59 Boiling point of liquid nitrogen according to the operating pressure

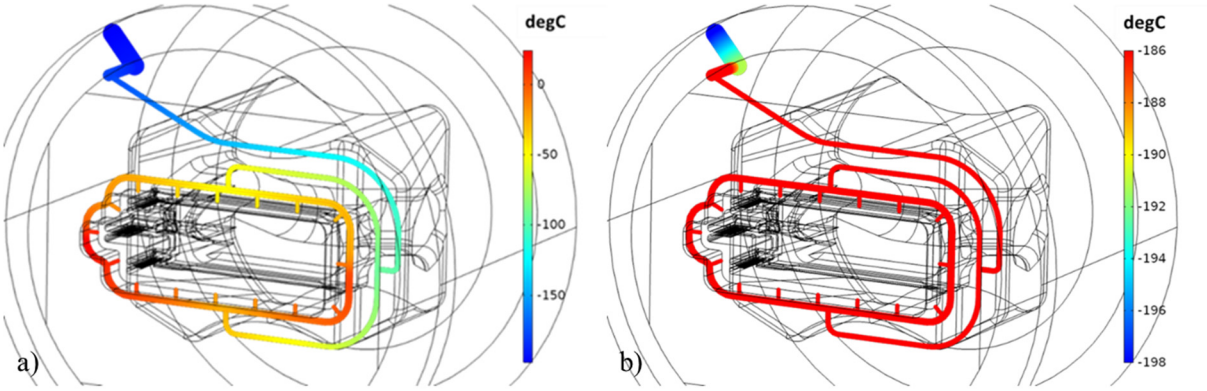

Fig. 60 Thermal map of liquid nitrogen into the channel (billet 12): a) range of temperature along the channel, b) gas formation along the channel

The proposed numerical model confirmed a good predictability of the results in terms of thermal field and extrusion load in the uncooled, gaseous cooled and liquid cooled extrusions. Moreover, the analysis clearly highlighted the limits of the tested cooling channel design, emphasising the importance of a proper tool to support the die design. However, this experimental campaign evidenced the main limitation of this first 1D numerical model. Indeed, since the phase change is not considered, it is not possible *a priori* to evaluate the gas formation, the transitory duration in liquid-

gaseous mixture state as well as the average percentage of nitrogen gas presented within the channel. Even if the simulation showed the strong limits of the selected cooling channel design, the liquid nitrogen cooling model overestimated the cooling efficiency. In the section 5.7, an integration of the numerical model based on homogeneous-flow approach will be proposed with the aim to solve the discussed limitations.

5.6 Numerical model of Hot Extrusion Process integrated within Optimization Platform: Automatic channel re-design (Benchmark 2011 Case Study)

The testing and the validation of the 3D numerical model of the extrusion process integrated with 1D model of cooling channel have brought excellent results at low computational time in terms of temperature and load prediction despite some shortcomings. The next step of the work is to propose a possible design methodology of the cooling channel perfectly integrable within the virtual prototyping phase of the die-set and matched with the requirement of the industrial framework. Many parameters are involved in the fluid-dynamic of the nitrogen flow [105] that strongly affect the cooling performances: position and geometry of the channel, inlet nitrogen parameters, nitrogen phase-change along the cooling path, thermal properties of the die among others etc. In addition, the experimental campaigns analysed during the PhD research evidenced many limits of channel design based only on die-makers experiences even if apparently seemed a good solution (i.e. Profilati case study). Therefore, this level of complexity can be more properly managed by means of numerical models and necessary demands for automatic, robust and comprehensive methodologies. Notably, the FE model of a nitrogen cooled extrusion is integrated in an optimization platform in order to iteratively and automatically adjusts the channel geometry and the process variables gaining to a final optimal solution in terms of thermal balance, cooling efficiency and nitrogen consumption. In this way, it is possible to test a large amount of design automatically, avoiding to manually and iteratively correct the channel design to obtain high cooling performances. The optimization is performed by means of the integration platform modeFRONTIER® and it is tested to virtual re-design the cooling channel of Benchmark 2011 case study that evidenced an unbalanced cooling around the bearings (sections 4.1 and 5.3). Overall, the optimization procedure starts from the variables' selection (Fig.61), that, in this case, are the cross-section properties along the channel and the nitrogen inlet pressure. Subsequently, the objective functions correlated to some outputs are chosen with the aim to guide and constraint the optimization algorithm towards the desired solution. The algorithm must be trained with an initial virtual design of experiment (DOE) properly selected. Different optimization strategies and optimization algorithm can be used within the modeFRONTIER® in accordance with the needs. Without going into the merits of this topic, two different optimization strategies are proposed and compared: in the first approach, 100 designs are generated using a genetic algorithm and automatically simulated by COMSOL, whilst, in the second approach, a meta-model is generated from an initial DOE of 100 design and then used to test a large number of designs without using the FE model.

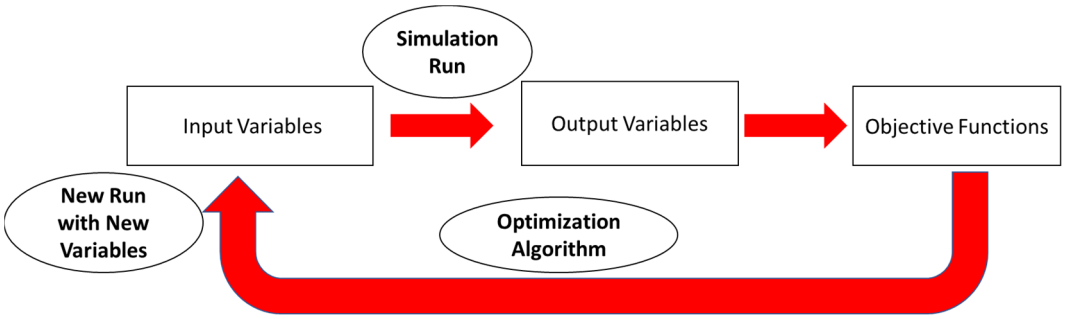

Fig. 61 Workflow of the optimization procedure

Since the computational time of about 1 hour for the simulation with nitrogen cooling is deemed excessive in order to test a significant number of channel designs in a relative short time, an equivalent numerical model is proposed in which the aluminium flow is replaced with equivalent thermal conditions to drastically reduce the required time of each simulation run.

5.6.1 Workflow Structure Design within the Optimization Platform

Recalling the Benchmark 2011 case study, an unbalanced cooling was found around the bearings with a higher drop of temperature in T5 and T3 compared to T1 (about 60 °C between T5 and T1). Therefore, the first aim of the re-design was to force the nitrogen flow towards the warmer areas around the bearings to balance the thermal gradient (Fig. 62). The cooling path was fixed because it is necessary the integration of CAD node to parameterize the pathway, and it will be an interesting future development. Therefore, the channel was divided into 10 segments within the COMSOL model (Fig. 63) in order to set the channel heights along the cooling path as input variables for the optimizer. Using the 1D model of the cooling channel, only the hydraulic diameter was employed in the fluid-dynamics equations (see section 5.1), then, that was enough to change the channel heights within the model, avoiding selecting two variables to characterize the cross-section shape of the channel. The channel height was allowed changing in the range from 1 mm to 10 mm, thus varying the hydraulic diameter from 1.7 mm to 7.5 mm along the planar path with the requirement to avoid excessive reduction of backer resistance. In the same way, the diameter of the transferring holes was varied between 2.5 mm to 6 mm. In terms of process parameters, the nitrogen inlet pressure was selected as input variable to analyse the nitrogen flow rate as a function of both channel design and valve opening. Its value was set variable in the reasonable range for industrial nitrogen plants (1.5-4 bars).

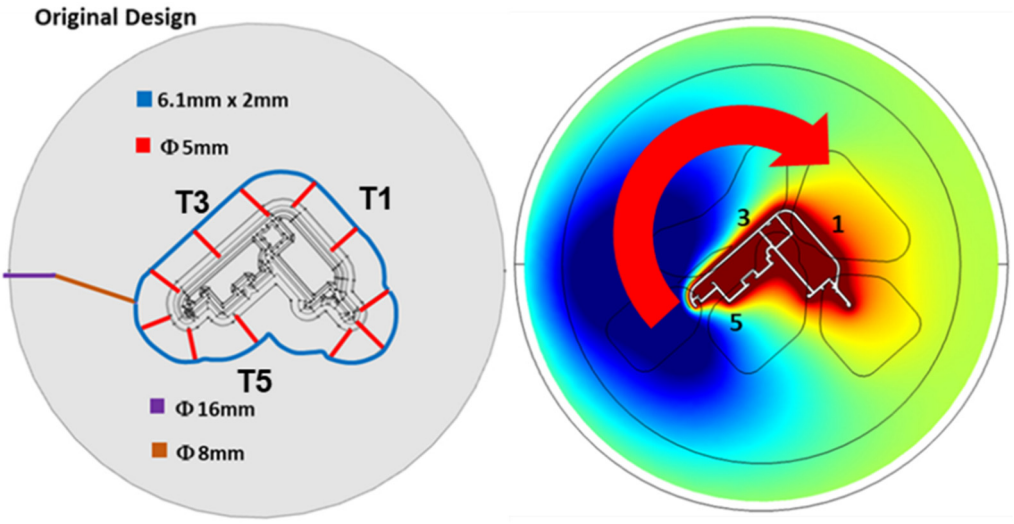

Fig. 62 Unbalanced cooling in the Benchmark 2011 case study

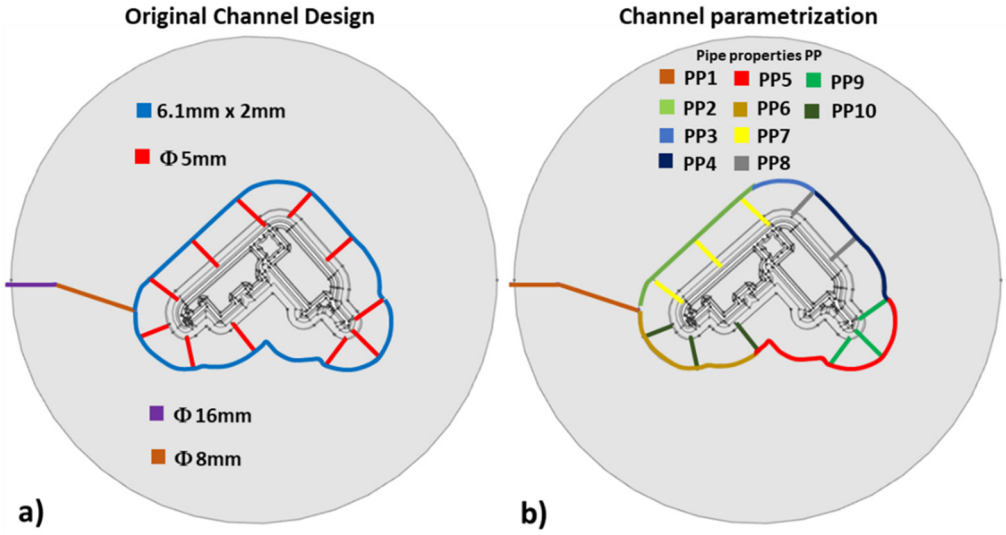

Fig. 63 Channel height parametrization along the cooling path: a) Original channel design; b) Channel divided into 10 parts

The monitored output after each run are the thermocouples' temperature and the nitrogen flow rate to control both the balancing of the cooling and the nitrogen consuming. Two objective functions were selected for the optimization. The first one (ind_error), imposed by Eq. (20), was aimed at balancing the temperature around the bearings (T1, T3, T5):

$$ind\_error = \sqrt{\frac{(T1-450)^2+(T3-450)^2+(T5-450)^2+(T1-T3)^2+(T1-T5)^2+(T3-T5)^2}{6}} + (1.01^{T1-450}-1)^2 + (1.01^{T3-450}-1)^2 + (1.01^{T5-450}-1)^2 \quad \textbf{(20)}$$

The first term of the equation under the square root drove the algorithm towards the thermal balance and the target temperature of 450°C. The other terms forced the algorithm to prefer colder solutions (e.g: the solution with T1, T2 and T5 at 400 °C is preferred to the one with all values at 500°C). The target temperature of 450 °C was selected to avoid thermal shocks in the die as well as to prevent an excessive drop of temperature in the exit profile. The second objective function was the minimization of the nitrogen flow rate in order to find a channel design that reduces the nitrogen consuming.

The COMSOL environment was integrated in the modeFRONTIER® workflow [117] by means of a DOS batch node connected to the input file of the FE model in order to update the channel design at each simulation run. The Fig. 64 shows the whole workflow created within the optimization platform. In the upper part of the workflow, the green icons represented the input variables, while the blue icons in the bottom were the outputs connected to the objective functions' nodes. The input variables were automatically selected and updated in the input file of the FE model at each run, while the outputs and the results of the objective functions were generated in the .txt file and inserted in the table inside modeFRONTIER for the subsequent analysis of the results.

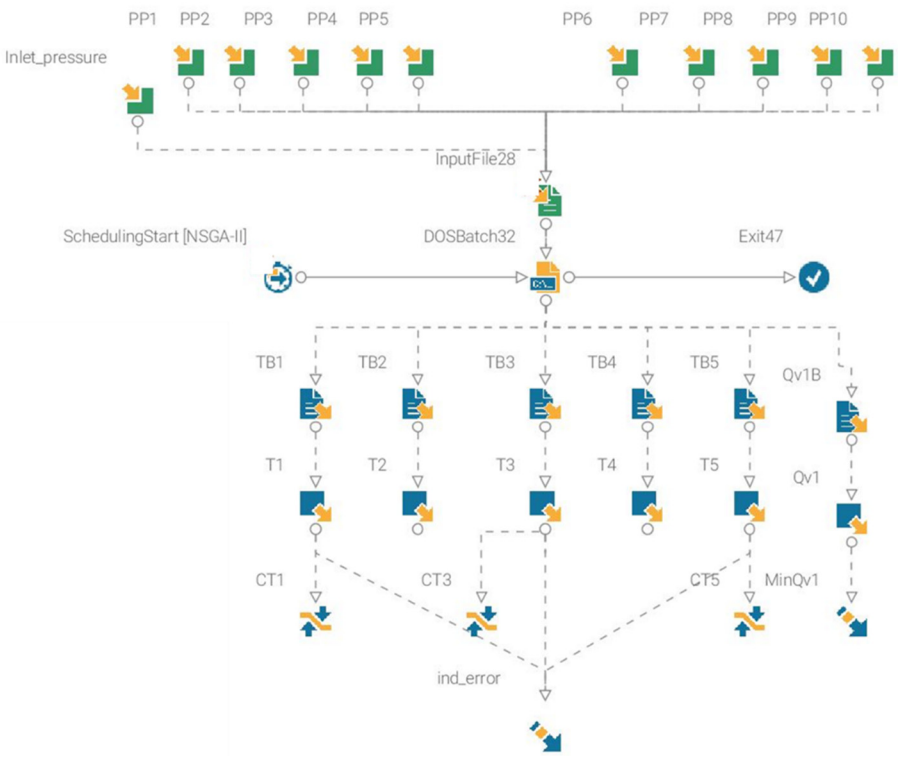

Fig. 64 modeFRONTIER ® workflow used in the channel design optimization

As previously mentioned, two different optimization strategies were proposed and compared. In the first one, the optimization algorithm was the Non-dominated Sorting Genetic Algorithm (NSGA-II) implemented in modeFRONTIER [117] with an initial population of 10 configurations identified with three different strategies: a random DOE sequence, a Pseudo-Random Sobol DOE sequence and the Uniform Latin Hypercube DOE sequence (ULH). The initial population was used to train the algorithm and it was chosen with strategies that avoid the clustering effect of uniform sampling. The number of generations evaluated was set to 10, while a mutation rate of 0.01 and a uniform crossover method with a 0.9 crossover rate were used. A total of 100 design (initial population*number of generations) were evaluated in 12 hours (laptop with Intel® core™ processor i7-7700HQ and Ram 16GB). Instead, in the second approach, starting from a Sobol DOE sequence of 100 tested designs, multiple response surfaces (RS) were created, one for each output variable, using the radial basis function (RB) interpolation tool. Then, the meta-models obtained were tested with the NSGA-II algorithm generating 10.000 design (100 initial design*100 generations) in less than 2 minutes. In summary, the low computational time of the first strategy allows to test a large number of designs using the FE model in automatic way. However, the computational time depends on the number of tested designs, and it can be time-consuming activity if the number becomes excessively high. Instead, in the second strategy, if the obtained meta-models are valid and representative of the investigated problem despite using a reduced number of designs for the training, then, it will be possible testing a very high number of solutions without time problems.

5.6.2 Equivalent numerical model of the porthole-die cooled with liquid nitrogen

In order to reduce the computational time of the FE model, the thermo-fluid dynamic study of the aluminium flow was replaced with equivalent thermal boundary conditions where the billet was in contact with the die. As well as reducing the number of the required elements, the model concerned only the thermo-fluid dynamic study of the nitrogen flow coupled with the thermal analysis of the

tooling set. Indeed, in the table 21 it may be noted that the billet and all that depend on it were not computed in this simplified model.

Table 21 Process Parameters and boundary conditions set for the simplified FE model (Benchmark 2011 case study)

Process Parameters	**Value**
Billet	Not computed
Die Temperature	500 °C
Container	Not computed
Ram	Not computed
Ram Speed	Not computed
Ram, Container/billet interface	Not computed
Die/billet interface	Heat exchange by convection
Bearings/billet interface	Heat exchange by convection
Inlet Nitrogen Pressure or Inlet nitrogen flow rate	2 bar (100%)
Inlet Nitrogen Temperature	-196 [°C]
Nitrogen Density Liquid (-196 °C, room pressure)	806.59 [kg/m^3]
Dynamic Viscosity Liquid (-196 °C, room pressure)	1.6137E-4 [Pa*s]
Nitrogen heat capacity at constant pressure Cp Liquid (-196 °C, room pressure)	2.041 [J/g*K]
Nitrogen thermal conductivity k Liquid (-196 °C, room pressure)	0.1465 [W/m*K]
Surface roughness of the channel (ε)	0.046 mm

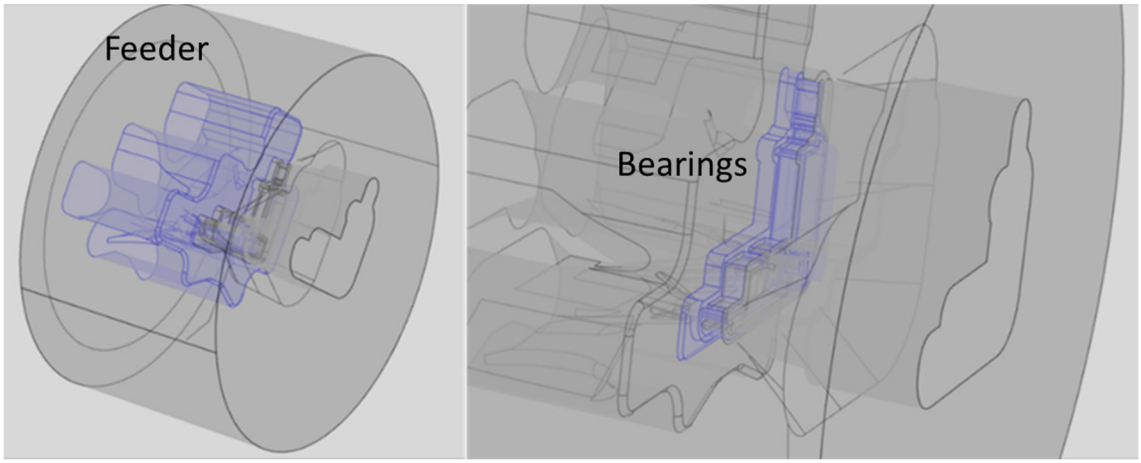

Fig. 65. Feeder and bearings surfaces where the boundary conditions replaced the heat-exchange with the aluminum flow

Moreover, the billet/die contact in the surfaces of the feeder and the bearings (Fig.65) was replaced using a convective heat flux with a temperature of 520 °C and 565 °C, respectively, for the feeder and the bearings, and using the same aluminium-steel heat transfer coefficient of 11000 W/mK. The selection of the boundary condition has been suggested by the numerical results obtained with the comprehensive model of the extrusion process. The computational time of the simplified model was about 5 min with a medium performance laptop (Intel® core™ processor i7-7700HQ and Ram 16GB), making feasible its integration in the optimization platform. In details, Figs. 66 and 67 show the thermal maps of the numerical models (100% of nitrogen flow rate) with and without the aluminium flow to prove the good comparability.

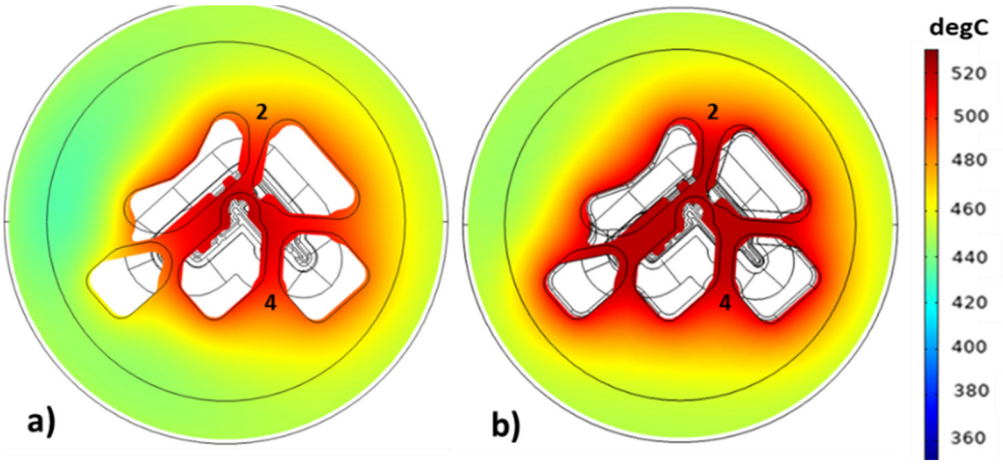

Fig. 66 Thermal field in the mandrel: a) full model b) equivalent model

In the mandrel, a slight general overestimation of the temperature was found in the equivalent model, probably in relation to the thermal boundary condition of 520 °C applied in all points of the feeder and the welding chamber. Instead, in the die an underestimation of the temperatures was evident nearby T1 in relation to the homogeneity of the temperatures in the bearings surfaces, while in the full model the bearings surfaces nearby T1 were warmer probably for different strain rate condition of the aluminium flow that increased locally the temperature. However, the goodness of the equivalent model comes from table 22 that reports the numerical-experimental comparison showing a peak error of only 1.4% in T5.

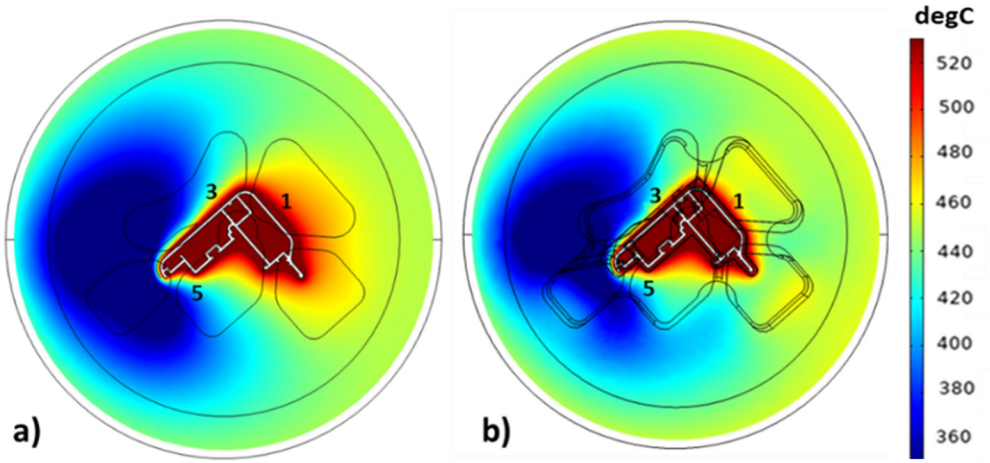

Fig. 67 Thermal field in the die: a) full model b) equivalent model

Table 22 Experimental-Numerical comparison for the equivalent model

	Thermocouples Temperature [°C]					Cooling
	T1	**T2**	**T3**	**T4**	**T5**	
Exp.	490	508	460	523	430	YES
Num.	484	514	460	517	436	YES
Err%	-1.2	1.2	0	-1.15	1.4	

5.6.3 Numerical results of the optimization procedures and selection of the new channel design

As previously mentioned, in the first approach the optimization algorithm NSGA-II was tested varying the DOE sequence generation by testing the random, the Sobol and the ULH sequences. As an example, Fig.68 summarizes the results of the optimization procedure using the Sobol DOE sequence in a bubble chart of the 4D design space: the bubbles represented the channel designs, in the x-axis they were reported as a function of a nitrogen flow rate, in the y-axis it was indicated the temperature deviation index (ind_error of Eq. 20), the diameter of the bubbles was related to the temperature of T1 that recorded the maximum temperature in the original design, and the colour of the bubbles represented the temperature of T5 that recorded instead the minimum temperature. The black bubble indicated the original design with a nitrogen flow rate of 8.7 l/min and an ind_error of 29. Meanwhile, the design positioned around the origin of the axis guaranteed solutions with thermal balance around the bearings and reduced nitrogen flow rate. For the selection of the optimal design, the linear Multiple-Criteria Decision-Making (MCDM) was used, selecting the weight of each objective function to obtain the design ranking. In this case, the same value of 0.5 was chosen for both the cooling balancing and the minimization of the nitrogen flow rate.

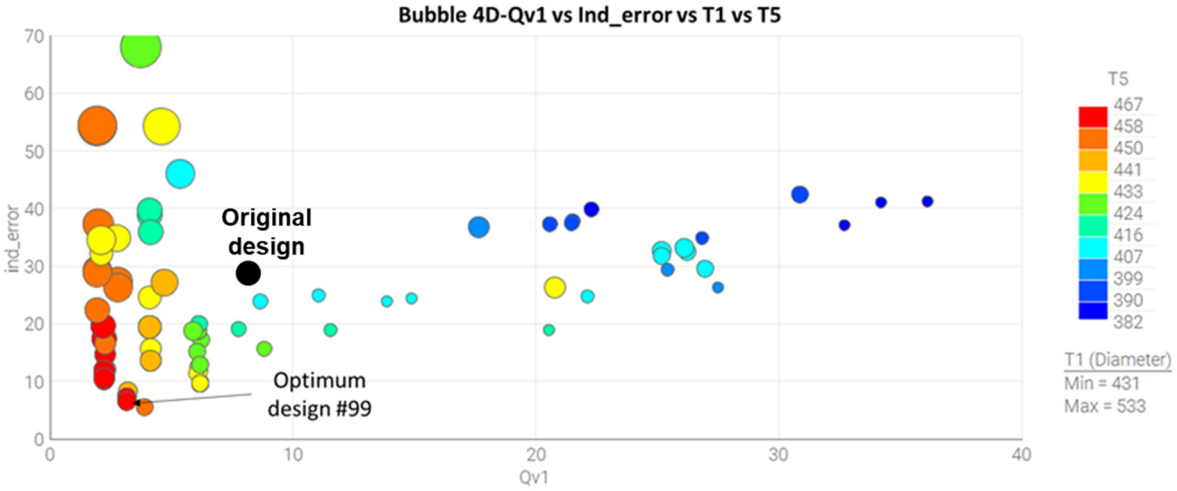

Fig. 68 Optimization results in the 4D design space using Sobol DOE sequence

In the Pareto front, as the result of the optimization with Sobol DOE sequence, the selected channel design (# 99) showed a temperature deviation index (ind_error) of 6.71 (T1=458°C, T3=453°C, T5=460°C) using a nitrogen flow rate of 3.13 l/min, thus obtaining the reduction of about 60% in terms of nitrogen consuming. In detail, Table 23 summarizes the temperature and nitrogen flow rate comparison between the three optimizations and the original design.

Table 23 Comparison between the original design and the design derived by the optimization

	#Design	T1 [°C]	T3 [°C]	T5 [°C]	Ind_error	Qv [l/min]
Original numerical design (100% nitrogen flow rate)		484	460	436		8.7
Random DOE/NSGA-II	95	462	454	436	15.85	4.22
Sobol DOE/NSGA-II	99	458	453	460	6.71	3.13
ULH DOE/NSGA-II	95	464	478	456	17.27	2.24

All three optimizations showed designs with good temperature balancing and reduced nitrogen flow rate if compared to the original one, however the best one was detected by the optimization started from the Sobol DOE. In addition, it can be notice that the solutions proposed with the Random and the ULH DOE were comparable in terms of temperature deviation, but the index value for the first one was lower since, as previously explained, a colder solution is preferred (436°C vs 478°C with a control value of 450°C).

The second optimization strategy started with the test of 100 designs generated by the Sobol sequence that were used to train meta-models in order to find relations between the input variable and the output results using the radial basis function (RB) interpolation tool. The meta-models were used to test 10000 designs (100 initial design*100 generation) in a very short time without the use of the FE model node. Fig. 69 reports the bubble chart of the 4D design space obtained with the meta-models. For the selection of the optimal design, the linear MCDM was used neglecting the unfeasible designs (i.e. those with negative nitrogen flow rate). For the same reason, in the Fig.69 the area of the unfeasible designs in the chart was truncate.

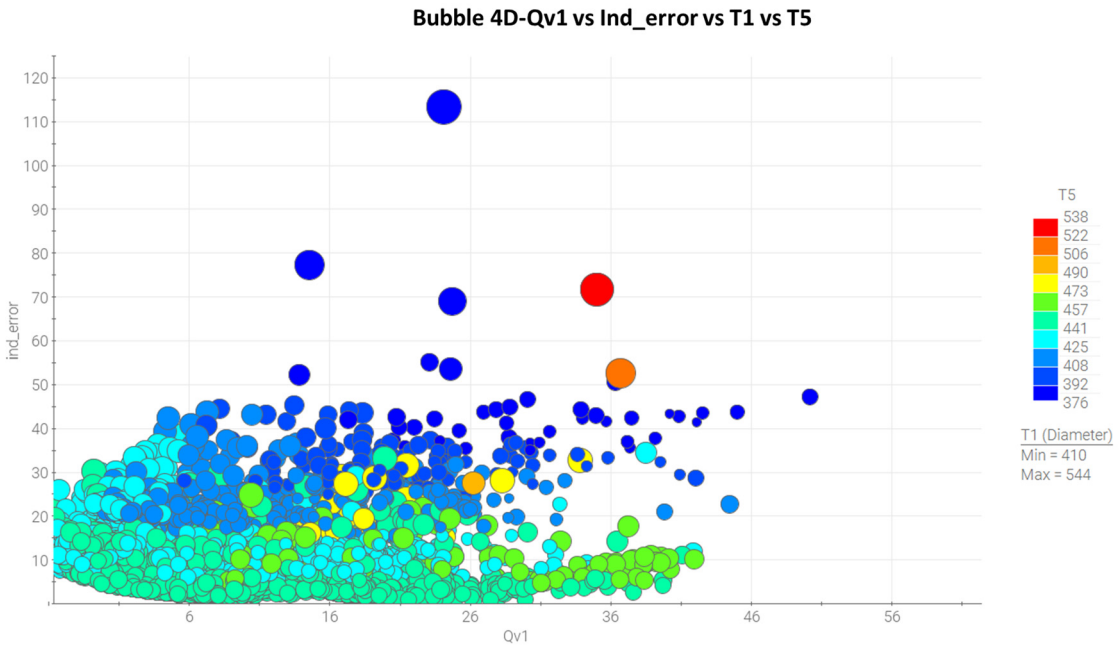

Fig. 69 Optimization results in the 4D design space using meta-models

In the Pareto front, the selected channel design (# 8004) showed the temperature deviation index (ind_error) of 2.77 (T1=453°C, T3=449 °C, T5= 448°C) and a nitrogen flow rate of 3.7 l/min. The selected design was then evaluated in COMSOL in order to test the reliability of the solution generated by the meta-models. Table 24 reports the comparison between the FE model and the meta-models results, evidencing the good matching in terms of temperature and nitrogen flow rate predictions (peak error -13.5%).

Table 24 Comparison between the meta-models and FE model results in terms of temperature and nitrogen flow rate prediction

	#Design	T1 [°C]	T3 [°C]	T5 [°C]	Ind_error	Qv [l/min]
Meta-models	8004	453	449	448	2.77	3.7
Comsol FE model	8004	466	450	455	10.37	3.2
Err%		2.9%	0.2%	1.6%		-13.5%

The solution achieved by means of the second strategy with meta-models apparently seemed better than the first one in terms of thermal balancing around the bearings. However, testing the selected design with the FE model it should be noted that the temperature deviation was comparable with the solution obtained with the first optimization strategy (Sobol DOE/NSGA-II). Improve the accuracy of the meta-models could lead to increase the potentiality of this second optimization strategy that allows testing a large number of configurations in a very short computational time.

In conclusion, Figs. 70 and 71 show the comparison between the original design and the optimal designs achieved with the two optimization strategies (Sobol DOE sequence and meta-models). The two new designs confirmed the success of the optimization procedure, obtaining an efficient and balanced cooling in the area around the bearings. Moreover, a reduction of about 60% was gained with both the optimized designs in terms of nitrogen consuming.

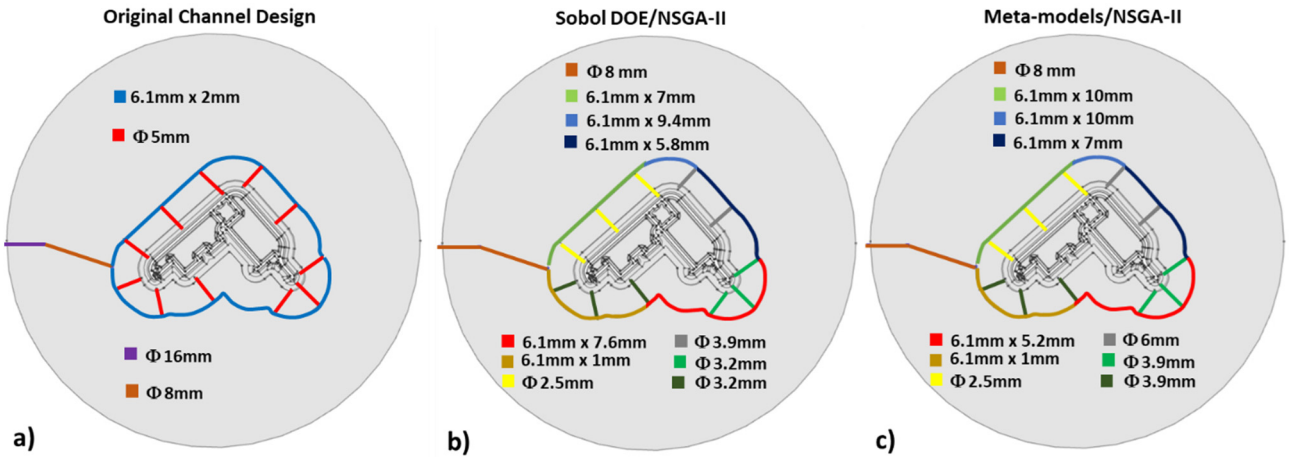

Fig. 70 Geometrical dimension of channel designs: a) Original design; b) Sobol DOE/NSGA-II design; c) Meta-Models/NSGA-II design

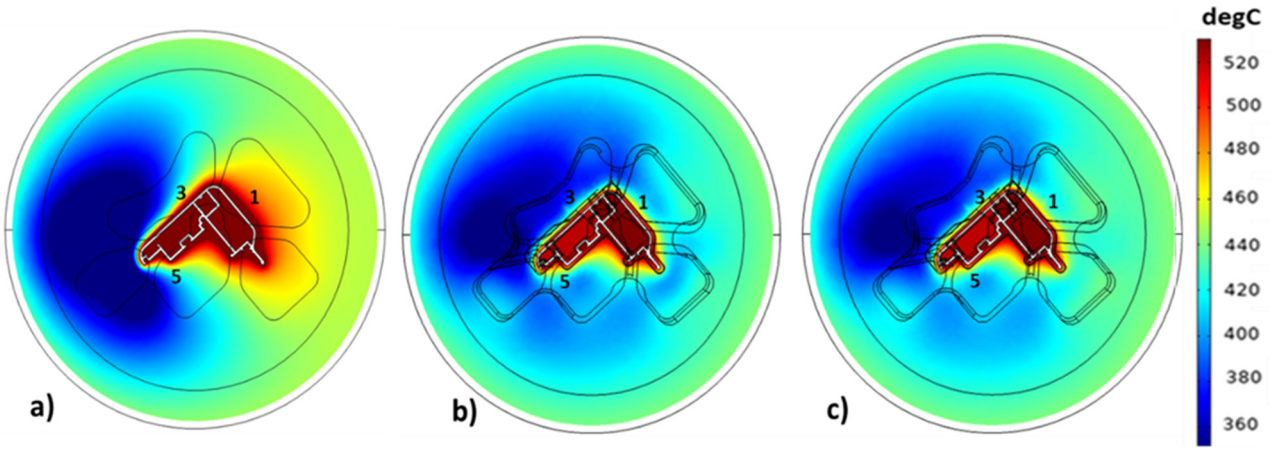

Fig. 71 Thermal field of the die: a) Original design b) Sobol DOE/NSGA-II design c) Meta-Models/NSGA-II design

5.7 A new numerical approach to evaluate the gas nitrogen generation within the channel: Homogenous Flow Model

5.7.1 Homogenous Flow Model

The 1D numerical model of nitrogen cooling, while demonstrating the issues of the proposed design, showed its greatest limit during the assessment of the Profilati case study, because the liquid nitrogen model overestimated the cooling efficiency of the channel. The experimental campaign demonstrated that the channel design caused a very long transitory and that during the last extrusion the stationary cooling condition probably was not still reached. Therefore, a mixture of liquid-gas nitrogen was present within the channel with the evolution in time of the gas nitrogen percentage. In this context, it is necessary the implementation of new model to take into account the gas nitrogen formation within the channel in terms of both pressure drop and heat exchange. Also in this case, the 1D approach is preferred to three-dimensional approach to avoid excessive computational complexity; in addition, the case studies presented in this PhD thesis have demonstrated the accuracy of the numerical results, even though performed on a single-phase nitrogen flow. However, the inherent complexity of modelling both phases – mostly related to the closure problem [113] – prompts to resort to the homogeneous-flow approach [118-119]: under the assumptions of same velocity for both liquid and gas phase (i.e., no liquid holdup) and no phase separation, the two-phase flow can be treated as a single-phase one, provided that its properties be appropriately modified to account for the actual

presence of gas and liquid. In this way, the momentum-conservation, the continuity equations as well as the conservation of energy presented in the section 5.2 are still valid. Notably, within the 1D equations previously described, the physical properties of the nitrogen are modified as a function of both liquid and gas nitrogen properties. Firstly, density ρ could be expressed as

$$\rho = \left(\frac{\omega_g}{\rho_g} + \frac{\omega_l}{\rho_l}\right)^{-1}, \tag{21}$$

where ω is mass fraction. The relationship between vapor quality and liquid mass fraction is relatively straightforward as $\omega_l = 1 - \omega_g$.

Viscosity of the homogeneous flow is also modeled to account for the presence of two phases. Notably, the classic formulation firstly proposed by Einstein and further developed to embody the effective viscosity of a two-phase flow [120] is employed to the purpose:

$$\mu = \mu_l \cdot \phi_l^{\left(\frac{\mu_l + 2.5\mu_g}{\mu_l + \mu_g}\right)}, \tag{22}$$

where liquid volume fraction is expressed as $\phi_l = (\rho/\rho_l)\omega_l$. Liquid and gas viscosity of nitrogen are implemented in the calculations, choosing the boiling point at room pressure (-196 °C). The small differences of single-phase properties in the application range (1/5 bars; -196/-170°C) do not justify the use of properties depended by temperature and pressure. In a similar manner to density and viscosity, specific heat capacity and thermal conductivity are also treated as properties of the homogeneous flow, which required appropriate formulations that combine the values for liquid and gas phase reported in available datasets [110]. To this end, the relationships proposed by Wang and Beckermann [121] are implemented, which consist of Eqns. (23) and (24) for specific heat capacity and thermal conductivity, respectively:

$$\rho \cdot c_p = \omega_l \rho_l c_l + \omega_g \rho_g c_{p,g}, \tag{23}$$

$$k = \omega_l k_l + \omega_g k_g. \tag{24}$$

The values computed for those properties are then used as an input in equations of section 5.2 to reconstruct the temperature field through conservation of energy. Also in this case, the physical properties of both liquid and gas nitrogen are chosen at the boiling point at room pressure. The implemented 1D model does not allow the density change along the channel, consequently, a constant density was selected, using a mixture with the 5% of gas mass fraction (mixture density equal to 82.3 kg/m^3). This assumption at the inlet of the channel is reasonable with the experimental evidence. Indeed, the supplied liquid nitrogen is at a temperature close to boiling point. The inlet nitrogen pressure is in the range of 3-5 bar – at least as the regulating valve is fully open and in such operating condition the boiling point is in the range -185/-179 °C [110]. The inlet nitrogen temperature is governed by the sub-cooler positioned upstream of the die, where the liquid nitrogen under pressure is cooled by means of tapped nitrogen brought to ambient pressure and consequently with lower boiling point (-196 °C at 1.01325 bar). Therefore, the liquid nitrogen enters within the channel with temperature equal or higher than -196 °C and very close to the boiling point at its operating pressure, so even the heat generated by friction losses yields to evaporation. The consistency of the density within the channel can be considered acceptable with these considerations because the differences in terms of density between mixture at 5% of gas and the 100% of gas is low (from 82.3 to 4.6 kg/m^3) if compared to the disparities of 200 times between the liquid and gas density (from 806.6 to 4.6 kg/m^3). However, the assumption of the constant density for the nitrogen can be considered the main limit of this new model and the way to consider this aspect without paying for an excessive

computational time will be further investigated. Even if the density is constant, the other physical properties are not constant and depend on the vapor quality. In this way, the effect of density change in terms of pressure drops and heat exchange is taken into account by the change of the dynamic viscosity and the heat transfer coefficient without losing the computing speed (Eqns. 14 and 22). As a first attempt, a linear function is employed to model the relationship between vapor quality and temperature of nitrogen homogeneous flow (Fig. 72) – by analogy with the experimental dataset by Rouhani [45] with respect to the degree of cooling – as a simple, yet representative trend that correlates experimental data. Notably, a linear increase of gas mass fraction with temperature is imposed in the calculation of all the involved properties, expressed by Eqns. (22), (23) and (24). That results in both augmented pressures drop and a decrease of heat-transfer rate as larger amounts of gas are generated within the channel. On the other hand, pressure drops within the channel are sufficiently low to make the dependence of gas mass fraction on pressure approximately negligible. For example, the maximum variation of nitrogen pressure amounts to 3.5 bar, considering 4.5 bar as the maximum inlet pressure and atmospheric pressure as the outlet pressure. Both extreme values are about one tenth of nitrogen critical pressure [114] and the impact of accounting for pressure decay on mixture specific volume is proved unremarkable in preliminary assessments. Despite the discussed assumptions, the new model allows to predict and evaluate the effect of the gas formation within the channel in terms of pressure drops and heat exchange, thus achieving more accurate results even when the channel design and process parameters compromise the cooling efficiency. Therefore, the assessment of the cooling efficiency for the Profilati case study has been repeated in order to analyze the potentiality of the homogenous-flow approach.

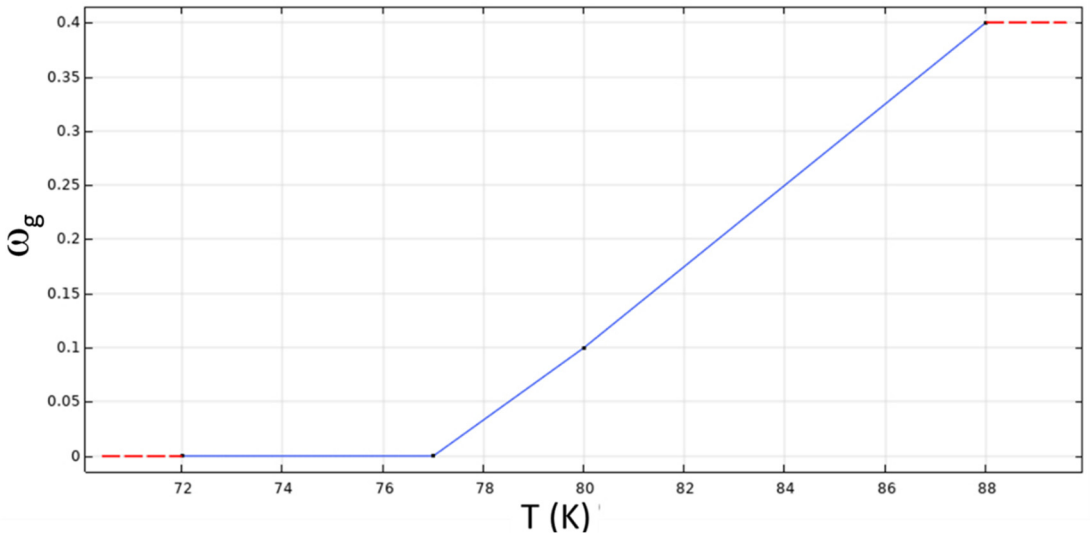

Fig. 72 Vapor quality as a function of homogeneous-flow temperature through a linear relationship

5.7.2 The Homogenous Flow Model tested on Profilati Case Study

Stationary and transient simulations were performed to test the homogeneous-flow approach. The stationary simulation was compared with the last extrusion, while the transient simulation was performed to analyze the thermal field evolution starting from the billet 12 when the connecting pipe began to be partially covered by ice and consequently a mixture of liquid and gas nitrogen flowed within the channel. In order to reduce the computational time, the transient analysis was implemented using the simplified thermal model without the aluminum flow with the same approach applied for FE model of the Benchmark 2011 case study to reduce the computational time within the optimization platform (section 5.6.2). Also in this case, the boundary thermal conditions to apply instead of the billet/die interface analysis were taken from the stationary simulation with the full comprehensive

model. In details, a non-constant convective heat flux was selected as imposed by a maximum temperature of 530 and 570 °C for the mandrel and the bearings, respectively, always setting heat transfer coefficient equal to 11000 W m^{-2} K^{-1}. In addition, during the billet-change a linear decrease of the reference temperature was imposed where the billet was in contact with the die (40 °C maximum in the bearings at the end of the billet change) to replicate actual cooling of the die during that time span. With regard to nitrogen cooling, for the first time a variable inlet pressure was imposed to virtually close the valve during the switching of billets. Table 25 summarizes all process parameters, boundary conditions and nitrogen properties used for the simulations.

Table 25 Process parameters, boundary conditions and nitrogen properties for Profilati case study using homogenous-flow approach

Process Parameters	**HFM (Stationary)**	**HFM (Transient from billet 12 to billet 17)**
Billet Temperature	480 °C	Not Computed
Die Temperature	Initial value steady state uncooled simulation (End of Billet 4)	Initial value steady state uncooled simulation (End of Billet 4)
Container Temperature	430 °C	Not Computed
Ram Temperature	440 °C	Not Computed
Temperature of backer surfaces in contact with press	280 °C	280 °C
Ram Speed	12 mm/s	Not Computed
Ram, Container/billet interface	No slip condition + Heat exchange by convection	Not Computed
Die/billet interface	No slip condition + Heat exchange by conduction	Heat exchange by convection
Bearings/billet interface	Slip condition + Heat exchange by conduction	Heat exchange by convection
Inlet Nitrogen Pressure	4 bar	4 bar
Inlet Nitrogen Temperature	-196°C	-196°C
Nitrogen Density (5% gas mass fraction)	82.3 kg/m^3	82.3 kg/m^3
Dynamic Viscosity	$\mu(\omega_g(T))$ Eq. 2 section	$\mu(\omega_g(T))$ Eq. 2 section
Nitrogen heat capacity at constant pressure Cp	Cp ($\omega_g(T)$) Eq. 3 section	Cp ($\omega_g(T)$) Eq. 3 section
Nitrogen thermal conductivity k	k ($\omega_g(T)$)	k ($\omega_g(T)$)

	Eq. 4 section	Eq. 4 section
Surface roughness of the channel (ε)	0.046 mm	0.046 mm

- *Steady-state analysis:*

Figs. 73 and 74 show the thermal map of the steady-state simulation, comparing the liquid nitrogen model with the homogenous-flow approach (17th extrusion). In the die, the thermal field obtained with the liquid nitrogen model presented a general slight underestimation of the temperature except for M4 (+1.0%), then, despite the good results, the liquid nitrogen modelling overestimated the cooling efficiency. Instead, the solution obtained with the HF model showed a general warmer thermal field, evidencing immediately the negligible effects of the cooling around the bearings. However, the substantial differences in terms of temperature prediction were clear in the backer, where the liquid nitrogen model greatly overestimated the refrigeration along the cooling path. In the HF thermal map, the cooling was notably effective from P1 to P2 and in P4 for its proximity to P2, but the gas formation along the channel limited the heat exchange and the drop of temperature registered by the other thermocouples.

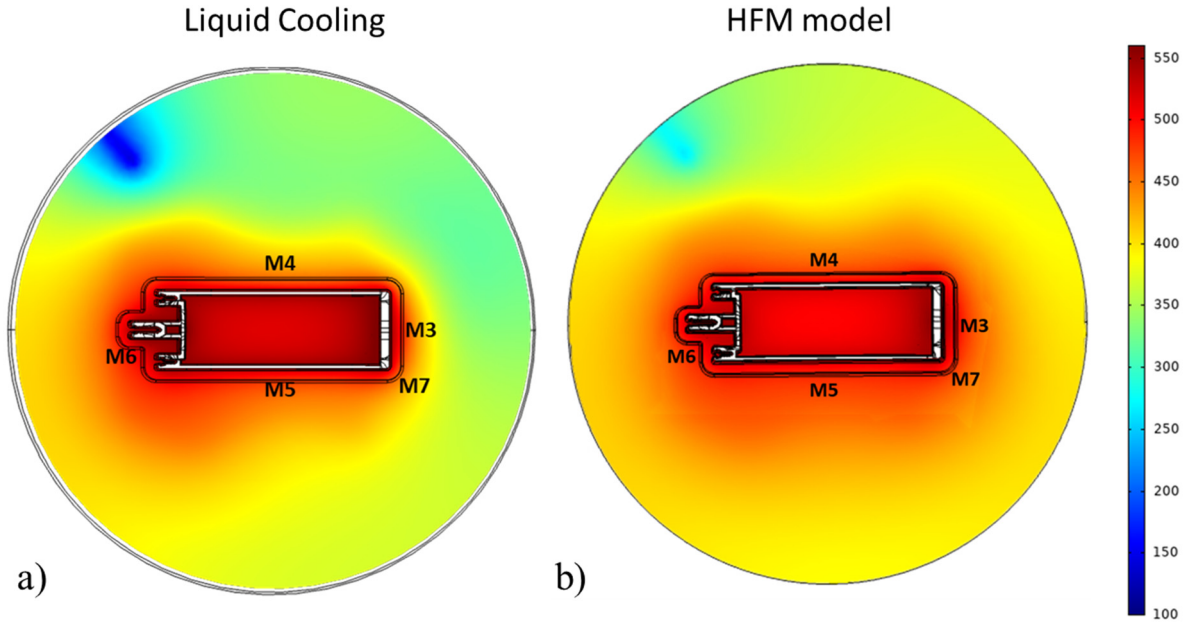

Fig. 73 Thermal map of the die in steady state condition: a) liquid cooled process, b) homogenous flow cooled process

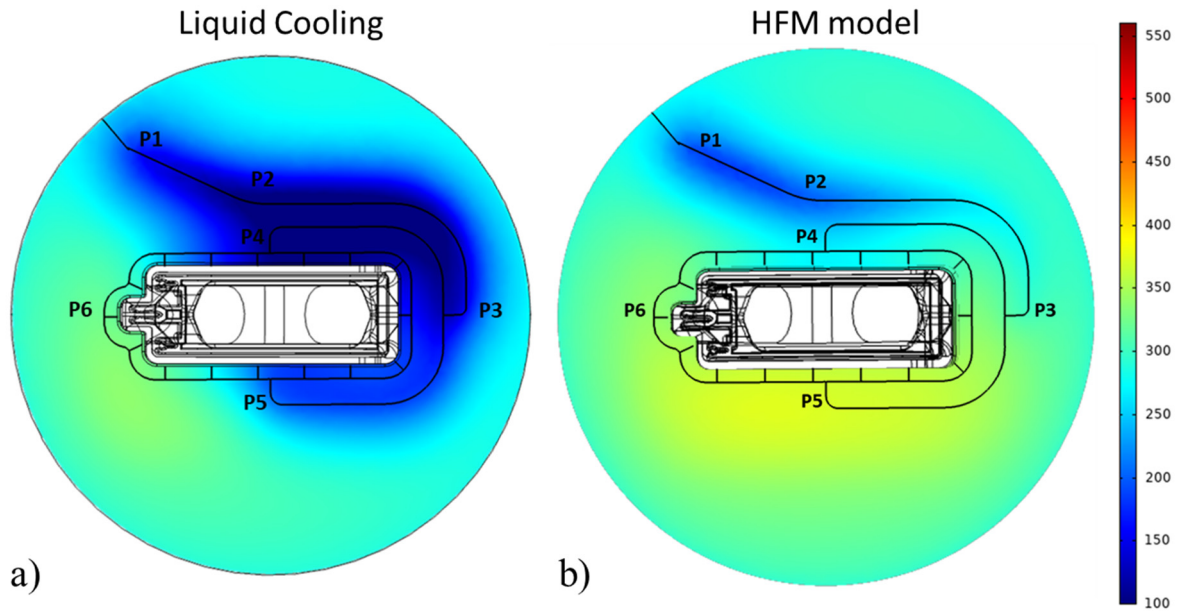

Fig. 74 Thermal map of the backer in steady state condition: a) liquid cooled process, b) homogenous flow cooled process

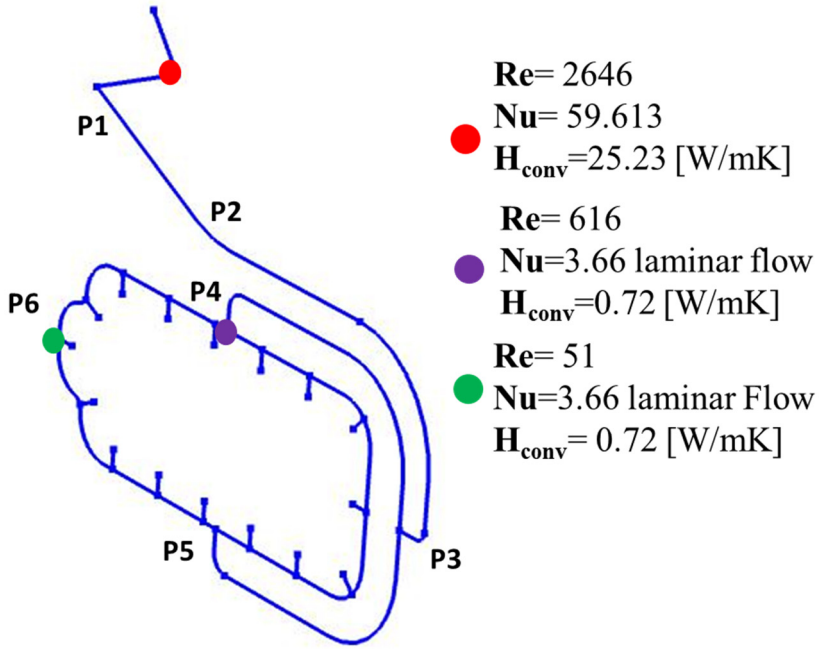

Fig. 75 Values of Reynolds, Nusselt number, and heat transfer coefficient within the 1D model of the cooling channel at the inlet of the nitrogen flow and at the locations closest to P4 and P6 probes.

This observation was substantiated by comparing the values of Reynolds number, Nusselt number and convective heat transfer coefficient resulting from the nitrogen-flow model at the inlet of nitrogen flow and at the specific locations within the channel, for example closest to the locations where P4 and P6 probes were placed (Fig. 75). The high values of Reynolds number at the inlet of nitrogen flow provided a high value of the Nusselt number and consequently a great heat transfer coefficient that allowed a significant drop of temperature nearby P1. Following the expected decrease in Reynolds and Nusselt number from the inlet to the aforementioned locations, it appeared that the heat transfer coefficient resulted considerably low at the location within channel closest to both P4 and P6 probes, also connected to the significant pressure drops that induce a laminar flow along much of the

channel. That reduced the heat-transfer rate at the former, thus resulting in the experimental cooling imbalance and ineffectiveness, which appeared well-captured by the numerical model. In details, Tables 26 and 27 report the experimental-numerical comparison for the last extrusion (billet 17), also evidencing the differences between the first numerical model and the new one. The homogenous-flow approach well captured the experimental phenomena in terms of thermal field prediction, especially if compared with the simulation with only liquid nitrogen flow. The maximum error was found in P4 with an underestimation of about 20%, but very lower than the -67.8% obtained with the single-phase model. Except for P4, the average errors were below the 5%, thus confirming the accuracy of the implemented model.

Table 26 Experimental-Numerical comparison in terms of temperature prediction in the backer (Billet 17): Liquid nitrogen model vs Homogenous flow approach

Billet 17	**Thermocouples Temperature [°C]**					
	P1	**P2**	**P3**	**P4**	**P5**	**P6**
Experimental	196	219	296	326	340	350
Liquid Numerical	190	120	195	105	200	321
%Err	-3.1%	-45.2%	-34.1%	-67.8%	-41.2%	-8,3%
HFM numerical	205	210	298	260	355	335
%Err	+4.6%	-4.1%	-1%	-20.4%	+4.4%	-4.3%

Table 27 Experimental-Numerical comparison in terms of temperature prediction in the die (Billet 17): Liquid nitrogen model vs Homogenous flow approach

Billet 17	**Thermocouples Temperature [°C]**				
	M3	**M4**	**M5**	**M6**	**M7**
Experimental	560	502	547	557	
Liquid Numerical	540	507	520	555	490
%Err	-3.6%	+1.0%	-4.9%	-0.4%	
HFM numerical	548	524	528	558	513
%Err	-2.1%	+4.4%	-3.5%	+0.2%	

- *Transient Analysis*

The transient simulation concerned the analysis of six extrusion processes, replicating the experimental condition from the billet 12 to the billet 17. The Fig. 76 shows the thermocouple temperatures predicted by the transient simulation and overlapped with the experimental data. The simulation started from the steady state uncooled condition, and the replacement of the aluminum flow with the boundary condition did not change the temperature deviation obtained with the full

model. The use of boundary condition variable with time allowed capturing the peak of temperature during the extrusion process as well as the cooling down during the billet change, partly exceeding the limit of transient simulations with pure Eulerian approach (section 5.2). In the die, the temperatures were not significantly influenced by the nitrogen cooling and the temperature drop was registered only during the billet change with a great matching with the experimental data. In the backer, during the simulation of the first cooled billet, a high temperature gradient was predicted both in P1 and in P2, obtaining a good overlap with the experimental results. During the subsequent extrusions, the good cooling trend was found also in P3, while a generally temperature underestimation was predicted in P4 obtaining during the last extrusion the maximum error of about 20%, the same predicted by the stationary analysis. Temperatures predicted in P5 and P6 showed respectively a slight underestimation and overestimation, but the errors were low and comparable with the uncertainty of thermocouple measurement. Therefore, the transient analysis showed the potentiality of the novel 1D cooling model in terms of temperature prediction also during complex transition phases as the billet change, allowing to obtain valuable information about the channel design quality. Indeed, a channel design that allows a good cooling of the die only after a very long transitory is anyway considered a not beneficial solution in terms of productivity and nitrogen consuming. While the stationary simulation allows to obtain rapidly information about the performances of the channel design with the aim to avoid worst solutions, the transient analysis of the best selected design adds important information about how extrusions are necessary to achieve an efficient cooling.

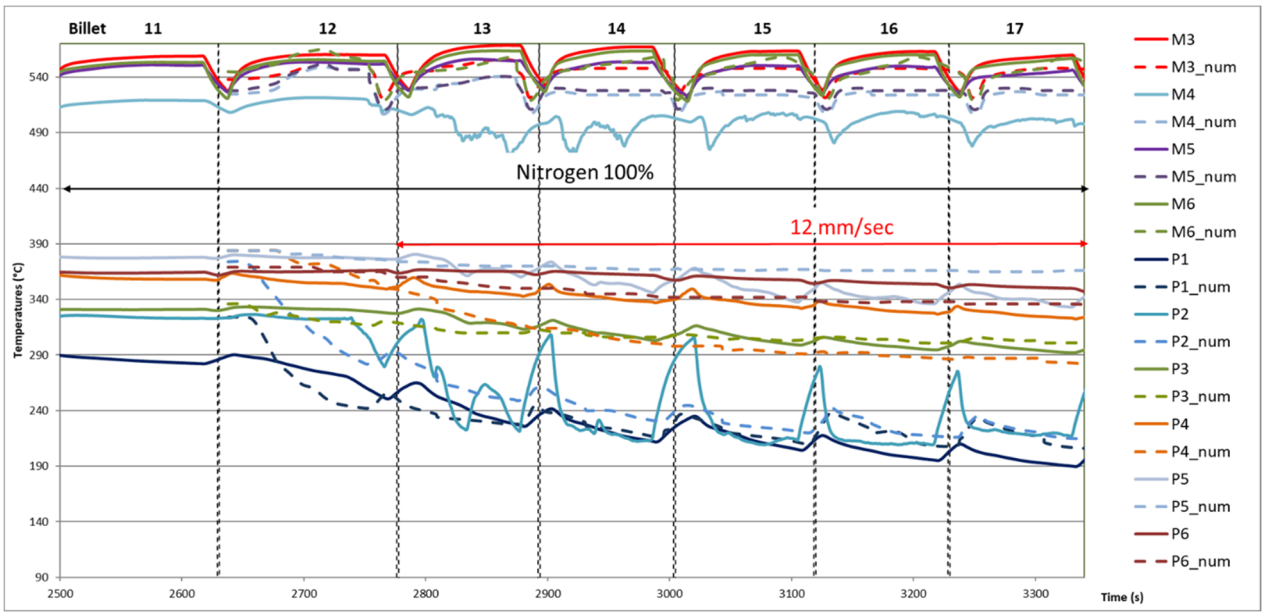

Fig. 76 Comparison between experimental and predicted trends of the extrusion process with cooling operated in transient state.

6 Experimental assessment of scrap length for charge welds and billet skin contamination

The contents of this chapter are focused on the experimental assessment of the intrinsic defects of the extrusion process: the charge welds and the billet skin contamination. In the section 2.5 it was presented the conditions that lead to the defects onset as well as how their evolution occurs along the profile length. The proposed experimental campaigns will be showed the current limits of the industrial practice in terms of scrap assessment, based on experience and inadequate approaches.

Three case studies will be deeply discussed: the Profilati case study already addressed for the nitrogen cooling, and the Indinvest case study with the analysis of two solid industrial profiles. The experimental campaigns will also evidence how time and cost consuming activity is the experimental evaluation of the extrusion defects, thus demonstrating how important the numerical approach can be in terms of scrap minimization at the design stage of the process with the aim to save time and costs.

6.1 Profilati Case Study

The profiles extruded during the assessment of the cooling efficiency were used to analyze also the evolution of the extrusion defects i.e. charge weld and billet skin contamination. The proper prediction of these defects allows reducing the material scrap as well as avoids selling to the customers extrudate with low mechanical properties and consequently of poor quality. The first aim of this experimental campaign was the assessment of the influence of the process parameters in terms of charge weld and billet skin evolution. Indeed, some works in literature highlighted the strong influence of the die geometry and the profile shape on the charge weld extent [89–92], but the impact of other parameters such as the extrusion speed and the die cooling can still be thoroughly examined. In Fig. 77 it is proposed the schematization for the selection of the billet transitions to analyze. The transition between the 2nd and 3rd billets as well as the one between the 3rd and the 4th billets were selected to investigate the charge weld behavior in the uncooled condition with 8 mm/s of ram speed. The transition between the 6th and the 7th billets represented the cooled condition with the nitrogen flow rate at 40%; the one between the 11th and the 12th billets constituted the cooled condition with the nitrogen valve fully opened; while the one between the 14th and the 15th billets identified the cooled condition at higher ram speed (12 mm/s). Some samples of the transition 5/6 were used for a preliminary polishing and etching tests.

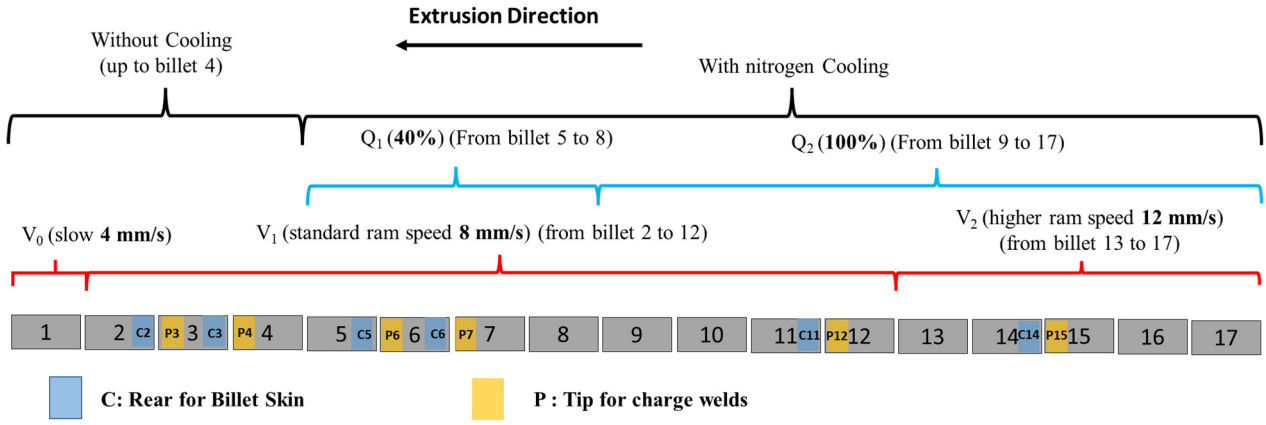

Fig. 77 schematization of the extrusion process for the selection of the billet transitions to analyze

For each transition, a profile length of about 7.50 m was collected: 5 m after the stopmark to evaluate the charge weld evolution and 2.50 m before the stopmark to find traces of skin contamination. The profiles were cut into samples of 100 mm, polished with abrasive papers, and subsequently etched in sodium hydroxide solution 30% in H2O (300g of NaOH for 1 l of H2O heated to 60 °C, etching time in the range of 45-90 sec) on the same side with respect to the extrusion direction. This etching was made with the aim to reveal the charge welds defect and the skin contamination on the cross section of each samples making the defects immediately visible to unaided eyes. In order to assess and quantify the defect pattern, each section was acquired through digital photography, then the area of the contour enclosing the defects was identified by coloring it and measuring the percentage of cross-

section contamination. In terms of charge weld extent, it was assumed that the extinction of the defect occurred at the 95% of the replacement in accordance with the industrial practice.

A specific nomenclature was chosen to identify the samples (Figs. 78-79): the first number represented the transition indicating the new billet extruded (i.e. it was used 7 for the transition between the 6th and the 7th billets); the mark + or – were used to specify the position after or before the stopmark respectively; the number after the mark indicated the distance from the stopmark in decimeters. Before the chemical etching, the samples were marked by means of laser texturing process (Fig.79), because the sodium hydroxide solution easily cancelled the inscription with the sharpie.

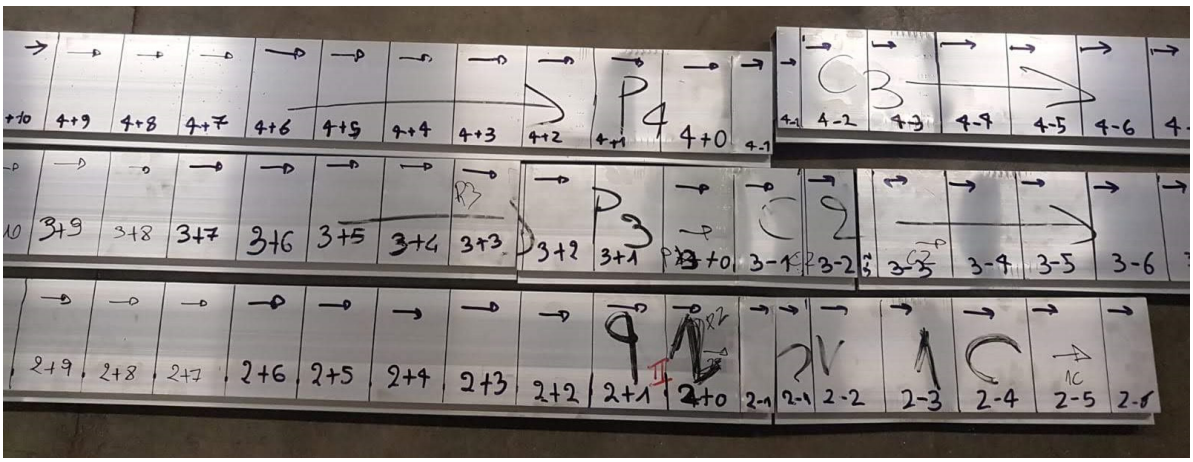

Fig. 78 An example of transition between subsequent billets before the cutting

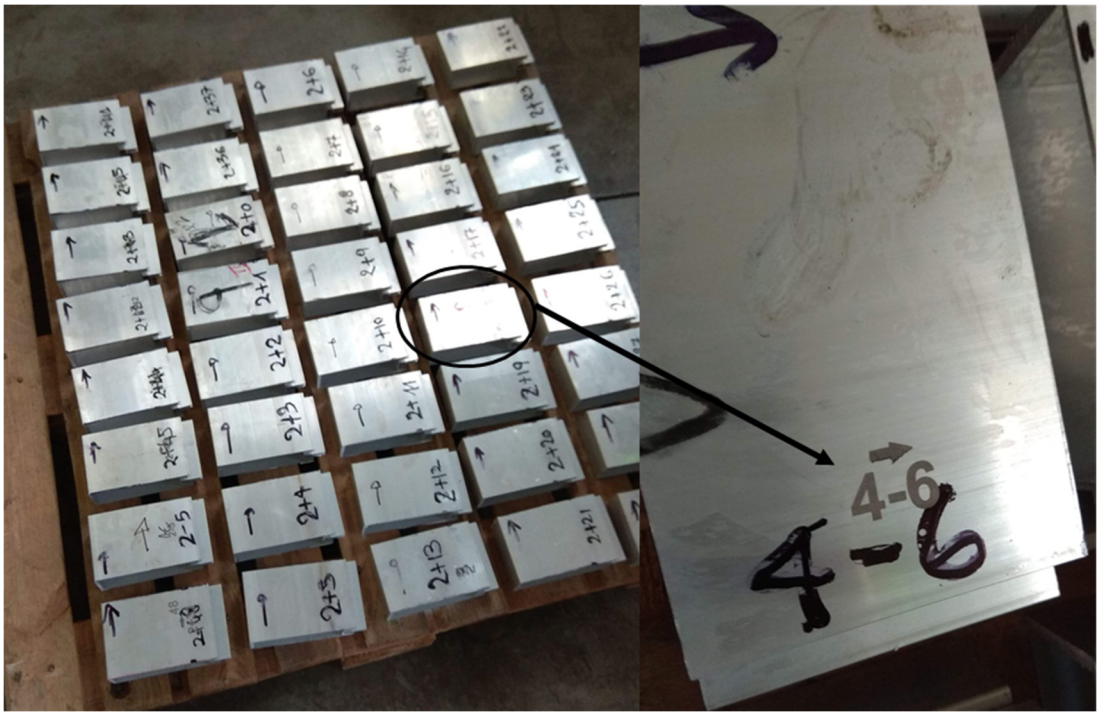

Fig. 79 An example of laser marking

In Fig. 80 it is shown an example of defect onset after etching. The area enclosed by the dark line represents the cross-section of the contaminated material flow that is the new billet replacement in case of charge welds or the billet skin flow in case of skin contamination. In some case studies, it is possible to appreciate, after the stopmark, the interaction between the two defects (see section 6.2).

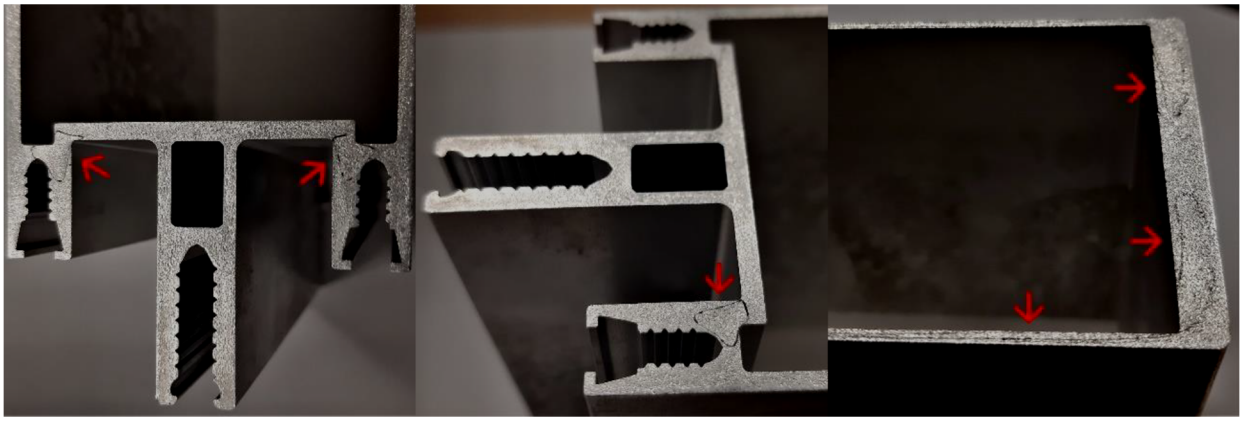

Fig. 80 An example of defect onset after etching

Figs. 81, 82, 83 and 84 showed the charge welds evolution for the four tested extrusion condition. The transition between the 3rd and the 4th billets (uncooled condition) showed the onset of the defect simultaneously in the bottom and upper area of the wings, in a cross section positioned at 1100 mm after the stopmark. Rapidly, the defect extended towards the long sides of the profile (4+13) and meanwhile the defect appeared also in the short side without wings (4+15). At 2200 mm far from the stopmark, the 95% of the cross-section area was replaced by the new billet material.

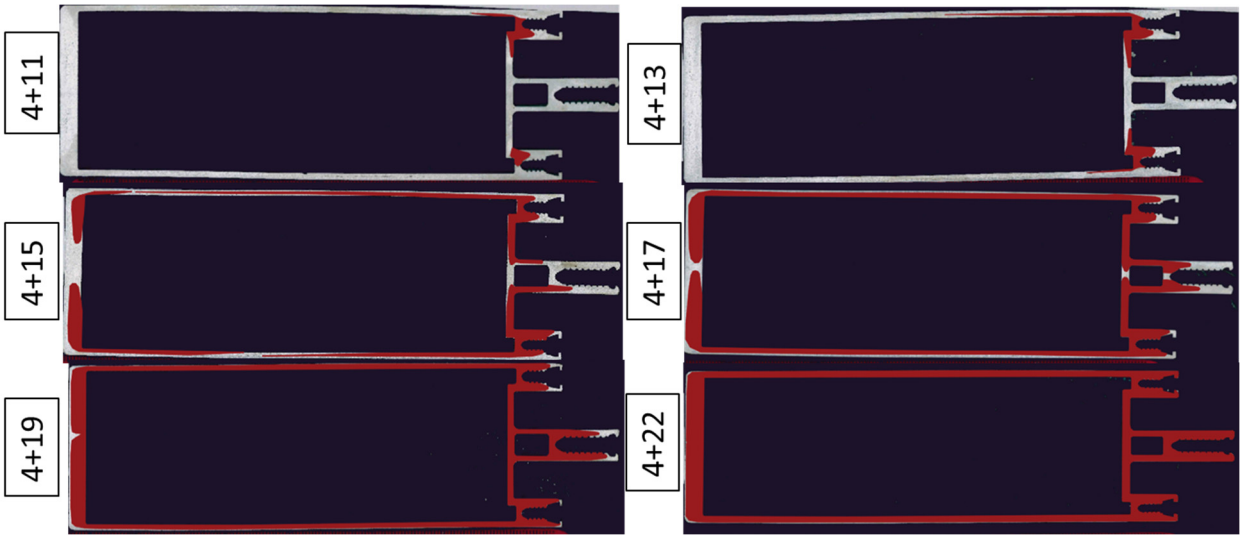

Fig. 81 Charge Evolution in the transition between the 3rd and the 4th billets

The transitions 11/12 (100% nitrogen flow rate, ram speed 8 mm/s) and 14/15 (100% nitrogen flow rate, ram speed 12 mm/s) showed a quite delayed onset of the defect, at 1300 mm far from the stopmark respect the 1100 mm of the uncooled condition, but the whole defect evolution was comparable in all three transitions. Differences between the start of the weld were small and not attributable at the varying process conditions. Indeed, the uncertainty about the cutting precision, about the depth of polishing as well as the issues in evaluating the defect evolution in thin-walled profile, make the small result deviations statistically possible. Moreover, the experimental campaign had proven the inefficiency of the nitrogen cooling, thus making its influence certainly negligible. In terms of extrusion speed, its increase did not cause an impact on the charge weld behavior and evolution, but probably different levels of speed should be tested before excluding its influence. In terms of skin contamination, no traces were found in the transitions 3/4, 11/12 and 14/15, thus demonstrating that the billet rest was enough to avoid the skin flow within the profile.

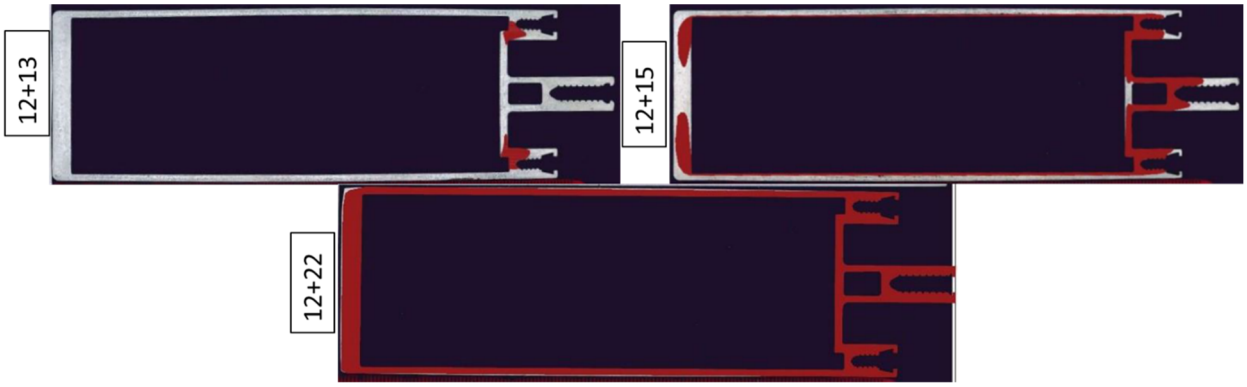

Fig. 82 Charge Evolution in the transition between the 11th and the 12th billets

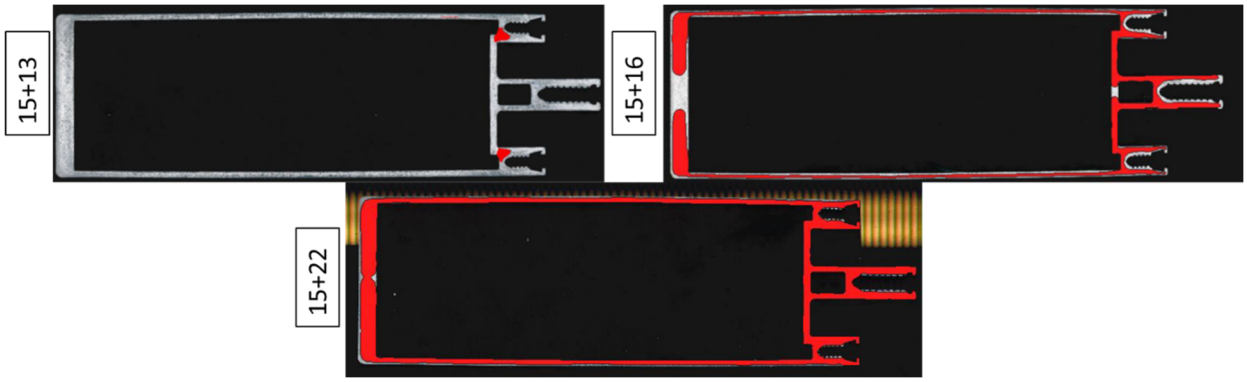

Fig. 83 Charge Evolution in the transition between the 14th and the 15th billets

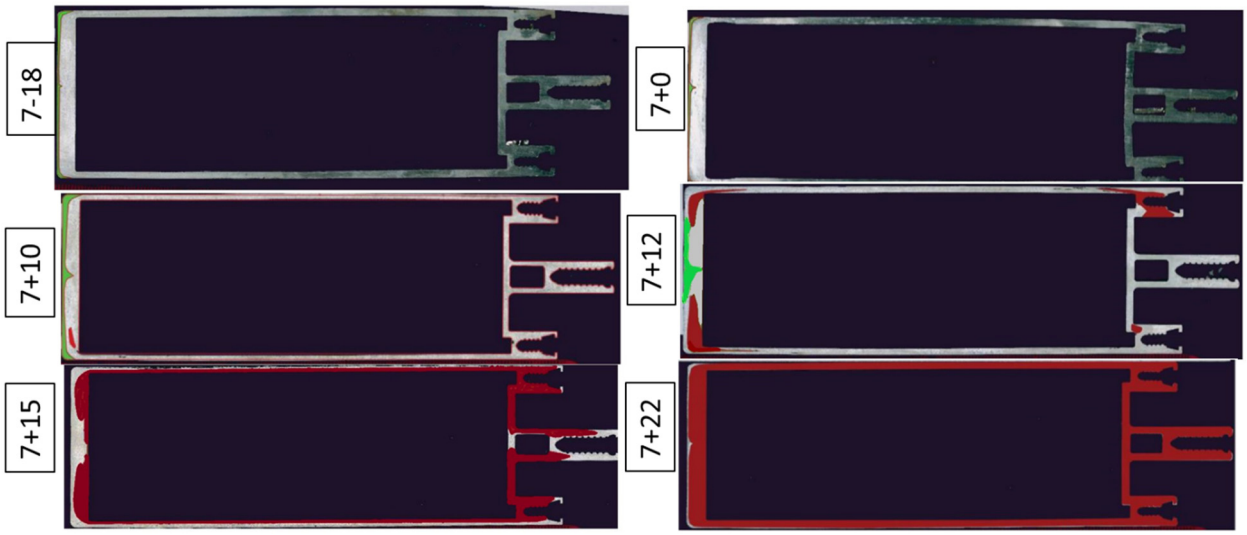

Fig. 84 Charge Evolution in the transition between the 6th and the 7th billets

Different evaluations were necessary for the transitions between the 6th and the 7th billets (40% of nitrogen flow rate, 8 mm/s of ram speed). Traces of contamination were found at 1800 mm before the stopmark nearby the outer edges of the short side without wings (Fig.84). In the figure, they were colored green to distinguish them from the charge weld in red. The contamination shape and dimension did not change neither at the stopmark nor further, but at 1000 mm after the stopmark a charge contamination appeared nearby the first one. At 1200 mm the charge weld flow became more evident in the short side and firstly appeared also in the wings. Afterwards, the charge weld replaced the behavior already seen in the other transitions, extinguishing at 2200 mm after the stopmark. The contamination found before the stopmark became greater during the interaction with the charge welds

(from 1200 mm to 1500 mm after the stopmark) becoming wider at the center of the side, but at distances higher than 1500 mm it was not possible to distinguish it by the charge welds. The first assumption about this defect was that billet skin was flowed into the profile, but the comparison in terms of billet rest with the other extrusions raises questions about this hypothesis. The table 28 summarizes the data collected in terms of billet rest, that for each transition is referred to the end of previous extrusion. Even if the chosen billet rest was constant and equal to 34 mm, the system's response of the press caused differences also in the range of 10-15 mm. The billet rest of the 6th extrusion (transition 6/7) was the lowest recorded (34 mm), but the small differences with both the 11th (36 mm) and the 14th (39 mm) extrusion did not justify the lack of skin contamination in the last two transitions analyzed. Indeed, to obtain a contamination at 1800 mm before the stopmark, the billet skin should enter in the die when an enough billet length remained to be extruded. In this case, with an extrusion ratio of 20 and a tooling set length (mandrel + die) of 184 mm, the skin contamination must enter in the die when a billet length of about 100 mm remained to be extruded (excluding the billet rest). Therefore, the differences of the billet rest in the range of 10-15 mm cannot caused in this case the occurrence or the absence of the defect in the extrudate.

Table 28 Billet rest in the analyzed transitions

Billet	Cooling	V_{ram}	Billet Rest
3rd	0%	8 mm/s	47 mm
6th	40%	8 mm/s	34 mm
11th	100%	8 mm/s	36 mm
14th	100%	12 mm/s	39 mm

From these premises it can be supposed that part of the contaminated materials accumulated during the whole process in the dead zones converged within the die while the sixth billet was extruding. The presence of this contamination did not affect the charge weld extent, but it modified the charge evolution at the beginning, shifting its first appearance in the short side without the wings.

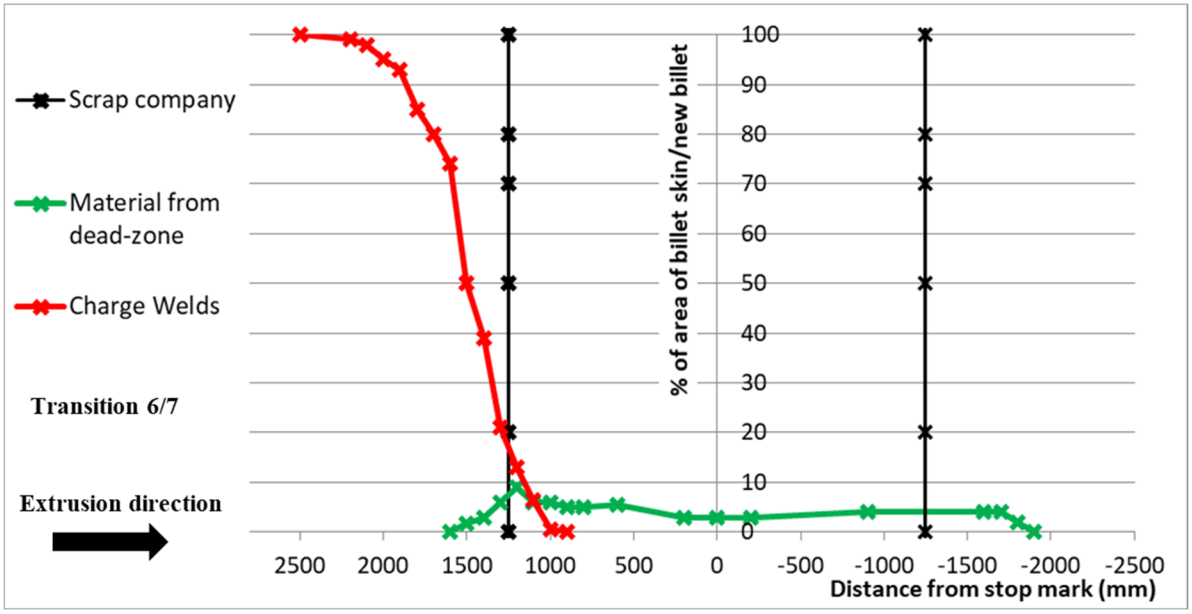

Fig. 85 Defect evolution in the transition 6/7 as a function of the distance from stopmark

The Fig. 85 shows the defects evolution of the transition 6/7 in terms of contaminated area within the profile evaluated at different distance from the stopmark. The x-axis values were inverted (values before the stopmark on the right) to represent the defect development by following the extrusion direction. Indeed, the contamination found before the stopmark was extruded before the billet change and in this case at the end of the sixth extrusion. Instead, the charge welds represented the replacement of the new billet material and it appeared within the profile during the extrusion of the subsequent billet. The scrap operated by the company was reported with black lines with the aim to evaluate if the discarded material was unnecessary or insufficient. The Fig. 86 reported the comparison between the analyzed transitions in terms of charge welds evolution, evidencing the small differences previously discussed. The transition between the 2nd and the 3rd billets, not representing another process condition, was reported only in the figure 86, but the same considerations made for the other billets were still valid.

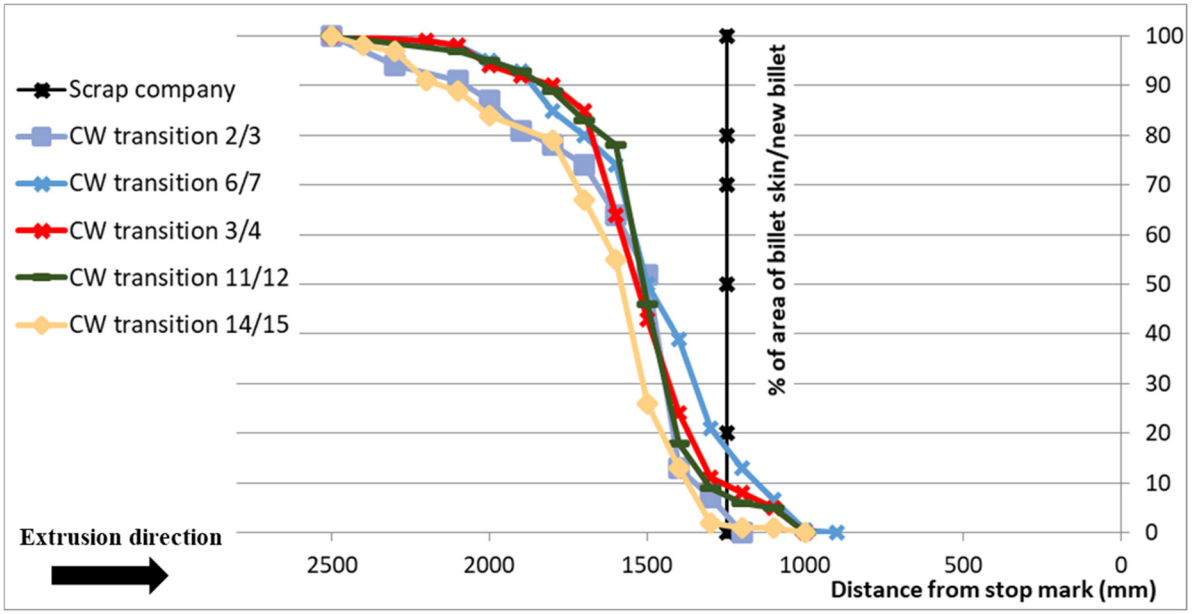

Fig. 86 Comparison in terms of charge welds development between the analyzed transitions

The experimental analysis of the charge weld and billet skin contamination revealed a charge extent of about 2200 mm after the stopmark and the absence of skin contamination with the billet rest used. The material flow from the dead zone found only during the sixth extrusion can be considered an exception. It was not possible to evaluate the influence of the nitrogen cooling and the changing of the ram speed seemed to be irrelevant in the investigated range. The scrap operated by the company of 2500 mm, symmetrically respect to the stopmark, underestimates the charge welds extent, and prevents the skin contamination unnecessarily (Figs. 85 and 86).

6.2 Indinvest Case Study

The Indinvest LT S.r.l. (Latina, Italy) had requested the analysis of the charge welds and billet skin evolution for two solid profiles regularly extruded in their plant. The geometry of the profiles as well as the 3D CAD of the dies are given in Fig. 87: Profile A presented a central thick section with a thin jagged appendix and a small bulge positioned respectively in the two extremes of the top side; Profile B showed a thick section with a massive side wing. The small area of Profile A (598.93 mm^2) suggested the use of a flat two-holes die to extrude two profiles simultaneously, while the Profile B (2761.35 mm^2) was extruded by means of flat die with a single opening. The Profile A was made by AA6063, while the Profile B using the AA6082, and both were extruded on an industrial 35 MN

press. Fifty billets were extruded for each production batch, and the investigated profiles sections were extracted in the transitions between the 6th and the 7th billets in order to be sure to select a steady-state process condition. In Table 29 all process parameters and the significantly geometry data of the billet and the tooling set are reported for both profiles.

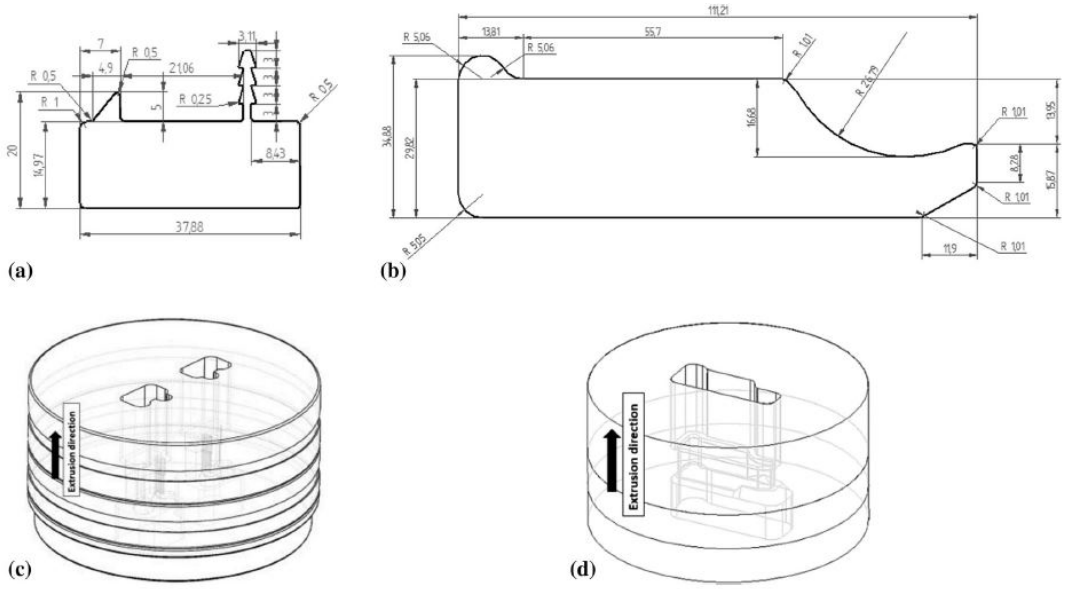

Fig. 87 Geometries of the profiles and of the dies under investigation: a, c profile A, b, d profile B

Table 29 Process parameters and Geometry data

Process parameters and geometry data	**Profile A**	**Profile B**
Aluminum alloy	AA6063	AA6082
Extrusion ratio	44	20
Ram speed, mm/s	6.44	7.64
Container temperature, °C	430	440
Billet temperature, °C	480	480
Die temperature, °C	450	450
Ram acceleration time, s	5	5
Billet length, mm	670	990
Billet diameter, mm	254	254
Container diameter, mm	264	264
Billet Rest length, mm	15	15

As clear in the table 29, the main differences were detected in the extrusion ratio (44 for Profile A and 20 for Profile B) and in terms of billet length (990 mm for Profile A and 670 mm for Profile B). A total length of 3500 mm was collected for the Profile A: 1600 mm after the stop mark for the charge welds evolution and 2000 mm before the stopmark to find the skin contamination. The whole industrial scrap was collected also for the Profile B: 1600 mm after the stop mark and 4200 mm before the stopmark. The profiles were initially cut into samples of 100 mm; then, for the extent of the profiles in which the defect was expected to increase rapidly, samples were further sectioned for an in-depth investigation. All the samples were then polished with abrasive papers and subsequently etched for about 90 sec in sodium hydroxide solution (30% in H2O at 60°C). In this case compared to thin hollow profiles (i.e. Profilati case study), the percentage of the cross-section area that presented

defects was easily measurable, since massive solid profiles were being analyzed. In order to quantitatively assess the defects trend, the percentage area containing the skin contamination and the new billet material has been computed by means of an image analysis tool of a CAD software on high-resolution pictures of each etched section of the two profiles. Here too, it was assumed that the extinction of the defect occurred at the 95% of the replacement in accordance with the industrial practice.

6.2.1 Profile A

In Figs. 88, 89, 90 and 91 the experimental evolution of the skin contamination and the charge welds is shown for the Profile A, following the distance from the stop mark (negative values indicates distances before the stopmark). Concerning the billet skin contamination, it did not evolve up to 100% on the profile section (as clearly evidenced in Figs. 88 and 89) but it remained roughly constant during ram stroke. The skin contamination was present in the sample further from the stopmark (-2000 mm), evidencing that a part of contaminated profile is probably sold. The percentage of contaminated area was in the range of 6-15% until 130 mm after the stopmark, then the new billet material began to interact with the skin. At this point (+147 mm), the charge welds extended to the center of the massive part of the profile, shifting and compressing the skin contamination towards the short side (Fig. 89). At 215 mm after the stopmark the skin was not distinguishable, and the charge welds almost filled the thick section of the profile (Fig. 90). At 297 mm far from the stopmark, the defect began to fill the jagged appendix and the small bulge, obtaining the 100% of section replacement at about 800 mm after the stopmark (Fig. 91). The high extrusion ratio (44) and the kind of the solid profile allowed a quick extinction of the defect (86% of replacement at +300 mm), slightly impeded by the presence of the appendixes. The Fig. 92 reports the development of skin contamination and charge welds within the profile section at different distances from stop mark: negative values on x-axis represent samples extracted from the end of the billet 6 (back-end defect) whilst positive ones represent samples extracted from the transition from billet 6th to 7th (front-end defect). Also in this case, the scrap of the company was not optimal, underestimating the skin contamination and overestimating the charge welds extent.

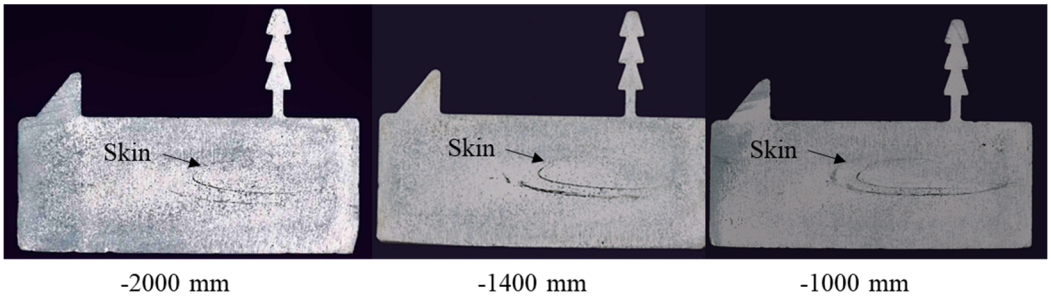

Fig. 88 Skin evolution in the Profile A before the stopmark

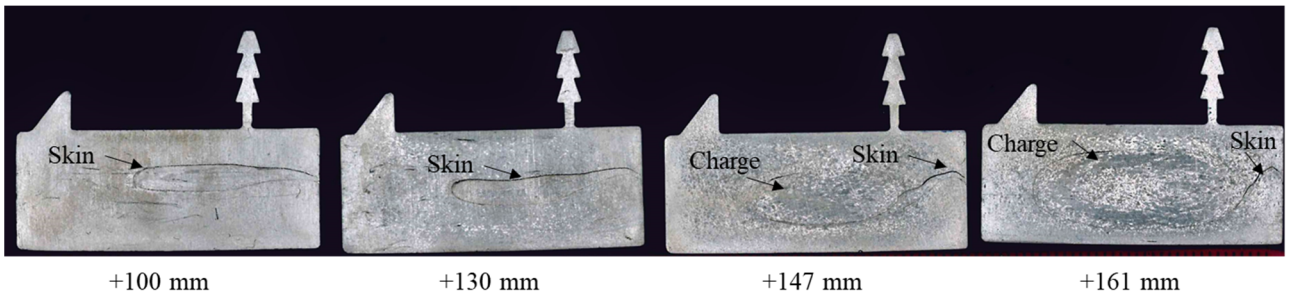

Fig. 89 Interaction between the skin contamination and the charge welds in the Profile A

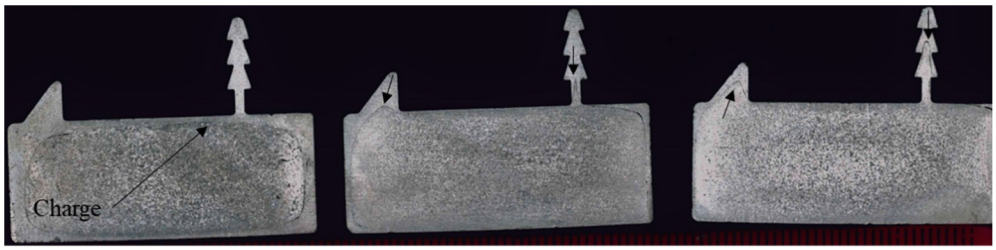

Fig. 90 Charge evolution in the Profile A (from +215 mm to +392 mm)

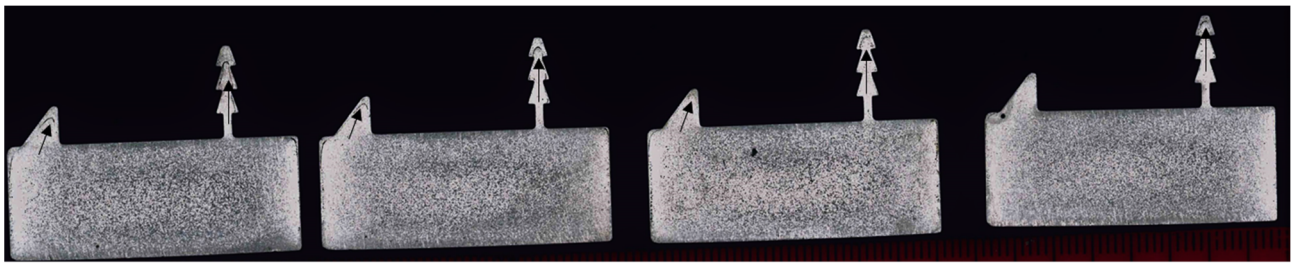

Fig. 91 Charge evolution in the jagged appendix of the Profile A

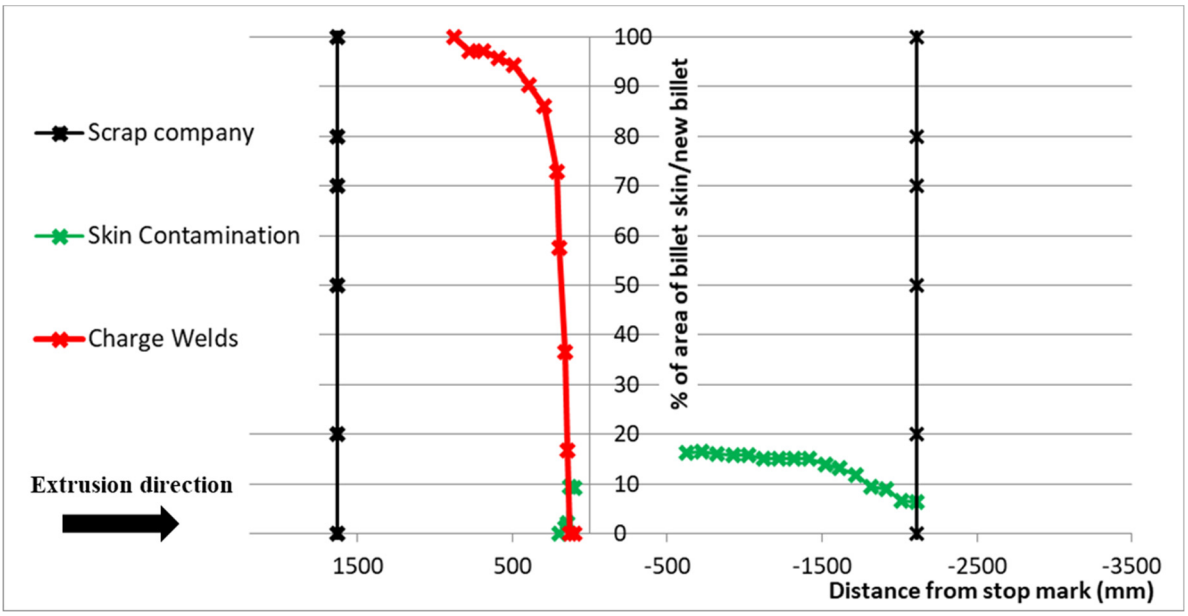

Fig. 92 Defect evolution in Profile A as a function of the distance from the stopmark

6.2.2 Profile B

In the Profile B (Figs. 93-94), the billet skin defect appeared in the center of the profile at -3700 mm from the stopmark, and it remained about constant in terms of contaminated area (12-15%) until near the stopmark (-500 mm). Then, it flattened out towards the short sides (4.5% at +68 mm), thus suggesting the upcoming of the charge weld defect that rapidly grew at 92 mm far from the stopmark, making not recognizable the skin defect (Fig. 94). The charge weld defect reached rapidly the 90% of the area replacement at +190 mm and up to 95%, and consequently its extinction, at +400 mm. As shown in the Profile A, the start of the defect contamination occurred in the center of the profile, due to the faster and unconstrained flowing of the material, then enlarging up to the complete filling of the section. However, as expected, Profile A showed a longer evolution of the charge weld according to the greater extrusion ratio and the higher shape complexity with respect to Profile B.

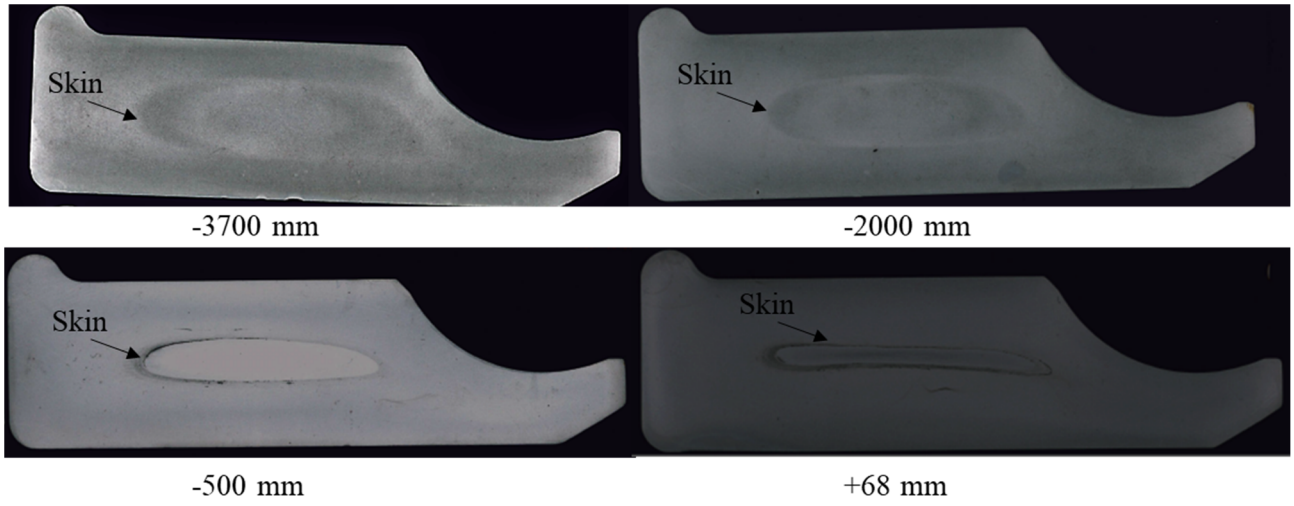

Fig. 93 Skin evolution in Profile B

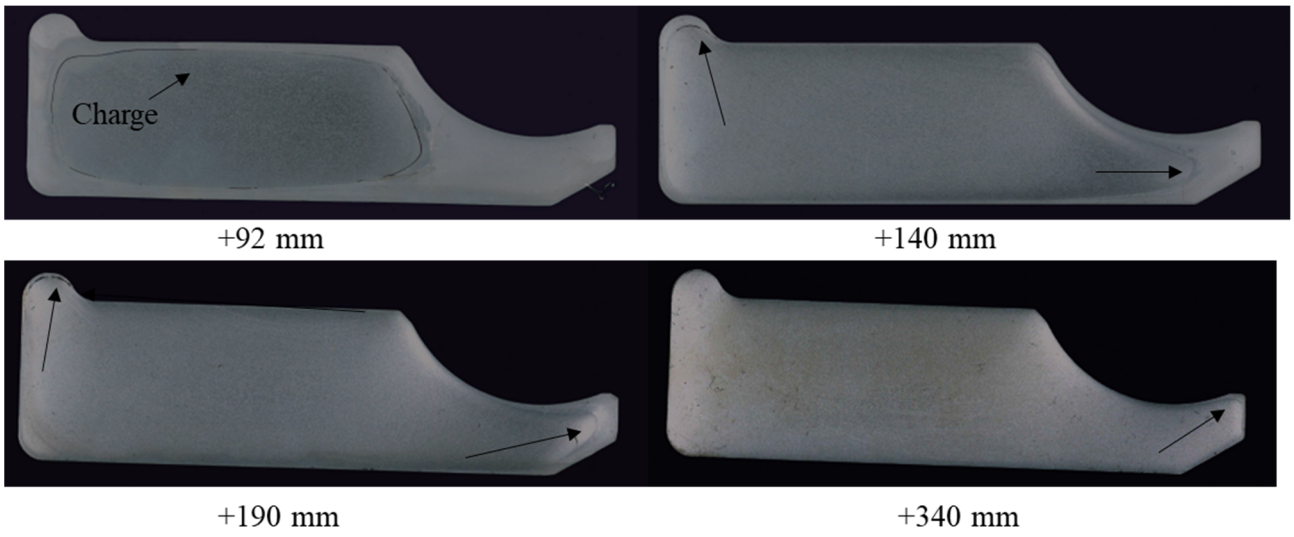

Fig. 94 Charge evolution in Profile B

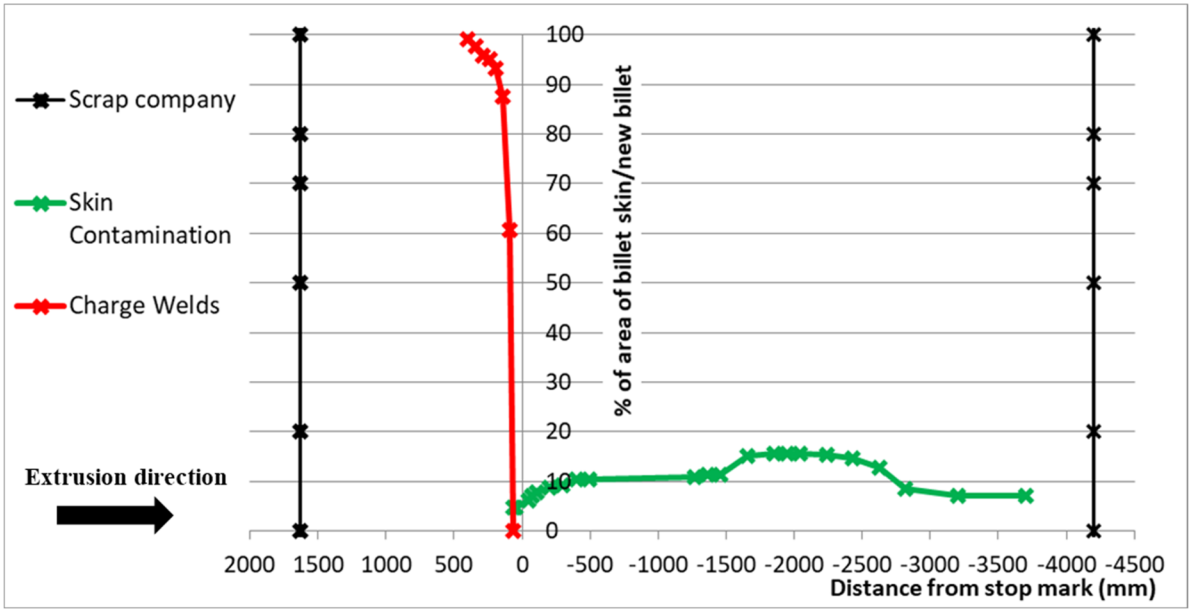

Fig. 95 Defect evolution in Profile B as a function of the distance from the stopmark

For the Profile B, the scrap for the skin contamination can be considered acceptable (4200 mm against the 3700 mm necessary), but the scrap for the charge was overestimated of four times (Fig.95).

7 Numerical modelling assessment for the prediction of the charge welds and the billet skin contamination

7.1 Numerical Modelling

The experimental campaigns showed that the industrial practice, based mainly on the experience, overestimated or underestimated the scrap length, discarding sound material in the first case and selling products with lower mechanical properties in the second case. Therefore, in this chapter, the potentiality of the FE model in terms of defect predictions will be deeply assessed with the aim to offer a valid numerical tool as supporting the industrial practice for the proper scrap evaluation. The numerical prediction of the charge welds and the billet skin contamination can be performed by means of different software dedicated to the extrusion process. Different numerical approach can be used: pure Eulerian, pure Lagrangian or Arbitrary Lagrangian-Eulerian Method. As previously mentioned in section 5.2, the mesh domain is fixed using the Eulerian approach, while with the Lagrangian approach the mesh domain follows the material flow changing its topology during the material deformation. The advantages of Eulerian approach are the reliability of the results in terms of thermal field, velocity field and extrusion load at the reduced computational time. However, some shortcomings with this approach could be the prediction of the profile distortion at the exit from the bearings, the analysis of the transient thermal field and extrusion load connected to both the die filling and the billet length reduction as well as the prediction of die filling issues. Instead, the Lagrangian method perfectly match with analysis that need to evaluate the evolution of the material flow under deformation. Nevertheless, this approach is very time-consuming in terms of computational time and the issues connected to mesh-distortion and remeshing when high deformations and high shape complexity occur, make difficult its use for the simulation of the extrusion process. In this context, the Arbitrary Lagrangian-Eulerian method exploits the advantages of both Lagrangian and Eulerian methods to mitigate the aforementioned shortcomings. In detail, the Lagrangian approach is used to simulate the billet upsetting and its length reduction during the process as well as the exit profile bending, while the Eulerian approach maintains fix the mesh within the die-set to avoid the mesh distortion and to reduce the computational time. Therefore, the ALE approach allows the calculation without changing the topological structure, then, it results faster than the adaptive remeshing method. These premises are necessary to understand why it is preferred an ALE approach to predict the extrusion defects. The Fig. 96 shows an example of charge welds and billet skin contamination evolution. It is immediately clear how an ALE approach can be helpful to evaluate the replacement of the new billet material within the profile as well as to follow the skin kinetics within the billet under deformation. The Eulerian approach can be used to predict the charge welds extent because it is enough the study of the material flow within the die that results independent by the billet movement within the container, instead, the billet under deformation must be analyzed for the skin contamination and the ALE approach is the best solution to avoid the issues of pure Lagrangian approach.

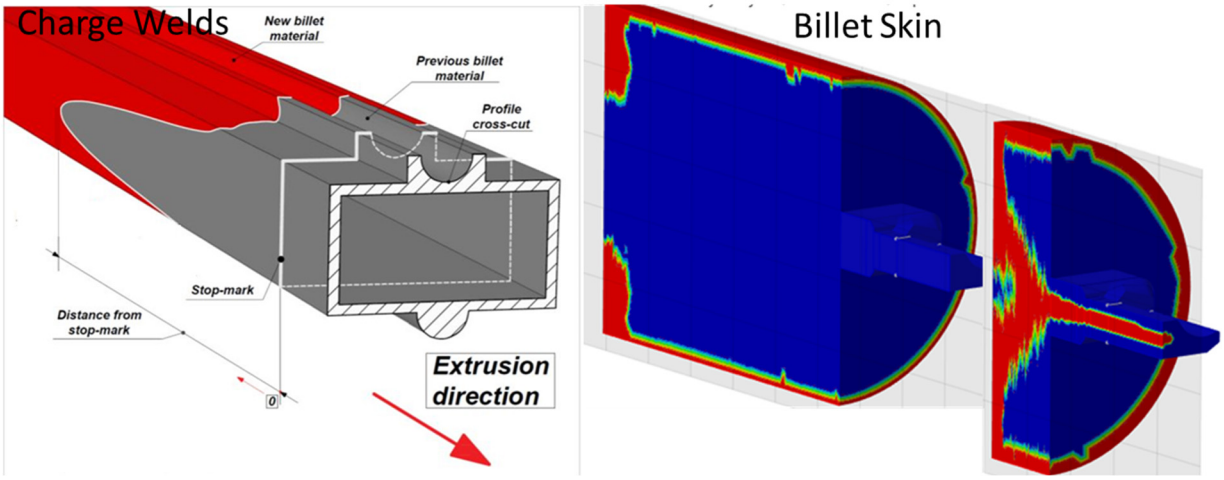

Fig. 96 An example of extrusion defect prediction: Charge Welds (on the left), Billet Skin contamination (on the right)

Therefore, in this PhD work two different software were used: Comsol Multiphysics for the simulation of the 3D extrusion process integrated with the 1D analysis of the nitrogen cooling, HyperXtrude® for the prediction and minimization of the scrap material derived from the charge welds and billet skin contamination. 3D numerical models were implemented within the HyperXtrude® environment using an ALE approach and they were tested in terms of charge welds and billet skin prediction comparing the numerical results with the data collected during the already discussed experimental campaigns. Unlike Comsol environment, HyperXtrude® is a software completely dedicated to the extrusion process and for this reason the preparation of the geometry, the selection of the boundary conditions as well as the mesh generation are simplified and customized for the extrusion process. However, a module to simulate the die nitrogen cooling is currently unimplemented within HyperXtrude® and from this point of view the Comsol environment allows more flexibility as showed in the chapter 5. As future developments of this project will be provided the integration of the ALE approach within Comsol for the scrap prediction as well as the integration of the nitrogen cooling within the HyperXtrude® environment with the aim to offer on a single platform the possibility to study and to optimize the extrusion process in all its aspects.

Despite the differences in terms of user interface, the setting of the process parameters and the boundary conditions within HyperXtrude® is the same seen within the Comsol environment. Notably, for the evaluation of charge welds and billet skin contamination it is enough the analysis of the material flow, replacing the tooling set with equivalent thermal and boundary conditions. Indeed, the computational time of transient simulations is very high in terms of defect prediction if compared with stationary thermal analysis (dozen of hours against at most few hours), and thereby it is useful to reduce the computed unnecessary domains. The table 30 reports the process parameters and the boundary conditions to set for the simulation. It is worth noting that also the heat exchange with the die is obtained by convection since it is not simulated, unlike the simulation of nitrogen cooling where the die is a computed domain. In this case, the table 30 reported in detail also the billet dimensions (length and diameter) as well as the billet rest, significant process parameters for the evaluation of the defects. Transient simulations of one extrusion are performed comparing the experimental-numerical results in terms of defect onset and defect evolution (distance from the stopmark).

Table 30 Process Parameters and boundary conditions set in the numerical models

Process Parameters	Value

Billet Diameter	Depends on the case study
Container Diameter	Depends on the case study
Billet Length	Depends on the case study
Billet Rest	Depends on the case study
Billet skin thickness	Depends on the case study
Billet Temperature	Depends on the case study
Die Temperature	Depends on the case study
Container Temperature	Depends on the case study
Ram Temperature	Depends on the case study
Ram Speed	Depends on the case study
Ram, Container/billet interface	No slip condition + Heat exchange by convection
Die/billet interface	No slip condition + Heat exchange by convection

7.2 Profilati Case Study: Experimental-Numerical Comparison

The first validation of the numerical model was tried with the Profilati case study. Recalling the experimental analysis, the charge welds extent resulted independent by the extrusion speed in the investigated range, and the billet rest was enough to avoid the skin contamination within the profile. Therefore, two transient simulations were performed in order to analyze the charge weld evolution at the two experimental extrusion speeds (8 mm/s and 12 mm/s). About the billet skin contamination, the billet rest was set equal to the minimum registered during the experimental campaign (34 mm) in order to analyze all cases with one simulation. The HyperXtrude® software allows to study simultaneously both the charge welds and the billet skin contamination. The ALE approach was implemented, using the Lagrangian approach for the billet under deformation within the container, while the Eulerian approach was used within the die and at the exit of the profile. As previously discussed, the Eulerian approach can be used for the prediction of the charge welds behavior, then, since the aim of the work the profile bending was not evaluated. The Fig. 97 shows the geometrical model already meshed. The different displayed colors indicate the sub-domains of the model (billet, billet skin, feeder, welding chamber, bearings zones etc.) and the user can easily divide the geometry, virtually cutting the domain along the extrusion direction. The use of sub-domains allows setting the

process parameters, the boundary condition as well as generating the mesh in an optimal way. In this case, the feeder and the welding chamber were included into the same sub-domain because under the same boundary conditions. A heat transfer coefficient of 11,000W/m^{2}°K was set between aluminum and the tool system not modelled, while for heat exchange with air, the heat transfer was set equal to 50 W/m^{2}°K with an air temperature of 50°C. Table 31 summarizes all process parameters and boundary conditions set for the simulation. In terms of billet skin thickness, a value of 0.5 mm was supposed, suggesting by the data collected in literature for other case studies [98-101].

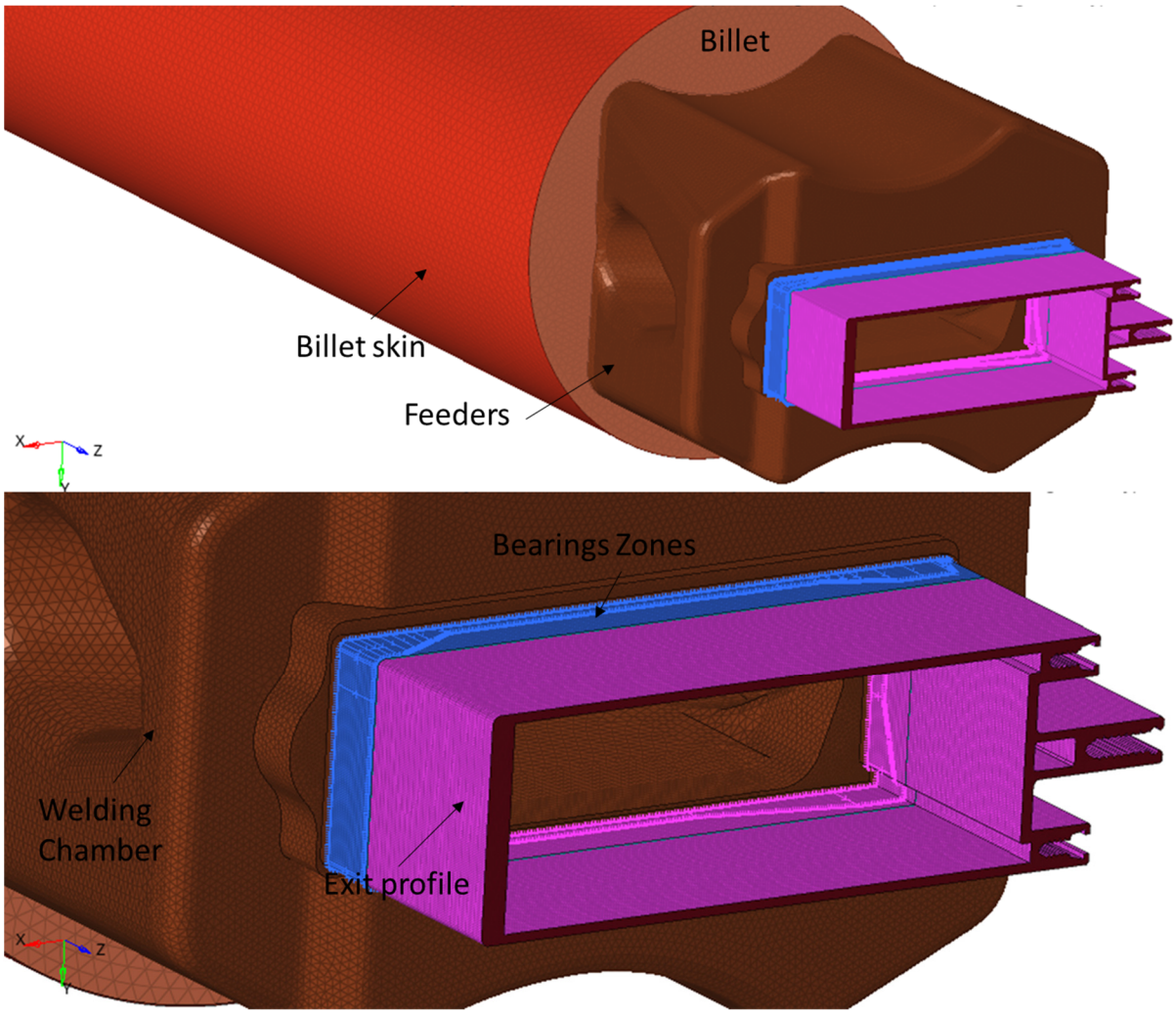

Fig. 97 The geometrical model for the simulation divided into sub-domains and already meshed

Table 31 Process parameters and boundary conditions set for Profilati case study (Simulations of charge welds and skin evolution)

Process Parameters	Value
Billet Diameter	203 mm
Container Diameter	211 mm
Billet Length	950 mm
Billet Rest	34 mm
Billet skin thickness	0.5 mm
Billet Temperature	480 °C

Die Temperature	510 °C
Container Temperature	430 °C
Ram Temperature	440 °C
Ram Speed	8 mm/s and 12 mm/s
Ram, Container/billet interface	No slip condition + Heat exchange by convection
Die/billet interface	No slip condition + Heat exchange by convection

In terms of aluminum flow stress, Hensel-Spittel plastic flow constitutive model [44-46] was used (Eq. 25), where σ is the flow stress, A is a material constant, ε the strain, $\dot{\varepsilon}$ the strain rate, T the temperature in Kelvin (see section 2.4). Respect to the sine hyperbolic law used within the Comsol environment, the strain dependence of the stress was considered, thus making the material model more accurate. Table 32 reports the Hensel-Spittel coefficients used for AA6060, as found in literature [44]. The mesh of the model consists of 2007124 tetrahedral mesh with a maximum mesh size of 5 mm in the billet, 3 mm in the feeder and 1.5 mm in the bearings zones. The billet skin was divided into 4 layers along the thickness in order to obtain accurate results.

$$\bar{\sigma} = A \cdot e^{m_1 T} \cdot \bar{\varepsilon}^{-m_2} \cdot \dot{\bar{\varepsilon}}^{-m_3} \cdot e^{\frac{m_4}{\bar{\varepsilon}}} \cdot (1+\bar{\varepsilon})^{m_5 T} \cdot e^{m_7 \bar{\varepsilon}} \cdot \dot{\bar{\varepsilon}}^{m_8 T} \cdot T^{m_9} \quad (25)$$

Table 32 Hensel-Spittel coefficients for AA6060 [44]

Flow stress parameters	**AA6060**
A parameter of Hansel-Spittel model	3400 MPa
m1 parameter of Hansel-Spittel model	$-6.1*10^{-3}$ K^{-1}
m2 parameter of Hansel-Spittel model	$1.25*10^{-1}$
m3 parameter of Hansel-Spittel model	$-1{,}39*10^{-2}$
m4 parameter of Hansel-Spittel model	$-2{,}6*10^{-3}$
m5 parameter of Hansel-Spittel model	$-5*10^{-4}$ K^{-1}
m7 parameter of Hansel-Spittel model	$2{,}8*10^{-3}$
m8 parameter of Hansel-Spittel model	$2*10^{-4}$ K^{-1}
m9 parameter of Hansel-Spittel model	0

Fig. 98 shows how the software simulated the charge welds evolution during the extrusion process. At time zero, the new billet material (in red) filled the volume within the container, while the old billet material (in blue) represented the material flow within the die. During the subsequent time steps, the new billet material started to interact with the old one within the die, then, in the third frame of

the Fig. 98 it is shown the full replacement of the old billet material in the cross-section of the profile. Notably, Fig. 99 depicts the experimental-numerical comparison within the cross section of the profile in terms of defect evolution at different distances from the stop-mark (billet 4, no cooling, 8 mm/s of ram speed).

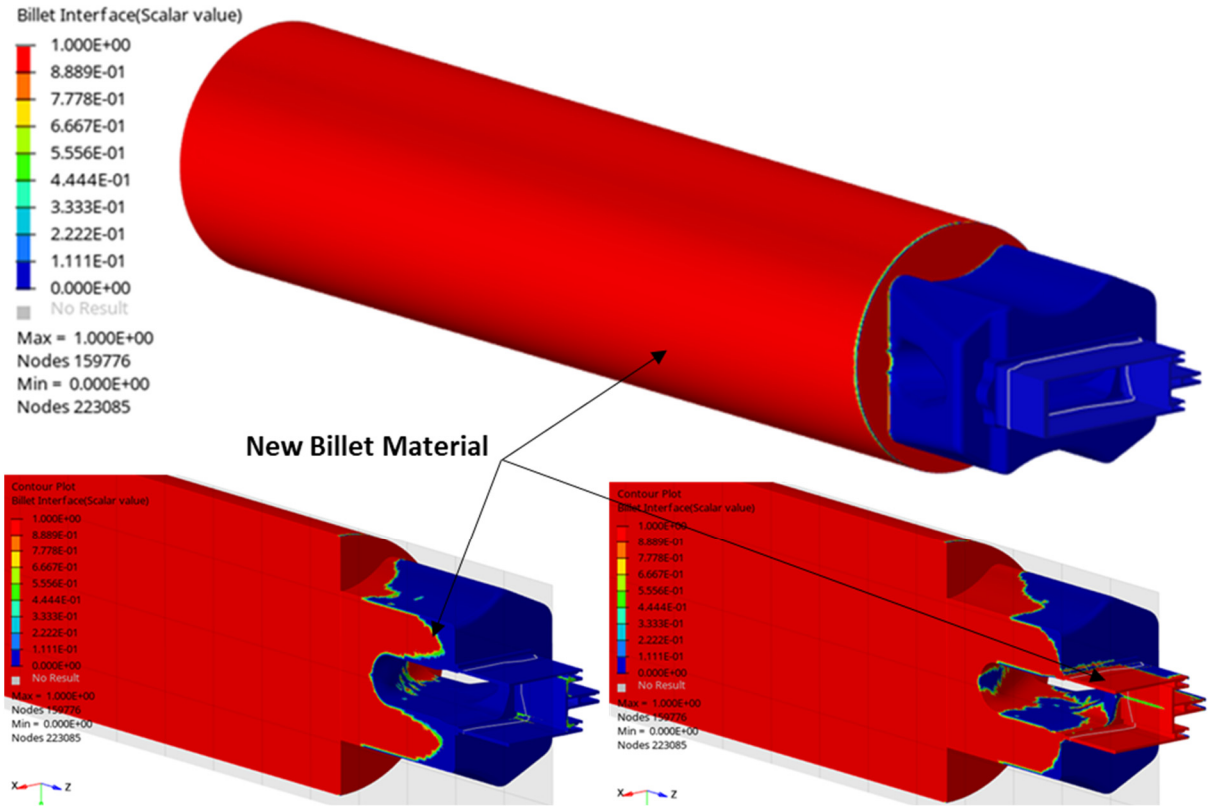

Fig. 98 Replacement of the old-billet material during the simulation of the extrusion process

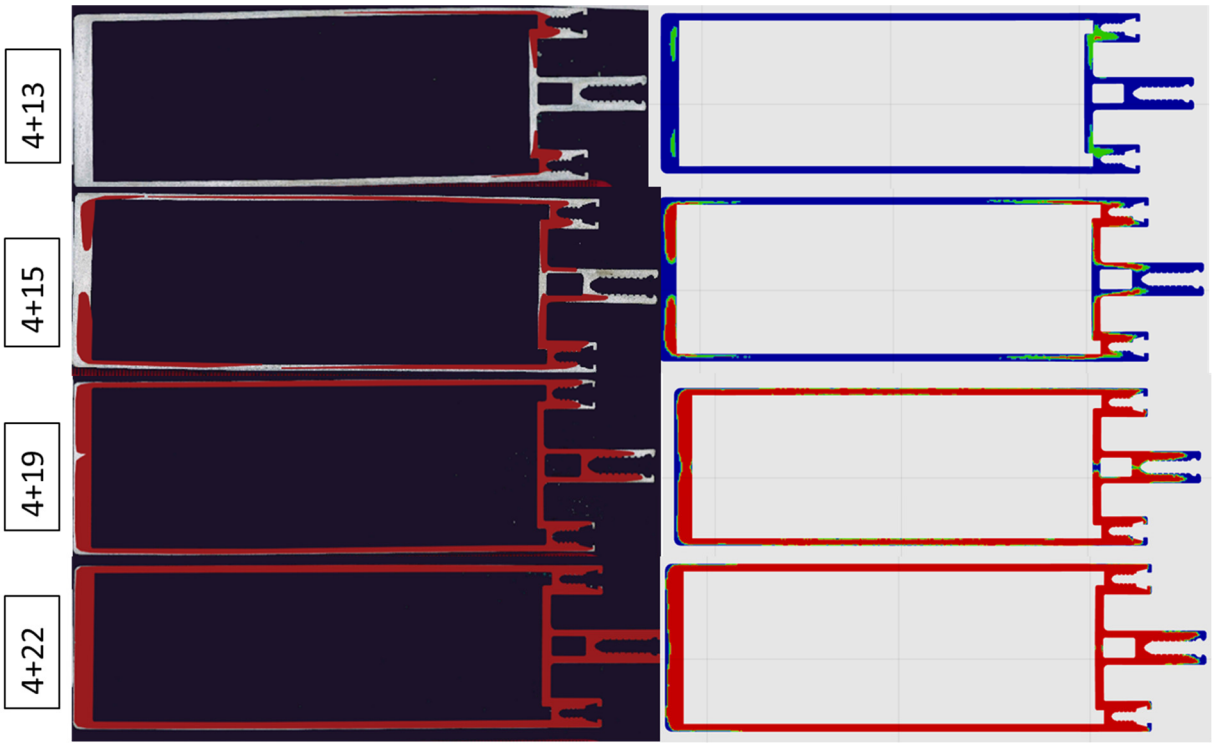

Fig. 99 Experimental-Numerical comparison in terms of old-billet replacement at different distances from the stopmark

The simulation evidenced a slight delay in terms of defect onset, indeed, the old-billet replacement appeared lower than the experimental one up to 1500 mm after the stopmark. However, at 1900 mm after the stopmark, the differences in terms of replacement were almost negligible and at 2200 mm a percentage of replacement higher than 95% were reached for both the experimental and numerical analysis. In addition, the experimental-numerical discrepancy appeared lower comparing the simulation results with the transitions 11/12 and 14/15 that showed a defect onset at 1300 mm after the stopmark. Recalling the experimental campaign, the transition between the 6th and 7th billets was an exception, because the material flow from the dead-zone interacted with the charge welds, phenomena that cannot be simulated with the implemented model. The Fig. 100 reports quantitatively the percentage evolution of the new billet material within the profile evaluated at different distance from the stopmark, comparing the numerical and the experimental trends. The good reliability and quality of the numerical results was immediately clear in the graph that evidences a great overlap between the experimental and numerical trends. It is worth noting that no differences were detected by the simulations in terms of defect evolution varying the extrusion speed, thus confirming partly the experimental evidence.

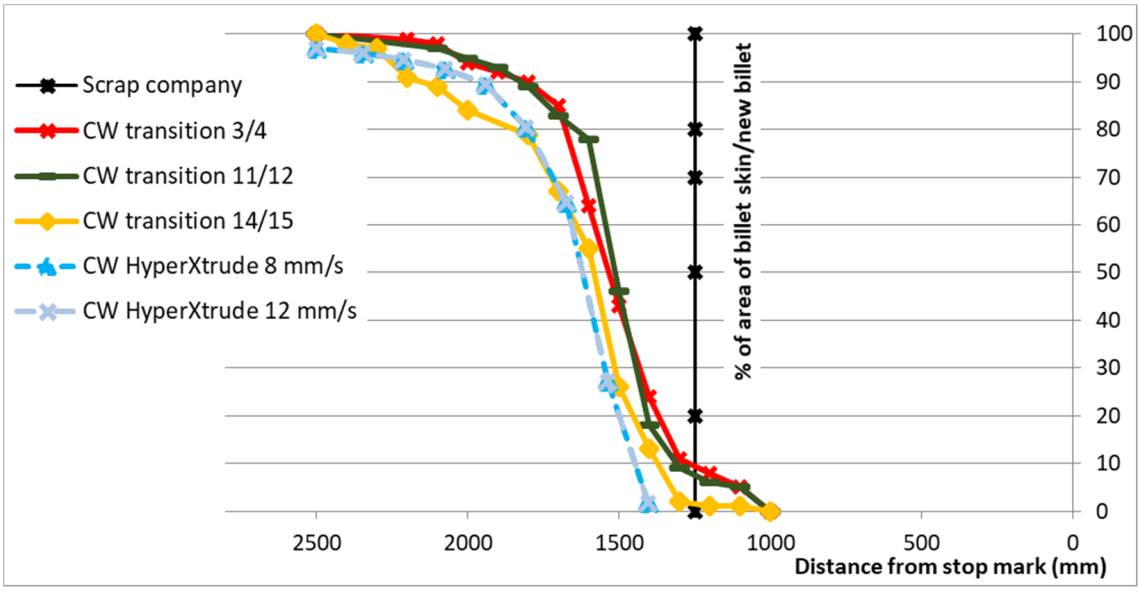

Fig. 100 Experimental-Numerical comparison in terms of percentage of old material replacement

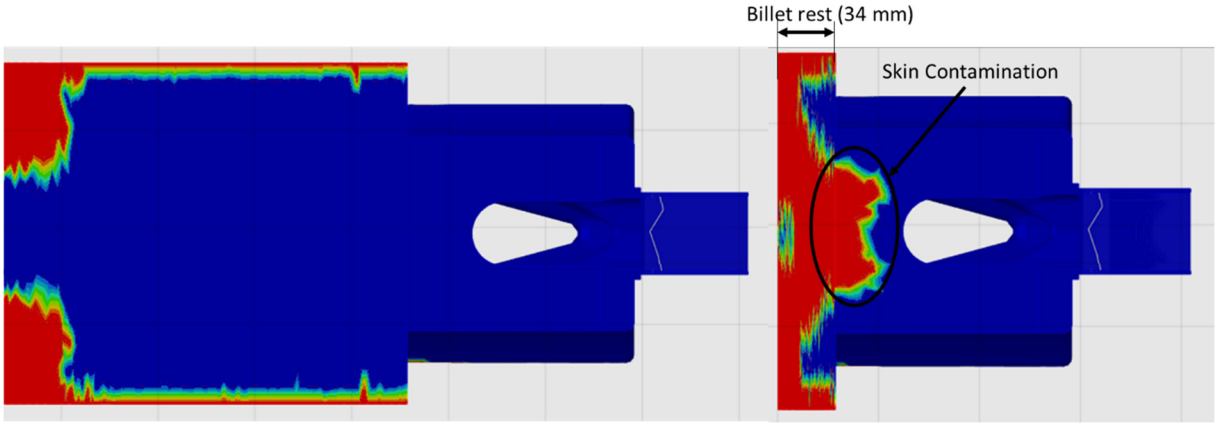

Fig. 101 Simulation of the billet skin contamination flow

In terms of skin evolution, the Fig. 101 showed the billet skin flow (in red) at two different time steps. It is worth nothing that at the end of the simulation, a large amount of the billet skin remained within the billet rest, thus avoiding a significant contamination of the profile. The small part that entered

within the die was located after the stopmark, because it will flow within the profile merely during the subsequent extrusion. Therefore, the simulation excluded the presence of skin contamination before the stopmark, confirming the experimental evidence. It is very hard to distinguish the skin contamination after the stopmark from the charge welds, especially in thin hollow profile, thereby, it was not possible to understand from the experimental data collected if the simulation correctly predicted the presence of skin contamination after the stopmark. Anyway, the good quality of the numerical results was proved in terms of charge welds and skin evolution, especially for the aim to predict and to minimize the scrap material. From this point of view, the table 33 summarizes the comparison in terms of scrap length between the experimental, theoretical, numerical, and industrial scraps. In this case, the numerical matching was perfect, while the theoretical formulas (see section 3.2) overestimated the scrap length for both charge welds and billet skin contamination. As previously discussed, the scrap operated by the company underestimated almost half the scrap after the stopmark and provided an unnecessary discard for the skin contamination. The potentiality of the simulation tool in terms of scrap optimization was also confirmed by the computational time of about 10 hours (Workstation: Intel(R) Core (TM) i7-9700 CPU @ 3.00GHz, 32 Gb Ram), certainly reasonable if compared with a very time-consuming experimental analysis and in keeping with the virtual prototyping industrial timeline.

Table 33 Scrap length evaluated with different strategies

Scrap Length	Experimental	1st Theoretical	2nd Theoretical	Numerical	Industrial
Charge Welds, 95% of replacement (After the stopmark)	2200 mm	2426 mm	3639 mm	2200 mm	1250 mm
Skin Contamination (Before the stopmark)	0 mm	675 mm	-	0 mm	1250 mm

7.3 Indinvest Case Study: Experimental-Numerical Comparison

In this section, the 3D numerical model of the extrusion process for the defects prediction was tested on the Indinvest case study. Recalling the experimental campaign, two solid profiles were analyzed in terms of charge welds and billet skin contamination: the high extrusion ratio and the great profile thickness promoted a rapid charge welds extinction, while the billet rest of 15 mm was not enough to avoid the skin contamination within the profile in both cases. Fig. 102 shows the mesh of the two profiles realized within HyperXtrude® environment. For the profile A, the symmetry was exploited to model only half of the geometry and to reduce the computational time. The total mesh consisted of 1209895 and 671780 tetrahedral elements for Profile A and Profile B respectively. Table 34 reports the process parameters and the boundary conditions set for both simulations, while Table 35 presents the Hensel-Spittel coefficients of the AA6063 (Profile A) and the AA6082 (Profile B).

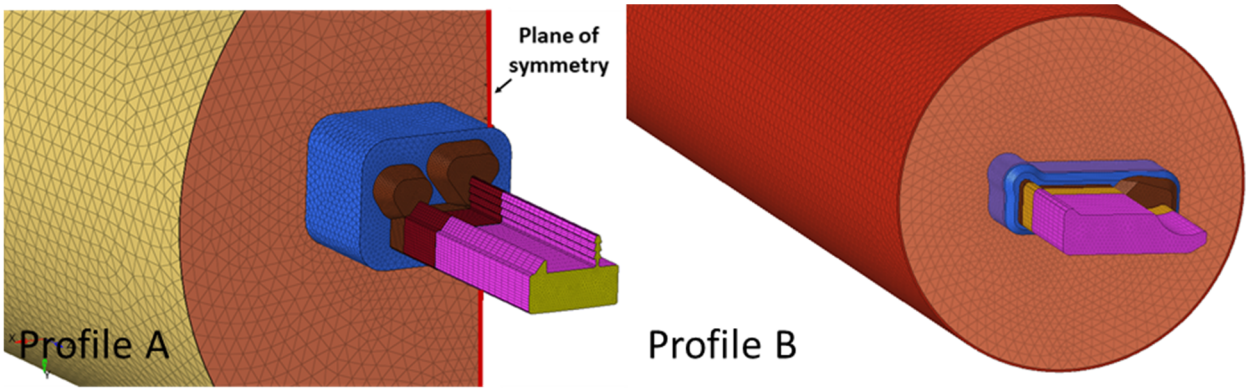

Fig. 102 The geometrical model for the simulations already meshed: a) Profile A, b) Profile B

Table 34 Process parameters and boundary conditions set for Indinvest case study

Process Parameters	Profile A	Profile B
Billet Diameter	254 mm	254 mm
Container Diameter	264 mm	264 mm
Billet Length	670 mm	990 mm
Billet Rest	15 mm	15 mm
Billet skin thickness	0.25 mm	0.25 mm
Billet Temperature	480 °C	480 °C
Die Temperature	450 °C	450 °C
Container Temperature	430 °C	430 °C
Ram Temperature	440 °C	440 °C
Ram Speed	6.44 mm/s	7.64 mm/s
Ram, Container/billet interface	No slip condition + Heat exchange by convection	No slip condition + Heat exchange by convection
Die/billet interface	No slip condition + Heat exchange by convection	No slip condition + Heat exchange by convection

Table 35 Hensel-Spittel coefficients for AA6063 [44] and AA6082[122] aluminum alloys

Flow stress parameters	AA6063	AA6082
A parameter of Hansel-Spittel model	1014,7 MPa	560000 MPa
m1 parameter of Hansel-Spittel model	$-4.38*10^{-3}$ K^{-1}	$-2.12*10^{-3}$ K-1
m2 parameter of Hansel-Spittel model	$2.43*10^{-1}$	$1.06*10^{-1}$
m3 parameter of Hansel-Spittel model	$-9,65*10^{-2}$	$9,8*10^{-2}$

m4 parameter of Hansel-Spittel model	$-4{,}38*10^{-4}$	$9.27*10^{-4}$
m5 parameter of Hansel-Spittel model	$-7.66*10^{-4}\ K^{-1}$	$-6.5*10^{-4}\ K^{-1}$
m7 parameter of Hansel-Spittel model	$2{,}94*10^{-2}$	$2{,}34*10^{-2}$
m8 parameter of Hansel-Spittel model	$2.91*10^{-4}\ K^{-1}$	$6.47*10^{-5}\ K^{-1}$
m9 parameter of Hansel-Spittel model	0	-1.208

A heat transfer coefficient of 11,000W/m^2°K was set between aluminum and the tool system not modelled, while for heat exchange with air, the heat transfer was set equal to 50 W/m^2°K with an air temperature of 50°C. Transient simulations of one extrusion were performed with a computational time of 6 hours and 2.5 hours for Profile A and Profile B respectively (Workstation: Intel(R) Core (TM) i7-9700 CPU @ 3.00GHz, 32 Gb Ram).

7.3.1 Profile A

Fig. 103 shows the experimental-numerical comparison in terms of charge welds evolution within the cross-section of the profile A. The defect onset, the old material replacement in the massive part of the profile as well as the replacement within the thin jagged appendix perfectly replicated the experimental trends. However, the implemented model did not allow to evaluate the interaction between the charge welds and the billet skin contamination, because they were carried out separately during the simulation. It could be necessary to implement a model of two subsequent extrusions to evaluate the charge-skin interaction, however, the results obtained with the current model were very complete and reliable in terms of scrap prediction and optimization.

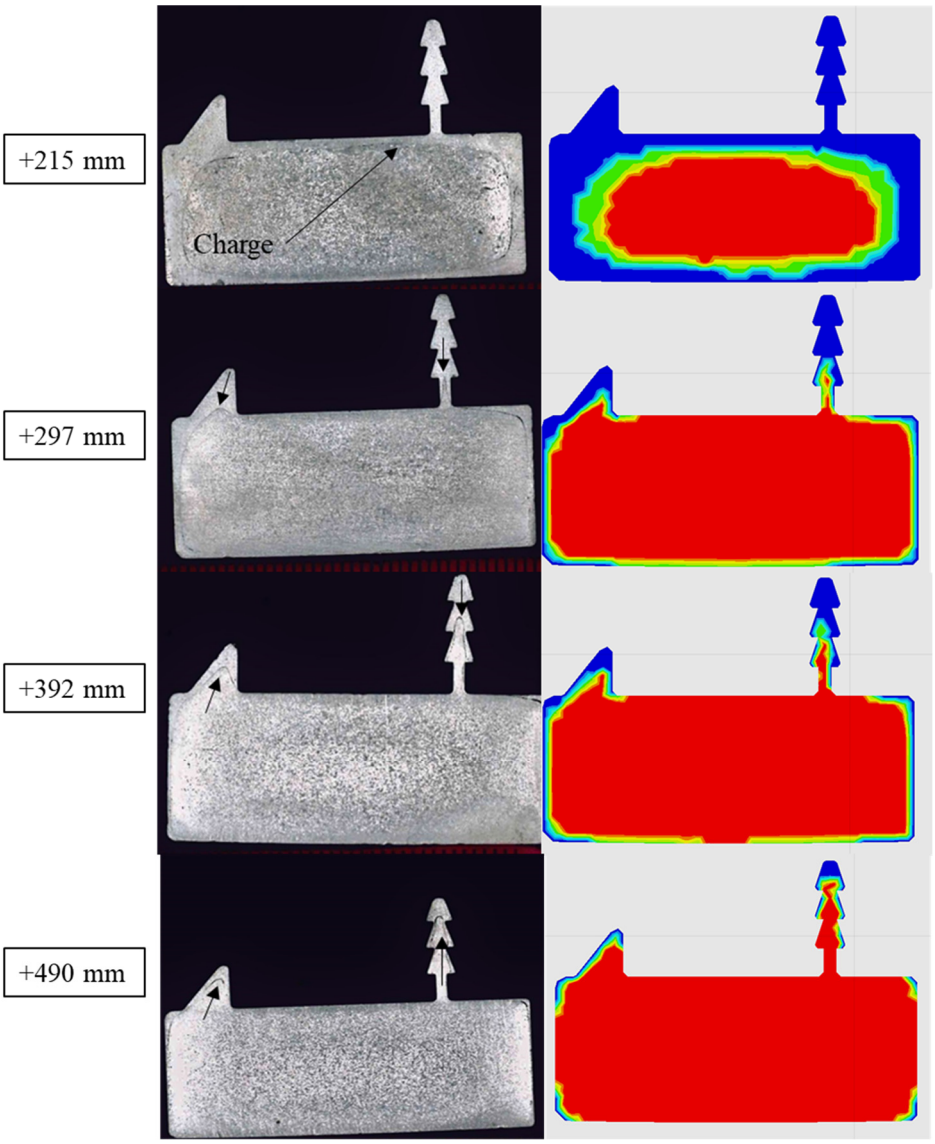

Fig. 103 Experimental-Numerical comparison in terms of old-billet replacement at different distances from the stopmark (Profile A)

In terms of skin prediction, the simulation overestimated the percentage of the contaminated area in proximity of the stopmark (Figs. 104 and 105) for both the not computed interaction with the charge welds and the mesh size that enlarged the skin defect. Indeed, experimentally it turned that the upcoming charge weld flattened the skin contamination, phenomena not simulated with the current numerical model. Moreover, the overestimation of the percentage of contaminated area could be reduced with a finer mesh, however, the significant increase of the computational time (almost twice) was not justified for the aim to predict the scrap length that would remain the same. About the skin contamination onset, it was not possible to evaluate the goodness of the numerical result due to missing experimental data for distances before the stopmark greater than 2000 mm. However, the simulation confirmed the experimental evidence of inadequate scrap length designed from the company to discard all skin contamination. Fig. 105 reports the comparison between the experimental and the numerical trends in terms of percentage of contaminated area of the profile, evidencing the almost perfect overlap of the results in terms of charge welds evolution.

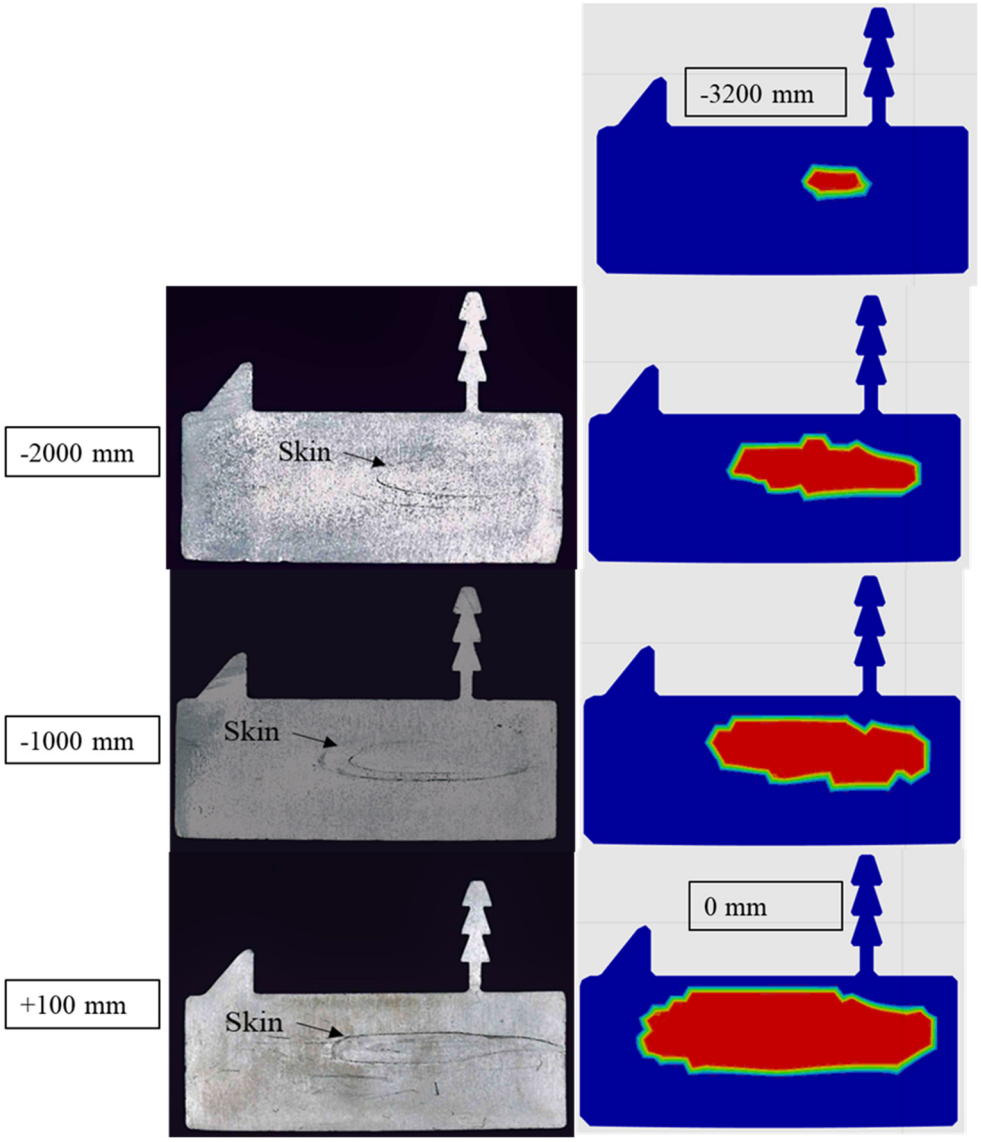

Fig. 104 Experimental-Numerical comparison in terms of skin contamination at different distances from the stopmark (Profile A)

In conclusion, the table 36 summarizes the comparison in terms of scrap length between the experimental, theoretical, numerical, and industrial scraps. In this case, the numerical matching was perfect, while the theoretical formulas underestimate the charge welds extent by about half. In terms of billet skin contamination, the estimated theoretical length was comparable with the numerical one (3320 mm and 3200 mm, respectively). As previously discussed, the scrap operated by the company overestimated over three times the scrap after the stopmark and provided an inadequate discard for the skin contamination.

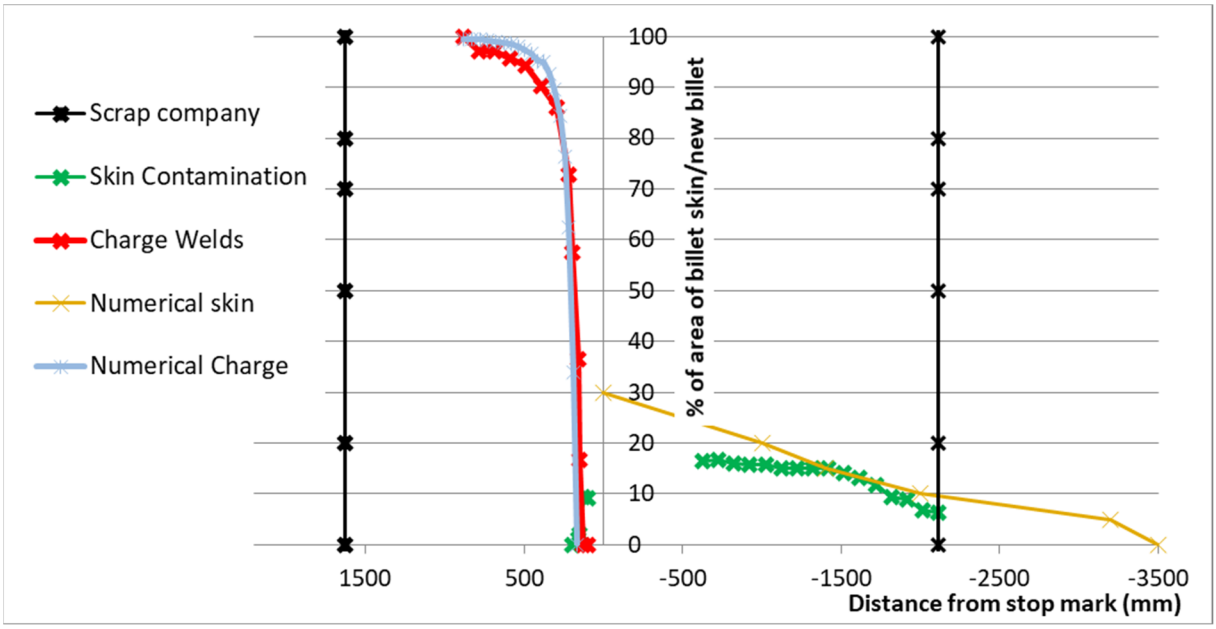

Fig. 105 Comparison between the numerical and the experimental trends of percentage contamination within the profile area (Profile A)

Table 36 Scrap length evaluated with different strategies (Profile A)

Scrap Length	Experimental	1st Theoretical	2nd Theoretical	Numerical	Industrial
Charge Welds, 95% of replacement (After the stopmark)	500 mm	240 mm	361 mm	500 mm	1600 mm
Skin Contamination (Before the stopmark)	At least 2000 mm	3320 mm	-	3200 mm	2000 mm

7.3.2 Profile B

Fig.106 shows the experimental-numerical comparison in terms of charge welds evolution within the cross-section of the profile B. Also in this case, the reliability of the numerical results was confirmed by the excellent forecast of the experimental trend. Moreover, Fig. 107 reports quantitatively the percentage evolution of the new billet material within the profile, evidencing the perfect overlapping of both the numerical and the experimental trends.

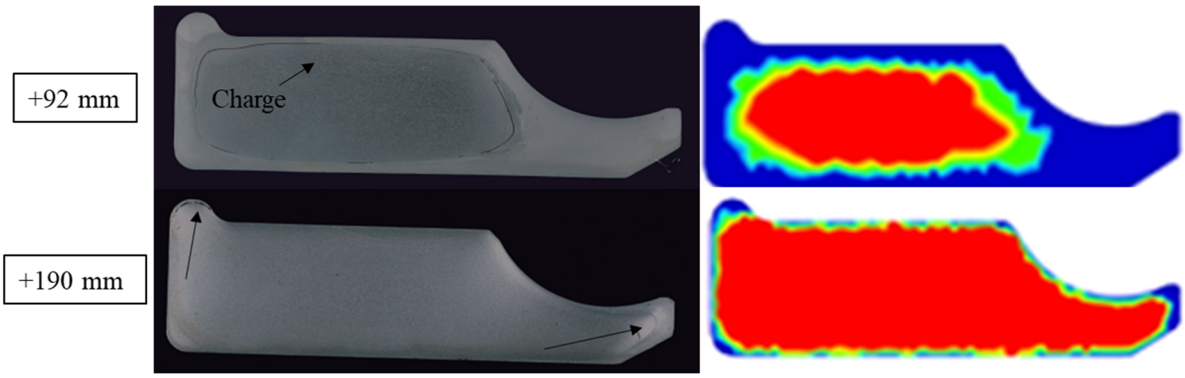

Fig. 106 Experimental-Numerical comparison in terms of old-billet replacement at different distances from the stopmark (Profile B)

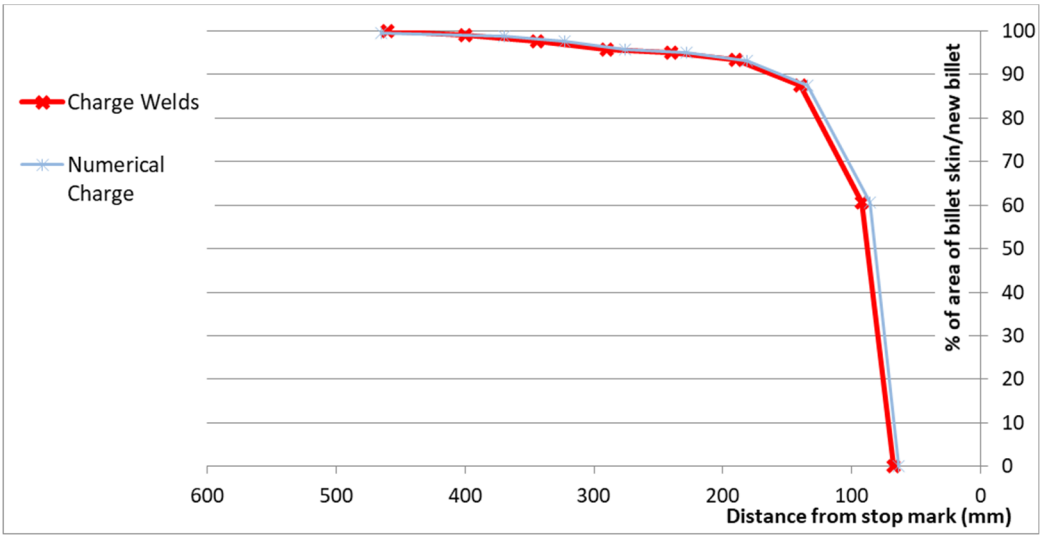

Fig. 107 Comparison between the numerical and the experimental trends of charge welds evolution (Profile B)

In terms of skin prediction, the simulation overestimated the percentage of the contaminated area in proximity of the stopmark (Figs. 107 and 108) for the same reasons previously discussed fort the Profile A. Fig.109 summarizes the experimental-numerical comparison in terms of defect evolution at difference distances from the stopmark. The perfect overlap of the experimental-numerical charge evolution trends (previously discussed), and the good prediction of the skin contamination onset confirmed the reliability of the implemented numerical model. Table 37 summarizes the comparison in terms of scrap length between the experimental, theoretical, numerical, and industrial scraps. In this case, the numerical matching was perfect, while the theoretical formulas underestimated both the charge welds and the skin contamination. As previously discussed, the scrap operated by the company overestimated over five times the scrap after the stopmark but provides an acceptable discard for the skin contamination (4200 mm respect the 3700 mm experimentally found).

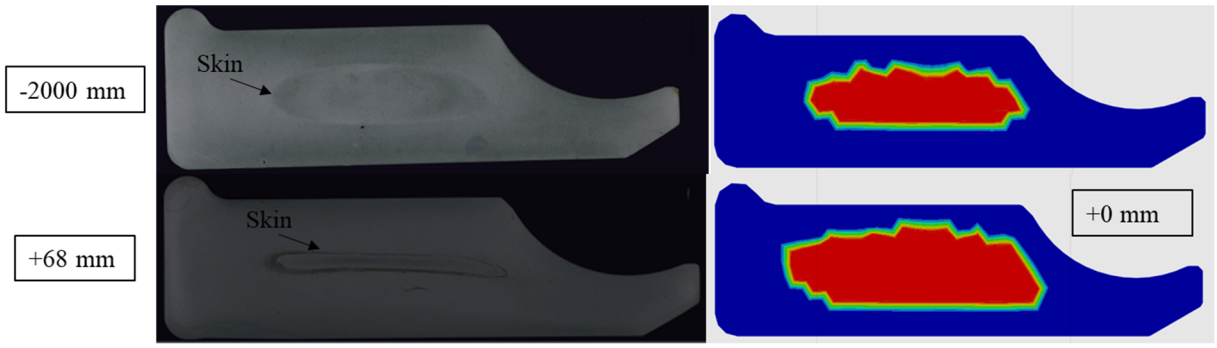

Fig. 108 Experimental-Numerical comparison in terms of skin contamination at different distances from the stopmark (Profile B)

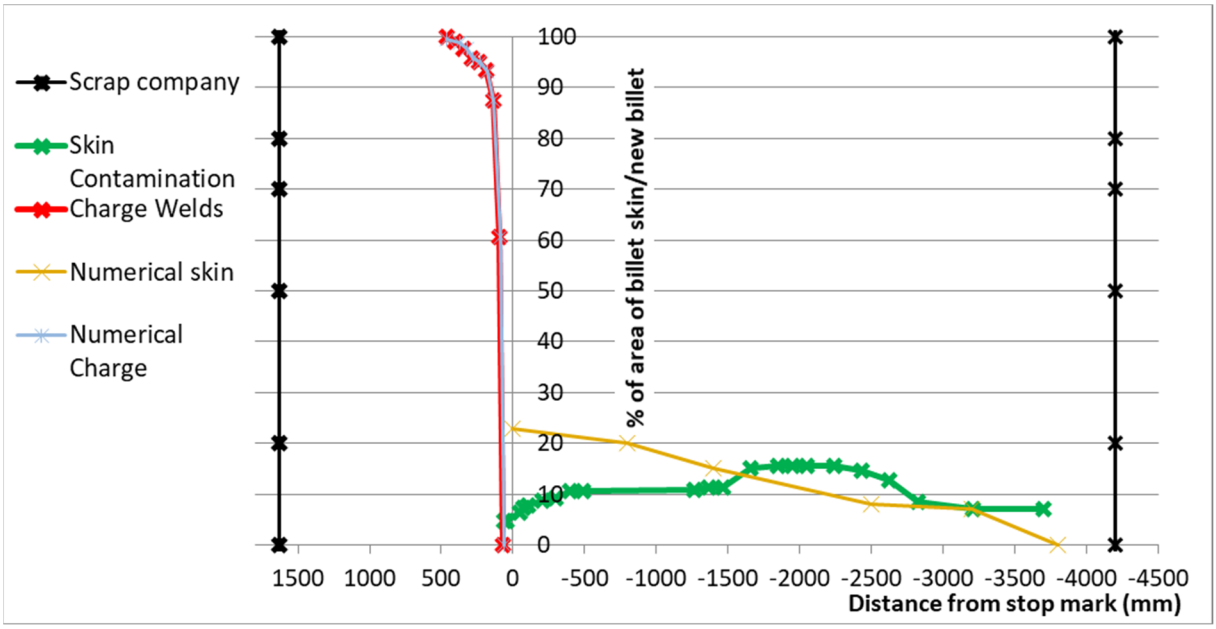

Fig. 109 Comparison between the numerical and the experimental trends of percentage contamination within the profile area (Profile B)

Table 37 Scrap length evaluated with different strategies (Profile B)

Scrap Length	Experimental	1st Theoretical	2nd Theoretical	Numerical	Industrial
Charge Welds, 95% of replacement (After the stopmark)	240 mm	133 mm	199 mm	240 mm	1600 mm
Skin Contamination (Before the stopmark)	3700 mm	2155 mm	-	3800 mm	4200 mm

8 Conclusion

This PhD thesis was focused on the experimental and the numerical assessment of the hot extrusion process of light alloys. Specifically, work was aimed at acquiring an in-depth knowledge of the temperature field developed during the process, mandatory to avoid surface defects and to improve the production rate. In this context, the literature review and the industrial practice revealed that the die cooled with liquid nitrogen offers a high-potential solution to localize the temperature drop nearby the exit of the extruded profile, where highest value are reached, further avoiding significant increases of the load since not affecting the billet deformability during the die filling. The use of liquid nitrogen demonstrated the possibility to double the extrusion speed if the cooling channel is properly designed. However, the literature review and the performed experimental campaigns evidenced that the way in which channel are nowadays designed does not allow an optimal cooling. Indeed, the investigated case studies proved the potentiality of liquid nitrogen cooling, but also the limits leading to unbalanced cooling and/or long transitory cooling phase marked by inefficient heat exchanges. In this scenario, the use of FE codes to predict the thermal field evolution during the extrusion process can offer the necessary support to die design with the aim to optimize the die and the process performances in all its aspect. The 1D model of cooling channel demonstrated its capabilities in all the tested case studies, obtaining in a low computational time average errors below 10% in terms of

thermal field prediction. In addition, the integration of the FE model within the optimization platform showed great possibilities in terms of automatic channel re-design. Notably, the virtual channel re-design of the Benchmark 2011 case study was successfully granted, automatically testing 100 designs in 12 hours and offering a new improved channel design with a balanced cooling around the bearings and with the reduction of the 60% of nitrogen consumption. Despite the accuracy of the presented numerical model, some shortcomings were revealed when a large amount of gas nitrogen is generated within the channel. Indeed, in these cases, the single-phase model using the properties of liquid nitrogen overestimated the cooling efficiencies with peak errors up to 70% where the gas formation reduced drastically the heat exchange with the die. Therefore, a new numerical model was tested based on homogenous fluid approach, where the two-phase flow is treated as a single-phase one, provided that its properties be appropriately modified to account for the actual presence of gas and liquid. The numerical model implemented for the Profilati case study confirmed the accuracy in terms of temperature prediction with a peak error of about 21% and an average error below the 7%. In addition, the transient analysis demonstrated the model potentiality in order to capture the transitory evolution of the thermal field and the gas formation within the channel.

In terms of scrap assessment, three experimental campaigns were performed, showing how the industrial practice are still inadequate in terms of evaluation of the proper scrap length with overestimation or underestimation of five times. In addition, the experimental assessment of the charge welds and the billet skin contamination is a very time and cost consuming activities, not worthwhile in the industrial context. Therefore, the state of art is focused on the analytical and numerical approaches to properly predict the defects evolution within the extruded profile. In this scenario, the proposed numerical model for the prediction of the charge welds and billet skin contamination, based on the Arbitrarian Lagrangian-Eulerian approach, was deeply tested and validated, obtaining an almost perfect matching in terms of defect onset and required scrap length.

The achieved numerical results about the temperature, load and defects prediction, suggest the reliability of the novel developed simulation tools and their potential integration in a flexible procedure to be used for virtual process and die design optimization, thus saving time for experimental trials and costs for inadequate or suboptimal solutions.

Future developments include the use of the ALE approach within the Comsol environment to simulate the scrap evolution during the extrusion process as well as the integration of the cooling module within the HyperXtrude® software. In addition, the improvement of the 1D model of the nitrogen cooling will be deeply study with the aim to taken into account the density changes along the cooling path. Another interesting aspect in terms of cooling channel design could be the use of the topological optimization to preliminarily start the design stage with an optimized cooling path. The final goal of this project, started within my own PhD work, is the integration on a single platform of the simulation of the extrusion process in all its aspect in order to assess and to optimize the process, taken into account simultaneously different objective functions such as strength criteria for the tooling set, scrap minimization and the productivity gain maintaining high standards in terms of profile quality and profile tolerances.

9 References

[1] P.K. Saha, Aluminum extrusion technology, ASM International, Materials Park, OH, USA, 2000.

[2] T. Sheppard, Extrusion of aluminum alloys, Springer, Boston, MA, USA 1999.

[3] Aluminum Extruders Council, Aluminum Extrusion Manual. 4.2 Edition, 2018.

[4] L.M. Tobin, The New Quality Landscape: Total Quality Management, Journal of System Management, Vol 41 (11), pp 8–14, 1990.

[5] B.J. Witcher, Total Marketing: Total Quality and the Marketing Concept, The Q. Review of Marketing, Winter 1990.

[6] H. Valberg, Comparison of metal flow in un-lubricated direct and indirect extrusion of aluminium alloys. Int J Mater Form, Vol 3, pp 387–390 2010.

[7] T. Sheppard, P.J. Tunnicliffe, S.J. Patterson, Direct and indirect extrusion of a high strength aerospace alloy (AA 7075), Journal of Mechanical Working Technology, Vol 6 (4), pp 313-331, 1982.

[8] K. Abrinia, K. Gharibi, An investigation into the backward extrusion of thin walled cans, Int J Mater Form, Vol 1, pp. 411–414, (2008).

[9] P.K. Saha, Thermodynamics and tribology in aluminum extrusion, Wear, vol. 218, pp. 179-190, 1998.

[10] A.R. Savkoor, Section 8.3 - Models of Friction, Handbook of Materials Behavior Models, JEAN LEMAITRE, Academic Press, pp.700-759,2001.

[11] J.A. Schey, Tribology in Metalworking, American Society for Metals, 1983

[12] A. Lawal, D.M. Kalyon, Nonisothermal extrusion flow of viscoplastic fluids with wall slip, International Journal of Heat and Mass Transfer, vol. 40, pp. 3883-3897, 1997.

[13] T.H.G. Megson, Chapter 14, Complex Stress and Strain, Structural and Stress Analysis (Fourth Edition), T.H.G. Megson, Butterworth-Heinemann, pp. 423-466, 2019.

[14] O. Cazacu, B. Revil-Baudard, Chapter 6, Elastic/plastic behavior of metallic materials in torsion and bending Plasticity of Metallic Materials, Elsevier, pp. 311-424, 2021.

[15] T. Björk, R. Westergård, S. Hogmark, Wear of surface treated dies for aluminium extrusion-a case study, Wear, Vol. 249 (3–4), pp. 316-323, 2001.

[16] K. Lukaszkowicz, L. A. Dobrzanski, G. Kokot, P. Ostachowski, Characterization and properties of PVD coatings applied to extrusion dies, Vacuum, Vol 86 (12), pp. 2082-2088, 2012.

[17] S. Abtahi, Interface Mechanisms on the Bearing Surface in Extrusion, Proc. Sixth International Aluminum Extrusion Technology Seminar, May 1996

[18] I. Flitta, T. Sheppard, Material flow during the extrusion of simple and complex cross-sections using FEM, Materials Science and Technology, Vol 21(6), pp. 648-656, 2005.

[19] L. Donati, L. Tomesani, M. Schikorra, N. Ben Khalifa, A. E. Tekkaya, Friction model selection in FEM simulations of aluminium extrusion, International Journal of Surface Science and Engineering, Vol 4, pp. 27-41, 2010.

[20] H. Valberg, Understanding metal flow in aluminium extrusion by means of emptying diagrams, Int J Mater Form, Vol 3, pp. 391–394, 2010.

[21] L. Zhu, K.A. Narh, K.S. Hyun, Investigation of mixing mechanisms and energy balance in reactive extrusion using three-dimensional numerical simulation method, International Journal of Heat and Mass Transfer, Vol. 48, pp. 3411-3422, 2005.

[22] Z. Peng, T. Sheppard, Study of surface cracking during extrusion of aluminium alloy AA 2014, Materials Science and Technology, Vol. 20 (9), pp. 1179-1191, 2004.

[23] S. Ngernbamrung, Y. Suzuki, N. Takatsuji, K. Dohda, Investigation of surface cracking of hot-extruded AA7075 billet, Procedia Manufacturing, Vol. 15, pp. 217-224, 2018.

[24] S.Z. Qamar, A.F.M. Arif, A.K. Sheikh, Analysis of product defects in a typical aluminum extrusion facility, Materials and Manufacturing Processes, Vol. 19, pp. 391-405, 2004.

[25] N.C. Parson, C.W. Jowett, C.V. Pelow, W.C. Fraser, Surface defects on 6xxx alloy extrusions, in: Proceedings of the 6th International Extrusion Technology Seminar, Vol. 1, pp. 57-67, 1996.

[26] S.Z. Qamar, T. Pervez, J.C. Chekotu, Die defects and die corrections in metal extrusion, Metals, Vol. 8, 380, 2018.

[27] A.F. Castle, T. Sheppard, Hot Working Theory Applied to Extrusion of Some Aluminum Alloys, Met Technol., Vol 3 (10),1976.

[28] A.F. Castle, Temperature Control in Aluminum Extrusion, Proc. Fifth International Aluminum Extrusion Technology Seminar, Aluminum Extruders Council and the Aluminum Associations, Inc.,1992.

[29] Y. Tashiro, H.Yamasaki, N. Ohneda, Extrusion Conditions and Metal Flow To Minimize Both Distortion and Variance of Cross-Sectional Shape, Proc. Fifth International Aluminum Extrusion Technology Seminar, 1992.

[30] P.K. Saha, R.K. Ghosh, Temperature Distribution During Hot Extrusion of Aluminum—Theoretical Evaluation, Indian J. Technol., Vol 17, 1979.

[31] P.K. Saha, Influence of Plastic Strain and Strain Rate on Temperature Rise in Aluminum Extrusion, Proc. Sixth International Aluminum Extrusion Technology Seminar, Vol 2, Aluminum Extruders Council and the Aluminum Associations, Inc., May 1996.

[32] L. Donati, M. El Mehtedi, Characterization Of Flow Stress Of Different AA6082 Alloys By Means Of Hot Torsion Test, AIP Conference Proceedings, Vol 1353, pp. 455-460, 2011.

[33] D. Li, A. Ghosh, Tensile deformation behavior of aluminum alloys at warm forming temperatures, Materials Science and Engineering: A, Vol 352 (1-2), pp. 279-286, 2003.

[34] J. Sarkar, T.R.G. Kutty, K.T. Conlon, D.S. Wilkinson, J.D. Embury, D.J. Lloyd, Tensile and bending properties of AA5754 aluminum alloys, Materials Science and Engineering: A, Vol 316 (1-2), pp. 52-59, 2001.

[35] H. Pouraliakbar, M. Pakbaz, S. Firooz, M. Reza Jandaghi, G. Khalaj, Study on the dynamic and static softening phenomena in Al–6Mg alloy during two-stage deformation through interrupted hot compression test, Measurement, Vol. 77, pp. 50-53, 2016.

[36] S. Ding, S. A. Khan, J. Yanagimoto, Flow behavior and dynamic recrystallization mechanism of A5083 aluminum alloys with different initial microstructures during hot compression, Materials Science and Engineering: A, Vol. 787, 2020.

[37] T. Bhujangrao, F. Veiga, C. Froustey et al., Experimental characterization of the AA7075 aluminum alloy using hot shear compression test, Archiv.Civ.Mech.Eng 21, Vol. 45, 2021.

[38] C. Bruni, M. El Mehtedi, Constitutive Equations for Finite Element Simulation, Key Eng Mater, Vol. 504-506, pp. 499-504, 2012.

[39] M. El Mehtedi, L. Balloni, S. Spigarelli, E. Evangelista, GI. Rosen, Hot Workability and Constitutive Equations of ZM21 Magnesium Alloy, Key Eng. Mat., Vol. 367 (79-86), 2008.

[40] K. Laber, A. Kawałek, S. Sawicki, H. Dyja, J. Borowski, D. Leśniak, H. Jurczak, Application of Torsion Test for Determination of Rheological Properties of 5019 Aluminium Alloy, Key Engineering Materials, Vol. 682, pp. 356–361, 2016.

[41] R. Pernis, J. Bidulská, T. Kvačarkaj, I. Pokorný, Application of The Torsion Test in Calculating The Extrusion Force, Archives of Metallurgy and Materials, 2011.

[42] S. Spigarelli, M. El Mehtedi, A New Constitutive Model for the Plastic Flow of Metals at Elevated Temperatures. J. of Materi Eng and Perform, Vol. 23, pp. 658–665, 2014.

[43] C.M. Sellars, W.J. McG Tegart, “Hot workability”, Int Metall Rev, Vol.17 (1), pp.1–24, 1972.

[44] M. El Mehtedi, S. Spigarelli, F. Gabrielli, L. Donati, Comparison study of constitutive models in predicting the hot deformation behavior of AA6060 and AA6063 Aluminum alloys. Materials Today: Proceedings; Vol. 2(10), pp. 4732–4739, 2015.

[45] Y.C. Lin, M.-S. Chen, and J. Zhong, Constitutive Modelling for Elevated Temperature Flow Behaviour of 42CrMo Steel, Comput. Mater. Sci., Vol. 42, pp 470–477, 2008.

[46] H.-Y. Li, D.-D. Wei, J.-D. Hu, Y.-H. Li, and S.-L. Chen, Constitutive Modeling for Hot Deformation Behavior of T24 Ferritic Steel, Comput. Mater. Sci., Vol. 53, pp 425–430, 2012.

[47] 10. J. Li, F. Li, J. Cai, R. Wang, Z. Yuan, and F. Xue, Flow Behavior Modeling of the 7050 Aluminum Alloy at Elevated Temperatures Considering the Compensation of Strain, Mater. Des., Vol. 42, pp 369–377, 2012.

[48] H.R. Rezaei Ashtiani, M.H. Parsa, and H. Bisadi, Constitutive Equations for Elevated Temperature Flow Behavior of Commercial Purity Aluminium, Mater. Sci. Eng., A545, pp. 61–67, 2015.

[49] N. Haghadi, A. Zarei-Hanzaki, and H.R. Abedi, The Flow Behavior Modeling of Cast A356 Aluminum Alloy at Elevated Temperatures Considering the Effect of Strain, Mater. Sci. Eng., A535, pp 252–257, 2012.

[50] Y.C. Lin, Y.-C. Xia, X.-M. Chen, and M.-S. Chen, Constitutive Descriptions for Hot Compressed 2124-T851 Aluminum Alloy over a Wide Range of Temperature and Strain Rate, Comput. Mater. Sci.,Vol.50, pp 227–233, 2010.

[51] I. Riero, V. Gutie´rrez, J. Castellanos, M. Carsı´, M.T. Larrea, and O.A. Ruano, A New Constitutive Strain-Dependent Garofalo Equation to Descrive the High-Temperature Processing of Materials: Application to the AZ31 Magnesium Alloy, Metall. Mater. Trans, Vol. 41A, pp 2396–2406, 2010.

[52] H. Wu, J. Yang, F. Zhu, and C. Wu, Hot Compressive Flow Stress Modelling of Homogenized AZ61 Mg Alloy Using Strain-Dependent Constitutive Equations, Mater. Sci. Eng., A574, pp 17–24,2013.

[53] X. Chen, Y. Du, K. Du, T. Lian, B. Liu, Z. Li, X. Zhou, Identification of the Constitutive Model Parameters by Inverse Optimization Method and Characterization of Hot Deformation Behavior for Ultra-Supercritical Rotor Steel, Materials, Vol. 14, 2021.

[54] R. Akeret, Extrusion welds—quality aspects are now centre stage. Proc of the 5th ET Semin, Vol. I, pp.319–336, 1992.

[55] L. Qiang, C. Harris, MR. Jolly MR, Finite element modelling simulation of transverse welding phenomenon in aluminium extrusion process. Mater Des, Vol. 24 (7), pp. 493–496, 2003.

[56] X. Zhang, D. Feng, X. Shi, S. Liu, Oxide distribution and microstructure in welding zones from porthole die extrusion, Trans Nonferrous Met Soc China, Vol. 23(3), pp.765–772, 2013.

[57] Y. Kim, K. Ikeda, Flow Behavior of the Billet Surface Layer in Porthole Die Extrusion of Aluminum, Metallurgical and Materials Transactions A, Vol. 31A, 2000.

[58] Aluminum Extruders Council, https://www.aec.org.

[59] S.N. Ab Rahim, M.A. Lajis, S. Ariffin, A review on recycling aluminum chips by hot extrusion process, Procedia CIRP, Vol. 26, pp. 761-766, 2015.

[60] J. Zasadziński, W. Libura, J. Richert, Fundamentals of advanced aluminum extrusion processes, in: Proceedings of the 8th International Extrusion Technology Seminar, Vol. 2, pp. 391-397, 2004.

[61] L.J. Matienzo, K.J. Holub, W. Vandatta, Investigation on surface defects produced during the extrusion of some aluminum alloys, Applications of surface science 15, pp. 307-320, 1982.

[62] L. Donati, L. Tomesani, The effect of die design on the production and seam weld quality of extruded aluminum profiles, J. Mat. Proc. Tech Vol.164-165, pp. 1025-1031, 2005.

[63] G. Liu, J. Zhou, J. Duszczyk, Predicting the variation of the exit temperature with the initial billet temperature during extrusion to produce an AZ31 profile, Int J Mater Form, Vol. 2, pp. 113–119, 2009.

[64] L. Donati, N.B. Khalifa, L. Tomesani, A.E. Tekkaya, Comparison of different FEM code approaches in the simulation of the die deflection during aluminium extrusion, Int J Mater Form, Vol. 3, pp. 375–378, 2010.

[65] N. Biba, A. Lishny, S, Stebunov, Finite Element Modelling of Complex Thin Profile Extrusion. AIP Conference Proceedings, Vol. 1353, pp. 425-430, 2011.

[66] N. Biba, S. Stebunov, A. Lishny, The Model for Coupled Simulation of Thin Profile Extrusion. Key Eng Mater, Vol. 504-506, pp. 505-510, 2012.

[67] A. Klaus, How to benefit from isothermal extrusion. Proceedings of the 11th International Extrusion Technology Seminar Vol.2, pp. 215-220, 2016.

[68] J.C. Benedyk, The evolution of the smart container: Achieving Isothermal Control in Extrusion. Light metal Age, pp.40-47, 2008.

[69] A. Farjad Bastani, T. Aukrust, S. Brandal, Study of isothermal extrusion of aluminum using finite element simulations. Int J Mater Form, Vol. 3, pp. 367–370, 2010.

[70] R. Holker, A. Jager, N.B. Khalifa, A.E. Tekkaya, New concepts for cooling of extrusion dies manufactured by rapid tooling. Key Engineering Materials, Vol 491, pp.223-232, 2011.

[71] F. Parvizian, T. Kayser, C. Hortig, B. Svendsen, Thermomechanical modeling and simulation of aluminum alloy behavior during extrusion and cooling, Journal of Materials Processing Technology, Vol. 209, pp. 876-883, 2009.

[72] T.J. Ward, R.M. Kelly, G.A. Jones, J.F. Heffron, The effects of Nitrogen - liquid and gaseous - on aluminum extrusion productivity, JOM - The Journal of The Minerals, Metals & Materials Society, vol. 36, pp. 29-33, 1984.

[73] P. Stratton, Raising productivity of aluminium extrusion with nitrogen, International Heat Treatment and Surface Engineering, vol. 2, pp. 105-108, 2008.

[74] A.F. Ciuffini, S. Barella, C. Di Cecca, A. Gruttadauria, C. Mapelli, L. Merello, G. Mainetti, M. Bertoletti, Surface quality improvement of AA6060 aluminum extruded components through liquid nitrogen mold cooling, Metals, Vol. 8, 409, 2018.

[75] H. Brodbeck, Experience Using Liquid Nitrogen for Die Cooling. Proceedings of the Third International Aluminum Extrusion Technology Seminar (ET 1984), Atlanta, Georgia, the Aluminum Extruders Council and the Aluminum Association, Vol 1, pp. 279-282, 1984.

[76] M.A. Marchese, J.J. Coston, Efficient Use of Liquid Nitrogen for Aluminum Extrusion Die Cooling and Inerting, Proceedings of Fourth International Aluminum Extrusion Technology Seminar (ET 1988), Chicago, Illinois, the Aluminum Extruders Council and the Aluminum Association. Vol. 2, pp. 83-88,1988.

[77] L. Donati, A. Segatori, B. Reggiani, L. Tomesani, PA Bevilacqua Fazzini, Effect of liquid nitrogen die cooling on extrusion process conditions, Key Engineering Materials, Vol. 491, pp. 215-222, 2012.

[78] R. Hölker, A. Jäger, N. Ben Khalifa, A. Erman Tekkaya, Controlling heat balance in hot aluminum extrusion by additive manufactured extrusion dies with conformal cooling channels, International Journal of Precision Engineering and Manufacturing, Vol. 14, pp. 1487-1493, 2013.

[79] R. Hölker, A. Erman Tekkaya, Advancements in the manufacturing of dies for hot aluminum extrusion with conformal cooling channels, The International Journal of Advanced Manufacturing Technology, Vol. 83, pp. 1209-1220, 2016.

[80] B. Reggiani, I. Todaro, Investigation on the design of a novel selective laser melted insert for extrusion dies with conformal cooling channels, The International Journal of Advanced Manufacturing Technology, Vol. 104, pp. 815-830, 2019.

[81] M. Mazur, P. Brincat, M. Leary, M. Brandt, Numerical and experimental evaluation of a conformally cooled H13 steel injection mould manufactured with selective laser melting, Int. J Adv. Manuf. Technol. Vol 93, pp. 881-900, 2017.

[82] A. Armillotta, R. Baraggi, S. Fasoli, SLM tooling for die casting with conformal cooling channels, Int. J Adv. Manuf. Technol., Vol. 71, pp. 573-583, 2014.

[83] A. Loukus, G. Subhash, M. Imaninejad. Mechanical properties and microstructural characterization of extrusion welds in AA6082-T4. Journal of Materials Science, Vol. 39, pp. 6561–6569, 2004.

[84] J.H. Zhu, B. Young, Effects of transverse welds on aluminum alloy columns, Thin-Walled Structures, Vol 45 (3), pp. 321-329,2007.

[85] S. Bingöl, M.S. Keskin, Effect of different extrusion temperature and speed on extrusion welds. Journal of Achievements in Materials and Manufacturing Engineering, Vol. 23(2), 2007.

[86] Finkelnburg WD, Scharf G. Some investigation on the metal flow during extrusion of Al alloys. In the proc. of the 5th Extrusion Technology Seminar, 1992; Chicago, USA.

[87] Jowett C, Adams J, Daughetee C, Lea G, Huff OA, Fossl N. Scrap allocation. In the Proc. of the 9th Extrusion Technology Seminar 2008; Florida, USA.

[88] P. Saha, Quality issues of hollow extrusions for aerospace applications, Proc. of the 9th Extrusion Technology Seminar, Florida, US, 2008.

[89] A.J. den Bakker, R.J. Werkhoven, R. van de Nolle, Influence of die geometry on charge weld evolution, In the Proc. of the ICEB - International Conference on Extrusion and Benchmark, pp. 57–64, 2013.

[90] Y. Mahmoodkhani, M.A. Wells, N. Parson, W. Poole, Numerical modelling of the material flow during extrusion of aluminium alloys and transverse weld formation. J Mater Process Technol, Vol. 214, pp. 688–700, 2014.

[91] T. Pinter, B. Reggiani, L. Donati, L. Tomesani, Numerical assessment of the influence of process and geometric parameters on extrusion welds and die deformation after multiple-cycles. Mater Today Proc Vol. 2(10), pp. 4856–4865, 2015.

[92] Yu JQ, Zhao GQ, Chen L (2016) Investigation of interface evolution, microstructure and mechanical properties of solid-state bonding seams in hot extrusion process of aluminum alloy profiles. J Mater Process Technol, Vol. 230, pp. 153–166.

[93] T. Hatzenbichler, B. Buchmayr, A. Umgeher, A numerical sensitivity study to determine the main influence parameters on the back-end defect. J Mater Process Technol, Vol. 182, pp.73–78, 2007.

[94] B. Reggiani, L. Donati, L. Tomesani (2013) Prediction of charge welds in hollow profiles extrusion by FEM simulations and experimental validation. Int J Adv Manuf Technol, Vol 69(5), pp.1855–1872, 2013.

[95] Y. Mahmoodkhani, M. Wells, N. Parson, C. Jowett, W. Poole, Modeling the formation of transverse weld during billet-on-billet extrusion. Materials, Vol. 7, pp. 3470–3480, 2014.

[96] T. Pinter, D. Antonios, B. Reggiani, A. Gamberoni, Charge weld scrap minimization by means of dead metal flow control in die design. Proc of the 11th ET Semin Vol. I, pp. 827–845, 2016.

[97] B. Reggiani, L. Donati, Experimental, numerical, and analytical investigations on the charge weld evolution in extruded profiles, Int J Adv Manuf Technol, Vol 99, pp. 1379–1387, 2018.

[98] T. Ishikawa, H. Sano, Y. Yoshida, N. Yukawa, J. Sakamoto, Y. Torzawa, Effect of Extrusion Conditions on Metal Flow and Microstructures of Aluminum Alloys, CIRP Annals 2006, Vol. 55 (1), pp. 275-278, 2006.

[99] T. Hatzenbichler, B. Buchmayr, Finite element method simulation of internal defects in billet-to-billet extrusion, Proc. of the Institution of Mechanical Engineers, Part B: Journal of Engineering Manufacture, Vol. 224, pp.1029-1042, 2010.

[100] C. Jowett, N. Parson, W. Fraser, J Hankin, K. Hicklin, Simulation of Flow of the Billet Surface into the Extruded Product. In the Proc. of the 7th Extrusion Technology Seminar, Vol. I pp. 27–42, 2000.

[101] S. Lou, Y. Wang, C. Liu et al., Analysis and Prediction of the Billet Butt and Transverse Weld in the Continuous Extrusion Process of a Hollow Aluminum Profile, J. of Materi Eng and Perform, Vol. 26, pp. 4121-4130, 2017.

[102] F. Klocke, K. Arntz, M. Teli, K. Winands et al., State-of-the-art Laser Additive Manufacturing for Hot-work Tool Steel, Procedia CIRP, Vol. 63, pp.58-63, 2017.

[103] Y. Chen, H. Chen et al., Numerical, and experimental investigation on thermal behavior and microstructure during selective laser melting of high strength steel, J. Manuf. Processes, Vol. 57, pp.533-542, 2020.

[104]. S. Cooke, K. Ahmadi, S. Willerth, R. Herring, Metal additive manufacturing: Technology, metallurgy and modelling, J. Manuf. Processes., Vol. 57, pp. 978-1003, 2020.

[105] A.J. Norwood, P.M. Dickens, R.C. Soar, R. Harris et al., Analysis of cooling channels performance, Int. J. Comput. Integ. M., Vol. 17 (8), pp. 669-678, 2004.

[106]. M.J. Hokzweissig, A. Taube, F. Brenne et al., Microstructural Characterization and Mechanical Performance of Hot Work Tool Steel Processed by Selective Laser Melting, Metall. Mater. Trans. B, Vol. 46, pp. 545-549, 2015.

[107] U. Scopioni Bertoli, A.J. Wolfer, M.J. Matthews et al., On the limitations of Volumetric Energy Density as a design parameter for Selective Laser Melting, Mat. Des. Vol. 113, pp. 331-340, 2017.

[108] D. Atwell, M. Barnett, Extrusion Limits of Magnesium Alloys. Metall and Mat Trans A, Vol. 38, pp. 3032-3041, 2007.

[109] A. Segatori, B. Reggiani et al., Effect of Process Parameters on Seam Weld Quality of ZM21 Tubes, Key Eng. Mat., Vol. 504-506, pp. 487-492, 2012.

[110] E.W. Lemmon, M.O. McLinden, D.G. Friend, Thermophysical properties of fluid systems, in: P.J. Linstrom, W.G. Mallard (Eds.), NIST Chemistry WebBook, Standard Reference Database no. 69, National Institute of Standards and Technology, Gaithersburg, MD, USA, 2018.

[111] COMSOL® Multiphysics 5.4 Release, https://www.comsol.com/release/5.4.

[112] M.V. Lurie, Modeling of oil product and gas pipeline transportation, Wiley, Weinheim, Germany, 2008.

[113] A. Dewan, Reynolds-averaged governing equations and closure problem, in: A. Dewan (Ed.), Tackling turbulent flows in engineering, pp. 43-48, Springer, Heidelberg, Germany, 2011.

[114] Properties of nitrogen, in: J.E. Jensen, W.A. Tuttle, R.B. Stewart, H. Brechna, A.G. Prodell (Eds.), Selected cryogenic data notebook, Report BNL 10200-R, Brookhaven National Laboratory, Upton, NY, USA, 1980.

[115] M. Nourani, A. S. Milani*, S. Yannacopoulos , "On the effect of different material constitutive equations in modeling friction stir welding: A review and comparative study on aluminum 6061, International Journal of Advances in Engineering & Technology, Mar. 2014, Vol. 7, Issue 1, pp. 1-20.

[116] B. Verlinden, A. Suhadi, L. Delaey "A generalized constitutive equation for an AA6060 aluminum alloy" Scripta Metallurgica et Materialia Vol.28, pp.1441-1446, 1993.

[117] https://www.esteco.com/modefrontier

[118] A. Husain, Applicability of the homogeneous flow model to two-phase flow, Ph.D. thesis, University of Cincinnati, Cincinnati, OH, USA, 1975.

[119] R. Balasubramaniam, E. Ramé, J. Kizito, M. Kassemi, Two phase flow modeling: Summary of flow regimes and pressure drop correlations in reduced and partial gravity, Report NASA/CR—2006-214085, National Aeronautics and Space Administration, Cleveland, OH, USA, 2006.

[120] D. Bedeaux, The effective shear viscosity for two-phase flow, Physica A: Statistical Mechanics and its Applications, Vol. 121, pp. 345-361, 1983.

[121] C.-Y. Wang, C. Beckermann, A two-phase mixture model of liquid-gas flow and heat transfer in capillary porous media – I. Formulation, International Journal of Heat and Mass Transfer, Vol. 36, pp. 2747-2758, 1993.

[122] A. Selvaggio, T. Kloppenborg, M. Schwane et al., Extrusion benchmark 2013 - Experimental analysis of mandrel deflection, local temperature and pressure in extrusion dies, Key Engineering Materials Vol. 585, pp. 13-22, 2014.

10 Research activities during the PhD

10.1 Key issues to be addressed

- Monitoring of the extrusion process of industrial profiles in terms of thermal gradient and extrusion load by means of dedicated, controlled experimental campaigns.
- Laboratory analysis of the profile defects extruded under different process conditions (cooled/uncooled process, variable ram speed)
- Laboratory tests for the mechanical characterization of selected aluminum alloys to be used as input data for numerical models.
- Simulation of the extrusion process for the prediction of the main process outputs (tools and profile temperatures, extrusion load, velocity gradient in the profile…)
- Simulation of the extrusion process in terms of scraps prediction and comparison with experimental data and analytical models reported in literature with the aim to minimize the scrap length.
- Simulation of the extrusion process with nitrogen cooling. Validation of the numerical model with experimental case studies.
- Benchmark of different simulation codes

- Implementation of an optimization platform for the hot extrusion process

10.2 Expected Results

- Validation of the numerical models of the extrusion process in terms of main outputs predictions (material flow, process load, thermal and velocity fields) by means of the comparison with experimental data.
- Development of numerical and analytical models for the prediction of the thermal gradient in the extrusion process with nitrogen cooling.
- Industrial experimentally testing of different cooling conditions
- Evaluation of the applicability of additive manufacturing technologies for the fabrication of extrusion dies with conformal cooling channels
- Experimental and numerical analyses on the prediction of the extrusion defects (charge welds, billet skin).

10.3 Activities carried out

During the first year of PhD, the research activities have been focused on the investigation of the main aspects of an extrusion process in terms of thermal fields, influences of process parameters and defects analysis. This was done throughout, a comprehensive literature review performed by means of the main research and scientific database. Concurrently, the study of the finite element method and the training with different Finite Element FE software were carried out. More specifically, the research activities carried out during this first year can be summarized as follow:

- Literature review and studying of the basic principles of the hot extrusion process of aluminium alloys
- Literature review and studying of the thermal problem in the extrusion process to understand what are the main solutions adopted in the industrial context.
- Literature review and studying of the main defects in the extrusion process. Analysis of the published literature on the numerical prediction of the extrusion defects in order to forecast the expected results with the commercial codes nowadays available.
- Assessment of the fundamentals of the fluid-dynamics theory for pressurized fluid within a channel.
- Training in the use of different software for plastic deformation processes (QForm Vx, Comsol Multiphysics, HyperXtrude). In addition, the implementation of a preliminary numerical model of the extrusion process was performed and verified against experimental case studies.
- Development of a preliminary numerical model of a nitrogen-cooling channel. The mono dimensional model of the cooling was integrated with the three-dimensional model of the extrusion process. First testing on Benchmark 2011 case study.

During the second year of PhD, more advances numerical models were implemented and validated aimed at the prediction of the main aspects of an extrusion process in terms of thermal fields, influences of process parameters, scrap assessment, cooling efficiency and defects analysis. During this year, two experimental campaigns were performed in collaboration with two different companies. The data acquired during the experimental campaigns were analyzed in detail to comprehend how phenomena were involved during the process and what are the key parameters to carry out robust and

efficient numerical models. In particular, the greatest efforts have been focused on numerical model of die nitrogen cooling, also introducing the study of gaseous phase. More specifically, the research activities carried out during this second year can be summarized as follow:

- Literature review on additive manufacturing applicability for the fabrication of conformal cooling channels in extrusion tools.
- First experimental campaign (Multi-die case study): monitoring of the thermal gradient during the extrusion process with and without nitrogen cooling under different conditions of extrusion speed and nitrogen flow rate. The functionality of the insert made with additive manufacturing technologies was tested evaluating the efficiency of the conformal cooling channel and the insert mechanical resistance under real process conditions.
- Second experimental campaign (Indinvest case study): Analysis of the charge welds, billet skin defects and micro-structure for solid industrial profile. Dedicated samples have been specifically prepared for the identification of the defects in the profile by cutting, polishing, grinding and chemical etching many profile slices.
- Development of robust numerical model of a nitrogen-cooling channel. The mono dimensional model of the cooling was integrated with the three-dimensional model of the extrusion process. The model was tested analyzing complex industrial case studies under different conditions of ram speed, nitrogen flow rate as well as of channel design. The model allows to evaluate the possible formation of gaseous phase within the channel.
- Third experimental campaign: Analysis of the charge welds, billet skin defects and micro-structure for solid industrial profile. Dedicated samples have been specifically prepared for the identification of the defects in the profile by cutting, polishing, grinding and chemical etching many profile slices.
- Implementation and validation of new numerical model for charge weld prediction with COMSOL Multiphysics software. The experimental-numerical comparison was performed with solid and hollow industrial profiles.
- Implementation of Lagrangian numerical model with Qform software to predict the billet skin flow within the profile.
- Numerical modelling of charge welds and billet skin evolution by means of HyperXtrude software using the Arbitrarian Lagrangian-Eulerian (ALE) approach. The experimental-numerical comparison was performed for Indinvest case study.
- Training in the use of software for multidisciplinary design optimization.

During the third year of PhD, improvements have been made in the implemented numerical models of the extrusion process in terms of thermal fields prediction in uncooled and nitrogen cooled process, scrap assessment and defects analysis. In addition, the last comprehensive experimental campaign was carried out, testing the cooling efficiency and the defect evolution for an industrial complex hollow profile (Profilati case study). In particular, a novel 1D numerical model of nitrogen cooling was proposed and validated with Profilati case study in order to take into account the phase change. The transient analysis of the extrusion of multiple billets was performed to analyze complex transition phases as the billet change and the nitrogen flow rate variations, allowing to acquire valuable information about the channel design efficiency. About the scrap assessment, an in-depth study was performed in terms of charge welds extent as a function of die design and extrusion ratio in order to propose an empirical formulation to be implemented within an optimization platform. Currently the optimization platform was successfully tested for the cooling channel re-design by varying the

channel geometry in an automatic way (Benchmark 2011 case study). More specifically, the research activities carried out during this third year can be summarized as follow:

- Third experimental campaign: monitoring of the thermal gradient during the extrusion process with and without nitrogen cooling under different conditions of extrusion speed and nitrogen flow rate. During the trials, a set of thermocouples in the tooling set was used to record the temperatures history during the process. Analysis of the charge welds and billet skin defects in an industrial profile. Dedicated samples have been specifically prepared for the identification of the defects in the profile by cutting, polishing, grinding and chemical etching many profile slices.
- Development of a novel numerical model of a nitrogen-cooling channel. The mono dimensional model of the cooling was integrated with the three-dimensional model of the extrusion process. The model takes into account the pressure drops caused by the gas formation along the channel. The tests were performed analyzing complex industrial case studies under different conditions of ram speed, nitrogen flow rate as well as of channel design.
- Implementation and validation of the transient analysis of the extrusion process of multiple billets under different cooling and ram speed conditions.
- The experimental-numerical comparison in terms of defect extent was performed for Profilati case study within the HyperXtrude environment.
- Numerical analysis of the charge weld extent as a function of die design and extrusion ratio.
- Implementation of the numerical model for the nitrogen cooling within the optimization platform.
- Testing of the virtual optimization of the cooling channel design for Benchmark 2011 case study.
- Preliminary design of a dedicated laboratory set up for testing the cooling channel performances of industrial extrusion dies.
- Writing of the PhD Thesis

11 Dissemination

11.1 International Journals

[J1] Negozio M., **Pelaccia R.**, Donati L., Reggiani B., Pinter T., Tomesani L. (2021). Finite Element Model Prediction of Charge Weld Behaviour in AA6082 and AA6063 Extruded Profiles. JOURNAL OF MATERIALS ENGINEERING AND PERFORMANCE, vol. 30, p. 4691-4699, ISSN: 1059-9495, doi: 10.1007/s11665-021-05752x

[J2] **Pelaccia, R.**, Negozio, M., Donati, L-, Reggiani, B., Tomesani, L. (2021). Extrusion of Light and Ultralight Alloys with Liquid Nitrogen Conformal Cooled Dies: Process Analysis and Simulation. JOURNAL OF MATERIALS ENGINEERING AND PERFORMANCE, p. 1-11, ISSN: 1059-9495, doi: 10.1007/s11665-021-06320-z

[J3] **Pelaccia, R.**, Reggiani, B., Negozio, M. et al. (2022). Liquid nitrogen in the industrial practice of hot aluminium extrusion: experimental and numerical investigation. Int J Adv Manuf Technol. https://doi.org/10.1007/s00170-021-08422-3

11.2 International Conferences

[C1] G. Valli, B. Reggiani, I. Todaro, **R. Pelaccia**, R. Squatrito, T. Pinter, E. Mainetti, Y. Rami, L. Donati, L. Tomesani, 2019. A novel 3D printed cooling insert for extrusion dies. In the Proceedings of the 11th Aluminum Two Thousand Congress, 2019, Treviso, Italy, 9-13 April.

[C2] **R. Pelaccia**, B. Reggiani, L. Donati, L. Tomesani, 2019. *Advanced modeling of die cooling with liquid nitrogen*. In the Proceedings of the 11th Aluminum Two Thousand Congress, 2019, Treviso, Italy, 9-13 April.

[C3] T. Pinter, E. Sicignano, **R. Pelaccia**, B. Reggiani**,** L. Donati, 2019. *Back-end and front-end scrap in direct extrusion: an estimation by means of finite element analysis*. In the Proceedings of the 11th Aluminum Two Thousand Congress, 2019, Treviso, Italy, 9-13 April.

[C4] **R. Pelaccia**, B. Reggiani, L. Orazi, L. Donati, 2019. *Numerical prediction of charge welds and coring defects in extruded profiles*. MTS Conference – Material Technologies in Silesia, Zawiercie, Poland, 13-16, October.

[C5] M. Negozio, **R. Pelaccia**, L.Donati, B. Reggiani, L. Tomesani, T. Pinter, 2020. *FEM validation of front end and back end defects evolution in a AA6063 and AA6082 aluminum alloys profiles*. Proceeding of the 23rd International Conference on Material Forming- ESAFORM, 4th-8th May (online virtual conference). Procedia Manufacturing 47, pp. 202-208 ISSN 2351-9789.

[C6] **R. Pelaccia**, M. Negozio, L. Donati, B. Reggiani, L. Tomesani, 2020. *Efficiency of conformal cooling channels inserts for extrusion dies*. Proceeding of the 23rd International Conference on Material Forming- ESAFORM, 4th-8th May (online virtual conference). Procedia Manufacturing 47, pp. 209-216 ISSN 2351-9789.

[C7] **R. Pelaccia**, B. Reggiani, L. Donati, L. Tomesani, 2020. *Modeling of Nitrogen Cooling in the Extrusion of Aluminum Alloys.* Accepted paper for the ET '20 - International Aluminum Extrusion Technology Seminar, scheduled for May 19-21, 2020 in Orlando Florida and Postponed Due to Coronavirus Threat, rescheduled for May 3-5 2022 [Accepted paper TH138]

[C8] T. Pinter, B. Reggiani, L. Donati, **R. Pelaccia**, M. Negozio, L. Tomesani, 2020. *Scrap Prediction in Direct Aluminum Extrusion*. Accepted paper for the ET '20 - International Aluminum Extrusion Technology Seminar, scheduled for May 19-21, 2020 in Orlando Florida and Postponed Due to Coronavirus Threat, rescheduled for May 3-5 2022 [Accepted paper TH112]

[C9] L. Donati, B. Reggiani, **R. Pelaccia**, G. Valli, I.Todaro, R. Squatrito, L. Tomesani, T. Pinter, E. Mainetti, Y. Rami, 2020. *Additive Manufacturing of H-13 Inserts for Optimal Extrusion Die Cooling*. Accepted paper for the ET '20 - International Aluminum Extrusion Technology Seminar, scheduled for May 19-21, 2020 in Orlando Florida and Postponed Due to Coronavirus Threat, rescheduled for May 3-5 2022 [Accepted paper EP152]

[C10] **Riccardo Pelaccia**, Marco Negozio, Barbara Reggiani, Lorenzo Donati, Luca Tomesani (2021). Analysis and optimization of cooling channels performances for industrial extrusion dies. In: Proceedings of the 24th International Conference on Material Forming (Extrusion & Drawing session). on line, 14-16 Aprile 2021

11.3 National Conferences

[CN1] B. Reggiani, L. Donati, L. Tomesani, **R. Pelaccia**, 2019. *A novel design concept of the extrusion dies*. Atti del XIV Convegno A.I.Te.M. - Associazione Italiana Tecnologie Manifatturiere, Padova, 09-11 Settembre 2019.

[CN2] **R. Pelaccia,** M. Negozio, L. Donati, B. Reggiani, L. Tomesani, 2022. Virtual shape and process optimization of nitrogen cooling in extrusion industry. Atti del XV Convegno A.I.Te.M.-Associazione Italiana Tecnologie Manifatturiere, Milano, 17-19 Gennaio 2022.

11.4 Contributions on Volume

[CV1] **R. Pelaccia,** B. Reggiani, I. Todaro, G. Valli, L. Donati, R. Squatrito, A. Fortunato, L. Tomesani, 2019. SLM of extrusion dies with liquid nitrogen cooling. Dodicesima giornata di studio Ettore Funaioli – 20 luglio 2018, pp. 39-40, Bologna, Società editrice Esculapio, ISBN: 978-88-9385-140-4.